Extreme Precipitation in Greenland and the Baffin Bay Region: Changes, Drivers, and Impacts on Land Ice

By:

Nicole Amber Loeb

A thesis submitted to the Faculty of Graduate Studies of

The University of Manitoba

In partial fulfillment of the degree of

Doctor of Philosophy

Department of Environment and Geography

Clayton H. Riddell Faculty of Environment, Earth, and Resources

University of Manitoba

Winnipeg, Manitoba, Canada

Copyright © 2025, Nicole Amber Loeb

Abstract

Small shifts in mean precipitation conditions can lead to larger changes in the most intense events, meaning that there is potential for increasing extreme precipitation in the Arctic as temperatures rise. Extreme precipitation can have substantial impacts on local communities and the physical climate system, including the surface mass balance (SMB) of land ice. This thesis investigates characteristics of extreme precipitation days (EPDs; > 95th percentile of wet days), focusing on their projected changes and impact on land ice SMB. Greenland and the eastern Canadian Arctic are the focus of this work due to the presence of numerous communities and large quantities of land ice that may be impacted. The research is divided into three studies;

Firstly, the ability of three atmospheric reanalyses to reproduce observed EPDs is evaluated. Despite challenges in matching the timing and location of individual events, the reanalyses generally reproduce the seasonality of EPDs and provide insight into the climatological statistics of events.

Next, the projected future changes in EPDs in the region are examined using Variable-Resolution Community Earth System Model (VR-CESM) simulations following a high emissions scenario and their connections to extratropical cyclones and atmospheric rivers (ARs) are explored. Most of the region sees large projected increases in EPD accumulations (>100 mm/year), particularly in the warm season tied to increasing AR occurrence. Conversely, southeastern Greenland sees a decrease, thought to be tied to reduced cyclone activity.

Finally, the role of EPDs in the seasonal SMB of the region's land ice is explored. Historically, EPDs contributed positively to seasonal SMB. Future EPDs continue to result in SMB increases in high elevation areas. However, they may lead to more variable and often negative SMB responses in the warm season in lower elevations, particularly in southwestern Greenland.

Together, this work provides an exploration of EPDs in the study region and their influence on the SMB of land ice. A better understanding of these processes allows for improved estimates of both the potential risks to communities related to EPDs and whether these events may accelerate or decelerate the contribution of the region's land ice to global sea level rise.

Acknowledgements

I would like to first express my gratitude to my co-advisors, Alex Crawford and Julienne Stroeve. Your expertise and support have been invaluable throughout this work. I appreciate your guidance in shaping this work, and your encouragement for me to pursue opportunities that arose during my studies, such as teaching and working with ECCC. I would also like to thank my internal committee members, Karen Alley, John Hanesiak, and Tim Papakyriakou, all of whom have provided helpful suggestions and feedback along the way. A special thank you to John who also served as my co-advisor for the first 2+ years of this degree. Additionally, thank you to Dr. Heini Wernli for serving as external examiner and providing insightful feedback on this work.

I am also very grateful for the great scientists that I have had the opportunity to collaborate with on this work. Many thanks to Jan Lenaerts, Adam Herrington, and the National Center for Atmospheric Research Land Ice Working Group for their help facilitating the VR-CESM simulations that became a vital part of this work, and to Annelise Waling for her help implementing the atmospheric river tracking algorithm. Also, to Michelle McCrystall, for assistance in comparing VR-CESM to CESM2 simulations. Thank you to Brice Noël for providing valuable expertise in interpreting the SMB analysis. Finally, I appreciate the reviewers whose comments helped to shape the papers within this thesis.

I am grateful to the Natural Sciences and Engineering Research Council of Canada (NSERC) for awarding me a CGS-D/PGS-D award to support me during this work, to Environment and Climate Change Canada for granting me an Atmospheric and Meteorological Graduate Supplement Scholarship, and to the selections committee of the D.G. & V.E. Barber Memorial Fellowship for awarding further financial support for this work. Additional funding was provided through Dr. Stroeve's Canada 150 Research Chair grant.

Finally, I am incredibly thankful to my family and friends for their support throughout my studies. Most of all, thank you to my fiancé, Greg. Your willingness to watch practice presentations and provide endless encouragement while I finished my studies will always be appreciated. Also, to our dog, Gretel, whose little snores beside me while I was writing brought such joy to this work.

Land Acknowledgement

This research was completed at the University of Manitoba located on original lands of Anishinaabeg, Ininiwak, Anisininewuk, Dakota and Dene peoples, and on the National Homeland of the Red River Métis. The study focuses on the lands of Inuit Nunangat and Kalaallit Nunaat.

We respect the Treaties that were made on these territories, we acknowledge the harms and mistakes of the past, and we dedicate ourselves to move forward in partnership with Indigenous communities in a spirit of Reconciliation and collaboration.

Table of Contents

Abstract ..... *ii*

Acknowledgements ..... *iii*

Land Acknowledgement ..... *iv*

List of Tables ..... *ix*

List of Figures ..... *x*

Chapter 1 Introduction *15*

1.1 Thesis motivation 15

1.2 Thesis objectives 16

1.3 Thesis outline 16

Literature cited 17

Chapter 2 Background *21*

2.1 Arctic precipitation in a changing climate 21

2.1.1 Precipitation observations 21

2.1.1.1 Observed precipitation in the Eastern Canadian Arctic and Greenland 21

2.1.1.2 Challenges in Arctic precipitation observations 22

2.1.2 Arctic precipitation atmospheric reanalyses and climate models 23

2.1.2.1 Historical Arctic precipitation in atmospheric reanalyses 23

2.1.2.2 Projections of Arctic precipitation with climate models 24

2.1.3 Extreme precipitation in the Arctic 25

2.1.4 Important feedbacks 26

2.1.5 Framework for quantifying drivers of change 28

2.2 Thermodynamic controls on extreme precipitation 29

2.2.1 Clausius-Clapeyron relationship 29

2.2.2 Sea ice and oceanic considerations 30

2.2.3 Energy Hypothesis 31

2.3 Dynamic controls on extreme precipitation 32

2.3.1 Atmospheric moisture transport 32

2.3.2 Large-scale circulation patterns 32

2.3.3 Discussion 35

2.4 Response of extreme precipitation and its drivers to a warming climate 35

2.4.1 Projections of thermodynamic and dynamic forcing 35

2.4.2 Impacts on cyclones and ARs 37
2.5 Impacts on Mass Balance 39
2.5.1 Factors contributing to land ice impacts 39
2.5.2 Case studies 41
2.5.3 Climatic factors 43
2.5.4 Discussion 44
2.6 Summary and Conclusion 45
2.6.1 Summary 45
2.6.2 Research Gaps 47
Literature cited 47
Chapter 3 Extreme Precipitation in the Eastern Canadian Arctic and Greenland: An Evaluation of Atmospheric Reanalyses 66
Abstract 66
3.1 Introduction 66
3.2 Materials and Methods 68
3.2.1 Reanalyses 68
3.2.1.1 ERA-5 68
3.2.1.2 MERRA-2 69
3.2.1.3 CFSR 69
3.2.1.4 Observations 69
3.2.2 Methodology 70
3.3 Results 72
3.3.1 Climatological Comparisons 72
3.3.2 Case Study 76
3.4 Discussion and Conclusion 78
Literature cited 79
Chapter 4 Projections and Physical Drivers of Extreme Precipitation in Greenland & Baffin Bay 85
Abstract 86
Plain Language Summary 86
4.1 Introduction 86
4.2 Data and Methods 88
4.2.1 VR-CESM Simulations 88

4.2.2 ERA5 89
4.2.3 Cyclone Tracking 89
4.2.4 AR Tracking 90
4.2.5 Assessment of extreme precipitation 90
4.3 Extreme precipitation events 91
4.3.1 Validation of historical simulations 91
4.3.2 Future changes in extreme precipitation 93
4.4 Drivers of extremes 96
4.4.1 Changes in cyclones and ARs 96
4.4.2 Relation of cyclones and ARs to extreme precipitation 99
4.5 Conclusions 101
Literature cited 102
Chapter 5 Modelling the Impacts of Historical and Future Extreme Precipitation Days on Seasonal Surface Mass Balance in the Eastern Canadian Arctic and Greenland 108
Abstract 108
5.1 Introduction 109
5.2 Data & Methodology 111
5.2.1 Model Simulations 111
5.2.1.1 Regional Atmospheric Climate Model (RACMO) 111
5.2.1.2 Variable-resolution Community Earth System Model (VR-CESM) 111
5.2.2 Methods 112
5.3 Extreme precipitation 114
5.4 SMB Response to Extreme Precipitation 116
5.4.1 Mean SMB Responses 116
5.4.2 Seasonal Context & Change 121
5.4.2.1 Cold Season 121
5.4.2.2 Warm Season 122
5.5 Discussion & Limitations 127
5.5.1 Connection to previous case studies 127
5.5.2 Model albedo differences 127
5.5.3 Limitations 128
5.6 Conclusions 129

Literature cited 131

Chapter 6 Summary and Conclusions..... 138

6.1 Summary of major contributions 138

6.2 Limitations and recommendations for future work 141

6.2.1 Systematic study of extreme precipitation changes in the region with a larger amount of model data..... 142

6.2.2 Analyze potential timeline of changes in extreme precipitation..... 143

6.2.3 Investigate connections between extreme precipitation and large-scale circulation .. 143

6.2.4 Connection of extreme precipitation characteristics to cyclone and AR parameters . 144

6.2.5 Investigate the longevity of impacts of extreme precipitation outside of the day and location/grid cell in which they occur, and how glacier dynamics are affected by these changes..... 144

6.3 Closing comments..... 145

Literature cited 146

Appendix A. Supplementary Material for Chapter 3..... 150

Appendix B. Supplementary Material for Chapter 4..... 155

Appendix C. Supplementary Material for Chapter 5..... 171

List of Tables

Table 3.1. Number of stations (N_s), observations (N_o), and extreme events (N_e) within each subregion. 71

Table 3.2. 2 x 2 contingency table. 72

Table 3.3. Extreme daily accumulation thresholds and the event frequency for each subregion relative to the observational threshold. Extreme thresholds are the mean of the individual thresholds from each station in the region weighted by the station's number of observations. ... 73

Table 3.4. Correlation coefficient between the reanalyses and observations for precipitation amounts in each subregion. Values in the overall column represent the correlations between the reanalyses and observations for all precipitation days with at least 1 mm of accumulation, while the extreme events column only includes days at or above the observed extreme threshold. 74

Table 3.5. HSS for the reanalyses in each subregion. $HSS_{\geq 1mm}$ refers to that of all precipitation days with at least 1 mm of accumulation (Equation 3.2), and ($HSS_{extreme}$) refers to extreme events using (Equation 3.3). 74

Table 5.1. DJFM IQR bootstrapping results for each subregion. The number of events indicates the total number of extreme precipitation days in DJFM in HIST and FUT. Actual interquartile range (IQR) is the IQR of SMB anomalies on extreme precipitation days in the period and Difference indicates the difference in IQR between the two time periods. Bold indicates a statistically significant change in IQR as determined by the bootstrapping methodology outlined in Section 5.2.2. 120

Table 5.2. As in Table 5.1, but for JJAS. 120

Table A.1. Details of each observation station analyzed. 150

Table A.2. Extreme event threshold accumulation, frequency (f_e), and number of days with at least 1 mm of accumulation for each station. Dashed lines separate the subregions. E, M, and C represent ERA-5, MERRA-2, and CFSR, respectively. 151

Table A.3. 95% Confidence interval (CI) for each subregion corresponding to the correlations provided in Table 3.4. Regions whose correlation is not statistically significant ($p \geq 0.05$) are italicized. 152

Table A.4. 3-by-3 cell group used for spatial offsetting analysis. The cell with a star indicates the cell containing the station. 152

Table B.1. Parameters used in the Crawford et al. (2021) Lagrangian cyclone tracking algorithm. 157

List of Figures

Figure 2.1. Mean annual (a) total precipitation and (b) snow fraction for 1980-2020 from ERA5. Blue (red) colours for snow fraction indicate areas where over half of the annual precipitation falls as snow (rain). 21

Figure 2.2. Conceptual model showing how sea ice concentration thermodynamically affects cyclone-associated precipitation in the Arctic in autumn (Sept-Oct) and winter (Dec-Mar). Arrow style shows the sign of correlation between variables, colour indicates season(s). Adapted from Crawford et al. (2022). © American Meteorological Society. Used with permission. 30

Figure 2.3. Sensitivity of extreme precipitation (mean annual highest single day accumulation total) in CMIP5 simulations to (a) thermodynamic forcing (where vertical velocity, ωe, is kept constant using the annual mean of 1950-2100), (b) sensitivity to dynamic contributions (difference between total extreme precipitation sensitivity and thermodynamic sensitivity), and the change in mean (c) vertically-integrated saturation specific humidity and (d) ωe (where negative indicates increased upward motion) during the occurrence of extreme precipitation. Differences are calculated relative to 1950-2005. Retrieved from Pfahl et al. (2017). Reproduced with permission from Springer Nature. 36

Figure 3.1. Map of the study region. Coloured circles show station locations within each subregion. 70

Figure 3.2. Taylor diagrams comparing accumulations for extreme events between products in each subregion. CFSR is not visible in b) due to the correlation falling below 0 and ERA-5 is overlain by MERRA-2 in f). 73

Figure 3.3. Percent of all extreme events in each product occurring in each month for all subregions. 75

Figure 3.4. Mean percent of annual precipitation attributed to extreme events based on a) ERA-5, b) MERRA-2, and c) CFSR. Circles show the relative contribution of extremes to annual precipitation for each station with at least 4 years of data. 76

Figure 3.5. Daily precipitation (≥ 5 mm) for 26-28 August 2011 from ERA-5 (a,d,g), MERRA-2 (b,e,h), and CFSR (c,f,i). The rows show data for 26 (a-c), 27 (d-f), and 28 (g-i) August 2011. Stippling indicates grid cells with daily accumulations above the extreme threshold. Stations are shown with black dots, filled circles, and filled diamonds if no precipitation, non-extreme precipitation, or extreme precipitation were observed, respectively. The color of filled station markers indicates the daily precipitation accumulation. The red square highlights the Kangerlussuaq region. 77

Figure 4.1. Maps showing surface topography from (a) ERA5, (b) VR-CESM, and (c) CESM2. Light contours are shown every 250 m and black dashed lines show the division of the subregions. 91

Figure 4.2. Comparisons of ERA5 to HIST for (a-d) mean annual precipitation, (e-h) extreme precipitation threshold, and (i-l) mean annual extreme precipitation. The third (c, g, k) and fourth (d, h, l) columns show the absolute and fractional differences between the products, respectively.

The relative difference is the fractional difference relative to ERA5 (i.e., (HIST-ERA5)/ERA5). 92

Figure 4.3. Comparisons of the native resolution CESM2-HIST to VR-CESM HIST for (a-d) mean annual precipitation and (e-h) extreme precipitation threshold. The relative difference is the fractional difference relative to CESM2 (i.e., (HIST-CESM2)/CESM2). 93

Figure 4.4. Mean (a-d) annual extreme precipitation and (e-h) percent of annual precipitation from extreme precipitation days in (a,e) HIST (1980-1999), (b,f) FUT (2080-2099) , (c,g) the difference between the two (FUT – HIST), and (d, h) the fractional difference relative to HIST (i.e., (FUT – HIST)/HIST). Only differences that are statistically significant ($p < 0.05$) are shown. 94

Figure 4.5. Daily precipitation distribution for all grid cells in each subregion (a-i, shown in the map) from ERA5 (1980-1999, black), HIST (1980-1999, blue), and FUT (2080-2099, green). Daily precipitation totals counts are binned every 5 mm. Vertical dashed lines indicate the mean extreme precipitation threshold in the subregion from each of ERA5 (black), HIST (blue), and FUT (green). 95

Figure 4.6. Mean total extreme precipitation accumulation in each in ERA5 (1980-1999, black), HIST (1980-1999, blue), and FUT (2080-2099, green) in each subregion (a-i). The map shows the location of each subregion. 96

Figure 4.7. Cyclone track densities from (a) ERA5 (1980-1999), (B) HIST (1980-1999), and (c) FUT (2080-2099). The differences between the future and historical conditions are shown in (c), with fractional differences (relative to HIST) shown in (e). Only differences that are statistically significant ($p < 0.05$) are shown. 97

Figure 4.8. As in Figure 4.7, but for number of AR days in each grid cell. 98

Figure 4.9. Fraction of all extreme precipitation days that are (a-d) cyclone-associated precipitation (CAP), (e-h) AR-associated, and (i-l) associated with both a cyclone and AR. Results are shown for (a,e,i) ERA5 (1980-1999), (b,f,j) HIST (1980-1999), (c,g,k) FUT (2080-2099) runs, and differences (FUT – HIST) are shown in (d,h,l). Only statistically significant differences ($p < 0.05$) are shown in (d,h,l). 100

Figure 5.1. Study domain map showing subregions used for analysis. 112

Figure 5.2. Mean monthly accumulation per grid cell from extreme precipitation in RACMO (blue lines), VR-CESM (orange lines), and ERA5 (black line) for the historical (1980-1998; solid lines) and future (2080-2098; dashed lines) in each subregion. 115

Figure 5.3. Mean monthly rain fraction for extreme precipitation days (solid lines, “EX”) and non-extreme days (dashed lines, “NON-EX”) in each subregion (a-i) from RACMO (blue lines) and VR-CESM (orange lines). The darker colours show the historical averages, and the lighter colours show the future projections. 116

Figure 5.4. Mean seasonal SMB in the region for the (a-d) cold season (DJFM) and (e-h) warm season (JJAS) for the historical period (1980-1998; a,c,e,g), and the difference between historical and future (2080-2098) periods (FUT – HIST; b,d,f,h) in RACMO (a-b, e-f) and VR-CESM (c-d, g-h). The solid purple line denotes the top of the ablation zone for the full simulation period.. 117

Figure 5.5. Average DJFM Daily mean SMB on extreme days vs. non-extreme days for all subregions (a-i). Each point represents one year. RACMO is shown in blue circles and VR-CESM is represented by orange/red squares, with the darker (lighter) colour showing historical (future) means. Dashed black lines show x = 0, y = 0, and x = y. 118

Figure 5.6. As in Figure 5.5, but for JJAS. 119

Figure 5.7. Mean DJFM $SMBex\ frac+$ for HIST (1980-1998; a, c) and projected changes (FUT (2080-2098) - HIST; b, d) from RACMO (a-b) and VR-CESM (c-d). $SMBex\ frac-$ is zero across the domain in both periods, and is therefore not shown. The solid purple line denotes the top of the ablation zone for the full simulation period, with the future ablation zone being shown on the DIFF panels (c-d)..... 122

Figure 5.8. Mean JJAS $SMBex\ frac+$ (a-b, e-f) and $SMBex\ frac-$ (c-d, g-h) for HIST (1980-1998; a-d) and projected changes (FUT (2080-2098) - HIST; e-h) from RACMO (a, c, e, g) and VR-CESM (b, d, f, h). The solid purple line denotes the top of the ablation zone for the full simulation period, with the future ablation zone being shown on the DIFF panels (e-h)..... 123

Figure 5.9. Mean anomalies on positive SMB JJAS extreme precipitation days in the historical period (1980-1998) from RACMO. Anomalies are calculated for the extreme precipitation day relative to ± 15 days surrounding the extreme precipitation day. The solid purple line denotes the top of the ablation zone for the full simulation period. Blue colours in each panel indicate anomalies that act to increase SMB. 124

Figure 5.10. As in Figure 5.9, but for future (2080-2098) positive SMB JJAS extreme precipitation days from RACMO. 125

Figure 5.11. As in Figure 5.9, but for future negative SMB JJAS extreme precipitation days from RACMO. 126

Figure A.1. Taylor diagrams comparing accumulations for extreme events between products in each subregion. The reanalysis accumulations are retrieved from the cell surrounding the station that produces the highest correlation with the station record to account for potential spatial offsets. CFSR is not visible in f) as it is overlain by ERA-5 and MERRA-2..... 153

Figure A.2. Histograms showing the cell with the highest correlation between the reanalyses and observations in each subregion. The cell numbers are as shown in Table A.4. 154

Figure A.3. Taylor diagrams comparing three-day accumulations for extreme events between products in each subregion to account for potential temporal offsets in the reanalyses. CFSR is not visible in c) due to the correlation falling below 0, and f) as it is overlain by MERRA-2. 154

Figure B.1. ARCTIC VR-CESM grid (adapted from Herrington et al., 2022)..... 156

Figure B.2. (a-c) March sea ice extent (years in which each grid cell exceeds 0.15 sea ice concentration of 18-year record), and (d-f) mean annual sea surface temperatures used from forcing CESM CMIP6 runs. Run 101 (f09_g17.CMIP6-SSP5-8.5.101) results are shown in (a,d), 102 (f09_g17.CMIP6-SSP5-8.5.102) in (b,e), and differences are shown in (c,f). 156

Figure B.3. Percent of all extreme events in reanalyses (ERA5, MERRA-2, CFSR) and VR-CESM HIST occurring in each month for all subregions (a-g), as in Figure 3.3 (Figure 3 of Loeb et al. (2022)) 158

Figure B.4. Mean percent of annual precipitation attributed to extreme events based on (a) ERA-5, (b) MERRA-2, (c) CFSR, and (d) VR-CESM HIST, as in Figure 3.4 (Figure 4 of Loeb et al. (2022)). Circles show the relative contribution of extremes to annual precipitation for each station with at least 4 years of data from the Second Generation Adjusted Daily Precipitation Dataset for Canada and Danish Meteorological Institute synoptic stations for Greenland. 158

Figure B.5. As in Figure 4.4, but for the results of the second VR-CESM future run (FUT-102). 159

Figure B.6. As in Figure 4.4, but for the results of the future CESM2 run. 160

Figure B.7. As in Figure 4.5, but including the results of the second VR-CESM future run (FUT-102). 161

Figure B.8. As in Figure 4.6, but including the results of the second VR-CESM future run (FUT-102). 161

Figure B.9. As in Figure 4.7, but for the results of the second VR-CESM future run (FUT-102). 162

Figure B.10. As in Figure 4.8, but for the results of the second VR-CESM future run (FUT-102). 163

Figure B.11. Mean pressure gradient associated with cyclones from (a) ERA5 (1980-1999), (B) HIST (1980-1999), and (c) FUT (2080-2099). The differences between the future and historical conditions are shown in (c), with fractional differences (relative to HIST) shown in (e). Only differences that are statistically significant ($p < 0.05$) are shown. 164

Figure B.12. As in Figure 4.9, but for winter (JFM). 165

Figure B.13. As in Figure 4.9, but for summer (JAS). 166

Figure B.14. As in Figure 4.9 (full year), but using a 600 km cyclone radius to determine cyclone-associated precipitation (CAP). 167

Figure B.15. As in Figure 4.9 (full year), but for the results of the second VR-CESM future run (FUT-102). 168

Figure B.16. As in Figure B.12 (JFM), but for the results of the second VR-CESM future run (FUT-102). 169

Figure B.17. As in Figure B.13 (JAS), but for the results of the second VR-CESM future run (FUT-102). 170

Figure C.1. As in Figure 5.2, but using the regional volume-based extreme precipitation definition, showing the mean monthly volume of extreme precipitation in each subregion. 171

Figure C.2. Mean seasonal SMB in the region for the (a-b) cold season (DJFM) and (c-d) warm season (JJAS) for the future period (2080-2098; SSP5-8.5) from RACMO (a, c) and VR-CESM (b,d). 171

Figure C.3. Difference in mean seasonal SMB between VR-CESM and RACMO for the (a-b) cold season (DJFM) and (c-d) warm season (JJAS) in the (a,c) historical period (1980-1998) and (b, d) future period (2080-2098; SSP5-8.5). The green (purple) colours indicate that VR-CESM (RACMO) has a higher seasonal SMB. 172

Figure C.4. Total number of extreme precipitation days occurring in each grid cell with positive SMB (a-h) or negative SMB (i-l) in the cold season (a-d) and warm season (e-l) in the historical (1980-1998; a,c,e,g,I,k) and future (2080-2098; b,d,f,h,j,l) periods. Counts from RACMO are shown in the first two columns (a-b, e-f, i-j) and VR-CESM is shown in the final two columns (c-d, g-h, k-l). 173

Figure C.5. Mean DJFM $SMBex\ frac+$ for FUT (2080-2098; SSP5-8.5) from (a) RACMO and (b) VR-CESM. The solid purple line denotes the top of the ablation zone for the full simulation period. 174

Figure C.6. Mean JJAS (a-b) $SMBex\ frac+$ and (c-d) $SMBex\ frac-$ for FUT (2080-2098; SSP5-8.5) from (a,c) RACMO and (b,d) VR-CESM. The solid purple line denotes the top of the ablation zone for the full simulation period. 174

Figure C.7. Mean extreme precipitation (a-d) accumulations and (e-h) rain fraction in HIST (1980-1998; a,c,e,g) and FUT (2080-2098; b,d,f,h) for $SMBex+$ (a-b, e-f) and $SMBex-$ (c-d, g-h) from RACMO. The solid purple line denotes the top of the ablation zone for the full simulation period. 175

Figure C.8. As in Figure C.7, but from VR-CESM. 176

Figure C.9. Mean anomalies on positive SMB JJAS extreme precipitation days in the historical period (1980-1998) from VR-CESM. Anomalies are calculated for the extreme precipitation day relative to $\pm$15 days. (Figure 5.9, but for VR-CESM) 177

Figure C.10. As in Figure C.9, but for future positive SMB JJAS extreme precipitation days. (As in Figure 5.10, but for VR-CESM) 178

Figure C.11. As in Figure C.9, but for historical negative SMB JJAS extreme precipitation days from RACMO. 179

Figure C.12. As in Figure C.9, but for historical negative SMB JJAS extreme precipitation days from VR-CESM. 180

Figure C.13. As in Figure C.9, but for future positive SMB JJAS extreme precipitation days. (As in Figure 5.11, but for VR-CESM.) 181

Chapter 1 Introduction

1.1 Thesis motivation

The Arctic climate has undergone major changes in recent decades due to anthropogenic climate change (e.g., Coulombe & Göbel, 2021; Serreze & Barry, 2011; Stjern et al., 2019). Temperatures in the Arctic are rising at a rate of up to four times faster than the global average (Ballinger et al., 2024; Rantanen et al., 2022), leading to drastic changes to the landscape and climate system (e.g., Bengtsson et al., 2011; Rawlins et al., 2010; Serreze & Barry, 2011; Stroeve et al., 2025; Stroeve & Notz, 2018). As temperatures have increased, sea ice concentrations have fallen dramatically (Stroeve et al., 2007; Stroeve & Notz, 2018), driving further warming due to the ice-albedo feedback (Curry et al., 1995; Serreze et al., 2009). This has led to major hydrological changes and an intensification of the Arctic water cycle (e.g., Bengtsson et al., 2011; Rawlins et al., 2010). The general increase in moisture brings higher precipitation accumulations in much of the Arctic but also causes a shift in the interannual variability of precipitation, leading to an increased likelihood of high intensity precipitation events (Pendergrass et al., 2017).

Precipitation is the main input to the surface mass balance (SMB) of land ice. The SMB describes the balance of surface accumulation and mass loss including processes such as accumulation from precipitation and deposition, melt, runoff, and refreezing of liquid water, but not including dynamic mass loss due to calving (Cogley et al., 2011; Dietrich et al., 2024). SMB changes have been studied in the Arctic (e.g., Fettweis et al., 2017; Lenaerts et al., 2013; Noël et al., 2018; Otosaka et al., 2023), but little work has illustrated the impacts of extreme precipitation. Precipitation increases ice mass if it falls as snow or falls as rain but then freezes. However, as precipitation phase and intensity changes, its impacts can vary drastically and become either positive or negative to the mass and stability of the ice. Case studies have illustrated varied impacts associated with past extreme precipitation events. For example, late summer rainfall events have been associated with extensive mass loss and melt (e.g., Box et al., 2022; Doyle et al., 2015). Conversely, intense snowfall can increase albedo and shield the ice below from melt for several days, reducing seasonal mass loss (e.g., Bailey & Hubbard, 2025; Oerlemans & Klok, 2004). The projected increase in precipitation variability and intensity, and shift towards rainfall, brings uncertainty into the role that extreme precipitation may play in the seasonal SMB in a warming climate.

These land ice changes have implications for global sea level rise (e.g., Bamber et al., 2018; Beckmann & Winkelmann, 2022; Edwards et al., 2021; Jacob et al., 2012). As extreme precipitation changes, it has the potential to influence the rate at which glacier loss contributes to increases in sea level. While SMB anomalies related to extreme precipitation do not alter the total potential sea level rise from the loss of a glacier or ice cap, it may accelerate or decelerate said mass loss. If there are more intense rainfall events, such as the case presented in Doyle et al. (2015), extreme precipitation may accelerate the contribution to sea level rise. Therefore, it is important to understand the relative importance of these events to climatological-scale SMB, which has not been previously quantified.

Changes in extreme precipitation events also impact local Indigenous communities through hazards such as flooding and the degradation of permafrost (Rinke et al., 2012), threatening

communities' access to food sources and infrastructure (Ford, 2009; Ford et al., 2010; Fox et al., 2023). Both increased precipitation rates and increased melt from nearby land ice can cause flooding in Arctic communities (Ford et al., 2010). Further, increased storminess can impede travel and therefore prevent communities from accessing services for days at a time (Fox et al., 2023). Developing a better understanding of the changes in extreme precipitation, and the implications for land ice, can help communities increase preparedness and awareness of potential impacts.

The Eastern Canadian Arctic Archipelago and Greenland are of particular interest in this concern because they contain approximately 11% of global land ice mass (Bamber et al., 2018). The region's land ice has been losing mass in recent decades as warming has increased, leading to longer and more intense melt seasons (e.g., Fettweis et al., 2017; Hugonnet et al., 2021; Noël et al., 2018). However, little work has been done to quantify extreme precipitation changes in the area, and how these extreme events influence the large quantity of land ice in the region.

1.2 Thesis objectives

This thesis aims to investigate changes in extreme precipitation events in the eastern Canadian Arctic and Greenland and how they impact the SMB of land ice in the study area using climate models. To achieve this, there are three specific objectives:

1. Investigate how well current models and atmospheric reanalyses capture extreme daily precipitation events in the region.
2. Examine the changes in extreme precipitation days in the study region by 2100 under a high emissions scenario and explore how driving processes, such as extratropical cyclones and atmospheric rivers, factor in to said changes.
3. Quantify the impacts and relative importance of extreme precipitation days to the seasonal SMB of land ice in the region in historical and future simulations.

1.3 Thesis outline

This thesis contains six chapters. Chapter 2 provides a comprehensive review of extreme precipitation in the Arctic, thermodynamic and dynamic drivers influencing precipitation changes, and the processes by which precipitation impacts land ice. Chapters 3 and 4 are composed of published peer-reviewed research papers, and Chapter 5 contains a manuscript currently undergoing peer-review, outlined below. A summary of the findings and their relevance is provided in Chapter 6.

Chapter 3 addresses the first research objective by comparing three commonly used atmospheric reanalyses to surface station observations of extreme precipitation ($\geq 95^{th}$ percentile of daily accumulations where at least 1 mm occurs) in the eastern Canadian Arctic and Greenland. By exploring a variety of metrics, the ability of reanalyses to reproduce observed extreme precipitation events is explored. This work was published in *Frontiers in Environmental Science*. Supplementary information for this paper is provided in Appendix A.

Loeb, N. A., Crawford, A., Stroeve, J. C., & Hanesiak, J. (2022). Extreme Precipitation in the Eastern Canadian Arctic and Greenland: An Evaluation of Atmospheric Reanalyses. *Frontiers in Environmental Science, 10*. DOI: 10.3389/fenvs.2022.866929

In Chapter 4, extreme precipitation days in historical and future simulations of the Variable-Resolution Community Earth System Model (VR-CESM) are explored to meet the second research objective. Changes in amount of extreme precipitation, seasonality, and importance of extremes to annual precipitation are investigated in the future simulations. Extratropical cyclone tracking and atmospheric river detection algorithms are employed to examine changes in the processes driving extreme precipitation in future projections. This work was published in the *Journal of Geophysical Research: Atmospheres.* Supplementary information for this paper is provided in Appendix B.

Loeb, N. A., Crawford, A., Herrington, A., McCrystall, M., Stroeve, J., & Hanesiak, J. (2024). Projections and Physical Drivers of Extreme Precipitation in Greenland & Baffin Bay. *Journal of Geophysical Research: Atmospheres, 129*(22), e2024JD041375. DOI: 10.1029/2024JD041375

Finally, the manuscript in Chapter 5 meets the third objective by exploring SMB, and its components, on extreme precipitation days in VR-CESM and the Regional Atmospheric Climate Model (RACMO). In this study, the relative importance of extreme precipitation days to seasonal SMB is explored and compared to non-extreme days for the cold (DJFM) and warm (JJAS) seasons. Through exploration of anomalies on extreme precipitation days associated with negative SMB and positive SMB, the changes in potential impacts in the future warmer climate are illustrated. This work has been submitted to *The Cryosphere* and is currently undergoing peer review. Supplementary information for this paper is provided in Appendix C.

Loeb, N.A., Crawford, A., Noël, B. P. Y., & Stroeve, J. (in review). Modelling the Impacts of Extreme Precipitation Events on Surface Mass Balance in the Eastern Canadian Arctic and Greenland. *Submitted to The Cryosphere* (egusphere-2025-995).

Literature cited

Bailey, H., & Hubbard, A. (2025). Snow Mass Recharge of the Greenland Ice Sheet Fueled by Intense Atmospheric River. *Geophysical Research Letters*, *52*(5), e2024GL110121. https://doi.org/10.1029/2024GL110121

Ballinger, T. J., Crawford, A., Serreze, M. C., Bigalke, S., Walsh, J. E., Brettschneider, B., et al. (2024). *Surface Air Temperature* (Arctic Report Card: Update for 2024). National Oceanic and Atmospheric Administration. Retrieved from https://arctic.noaa.gov/report-card/report-card-2024/surface-air-temperature-2024/

Bamber, J. L., Westaway, R. M., Marzeion, B., & Wouters, B. (2018). The land ice contribution to sea level during the satellite era. *Environmental Research Letters*, *13*(6), 063008. https://doi.org/10.1088/1748-9326/aac2f0

Beckmann, J., & Winkelmann, R. (2022). Effects of extreme melt events on ice flow and sea level rise of the Greenland Ice Sheet. *The Cryosphere Discussions*, 1–23. https://doi.org/10.5194/tc-2022-145

Bengtsson, L., Hodges, K. I., Koumoutsaris, S., Zahn, M., & Keenlyside, N. (2011). The changing atmospheric water cycle in Polar Regions in a warmer climate. *Tellus A: Dynamic Meteorology and Oceanography*, *63*(5), 907–920. https://doi.org/10.1111/j.1600-0870.2011.00534.x

Box, J. E., Wehrlé, A., van As, D., Fausto, R. S., Kjeldsen, K. K., Dachauer, A., et al. (2022). Greenland Ice Sheet Rainfall, Heat and Albedo Feedback Impacts From the Mid-August 2021 Atmospheric River. *Geophysical Research Letters*, *49*(11), e2021GL097356. https://doi.org/10.1029/2021GL097356

Cogley, J. G., Hock, R., Rasmussen, L. A., Arendt, A. A., Bauder, A., Braithwaite, R. J., et al. (2011). *Glossary of Glacier Mass Balance and Related Terms* (IHP-VII Technical Documents in Hydrology No. No. 86, IACS Contribution No. 2) (p. 124). Paris, France: UNESCO-IHP. Retrieved from https://wgms.ch/downloads/Cogley_etal_2011.pdf

Coulombe, P. G., & Göbel, M. (2021). Arctic Amplification of Anthropogenic Forcing: A Vector Autoregressive Analysis. *Journal of Climate*, *34*(13), 5523–5541. https://doi.org/10.1175/JCLI-D-20-0324.1

Curry, J. A., Schramm, J. L., & Ebert, E. E. (1995). Sea Ice-Albedo Climate Feedback Mechanism. *Journal of Climate*, *8*(2), 240–247. https://doi.org/10.1175/1520-0442(1995)008<0240:SIACFM>2.0.CO;2

Dietrich, L. J., Steen-Larsen, H. C., Wahl, S., Faber, A.-K., & Fettweis, X. (2024). On the importance of the humidity flux for the surface mass balance in the accumulation zone of the Greenland Ice Sheet. *The Cryosphere*, *18*(1), 289–305. https://doi.org/10.5194/tc-18-289-2024

Doyle, S. H., Hubbard, A., van de Wal, R. S. W., Box, J. E., van As, D., Scharrer, K., et al. (2015). Amplified melt and flow of the Greenland ice sheet driven by late-summer cyclonic rainfall. *Nature Geoscience*, *8*(8), 647–653. https://doi.org/10.1038/ngeo2482

Edwards, T. L., Nowicki, S., Marzeion, B., Hock, R., Goelzer, H., Seroussi, H., et al. (2021). Projected land ice contributions to twenty-first-century sea level rise. *Nature*, *593*(7857), 74–82. https://doi.org/10.1038/s41586-021-03302-y

Fettweis, X., Box, J. E., Agosta, C., Amory, C., Kittel, C., Lang, C., et al. (2017). Reconstructions of the 1900–2015 Greenland ice sheet surface mass balance using the regional climate MAR model. *The Cryosphere*, *11*(2), 1015–1033. https://doi.org/10.5194/tc-11-1015-2017

Ford, J. D. (2009). Vulnerability of Inuit food systems to food insecurity as a consequence of climate change: a case study from Igloolik, Nunavut. *Regional Environmental Change*, *9*(2), 83–100. https://doi.org/10.1007/s10113-008-0060-x

Ford, J. D., Bell, T., & St-Hilaire-Gravel, D. (2010). Vulnerability of Community Infrastructure to Climate Change in Nunavut: A Case Study From Arctic Bay. In G. K. Hovelsrud & B. Smit (Eds.), *Community Adaptation and Vulnerability in Arctic Regions* (pp. 107–130). Dordrecht: Springer Netherlands. https://doi.org/10.1007/978-90-481-9174-1_5

Fox, S., Crawford, A., McCrystall, M., Stroeve, J., Lukovich, J., Loeb, N., et al. (2023). Extreme Arctic Weather and Community Impacts in Nunavut: A Case Study of One Winter's Storms

and Lessons for Local Climate Change Preparedness. *Weather, Climate, and Society*, *15*(4), 881–892. https://doi.org/10.1175/WCAS-D-23-0006.1

Hugonnet, R., McNabb, R., Berthier, E., Menounos, B., Nuth, C., Girod, L., et al. (2021). Accelerated global glacier mass loss in the early twenty-first century. *Nature*, *592*(7856), 726–731. https://doi.org/10.1038/s41586-021-03436-z

Jacob, T., Wahr, J., Pfeffer, W. T., & Swenson, S. (2012). Recent contributions of glaciers and ice caps to sea level rise. *Nature*, *482*(7386), 514–518. https://doi.org/10.1038/nature10847

Lenaerts, J. T. M., Angelen, J. H. van, Broeke, M. R. van den, Gardner, A. S., Wouters, B., & Meijgaard, E. van. (2013). Irreversible mass loss of Canadian Arctic Archipelago glaciers. *Geophysical Research Letters*, *40*(5), 870–874. https://doi.org/10.1002/grl.50214

Noël, B., van de Berg, W. J., van Wessem, J. M., van Meijgaard, E., van As, D., Lenaerts, J. T. M., et al. (2018). Modelling the climate and surface mass balance of polar ice sheets using RACMO2 – Part 1: Greenland (1958–2016). *The Cryosphere*, *12*(3), 811–831. https://doi.org/10.5194/tc-12-811-2018

Oerlemans, J., & Klok, E. J. L. (2004). Effect of summer snowfall on glacier mass balance. *Annals of Glaciology*, *38*, 97–100. https://doi.org/10.3189/172756404781815158

Otosaka, I. N., Shepherd, A., Ivins, E. R., Schlegel, N.-J., Amory, C., van den Broeke, M. R., et al. (2023). Mass balance of the Greenland and Antarctic ice sheets from 1992 to 2020. *Earth System Science Data*, *15*(4), 1597–1616. https://doi.org/10.5194/essd-15-1597-2023

Pendergrass, A. G., Knutti, R., Lehner, F., Deser, C., & Sanderson, B. M. (2017). Precipitation variability increases in a warmer climate. *Scientific Reports*, *7*(1), 17966. https://doi.org/10.1038/s41598-017-17966-y

Rantanen, M., Karpechko, A. Y., Lipponen, A., Nordling, K., Hyvärinen, O., Ruosteenoja, K., et al. (2022). The Arctic has warmed nearly four times faster than the globe since 1979. *Communications Earth & Environment*, *3*(1), 1–10. https://doi.org/10.1038/s43247-022-00498-3

Rawlins, M. A., Steele, M., Holland, M. M., Adam, J. C., Cherry, J. E., Francis, J. A., et al. (2010). Analysis of the Arctic System for Freshwater Cycle Intensification: Observations and Expectations. *Journal of Climate*, *23*(21), 5715–5737. https://doi.org/10.1175/2010JCLI3421.1

Rinke, A., Matthes, H., Christensen, J. H., Kuhry, P., Romanovsky, V. E., & Dethloff, K. (2012). Arctic RCM simulations of temperature and precipitation derived indices relevant to future frozen ground conditions. *Global and Planetary Change*, *80–81*, 136–148. https://doi.org/10.1016/j.gloplacha.2011.10.011

Serreze, M. C., & Barry, R. G. (2011). Processes and impacts of Arctic amplification: A research synthesis. *Global and Planetary Change*, *77*(1–2), 85–96. https://doi.org/10.1016/j.gloplacha.2011.03.004

Serreze, M. C., Barrett, A. P., Stroeve, J. C., Kindig, D. N., & Holland, M. M. (2009). The emergence of surface-based Arctic amplification. *The Cryosphere*, *3*(1), 11–19. https://doi.org/10.5194/tc-3-11-2009

Stjern, C. W., Lund, M. T., Samset, B. H., Myhre, G., Forster, P. M., Andrews, T., et al. (2019). Arctic Amplification Response to Individual Climate Drivers. *Journal of Geophysical Research: Atmospheres*, *124*(13), 6698–6717. https://doi.org/10.1029/2018JD029726

Stroeve, J., & Notz, D. (2018). Changing state of Arctic sea ice across all seasons. *Environmental Research Letters*, *13*(10), 103001. https://doi.org/10.1088/1748-9326/aade56

Stroeve, J., Holland, M. M., Meier, W., Scambos, T., & Serreze, M. C. (2007). Arctic sea ice decline: Faster than forecast. *Geophysical Research Letters*, *34*(9). https://doi.org/10.1029/2007GL029703

Stroeve, J., Notz, D., Dawson, J., Schuur, E. A. G., Dahl-Jensen, D., & Giesse, C. (2025). Disappearing landscapes: The Arctic at +2.7°C global warming. *Science*, *387*(6734), 616–621. https://doi.org/10.1126/science.ads1549

Chapter 2 Background

The Arctic is a region experiencing faster warming than the global mean, driving an amplification of the hydrological cycle (Bengtsson et al., 2011; Rawlins et al., 2010). Observations and climate model projections have shown increasing precipitation across the Arctic (e.g., Bintanja & Selten, 2014; McCrystall et al., 2021; Yu & Zhong, 2021). In addition to the increase in precipitation, observations and modelling studies have shown increased variability because of climate change, notably favouring more intense precipitation rates (e.g., Bintanja et al., 2020; Pendergrass et al., 2017; Scoccimarro & Gualdi, 2020; Walsh et al., 2020). As temperatures have increased, sea ice concentrations have fallen dramatically (e.g., Stroeve et al., 2007; Stroeve & Notz, 2018), and glaciers and the Greenland Ice Sheet (GrIS) have begun to lose ice mass (e.g., Box, Hubbard, et al., 2022; Hugonnet et al., 2021; Noël et al., 2018), leading to drastic changes to the climate system.

2.1 Arctic precipitation in a changing climate

2.1.1 Precipitation observations

2.1.1.1 Observed precipitation in the Eastern Canadian Arctic and Greenland

Based on 1980-2020 averages from the fifth-generation reanalysis from the European Centre for Medium-range Weather Forecasts (ERA5), Southeastern Greenland tends to see the most annual precipitation in the study region, most of which falls as snow (Figure 2.1). Other regions, such as Ellesmere Island and inland on the Greenland Ice Sheet, see very little precipitation. Most precipitation falls close to the shore because steep topography promotes orographic precipitation processes (Jonassen et al., 2020; Schuenemann & Cassano, 2010). High altitude regions of the GrIS and ice caps of Ellesmere Island receive virtually all of their precipitation in the form of snowfall (Figure 2.1b). However, rainfall is becoming more common as temperatures rise; rainfall was observed at the GrIS Summit for the first time in August 2021 (Box et al., 2022), making it unlikely that any areas in the study region do not receive any rainfall.

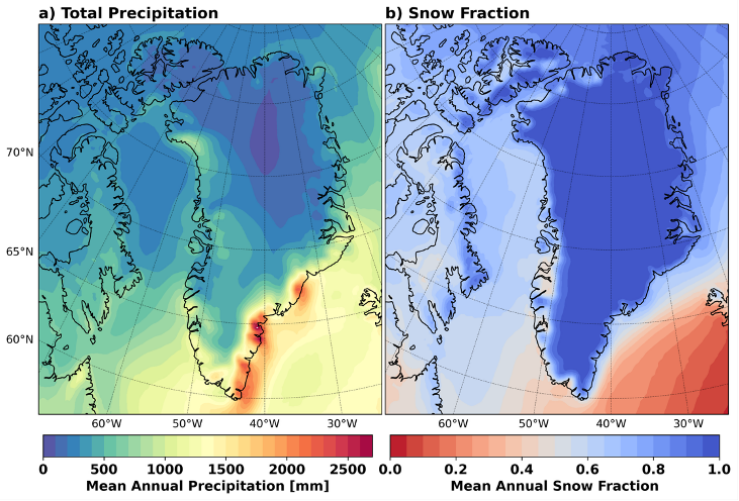

Figure 2.1. Mean annual (a) total precipitation and (b) snow fraction for 1980-2020 from ERA5. Blue (red) colours for snow fraction indicate areas where over half of the annual precipitation falls as snow (rain).

Extratropical cyclones often become occluded and quasi-stationary over Baffin Bay, bringing precipitation to the eastern shores of Baffin Island for an extended period (Intihar & Stewart, 2005). Cyclonic activity in the Baffin Bay region typically peaks in autumn or early winter (Gascon et al., 2010; Zahn et al., 2018). Due to the reliance on cyclones, the annual precipitation totals in the eastern Canadian Arctic can vary dramatically depending on the number and strength of systems entering the region.

Southeastern Greenland is also a region of substantial cyclonic activity due to the north-Atlantic storm track, which commonly brings systems into the area. Precipitation is often concentrated along the coast due to the steep topography, yielding high precipitation rates and accumulations (Schuenemann & Cassano, 2010; Serreze et al., 1997). Peak cyclonic activity typically occurs in the winter on the southeast coast of Greenland (Schuenemann & Cassano, 2010).

Robust Arctic-wide annual precipitation increases have not been consistently observed yet (e.g., Boisvert et al., 2018; Gascon et al., 2010), likely due to the relatively short observation period and large interannual variability in precipitation. However, observational studies have suggested that local evaporation, and therefore tropospheric moisture, is increasing (e.g., Boisvert & Stroeve, 2015; Kopec et al., 2016; Serreze et al., 2012) and more precipitation is falling as rain or freezing rain (e.g., Boisvert et al., 2018; Hanesiak & Wang, 2005).

2.1.1.2 Challenges in Arctic precipitation observations

Precipitation observations, particularly in regions where solid precipitation occurs, are notoriously difficult (e.g., Rasmussen et al., 2012; Yang et al., 1995). In the Arctic, challenges exist related both to the observation techniques themselves, as well as the sparse observational network. Issues such as wind undercatch, wetting loss, and the remoteness of observation sites pose difficulty in obtaining high quality measurements.

Wind undercatch refers to when precipitation particles, generally snow, are blown around or out of a precipitation gauge leading to underestimation of precipitation rates and accumulations (e.g., Goodison et al., 1998; Wagner et al., 2021). The wind field is altered by the presence of the precipitation gauge, leading to the development of turbulence around the collector which can deflect snow particles and cause a reduction in the amount of precipitation measured (Goodison et al., 1998; Groisman & Legates, 1994; Sevruk & Klemm, 1989). Precipitation accumulations can be underestimated by up to 50% due to wind undercatch alone (Rasmussen et al., 2012), although blowing snow may also falsely increase measurements (Goodison et al., 1998; Yang et al., 2000).

Depending on the sampling period of measurement instrumentation, it is possible that some captured precipitation is lost via evaporation, referred to as wetting loss (e.g., Collier, 2000; Groisman & Legates, 1994). If long sampling periods are used, wetting losses can reduce precipitation observations by up to approximately 20% (Metcalfe & Goodison, 1993).

Finally, the sparse observational networks in the Arctic pose a substantial challenge in understanding Arctic precipitation patterns. Much of the Arctic is very remote, meaning that deploying and maintaining ground-based instrumentation for extended periods is difficult or impossible. Even in more populated regions, observational networks are often sparse and subject

to budget cuts, such as in Canada where the number of active observation sites has been declining since the 1990s (Mekis et al., 2018).

To avoid some of these challenges, satellite-based observations of precipitation are commonly used in the Arctic. These observations can help to fill in gaps in surface observational networks. Also, these measurements are not subject to many of the common biases of surface observations, like wetting losses and wind undercatch. However, satellite observations are subject to a variety of other limitations, such as the high cost of satellite instrumentation and lack of ground truth to verify measurements (Levizzani et al., 2011; Liu & Curry, 1997). For example, space-borne measurements often cannot resolve snowfall from shallow cloud layers, causing a negative bias in overall precipitation estimations (Levizzani et al., 2011; Norin et al., 2015; Wood, 2011). Algorithms developed must make assumptions about ice cloud structure, which is still not sufficiently understood due to the lack of microphysical observations, potentially leading to inaccurate retrievals (Levizzani et al., 2011; Liu & Curry, 1997).

Gridded interpolated observation-based products also exist to try to fill in gaps and blend available observations. For example, the Global Precipitation Climatology Product (GPCP) from the World Climate Research Program's Global Energy and Water Cycle Experiment (Adler et al., 2003, 2018) is a popular dataset. Observations from several satellite-based sensors are input and combined with surface station gauge data from the National Oceanic and Atmospheric Administration's Global Historical Climate Network and Climate Assessment and Monitoring System, then complex data merging and statistical interpolation is performed to yield a continuous gridded dataset (Adler et al., 2003). While this can help provide an estimation of precipitation patterns, there are additional uncertainties using interpolation techniques in data sparse areas like the Arctic (Rapaić et al., 2015). Additionally, GPCP is very coarse (2.5° x 2.5° spatial resolution), meaning it cannot give insight into regional- or local-scale precipitation.

2.1.2 Arctic precipitation atmospheric reanalyses and climate models

2.1.2.1 Historical Arctic precipitation in atmospheric reanalyses

Because of the difficulty in obtaining long-term, reliable Arctic precipitation observations, atmospheric retrospective analyses, or reanalyses, are used commonly in studies of Arctic precipitation. Atmospheric reanalyses blend available observations with output from numerical weather prediction models. Reanalyses provide a gridded view of historical climate produced by atmospheric models run over many decades while incorporating millions of observations at regular intervals to make sure that the model remains close to the observed conditions (Riddaway, 2014). Generally, variational analysis techniques are used for data assimilation in reanalyses (A. P. Barrett et al., 2020). Variational analysis means that the analysis is produced by minimizing the difference between the forecast from earlier observations and observations at analysis time (Talagrand, 2010). These products are designed with the goal of providing a more homogenous record of atmospheric variables (Riddaway, 2014).

Many comparisons of reanalyses to Arctic climate variables have been performed, and it has been found that agreement with observations is generally lower for precipitation than other variables, such as temperature, since fewer precipitation observations are assimilated leading to more dependence on model setup (e.g., Avila-Diaz et al., 2021; Diaconescu et al., 2018; Lindsay

et al., 2014; Rapaić et al., 2015). Several modern reanalyses have been shown to agree well with annual and seasonal precipitation patterns in the Arctic (e.g., A. P. Barrett et al., 2020; Lindsay et al., 2014). However, there is more disagreement with observations when looking at short-term (e.g., daily) precipitation accumulations and small-scale spatial variability (e.g., A. P. Barrett et al., 2020). Several studies have also noted that reanalyses tend to produce higher accumulations than observed in the Arctic, with more precipitation falling as rain rather than snow (e.g., A. P. Barrett et al., 2020; Boisvert et al., 2018; Edel et al., 2020; Lindsay et al., 2014; Rapaić et al., 2015). While these limitations are important to bear in mind, reanalyses are still considered one of the best tools for verifying historical precipitation statistics from climate models.

2.1.2.2 Projections of Arctic precipitation with climate models

A climate model is a mathematical representation of the physical climate system, often made up of component models representing portions of the system, such as the atmosphere, land surface, and ocean, that may be partially or fully coupled (i.e., interactive) with each other during a simulation (Gettelman & Rood, 2016). These models can be used to produce long-term simulations of the climate that are temporally and spatially continuous. Precipitation is often considered one of the variables with the highest uncertainty in climate modeling as microphysical precipitation processes are often poorly represented (e.g., Bochow et al., 2024; Lopez, 2007). Precipitation relies on complex, small-scale processes that are difficult to represent accurately in models. For example, precipitation patterns in regions with complex terrain depend heavily on orographic lift, which can only be captured in models if the landscape is adequately captured. Additionally, even large-scale circulation changes may be poorly constrained, such as near Greenland in simulations from the fifth phase of the Coupled Model Intercomparison Project (CMIP5) (Hanna et al., 2018).

Typically, models with a higher spatial resolution provide more accurate representations of precipitation, particularly for high-intensity events (e.g., Cai et al. 2018; Diro and Sushama 2019). Methods of downscaling coarse-resolution climate models have been developed using statistical and dynamic methods. Statistical downscaling involves applying a statistical model to interpolate values within grid cells and may use information such as topography within the grid cell to increase accuracy (e.g., Noël et al. 2016). Dynamical downscaling involves using the coarse model results as forcing for a higher-resolution regional climate model, meaning that the downscaling is physically based rather than based on statistics (e.g., Cai et al. 2018; Noël et al. 2020). Both statistical and dynamical downscaling methods have improved agreement between modelled precipitation and observations (e.g., van Kampenhout et al. 2019; Cai et al. 2018).

Climate projections have shown major increases in precipitation totals and variability across the entire Arctic (e.g., Bintanja et al., 2020; Bintanja & Selten, 2014; Kolbe, Bintanja, et al., 2023; Pendergrass et al., 2017). Following the Clausius-Clapeyron equation, warmer air can hold approximately 6-7% more water vapour per 1°C warming (Bengtsson et al., 2011). This translates to an increase in precipitation of 1-3% per degree of warming globally, but the increase is much larger in the Arctic at an increase of approximately 4.5% per degree (Bintanja & Selten, 2014). Because of this, it is expected that the Arctic climate will become much wetter as it warms (e.g., Serreze et al. 2012; Boisvert and Stroeve 2015, McCrystall et al. 2021).

Results from CMIP6 show an even higher sensitivity of Arctic precipitation to warming than previous projections, with the largest increases occurring in summer and autumn (Kolbe, Bintanja,

et al., 2023; McCrystall et al., 2021). Bochow et al. (2024) found that annual precipitation in Greenland rose by 6.09% per 1°C warming in CMIP6 simulations following SSP5-8.5, aligning more closely with the Clausius-Clapeyron relationship. Along with increased precipitation totals, much of the Arctic is expected to see a shift towards precipitation falling in the form of rain rather than snow. By 2100, rain is expected to become the dominant form of precipitation across much of the Arctic due to the strong atmospheric warming (Bintanja & Andry, 2017; Thompson-Munson et al., 2025). McCrystall et al. (2021) found a statistically significant decrease in autumn snowfall in the eastern Canadian Arctic associated with an increase in rainfall when comparing the end of the 21st century to the beginning in CMIP6 simulations.

2.1.3 Extreme precipitation in the Arctic

A variety of definitions have been used to classify extreme precipitation globally and in the Arctic. Pendergrass (2018) explored several commonly used extreme daily precipitation thresholds, illustrating how the selected threshold may account for a very different portion of annual precipitation depending on the precipitation distribution at your location of interest. In this study, extreme precipitation is defined as daily accumulations at or above the 95th percentile of wet days (≥ 1 mm), one of the definitions outlined by Pendergrass (2018). This definition was selected as it is a moderate definition that results in appropriate sample sizes even in areas with low data availability and removes the spurious frequent drizzle in many parts of the Arctic in gridded datasets (e.g., A. P. Barrett et al., 2020). This definition has been used in several Arctic precipitation studies (e.g., Diaconescu et al., 2018; J. Liu et al., 2021) and is one of the 27 core climate extreme indices defined by the Expert Team on Climate Change Detection and Indices (Peterson et al., 2001; WCRP, 2021). Other common definitions include the 95th percentile of all daily precipitation (e.g., Serreze et al., 2022; Yu & Zhong, 2021), the 99th percentile (Pfahl & Wernli, 2012; e.g., Serreze et al., 2015, 2022; de Vries, 2021), and the highest annual daily precipitation rate (e.g., Pfahl et al., 2017).

Extreme precipitation has been shown to exhibit more dramatic changes in a warming climate than mean precipitation rates (e.g., Fischer & Knutti, 2016; Myhre et al., 2019; Pendergrass et al., 2017). These events can have substantial impacts on other aspects of the climate system, such as sea ice (e.g., Dou et al., 2019) and glaciers (e.g., Doyle et al., 2015), as well as local communities (e.g., Ford et al., 2010). To accurately predict these changes in precipitation extremes, it is essential to understand the processes causing them.

Historically, extratropical cyclones (hereafter referred to as “cyclones” or “storms”) drive the majority of precipitation in the Arctic (e.g., Bintanja & Selten, 2014; Chen et al., 1997; Schuenemann et al., 2009). A cyclone is a synoptic-scale low-pressure system in which air converges towards the center, driving upward motion and precipitation (Catto, 2016). Cyclones generally have fronts extending away from the low-pressure center that trigger precipitation at a broader scale. These systems are transient eddies in the background circulation that transport energy and moisture as they propagate (Seager et al., 2010). The warm conveyor belt (WCB) of cyclones is often associated with heavy cyclone-associated precipitation. The WCB is a region of warm, moist air that rises within a cyclone, typically moving poleward and ascending to the jet stream level above the warm front (Browning & Pardoe, 1973; Heitmann et al., 2024; Wernli & Davies, 1997). Air parcels in the WCB typically originate in the warm sector of the cyclone and

rise from the near-surface to jet stream level (Wernli & Davies, 1997). Intense latent heat release during ascent can drive intense precipitation rates within the WCB (Pfahl et al., 2014) and intensify cyclones (Binder et al., 2016).

Cyclones account for upwards of 75% of total precipitation in Arctic regions (Hawcroft et al., 2012). Particular areas of the Arctic are favoured for cyclone activity, such as southeastern Greenland and Iceland along the North Atlantic storm track (Vavrus, 2013). Previous studies have suggested that extreme winter precipitation events in the Canadian Arctic Archipelago were consistently driven by cyclones moving through the area, with the amount of accumulation depending on the location relative to the storm track (Intihar & Stewart, 2005; Serreze et al., 2015, 2022).

Another feature driving precipitation in the Arctic is atmospheric rivers (ARs). An AR is a long, narrow corridor of enhanced water vapour transport in the atmosphere (Dacre et al., 2015). They are typically identified via gradients in vertically integrated water vapour transport (IVT); a common threshold for AR identification in the Arctic is a minimum IVT of 250 kg m^{-1} s^{-1} (e.g., Ralph et al., 2018; Rhoades et al., 2020). ARs are commonly associated with WCBs within cyclones (Bao et al., 2006; Dacre et al., 2015). Dacre et al. (2019) found that a low-level feeder airstream brings moisture near the base the WCB, where convergence near the cold front results in a pooling of moisture that can generate an AR, further feeding strong moisture transport within the WCB. This agrees closely with other conceptual models (e.g., Browning & Pardoe, 1973; Payne et al., 2020; Wernli & Davies, 1997).

ARs have been shown to have significant hydrological impacts in the Arctic due to the presence of both heat and ample moisture for precipitation, causing the rainfall fraction to increase (Mattingly et al., 2018). For example, an AR brought the first observed rainfall to the GrIS Summit Station in August 2021 (Box, Wehrlé, et al., 2022). Lauer et al. (2023) found that ARs accounted for ~40% of precipitation during an early summer field campaign in the North Atlantic sector of the Arctic, but played a smaller role in observations in spring, when only ~16% of precipitation was AR-related. It is suggested that ARs will become more common at high latitudes as the climate warms (Wang et al., 2024; Wille et al., 2025; Zhang et al., 2021).

The distribution of intense precipitation in the Arctic is also heavily influenced by orography, such as coastal southeast Greenland. Here, precipitation is typically brought by cyclones bringing onshore flow, which causes orographic lift as the air moves over the steep mountains along the coast (Chen et al., 1997; Jonassen et al., 2020). Orographic lift was also noted to be a pivotal mechanism driving extreme winter snowfall events in the Canadian Arctic Archipelago (Intihar & Stewart, 2005; Serreze et al., 2022).

2.1.4 Important feedbacks

There are a variety of important feedbacks that act to enhance or dampen the changes explored throughout this paper. In this section, I will introduce some of the most influential feedbacks: the ice-albedo feedback, the water vapour feedback, lapse rate feedback, and the glacier melt-elevation feedback.

The ice-albedo feedback mechanism denotes a powerful cycle enhancing radiative heating (Curry et al., 1995; Kellogg, 1983). Snow and ice have relatively high albedos, meaning that they reflect the vast majority of incoming solar radiation, reducing heating (Warren, 1982). Rising temperatures lead to increased melt of snow and ice surfaces, causing them to decrease in areal coverage. As snow and ice retreat, darker surfaces below (such as open water, vegetation, or rock) are exposed. These darker surfaces have lower albedos, leading to more absorption of radiation, causing an increase in temperature, producing more melt, and initiating a positive feedback cycle. This effect is seen in a variety of ways in the Arctic, including the loss of sea ice revealing darker, open ocean surface (e.g., Curry et al., 1995), as well as snowmelt and loss of glacial ice revealing darker underlying surfaces (e.g., Warren, 1982). The ice-albedo feedback is considered to be one of the main contributors to the Arctic amplification of climate change (e.g., Curry et al., 1995; Serreze et al., 2009).

The water vapour feedback describes the relationship between temperature and atmospheric water vapour content (Rind et al., 1991). As the temperature of air increases, it can hold more water vapour (discussed further in Section 2.2.1). This increase in water content drives increases in condensation, which in turn releases latent heat. The latent heat release causes temperatures to rise further, creating a positive feedback loop that increases temperature and atmospheric moisture holding capacity, leading to further warming assuming ample moisture availability. This tends to lead to the atmosphere holding more moisture and becoming more unstable, promoting intense precipitation where it occurs.

The water vapour feedback cycle is closely connected with the lapse rate feedback in the Arctic (Boeke et al., 2021). The lapse rate feedback describes how, as the atmosphere warms, more longwave radiation is lost to space at the top of the atmosphere (Manabe & Wetherald, 1975). This results in a negative feedback when considering total global warming and in the tropics, where deep convection allows for warming throughout the troposphere, leading to more heat being lost at the top of the atmosphere and regulating the amount of atmospheric warming (Hansen et al., 1997). However, in the Arctic, the warming is highest near the surface resulting in a steeper lapse rate and positive feedback by which the lower atmosphere continues to heat (Boeke et al., 2021). The ice-albedo feedback drives surface heating, and the water vapour feedback takes place in the lower troposphere, enhancing low-level warming in the Arctic and leading to steeper lapse rates, particularly in autumn and winter (Boeke et al., 2021).

Several additional feedbacks relating to cloud cover can occur in the Arctic which can operate differently over bright- and dark-coloured surfaces. Over dark surfaces, enhanced cloud cover with high liquid water content due to increased temperature can reflect more incoming solar radiation, which can lead to a cooling effect and a negative feedback cycle (Goosse et al., 2018). This effect may occur over dark open water surfaces during the warm season in the Arctic. Conversely, the presence of optically thick clouds over bright surfaces, such as snow or sea ice, instead enhances downwelling longwave radiation, resulting in a warming effect and a positive feedback cycle that increases temperatures and cloudiness (Goosse et al., 2018; Vavrus, 2004). This effect has been tied to enhanced sea ice loss in the Arctic (e.g., Kay & Gettelman, 2009). For example, the positive downwelling longwave radiation anomalies due to increased cloudiness associated with moisture intrusions has been shown to result in earlier sea ice melt onset in the Arctic (Mortin et al., 2016). This positive feedback generally plays a larger role in Arctic climate changes than the negative feedback due to the presence of brightly coloured snow and ice surfaces

across the Arctic for much of the year. Increases in cloudiness are expected due to rising atmospheric moisture in the warmer future climate. However, climate models often struggle in reproducing accurate cloud cover over areas such as Greenland (e.g., Herrington et al., 2022), meaning that their role in future climate changes may be insufficiently captured in current models.

Finally, the melt-elevation feedback refers to a positive feedback mechanism accelerating the mass loss of glaciers (e.g., Boers & Rypdal, 2021; Levermann & Winkelmann, 2016). Increased temperatures promote the melting of land ice, which in turn causes the ice surface to decrease in elevation. As the ice surface becomes lower, it is exposed to higher temperatures and is more prone to ablation (Levermann & Winkelmann, 2016), reducing the elevation further and potentially leading to a dramatic acceleration of mass lass (e.g., Beckmann & Winkelmann, 2022).

It is also important to consider that the feedbacks influence one another, such as the melt-elevation feedback reducing ice area and revealing lower albedo surfaces, which can increase temperature through the ice-albedo feedback, causing more melt and supporting both cycles to go on. Similarly, the water vapour feedback over the ocean can lead to a warming of the atmosphere and melting of sea ice, which allows more open water for evaporation and lower albedo to enhance warming (Villamil-Otero et al., 2018). All of these feedbacks, and more, contribute to and are affected by changes in precipitation in the Arctic, which will be explored throughout the rest of this chapter.

2.1.5 Framework for quantifying drivers of change

When investigating the causes behind climatic changes, a common framework is attributing changes to thermodynamic or dynamic drivers. In general, thermodynamic changes to precipitation refer to changes due to moisture availability, whereas dynamic changes indicate those caused by differing moisture transport due to circulation and convergence patterns (e.g., Norris et al., 2019; Pfahl et al., 2017; Seager et al., 2010; Yettella & Kay, 2017). The majority of this work has investigated the causes of changes in mean precipitation but can give insight into the drivers of extremes in a warming climate. Using this type of differentiation, a greater understanding of the processes driving precipitation changes can be achieved, allowing for a deeper understanding of potential changes in the future.

The subsequent sections are organized as follows: Important thermodynamic and dynamic processes influencing precipitation rates and distributions are introduced in Sections 2.2 and 2.3, respectively. Section 2.4 details how the thermodynamic and dynamic factors interact to produce precipitation patterns and projections of how they may change in a warming climate. The impacts of extreme precipitation and the factors influencing it on glacier/ice sheet mass balance are explored in Section 2.5.

2.2 Thermodynamic controls on extreme precipitation

2.2.1 Clausius-Clapeyron relationship

As air temperatures increase, the saturation vapour pressure increases following the Clausius-Clapeyron relationship (e.g., Brown, 1951). Stull (2017) provides the following equation to find saturation vapour pressure (e_s) at a given temperature (T) following the Clausius-Clapeyron relationship;

$$e_s = e_0 \cdot exp\left[\frac{L}{R_v} \cdot \left(\frac{1}{T_0} - \frac{1}{T}\right)\right] \tag{2.1}$$

where e_0 is the saturation vapour pressure at a reference temperature, T_0, and L and R_v represent the latent heat of vapourization and water vapour gas constant, respectively. This shows an exponential relationship between the moisture-holding capacity of air and temperature, meaning that air can hold more moisture at a rate of 6-7% per degree of warming (e.g., Bengtsson et al., 2011; Trenberth et al., 2003). This increase in moisture applies to all locations and levels, suggesting an amplification of the hydrological cycle in the Arctic without drastically altering the distribution of moisture (Norris et al., 2019). The increased atmospheric moisture can lead to the pattern of precipitation changes referred to as "wet gets wetter, dry gets drier" (e.g., Held & Soden, 2006; Seager et al., 2010), whereby the historical hydrological cycle is simply amplified.

Globally, mean precipitation is expected to increase by 1-3% per degree of warming as a result of the increased moisture-holding capacity of warmer air (Allen & Ingram, 2002; Held & Soden, 2006), but the increase in the Arctic is closer to 4.5% per degree (Bintanja & Selten, 2014). Precipitation extremes are expected to increase faster than the mean; Pfahl et al. (2017) found a projected increase of upwards of 7% per degree of warming in the mean annual maximum daily precipitation amount over the entire Arctic owing to increased atmospheric moisture. Rates of increases reached as high as 10% over Greenland. This is supported by Norris et al. (2019), where the high latitudes were projected to see the most substantial relative contribution of thermodynamics to increases above the 75th percentile of daily precipitation rates. This suggests that direct impacts from warmer temperatures alone can drive rising precipitation in the Arctic.

Increased atmospheric moisture provides an enhanced opportunity for extreme precipitation, but the true response may be more complex than a simple increase. While the amount of moisture in the air is expected to increase following the Clausius-Clapeyron relationship, Vihma et al. (2016) found evidence that relative humidity over Arctic land surfaces may decrease in some regions in CMIP5 model projections. This is because the moisture availability may not increase quickly enough to maintain constant or increasing relative humidity levels as the air temperature rises. This is consistent with the precipitation sensitivity being observed to be lower than the Clausius-Clapeyron relationship (e.g., Allen & Ingram, 2002; Bintanja & Selten, 2014; Held & Soden, 2006). Loriaux et al. (2017) performed simulations exploring the response of precipitation intensity to varied atmospheric moisture in the Netherlands and found that average precipitation rate tends to decrease with increased relative humidity. This is hypothesized to be because higher humidity allows precipitation to occur sooner than in a drier atmosphere, which results in more, weaker precipitation and reduces the probability of developing extreme precipitation. However, it is expected that this increase in weak precipitation will be at the expense of moderate rates, and extremes will still be enhanced by higher atmospheric moisture (e.g., Pfahl et al., 2017).

2.2.2 Sea ice and oceanic considerations

The loss of sea ice allows for more open water that can evaporate freely into the atmosphere. Years with low September sea ice minima tend to have higher cyclone-associated precipitation in the autumn in atmospheric reanalyses (Stroeve et al., 2011). Kopec et al. (2016) found that atmospheric moisture from local evaporation increases at a rate of 18.2 ± 4.6% and 10.8 ± 3.6% per 100,000 km^2 of sea ice lost in the Canadian Arctic and Greenland Sea regions, respectively. However, previous studies found that the relationships between other cyclone intensity metrics that may predict extreme precipitation and sea ice cover were less direct (e.g., Koyama et al., 2017; Stroeve et al., 2011).

Declining sea ice cover can also contribute to thermodynamic changes in the atmosphere, favouring intense precipitation by altering the static stability of the lower troposphere. Crawford et al. (2022) developed a conceptual model of the local impacts of varied sea ice concentrations on winter and autumn cyclone development (Figure 2.2). As sea ice concentrations fall and more open water is exposed, there are stronger sensible and latent heat fluxes towards the atmosphere, particularly in the winter when the water is much warmer than the air (Hay et al., 2022; Screen & Simmonds, 2010). This increases the temperature in the low levels (Screen & Simmonds, 2010), causing a reduction in stability as the warmer air is more buoyant than the cooler overlying air (e.g., Schweiger et al., 2008), encouraging convection and increasing the Eady growth rate. The Eady growth rate describes the potential for cyclogenesis based on atmospheric stability and vertical wind shear (Eady, 1949). This resulted in more intense cyclones and greater cyclone-associated precipitation in the Arctic during the winter and early spring (e.g., Crawford et al., 2022; Valkonen et al., 2021), thereby increasing the risk of extreme precipitation.

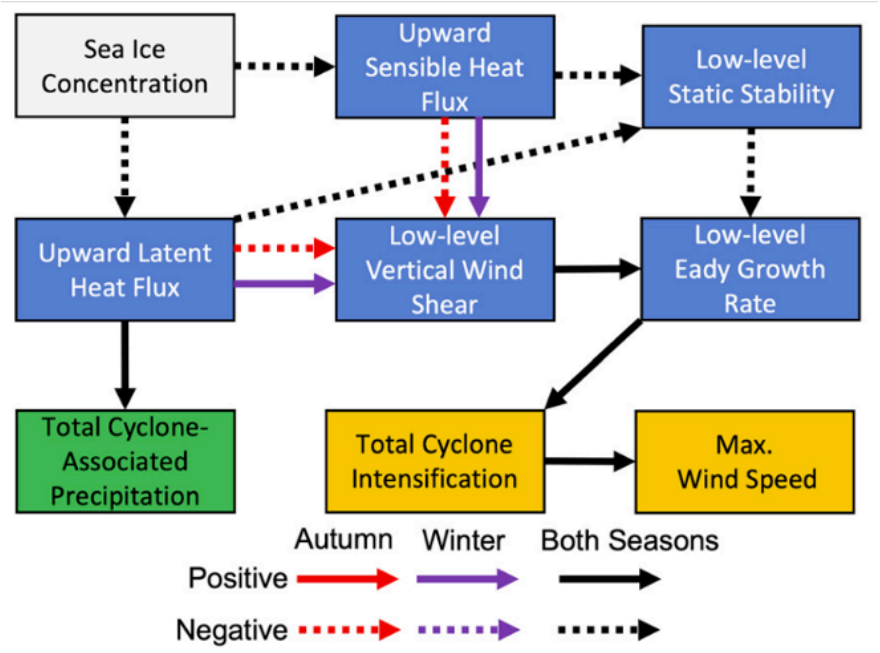

Figure 2.2. Conceptual model showing how sea ice concentration thermodynamically affects cyclone-associated precipitation in the Arctic in autumn (Sept-Oct) and winter (Dec-Mar). Arrow style shows the sign of correlation between variables, colour indicates season(s). Adapted from Crawford et al. (2022). © American Meteorological Society. Used with permission.

Sea ice loss has the largest impact on evaporation and precipitation rates in the autumn and winter, as it creates a strong temperature gradient between the water surface and cold air above (Bintanja & Selten, 2014). As the sea ice edge shifts in location, the area with the strongest temperature gradient between the warm ocean and cold sea ice also moves, shifting the location of heightened cyclone development and precipitation enhancement (Crawford et al., 2022). However, the actual impacts of these changes on cyclone development have not been clear. For example, the lowering of sea ice extent during September and October, when sea ice is at an annual minimum, tends to still decrease static stability but lower the wind shear (Crawford et al., 2022). These changes effectively cancel each other out, resulting in little impact on cyclogenesis or precipitation processes.

2.2.3 Energy Hypothesis

Another important factor in precipitation changes in the Arctic is differences in the energy balance. The energy hypothesis suggests that increases in global precipitation in a warming climate are subject to energy constraints to maintain balance in the troposphere (Allen & Ingram, 2002). As the lower atmosphere warms, it emits more longwave radiation, and more is lost to space, causing radiative cooling of the atmosphere (Allen & Ingram, 2002). The cooling promotes condensation of moisture and latent heat release, leading to increased precipitation rates (Allen & Ingram, 2002). The energy hypothesis indicates that magnitude of precipitation increases are controlled by the rate of radiative cooling driving latent heat release (Allen & Ingram, 2002).

In the Arctic, Pithan and Jung (2021) analyzed the connection between the Arctic hydrological cycle and energy balance in CMIP6 projections in which sea ice is held constant. Their Figure 2 illustrates the zonally averaged seasonal temperature sensitivity of precipitable water and changes to energy balance components. In the summer, increases in precipitable water are apparent, with the largest relative increases being found in the Arctic (Figure 2a of Pithan & Jung, 2021). It was found that precipitation amounts were more sensitive to radiative cooling than moisture availability in the winter when increases in precipitable moisture were modest. Poleward of 60°N, mean latent heat release from precipitation closely follows the radiative cooling curve (Figure 2b of Pithan & Jung, 2021), suggesting that the energy hypothesis might help to explain the increases in Arctic winter precipitation.

While energy constraints may be important for mean precipitation, it is hypothesized that the role is more minor when considering intense precipitation events (Allen & Ingram, 2002; Pendergrass & Hartmann, 2014), so it is not likely to play a pivotal role in producing precipitation extremes. Nevertheless, it may act to change the frequency of high-intensity precipitation by promoting weaker rates, thereby reducing extremes, or slightly increasing the rate of existing precipitation.

2.3 Dynamic controls on extreme precipitation

2.3.1 Atmospheric moisture transport

While temperature (and therefore atmospheric moisture) is increasing globally, dynamics can determine where the precipitation will form and fall based on locations of convergence (Trenberth et al., 2003). Regions in which humid air converges tend to favour convection and the most intense precipitation, as ample moisture is present and the horizontal convergence provides a triggering mechanism for vertical motion (e.g., Hudson, 1971). The discussion of how dynamic controls affect precipitation in polar regions often revolves around the concept of atmospheric moisture transport (AMT). AMT refers to the movement of atmospheric moisture, and here we are concerned with poleward AMT from the warmer lower latitudes toward the poles (e.g., Bintanja et al., 2020; Villamil-Otero et al., 2018). AMT is always occurring, but the strength varies. Typically, the most substantial AMT occurs in the warm sector of a cyclone where humidity and temperatures are higher than the surrounding air (Woods et al., 2013). Naakka et al. (2019) found that the strength of AMT depends more on the humidity of the air than the strength of the winds.

In the high latitudes, cyclones are the primary mechanism of AMT (Konstali et al., 2024). Fearon et al. (2021) found that cyclones accounted for 74% of AMT across 70°N between 1998 and 2018. These systems often carry abundant moisture for long distances before entering the Arctic; Trenberth et al. (2003) suggested that moisture may be transported up to 3200 km by a cyclone before falling as precipitation. ARs are also important to consider as they represent areas of enhanced AMT with a meridional component, often embedded within a cyclone (Zhang et al., 2021). Periods of strong AMT are often referred to as “moisture intrusions” (e.g., Woods et al., 2013); Woods et al. (2013) defined winter Arctic moisture intrusions as vertically integrated meridional moisture fluxes of upwards of 200 Tg d^{-1} deg^{-1} across 70°N, which was the 90th percentile value. Villamil-Otero et al. (2018) found that the intensity and propagation speed of a cyclone were typically more important than the number of cyclones when predicting AMT into the Arctic based on reanalyses.

In general, AMT alone does not necessarily produce precipitation extremes. However, the locations of enhanced AMT are more likely to see intense precipitation rates. In the Arctic, strong AMT is typically associated with warmer, southerly flow with temperatures further enhanced by latent heat release (e.g., Fearon et al., 2021; Woods et al., 2013). This leads to lower static stability and convective enhancement of the precipitation (e.g., Komatsu et al., 2018), tending to increase accumulation rates.

2.3.2 Large-scale circulation patterns

The amount of AMT and movement of cyclones into the Arctic is closely related to the large-scale circulation of the region. More specifically, the polar jet stream's orientation and strength can strongly impact the movement of moisture and the development of cyclones and their propagation in the high latitudes (Hurrell et al., 2003). The polar jet stream exists where there are strong meridional temperature gradients between cold polar and warm tropical air, creating a strong baroclinic zone where disturbances (cyclones) develop (Hall et al., 2014). Cyclones, in turn, can impact the jet stream by perturbing the baroclinic zones and through alterations of the momentum flux (e.g., Federer et al., 2024; Hall et al., 2014; Panetta & Held, 1988; Smith et al., 2022). In

general, cyclones' momentum flux is oriented in opposition to the direction of propagation and tends to enhance and decelerate zonal flow in the region of cyclogenesis and cyclolysis, respectively (Smith et al., 2022).

The most common paths of cyclone propagation are referred to as storm tracks (e.g., Shaw et al., 2016). Storm tracks are also generally the regions of strongest energy and moisture transport, as cyclones bring warm, moist air poleward (Shaw et al., 2016). The strongest AMT into the Arctic generally occurs in the north Pacific and north Atlantic sectors, near the end of major storm tracks (e.g., Bengtsson et al., 2011; Dufour et al., 2016). Regions in which cyclones occlude and become quasi-stationary at the end of their life cycle tend to receive substantial AMT (e.g., Bengtsson et al., 2011; Dufour et al., 2016). Such regions include the Canadian Arctic Archipelago, the Gulf of Alaska, and Scandinavia (Intihar & Stewart, 2005; Naakka et al., 2019).

If the steering flow is oriented more meridionally, more moisture is transported into the Arctic (Fearon et al., 2021). Liu and Barnes (2015) found that periods of extreme AMT into the Arctic were often associated with Rossby waves breaking. Rossby waves are meanders in the jet stream that develop due to the conservation of potential vorticity in a rotating fluid (Holton, 2004). Breaking refers to when the wave reaches a critical amplitude and an overturning of potential vorticity occurs, often resulting in blocking events (Holton, 2004). A blocking event (or pattern) occurs when an anomalous quasi-stationary ridge of high pressure interrupts the zonal flow and forces strong meridional flow in the troposphere, often for extended periods (Auger et al., 2017; Legras & Ghil, 1985; Woods et al., 2013). This pattern can result in enhanced AMT events into the Arctic (e.g., C. Liu & Barnes, 2015; Strong & Magnusdottir, 2008). During blocking events, the jet stream and accompanying cyclones are forced poleward on the western flank of the upper level ridge and cold, dry air moves equatorward east of the high (e.g., Auger et al., 2017). This means that the western edge sees strong AMT supporting intense precipitation, but the eastern edge does not. For example, Greenland blocking events often see the shifting of the Icelandic low southwards and deflection of cyclones towards southwestern Greenland, whereas the North Atlantic storm track would usually favour storms impacting southeastern Greenland and Iceland in the absence of a blocking high (Auger et al., 2017). Blocking events are hypothesized to increase in frequency in a warming climate (e.g., B. S. Barrett et al., 2020; Hanna et al., 2016) but are generally not well captured in climate models (Hanna et al., 2018). The orientation of the jet stream, and therefore storm tracks, depends on large-scale pressure patterns, referred to as modes of climate variability (Hall et al., 2014).

Modes of climate variability are recognized as explanations for medium- to long-term (often weekly to seasonal) fluctuations in the general atmospheric circulation patterns at a hemispheric scale (Lorenz, 1951). These patterns give insight into jet stream variability (Hall et al., 2014) and, therefore, the development and propagation of systems that may produce extreme precipitation. Many modes are defined using empirical orthogonal function analysis (also referred to as principal component analysis), whereby the covariance between a complex set of related variables is used to create a new set of components that describe patterns and variability in the system (Jolliffe, 2002). Relevant modes for Arctic precipitation distribution include the North Atlantic Oscillation (NAO) and Arctic Oscillation (AO).

The NAO refers to variation in the intensity of zonal winds over the North Atlantic due to pressure variability of the Icelandic low and subtropical high-pressure zone (Bromwich et al., 1999; Serreze et al., 1997). The NAO index is calculated as the difference between the normalized

mean sea level pressure of Stykkisholmur, Iceland and Lisbon, Portugal (Hurrell, 1995). A negative (positive) NAO phase leads to more meridional (zonal) flow across the North Atlantic. This means that the negative phase promotes more AMT into the Arctic via the North Atlantic sector, the Arctic's strongest AMT source region (Villamil-Otero et al., 2018), and would tend to support the development of extreme precipitation in the region. A positive NAO phase in winter generally leads to lower precipitation totals across the Canadian Arctic and Greenland as storms in the Atlantic tend to be shifted from the typical storm track, enhancing precipitation over Scandinavia instead (Bromwich et al., 1999; Hurrell et al., 2003).

The AO is defined as the first empirical orthogonal function of winter sea level pressure in the Northern Hemisphere (Thompson & Wallace, 1998). The positive (negative) phase of the AO is associated with lower (higher) pressure over the Arctic and higher (lower) in the midlatitudes (Thompson & Wallace, 1998). This results in the shifting of the polar jet stream and, therefore, alters storm tracks (Thompson & Wallace, 2001). Using reanalysis datasets, Oshima and Yamazaki (2004) found a statistically significant relationship between the AO phase and AMT into the Arctic from the Atlantic Ocean. The AO can also cause a shift in the distribution of precipitation, such as decreasing the amount of accumulation in southwestern Greenland during the positive phase due to reduced southwesterly flow, similar to the positive NAO phase (Mosley-Thompson et al., 2005). The NAO and AO are highly correlated, with the largest differences existing during the winter (Thompson & Wallace, 1998). They are often combined into a singular annular mode describing Northern Hemisphere pressure patterns called the Northern Annular Mode (e.g., Thompson & Wallace, 2001). Annular modes are large-scale patterns of climate variability, typically consisting of zonal patterns of pressure variations (Lorenz, 1951). While combining the NAO and AO is useful for large-scale studies, keeping them separated can be helpful to focus on the Atlantic sector, where both play an important role and their small differences are more relevant than in other parts of the Arctic.

Large-scale modes of climate variability, including the NAO and AO, play an essential role in the occurrence and distribution of extreme precipitation in the Arctic, particularly through their influence on the jet stream and, therefore, propagation of cyclones (Hurrell et al., 2003). As they modes cycle, they alter the path of typical storm tracks, resulting in a redistribution of precipitation. For example, blocking events bringing heavy precipitation to western Greenland tend to be associated with negative NAO phase (e.g., Box et al., 2005; Gallagher et al., 2020; Neff, 2018), whereas the positive NAO phase promotes zonal flow (Auger et al., 2017). Berdahl et al. (2018) suggests that the location of the Icelandic Low alone has a higher correlation with winter precipitation totals in southeastern Greenland than the NAO or AO index. They found that moisture transport into the region increases by up to 40% when the low is positioned further west than average, allowing moist southeasterly winds to bring heavy precipitation to the area. In general, the amount of AMT in the Arctic is closely related to the NAO and AO indices since they have a direct impact on the mean flow patterns (e.g., Hall et al., 2014; Villamil-Otero et al., 2018). This, in turn, affects extreme precipitation by altering regions of moisture convergence and distribution (e.g., Pfahl et al., 2017).

2.3.3 Discussion

The impact of AMT on precipitation in the Arctic varies seasonally and regionally, with further influence from the phase of modes of climate variability and jet stream characteristics. The North Atlantic storm track is a region of intense AMT from south of Greenland across to Scandinavia and eastward, bringing the strongest meridional AMT in the autumn and winter (e.g., Figure 1a,d of Naakka et al., 2019). The North Pacific storm track exhibits deep AMT reaching the central Arctic Ocean in the summer months (e.g., Figure 1c of Naakka et al., 2019) but is generally weaker than that of the North Atlantic sector. AMT in the Eurasian Arctic shows less variability, flipping between weakly positive and negative AMT throughout the year.

Periods of strong AMT fuel most extreme precipitation events in the Arctic (e.g., Kolbe, Sonnemans, et al., 2023). For example, southeastern Greenland is one of the regions receiving the most frequent extreme precipitation in the Arctic as cyclones move along the North Atlantic storm track (Hanna et al., 2006; Schuenemann & Cassano, 2010; Serreze et al., 1997). This region experiences particularly intense precipitation because of its complex topography. As storms move towards the coast, the air is forced upwards over the steep mountains, causing orographic enhancement of the precipitation, as discussed in Section 2.1.1. This is seen in various mountainous parts of the Arctic, such as the Canadian Arctic Archipelago (Intihar & Stewart, 2005) and Svalbard (Serreze et al., 2015). Many areas of the Arctic, including those where orographic enhancement is important, are very dependent on cyclones for precipitation and experience large interannual variability depending on the storms that reach the region, which is often determined by the large-scale circulation patterns (e.g., Zahn et al., 2018).

2.4 Response of extreme precipitation and its drivers to a warming climate

2.4.1 Projections of thermodynamic and dynamic forcing

Thermodynamic changes tend to amplify the hydrological cycle globally, whereas dynamic factors tend to bring about regional changes (Norris et al., 2019). Historically, Arctic precipitation is primarily driven by cyclones transporting moisture into the region, but the majority of observed and projected precipitation changes have been attributed to increased local evaporation (e.g., Bengtsson et al., 2009; Bintanja & Selten, 2014; Skific et al., 2009; Yu & Zhong, 2021). However, the increase in atmospheric moisture also enhances dynamic changes. For example, Bengtsson et al. (2011) found an increase in net AMT of 29% by the year 2100 relative to 20th-century averages in a moderate climate change scenario. This suggests that dynamic factors are vital to understanding the distribution of precipitation in the Arctic, but thermodynamic effects are expected to be more important for understanding the magnitude of future changes in precipitation.

Pfahl et al. (2017) explored global estimations of the contributions of thermodynamic and dynamic factors to changes in extreme precipitation in CMIP5 models (Figure 2.3). Here, extreme precipitation is defined as the mean annual maximum daily precipitation rate. In the Arctic, the greatest contribution to increasing extreme precipitation is from thermodynamics, where an increase in vertically integrated water vapour of over 10% per degree of warming is seen for the entire Arctic (Figure 2.3c). Conversely, the dynamic factors are shown to either have little impact or a negative contribution to extreme precipitation. For example, a clear negative trend in dynamic

contributions is evident along the southeastern coast of Greenland (Figure 2.3b), where fewer and weaker cyclones are projected to impact (e.g., Yettella & Kay, 2017).

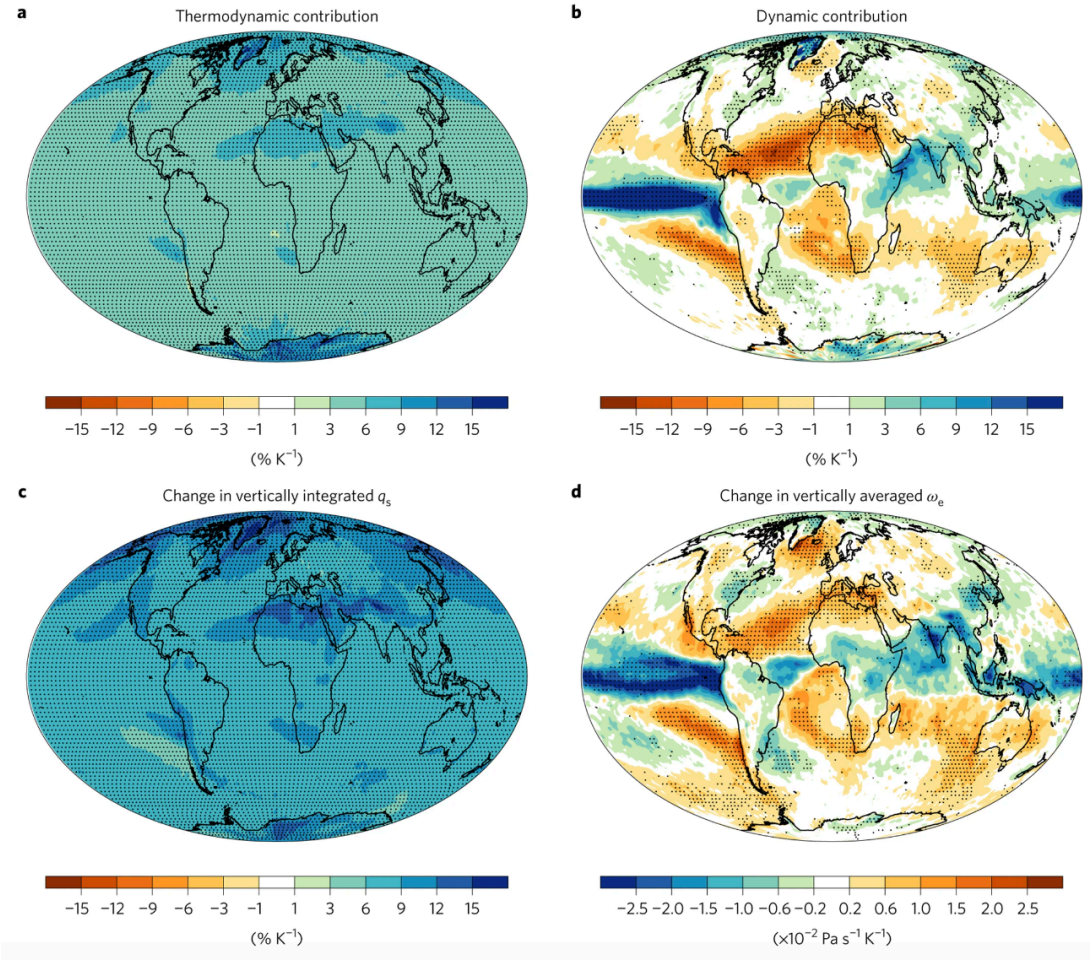

Figure 2.3. Sensitivity of extreme precipitation (mean annual highest single day accumulation total) in CMIP5 simulations to (a) thermodynamic forcing (where vertical velocity, ω_e, is kept constant using the annual mean of 1950-2100), (b) sensitivity to dynamic contributions (difference between total extreme precipitation sensitivity and thermodynamic sensitivity), and the change in mean (c) vertically-integrated saturation specific humidity and (d) ω_e (where negative indicates increased upward motion) during the occurrence of extreme precipitation. Differences are calculated relative to 1950-2005. Retrieved from Pfahl et al. (2017). Reproduced with permission from Springer Nature.

Bintanja and Selten (2014) demonstrated that the anticipated growth in Arctic winter precipitation during the 21st century is predominantly a consequence of heightened evaporation resulting from sea ice loss. Projections suggest that the interannual variability of surface temperature will decrease in the Arctic as sea ice declines, leading to relatively low interannual variability in local evaporation from the open water surface (Boer, 2009). This suggests that as the Arctic becomes ice-free, the variability in thermodynamic factors influencing precipitation will be reduced. While the thermodynamic effect has been tied most closely to the increase in precipitation totals, Bintanja et al. (2020) showed that the majority of increases in interannual precipitation variability in CMIP5 simulations were linked to changes in AMT, with the most substantial variability occurring during the summer.

Bintanja and Selten (2014) also explored the seasonality of the forcings of precipitation increases in CMIP5 models. During winter months, the vast majority of precipitation increases are linked to increased evaporation tied to the loss of sea ice cover. Authors were able to attribute evaporative increases to sea ice loss by calculating differences in evaporative fluxes over only regions of sea ice retreat summed over 10-year periods. Conversely, the rise in summer precipitation is primarily attributed to an intensified flow of moisture into the region from lower latitudes. More recent studies using CMIP6 projections supported these findings (e.g., Kolbe, Bintanja, et al., 2023). Skific et al. (2009) investigated seasonal projections of atmospheric moisture in the Arctic from the Community Climate System Model (CCSM). Overall, thermodynamics were once again found to have the most significant impacts, except for a dynamically-driven increase in moisture in the Barents Sea region owing to strengthened AMT. Dynamic factors were also shown to support thermodynamic increases in the Central Arctic Ocean during the summer and North Atlantic in autumn, agreeing with the seasonal cycle of transport into the Arctic region found by Bintanja and Selten (2014).

While thermodynamic and dynamic contributions to precipitation changes can be approximated, it is difficult to truly separate their impacts due to their interconnectedness (e.g., Kolbe, Bintanja, et al., 2023). For example, AMT can directly influence precipitation rates, but it can also cause feedbacks with other parts of the climate system, altering precipitation indirectly, such as through the water vapour feedback. AMT has been noted to explain approximately 40% of the variability in the downward longwave radiation flux in the Arctic due to the increased presence of low-level clouds when more moisture is present (Woods et al., 2013). Temperatures may then rise as a result of both greater downward longwave radiation and amplified latent heat release from condensation (Rind et al., 1991). This can lead to a decrease in sea ice thickness (Morrison et al., 2012) and an increase in local moisture availability as more water surface is uncovered. Additionally, the destabilization of the lower troposphere, as discussed in Section 2.2.2, as well as increased low-level temperatures via the ice-albedo and water vapour feedbacks, can promote convective precipitation within or independent of cyclones (Parker et al., 2022).

As extremes are rare by nature, it is difficult to study them systematically due to a lack of observations to constrain their characteristics and drivers to best understand potential changes in the future (e.g., Otto, 2019). Pfahl et al. (2017) showed that the dynamic contribution to changing extreme precipitation caused the vast majority of the disagreement between model projections, with Greenland and the central Arctic Ocean containing some of the highest degrees of uncertainty outside of the tropics. The thermodynamic changes are typically less uncertain as the relationship between temperature and moisture-holding capacity of air is well understood (e.g., Norris et al., 2019; Pfahl et al., 2017).

2.4.2 Impacts on cyclones and ARs

As discussed in Section 2.4.1, the warmer atmosphere holding more moisture acts to increase precipitation globally, including within cyclones and ARs (e.g., Kolbe, Sonnemans, et al., 2023; Yettella & Kay, 2017), whereas dynamic factors tend to have more complex impacts (e.g., Seager et al., 2010). Yettella and Kay (2017) found that greater than 90% of increases in cyclone-associated precipitation in projections of the 21st century were related to increased atmospheric moisture rather than changing cyclone intensity or frequency. Because of this, precipitation

extremes associated with cyclones are likely to increase even without drastic changes in cyclone intensity metrics, such as depth (e.g., Yettella & Kay, 2017).

By definition, increasing moisture would intensify ARs because integrated water vapour transport is a typical measure of AR intensity (e.g., Dacre et al., 2015). Previous studies have found increased precipitation from ARs globally in projections due to amplified atmospheric moisture (Kolbe, Sonnemans, et al., 2023; O'Brien et al., 2022; Zhang et al., 2021). Arctic ARs are expected to increase in a warming climate almost solely due to thermodynamic increases, with dynamic changes acting to reduce AR potential across the Arctic outside of the Barents and Kara Sea regions in projections by Kolbe, Sonnemans, et al. (2023). Nellikkattil et al. (2023) found that extreme precipitation became 10% (20%) more likely to occur with Arctic ARs in an atmospheric CO_2 doubling (quadrupling) experiment, with some of the largest increases being found in regions such as southwest Greenland and Alaska, where orography enhances precipitation rates.

Changes in large-scale circulation could result in precipitation occurring in different areas in the warming climate. For example, Stroeve et al. (2011) noted a rise in cyclone-associated precipitation attributed to alterations in atmospheric circulation patterns, bringing more frequent and stronger cyclones into the Arctic. Conversely, previous studies have suggested a southeastward shift and weakening of the North Atlantic storm track tied to sea ice loss, which would bring fewer intense cyclones to regions like southeastern Greenland that are currently hotspots for cyclone activity (e.g., Joos et al., 2023; Yettella & Kay, 2017). The Pacific sees an opposite response, where the North Pacific storm track shifts northward with increasing warming and brings more cyclones into the Arctic (Priestley & Catto, 2022). Some studies have suggested that NAO and AO are trending towards becoming more positive (e.g., Gillett & Fyfe, 2013), which tends to reduce the occurrence of strong meridional circulation and, therefore, the number of cyclones and ARs bringing moisture into the central Arctic (e.g., Baek et al., 2023), likely reducing intense precipitation in regions such as Greenland with increases in Scandinavia. However, the trend in NAO and AO phase is not universally seen in climate projections and is relatively uncertain (e.g., Kolbe, Sonnemans, et al., 2023). Kolbe, Sonnemans, et al. (2023) found that almost all of the interannual variability in Arctic ARs was linked to the position and speed of the midlatitude jet stream, highlighting the importance of understanding jet stream variability to predict heavy precipitation.

Another dynamic element that could contribute to changes in the distribution of cyclone-associated precipitation is the propagation speed of systems. Previous studies have indicated that in a warming Arctic with reduced sea ice, the propagation of cyclones through the region is anticipated to decelerate (Crawford et al., 2023; Hay et al., 2023; Priestley & Catto, 2022). This can lead to storms impacting the same areas for more extended periods, contributing to higher precipitation totals. Coupled with the increased moisture within cyclones due to thermodynamic changes, the risk of extreme precipitation accumulations may increase due to the slower movement of storm systems. This risk is even greater in regions where topography may further amplify the precipitation (e.g., Chen et al., 1997; Intihar & Stewart, 2005).

In addition to altered propagation speeds, the warming Arctic climate is leading to changes in cyclone frequency. Zahn et al. (2018) assessed 30-year trends (1981-2010) in cyclone characteristics in reanalyses and found varied patterns. In the winter, storms have become less frequent in eastern Greenland and the Eurasian Arctic and more frequent in Svalbard and the Beaufort Sea. In summer, decreases in frequency are found in the northern Baffin Bay region and

the Beaufort Sea. In contrast, increases are shown in the Laptev Sea and the western Canadian Arctic Archipelago. In a similar analysis of ARCTIC CORDEX reanalysis and model-driven regional climate model simulations, Akperov et al. (2019) found similar patterns in trends, but illustrated some disagreement between simulations. The loss of sea ice acts to enhance cyclogenesis in winter (e.g., Crawford et al., 2022), as explored in Section 2.2.2, but this does not mean cyclones are expected to become more frequent everywhere sea ice is lost.

All of these discussed alterations of cyclone and AR characteristics can lead to changes to intense precipitation in the Arctic since many extreme events are tied to these systems (e.g., Serreze et al., 2022; Yu & Zhong, 2021). The thermodynamically-driven increase in moisture is credited as the most significant factor in the intensification of precipitation, including within cyclones and ARs (e.g., Pfahl et al., 2017; Yettella & Kay, 2017; Yu & Zhong, 2021). However, the factors explored here illustrate how dynamic changes to large-scale circulation can modify the locations in which these systems impact (e.g., Pfahl et al., 2017; Priestley & Catto, 2022; Yu & Zhong, 2021), therefore changing the frequency and intensity of extreme precipitation across the Arctic.

2.5 Impacts on Mass Balance

2.5.1 Factors contributing to land ice impacts

Extreme precipitation can have complex impacts on the mass balance of land ice depending on factors such as its timing, intensity, and phase. Mass balance refers to any changes in the ice mass of a glacier over time, including dynamic, internal, and surface processes (Cogley et al., 2011). The surface mass balance (SMB) is the difference between accumulation and ablation at the ice surface (Cogley et al., 2011). Precipitation is the primary input to the SMB of land ice, although deposition of water vapour has been observed to account for up to ~10% of summer accumulations in the accumulation zone of the GrIS (Dietrich et al., 2024). However, the impacts of precipitation on land ice may become more complex as precipitation variability increases (e.g., Pendergrass et al., 2017) and its phase shifts towards more rainfall (e.g., Bintanja & Andry, 2017). Thompson-Munson et al. (2025) found that all of the GrIS may experience rainfall under 21st century warming projections. In this section, several factors influencing how land ice may respond to extreme precipitation are explored.

One component that may cause a shift in the way ice responds to extreme precipitation is via the firn layer. Firn refers to snow that has been present on top of a glacier for at least one melt season but has not yet compacted into ice (Cogley et al., 2011). This means that pore space exists within the layer, and liquid water at the surface of a glacier may percolate into the firn and be retained. Generally, this occurs through freezing the water into an ice lens, capillary forces holding the water in place, or storage within a firn aquifer (e.g., Forster et al., 2014; Noël et al., 2022). While this can help to mitigate mass loss, it can also introduce new vulnerabilities. For example, water refreezing into an impermeable ice lens (also referred to as an ice slab) can make the pore space below inaccessible (e.g., Machguth et al., 2016), and it releases latent heat at the depth of freezing, warming the ice (e.g., van Pelt et al., 2016). The formation of ice slabs within the firn layer can be impactful on future mass balance, but the magnitude of their impact depends on factors such as the future development of the firn layer atop the ice and the thickness of the ice layer. Firn growth occurs through snow accumulation on ice that compacts over the course of months (Zwally

& Jun, 2002). If less snowfall occurs, less firn will develop, leading to differing impacts resulting from events such as intense rainfall. Firn compaction also occurs more quickly under higher temperatures (Zwally & Jun, 2002), leading to the degradation of the firn layer. If an ice slab develops, its impact on mass balance may be offset by the development of thick firn atop the ice, meaning more pore space is available for water retention (Ashmore et al., 2020). However, ice slabs have been shown to substantially impact runoff in Greenland and the Canadian Arctic. In a modelling experiment, Ashmore et al. (2020) investigated the role of ice slabs in the SMB of Devon Ice Cap in the Canadian Arctic and found little impact on SMB until the slab grew to thicknesses close to 1 m, at which point the slabs became largely impermeable. MacFerrin et al. (2019) found that the runoff area of the GrIS has increased by 26 $\pm$ 3% from 2001 to 2014 due to the formation of ice slabs that are multiple metres thick, preventing the percolation of water into the depths of the firn layer.

Historically, it is estimated that firn retained approximately half of all rain and meltwater on the GrIS, drastically reducing the potential mass loss (Harper et al., 2012). However, there is a finite amount of pore space within the firn layer on any glacial ice. As the climate warms, more rainfall and melt occur, which means the pore space is being filled. This creates the potential for a tipping point in which little refreezing and retainment of liquid water can occur (e.g., Noël et al., 2017, 2022). Projections of GrIS SMB under SSP5-8.5 show that its refreezing capacity may begin to fall before the end of the 21st century, with southwest Greenland showing the earliest drop in refreezing potential (Noël et al., 2022). However, Medley et al. (2022) found that GrIS firn air content fell by 5% between 1996 and 2019, indicating an earlier decrease in water-holding capacity. Many glaciers on Baffin Island have been shown to be already experiencing reduced refreezing capacity and accelerated mass loss (Noël et al., 2018). This means that extreme rainfall events that previously may have led to a mass gain will be more likely not to be captured by the firn and instead promote melt through latent heat release, and meltwater (e.g., Doyle et al., 2015; Harper et al., 2023).

Extreme precipitation's influence on glacier dynamics is also important to consider. As water percolates, it may reach the bed beneath the ice and lubricate the underlying surface, changing how the glacier moves (e.g., Cuffey & Paterson, 2010). This can cause dramatic increases in ice flow (e.g., Doyle et al., 2015). During the melt season, glaciers tend to produce an efficient drainage system to deal with the presence of liquid water (e.g., Bartholomew et al., 2010, 2012). However, at the beginning of the melt (or during other seasons), organized channels do not exist, and water is not moved effectively (Bartholomew et al., 2012). This can result in water pressure building up between the ice and the underlying bed, resulting in a lower effective pressure, which reduces drag and allows the ice to flow more quickly (e.g., Iken & Bindschadler, 1986). As more intense rainfall is expected to occur in the Arctic, reaching higher elevations inland (e.g., Bintanja & Andry, 2017), this accelerated ice motion may become more common. This increased flow can trigger the glacier melt-elevation feedback as more ice moves to lower elevations (e.g., Levermann & Winkelmann, 2016) and promote further ice loss.

Albedo considerations are also critical in understanding the response of ice to heavy precipitation. Individual events may have very different impacts on land ice because of variations in albedo due to the presence or absence of snow (Warren, 1982). The characteristics of the snow are also important, as snow metamorphism can cause sizeable shifts in its optical properties (Warren, 1982). Generally, older, compacted snow or wet snow have lower albedos than fresh

snow, causing higher absorption of energy and increased temperatures (Shea et al., 2005; Warren, 1982). This means that an event that brings fresh snowfall to a glacier's surface typically causes an increase in albedo, reflecting more shortwave energy and cooling the surface (Oerlemans & Klok, 2004). This results in an increase in mass balance and a reduction in melt if it occurs during the melt season. However, the opposite effect can occur if an event brings intense rainfall. The presence of liquid water generally leads to a darkening of the ice or snow surface (Cuffey & Paterson, 2010; Shea et al., 2005). The increased absorption leads to rising temperatures and heightened potential for melt and ice loss. Additionally, the loss of ice can trigger the ice-albedo feedback and enhance warming, causing further ice loss (Kellogg, 1983).

2.5.2 Case studies

These impacts are poorly understood in a climatological context due to their non-linearity and rarity, but several case studies have shown the potential for drastically different results. Doyle et al. (2015) presented observations showing how a late-summer heavy cyclonic rainfall event in western Greenland resulted in intense runoff and mass loss in August 2011. Some areas in western Greenland received approximately 20% of the average annual precipitation (as rain) in seven days following the conclusion of the melt season. The cyclone brought warmer temperatures, and authors found that the presence of liquid water on the bare ice released latent heat as it froze to the surface and sensible heat due to water being above freezing, causing surface temperatures to rise to the melting point and drive further mass loss. The introduction of substantial amounts of liquid water after the melt season had ended caused a dramatic increase in ice flow. Velocities nearly doubled at some measurement sites, and the increased speed reached approximately 140 km into the GrIS interior. This increased flow caused ice discharge and could have contributed to the melt-elevation feedback as more ice moved downslope.

Impacts from an anomalous late October rainfall event in the accumulation zone of Jakobshavn glacier in the western GrIS were documented by Harper et al. (2023). A cyclone brought temperatures to near 0°C up to 2000 m elevation at the beginning of the rainfall event on 30 October 2008, producing extreme precipitation rates. Temperatures of the ice prior to the event were well below freezing but rose by tens of degrees due to the warmer air temperatures and latent and sensible heat from the rainfall. An estimated 10 MJ m^{-2} of energy was added to the firn layer in the study area. It took 5-8 weeks for sites to return to the prior energy state, and the amount of refreezing was 20-100% of the total refreezing of the previous melt season. Glaciers develop effective channels for liquid water percolation and runoff during the melt season, allowing water to percolate deep into the firn layer before refreezing (Ashmore et al., 2020). However, since this occurred in the cold season, authors noted that refreezing within the firn occurred at shallower depths, which may have made the firn below inaccessible, reducing future recapture of melt or rainwater.

Box et al. (2022) explored observations of the August 2021 AR that brought the first observed rainfall to the top of the GrIS. Rainfall was observed over most of southern and western Greenland on 13-14 August, reaching Summit station, with heavy precipitation reaching up to ~2000 m altitude. Authors found that the majority of impacts were tied to warm temperatures, reaching slightly above 0°C. However, the effect of the heavy rainfall acted to exacerbate melt from increased temperatures. For example, the addition of liquid water at the surface meant more

liquid freezing into impermeable ice lenses in the firn layer. As the water froze at different depths, it caused alterations to the thermal profile of the ice as the freezing released latent heat. These impacts were seen well into the accumulation region of the western GrIS and may have caused the region to be more vulnerable to future melt.

The extreme GrIS melt event of July 2012 was found to be tied to a similar synoptic setup as the cases presented by Doyle et al. (2015) and Box et al. (2022), with a ridge over/east of Greenland and a low upstream leading to enhanced southerly flow towards southern and western Greenland (Hermann et al., 2020). The melt area during the event was found to cover 94.8% of GrIS area (Hermann et al., 2020) and some of the highest observed melt rates were seen in some of the lower ablation areas (up to 28 cm day^{-1} ice equivalent; Fausto et al., 2016). While this event is not typically viewed as a precipitation-related event, southwestern Greenland received multiple days of intense rainfall throughout the anomalous period which was tied to enhanced mass loss (Hermann et al., 2020). Indeed, Fausto et al. (2016) illustrated that non-radiative surface energy fluxes dominated the ablation zone surface energy budget across western and southern Greenland during the event, suggesting the potential increase in melt events dominated by non-radiative fluxes if cyclonic activity increases in the region. The domination of non-radiative fluxes was also seen to be the case for melt related to heavy rainfall events in Qassimiut in southern Greenland (Teng et al., 2025).

Conversely, Bailey and Hubbard (2025) presented an analysis of a March 2022 AR event impacting southeastern Greenland. In this case, surface air temperatures remained near 0°C and heavy snowfall occurred. The added snow mass during the AR event was found to offset seasonal melt and mass loss over the 2021-2022 season by approximately 8%. This snowfall increased surface albedo (by approximately 3-7%), delaying the beginning of the melt season. The albedo anomaly was long-lasting; the regional albedo in the upper ablation zone in southeastern Greenland was observed to have anomalously high albedo in June-August 2022. This demonstrates that impacts associated with ARs on the GrIS can vary drastically depending on timing.

Oerlemans and Klok (2004) showed how a heavy snowfall event in the Swiss Alps during the summer led to a multi-day slowing of melt observed at Morteratschgletscher in Switzerland. A cyclone brought a strong cold front across central Europe on 10 July 2000, which brought maximum daily temperatures on the glacier from approximately 18°C to 3°C. Approximately 20 cm of snow fell at low altitudes, with closer to 50 cm accumulating near the equilibrium line. The equilibrium line represents the location on the glacier at which melt/seasonal ablation occurs below and net accumulation occurs above. This caused a sharp increase in albedo by roughly 0.25. Observations showed that this increase in albedo lasted for one week as the snow slowly melted. Using an SMB model, the authors showed that the storm brought a total of 224 mm w.e. of mass when averaged over the entire glacier but had a positive SMB impact of 354 mm w.e. due to both the added snow as well as the increased albedo, shielding the underlying ice and lowering surface temperatures. The addition of fresh snow increases snowpack cold content, which refers to the temperature deficit that must be overcome for melt to occur, further preventing melt (Jennings et al., 2018). This further illustrates how heavy precipitation can positively impact the mass balance of glaciers and dampen seasonal melt.

Finally, Box et al. (2005) assessed how a persistent Greenland blocking pattern led to strong precipitation anomalies across the GrIS from September 2002 to April 2003. This pattern brought more frequent, intense storms to southeastern Greenland, where orographic lift enhanced

precipitation, leading to severe precipitation rates. This produced high albedos and a deep snow cover protecting the southeastern GrIS from melt as the warm season began. In contrast, a negative precipitation anomaly of up to 370 mm was seen in southwestern Greenland due to the prolonged blocking pattern. This meant that there was little to no seasonal snow cover in the ablation zone, leading to a lower albedo than usual, promoting earlier and increased melt as temperatures rose as spring began. Authors noted that the following melt season saw roughly 73 km^3 more ice melt/freshwater discharge from the ice sheet than average, the majority of which came from the southwestern sector. This highlights the sensitivity of the GrIS to precipitation variability, particularly in the quickly changing southwestern region.

Because of these differing impacts, it is crucial to understand how extreme precipitation is changing in terms of seasonality, phase, frequency, and intensity. It is also important to understand the properties of land ice as the climate shifts, as impacts may vary if the ice becomes more vulnerable as firn pore space is depleted and the melt-elevation feedback accelerates loss (e.g., Wei et al., 2022).

2.5.3 Climatic factors

Since little work has been done that illustrates the long-term impacts of extreme precipitation on land ice in a changing climate, I will explore the influence of various factors that control precipitation extremes (discussed in Sections 2.2-2.4) on land ice. By gaining a better understanding of their contribution to the mass balance of land ice surrounding Baffin Bay, one can theorize how extreme precipitation may play a role.

The location of the Icelandic low-pressure center has a direct impact on winter accumulation in the southeastern GrIS (Auger et al., 2017; Berdahl et al., 2018), but the GrIS also plays a role in the location of the Icelandic low, as explored by Chen et al. (1997). As air is forced upwards moving over the GrIS, lee cyclogenesis can occur based on the conservation of potential vorticity, generating cyclones moving away from Greenland. However, as the ice sheet melts and redistributes mass over very long time periods, it may not reach as high of altitudes and become flatter. This would lead to less lee cyclogenesis and position the Icelandic low further west towards Greenland, increasing the potential for more precipitation to fall over the ice sheet. The increased precipitation would add mass to the ice sheet, thereby creating a negative feedback loop. As the climate warms, the altered circulation patterns and increased atmospheric moisture owing to external factors may modify this balance by redistributing precipitation (e.g., Auger et al., 2017), more intense precipitation rates (e.g., Pfahl et al., 2017), more rainfall than snowfall (e.g., McCrystall et al., 2021), and more vulnerable ice being lost quickly in the warming climate (e.g., Box, Hubbard, et al., 2022).

The phases of various modes of climate variability also impact the precipitation falling on land ice, as well as the conditions of the ice at the time of the intense precipitation. Previous studies have shown clear correlations between the NAO phase and accumulation on the GrIS (e.g., Bjørk et al., 2018; Bromwich et al., 1999). Bjørk et al. (2018) explored how the NAO phase impacted GrIS annual accumulation using atmospheric reanalyses and satellite imagery. As discussed in Section 2.3.2, the positive NAO phase promotes cyclones traversing the North Atlantic storm track and bringing heavy winter snowfall to eastern and northern Greenland and drier than average

conditions on the west. Conversely, the negative NAO phase drives higher than normal precipitation to the northwestern GrIS as more cyclones move northward through Baffin Bay, leaving dry conditions to the east. This suggests that the eastern (western) GrIS is likely to see more extreme precipitation events occurring during the positive (negative) NAO phase. However, this also may indicate that extended periods of either phase can make the ice in a region more susceptible to loss. For example, an extended positive (negative) NAO phase can leave the central/western (eastern) GrIS lacking in the development of firn and therefore more vulnerable to heavy rainfall, as observed by Doyle et al. (2015). This is supported by Mosley-Thompson et al. (2005), who found that the central west GrIS was the region whose accumulation is most sensitive to the NAO phase based on ice core records. However, the exact impacts of these patterns depend on the timing and phase of precipitation.

As with extreme precipitation in general, cyclones and ARs can have complex impacts on land ice in the Arctic. Mattingly et al. (2018) investigated the impacts of ARs on GrIS SMB and showed that they can bring about positive and negative SMB impacts depending on the location and timing of the event (Figure 8 of Mattingly et al., 2018). ARs impacting eastern Greenland in any season typically result in strong accumulation in southeastern Greenland. In contrast, those making landfall in western Greenland tend to bring enhanced ablation to lower elevations of both the eastern and western edges of the ice sheet, with more accumulation at high elevations. The authors noted that the substantial accumulation tends to outweigh increased melt in the western GrIS, even during summer ARs. Notably, strong western Greenland ARs tend to cause mass loss on the eastern GrIS even in the winter due to the heat associated with the system. This heat can also promote the type of cold season heavy rainfall observed by Harper et al. (2023), as discussed in Section 2.5.2. This suggests that ARs may bring about extreme precipitation resulting in a mass increase for part of the GrIS at the expense of other regions. Previous studies have not investigated the direct impact of ARs on the SMB of the glaciers of the eastern Canadian Arctic Archipelago. However, Kolbe, Sonnemans, et al. (2023) showed that southeastern Baffin Island is expected to see moderate increases in AR activity, similar to that of eastern Greenland, which could spur more intense precipitation events over the region's glaciers. Little et al. (2019) found similar complex impacts of ARs on glaciers in New Zealand, where ARs were associated with both extreme ablation and extreme snowfall events, depending on the phase of precipitation and timing. Similar impacts could be expected in the Canadian Arctic as ARs increase.

2.5.4 Discussion

The thermodynamic changes to extreme precipitation are driving precipitation increases broadly, with virtually the entire Arctic seeing more precipitation (Norris et al., 2019; Pfahl et al., 2017). Dynamic contributions vary more drastically spatially and temporally (Norris et al., 2019; Pfahl et al., 2017). The factors leading to changes in extreme precipitation are also changing glacier conditions (in terms of snow cover, dynamics, temperature, etc.), which is important to consider when assessing the potential impacts that these events may have in the future. The increasing temperature and atmospheric moisture bring a higher risk of impactful cyclone and AR events in the Arctic, particularly those with rainfall as opposed to snowfall (e.g., Lenaerts et al., 2020). Doyle et al. (2015) found that not only is rainfall increasing over the GrIS but it is also shown to be more common later in the summer/autumn, leading to the potential for more high runoff events (e.g., Box, Wehrlé, et al., 2022; Doyle et al., 2015; Harper et al., 2023). Box et al. (2023) further

illustrated this through the investigation of extreme rainfall events over the GrIS during 1991-2021, finding that both total rainfall and rainfall fraction have increased by upwards of 30% during the study period.

When investigating the impacts of intense precipitation events, it is essential to consider not only the direct impacts, such as the adding of mass to a glacier and latent heat release of rainfall freezing to the ice (e.g., Box et al., 2023; Oerlemans & Klok, 2004), but also the indirect effects that play a role in altering ice properties, largely through the mechanisms explored in Section 2.5.1. For example, the albedo may increase with heavy snowfall (e.g., Oerlemans & Klok, 2004) or decrease with intense rainfall (e.g., Box, Wehrlé, et al., 2022; Doyle et al., 2015), but the impact generally lasts for days to weeks and can alter the amount of seasonal melt. Box et al. (2023) presented two cases of extreme rainfall in southern Greenland and concluded that the rainfall increased melt rates by 16 $\pm$ 4% during the event but had a more extensive influence indirectly through refreezing into ice lenses at depth and altering snow metamorphism resulting in a lower surface albedo and triggering further melt. In a study of the surface energy balance during extreme rainfall events in southern Greenland, Teng et al. (2025) found that the rain heat flux was relatively small compared to other terms (contributing less than 5% to total melt energy), but surface melt during extreme rainfall events was found to increase by an average of 17.9 and 46.7% relative to the previous day at the two stations studied. The climatic conditions occurring alongside extreme precipitation can have substantial impacts on land ice, such as the presence of optically thick clouds leading to cloud radiative feedbacks (e.g., Goosse et al., 2018; Teng et al., 2025; Vavrus, 2004) and dramatic temperature changes (e.g., Box et al., 2022; Hermann et al., 2020; Oerlemans & Klok, 2004) that must be considered as well.

Extreme precipitation events are rare by nature, and little systematic study of their impacts has been conducted. As the climate warms, the increased temperatures have had the largest impact on the degradation and loss of land ice mass (e.g., Dowdeswell et al., 1997; Hanna et al., 2014, 2021; Mattingly et al., 2023; McLeod & Mote, 2016; Mote, 2007), so fewer studies have been conducted examining the consequences of individual precipitation events. However, it is important to understand how these anomalous events factor into future mass balance, particularly as the ice becomes more vulnerable to change and intense precipitation becomes more common in the new Arctic climate.

2.6 Summary and Conclusion

2.6.1 Summary

As the Arctic warms, the processes influencing precipitation are changing. Overall, this is leading to an increase in precipitation rates and promoting extremes, but also changing the distribution of moisture across the Arctic (Bengtsson et al., 2011). Both thermodynamic and dynamic factors are driving these precipitation changes. Broadly, thermodynamic-related precipitation changes are driven by increased atmospheric moisture-holding capacity as temperatures rise, and dynamically driven changes arise from altered large-scale circulation and moisture convergence patterns (e.g., Norris et al., 2019; Pfahl et al., 2017; Seager et al., 2010; Yettella & Kay, 2017). These changes are further impacted and driven by various feedback cycles within the Arctic climate system, such as the ice-albedo, water vapour, and lapse rate feedbacks.

Thermodynamic moisture increases are governed by the Clausius-Clapeyron relationship, whereby the moisture-holding capacity of air increases by 6-7% per degree of warming. This alone strengthens the hydrological cycle, particularly in the Arctic, where surface warming is greatest. This results in a mean precipitation increase of approximately 1-3% globally but a higher rate of 4.5% per degree in the Arctic (Bintanja & Selten, 2014). This change alone tends to favour increases in precipitation rates but is further enhanced by the loss of sea ice, providing an ample moisture source from the open ocean surface and destabilizing the lower troposphere, which encourages convection and can intensify cyclones (Crawford et al., 2022). Energy constraints may also play a role in Arctic precipitation patterns, particularly in winter, where radiative cooling can force weak precipitation or act to slightly enhance existing precipitation rates (Pithan & Jung, 2021).

The Arctic largely relies on cyclones and ARs bringing moisture from lower latitudes polewards to drive extreme precipitation (Fearon et al., 2021). These intense AMT events bring both heat and moisture to enhance precipitation rates. The occurrence and distribution of cyclones and ARs, and therefore AMT, depends on factors such as jet stream characteristics and modes of climate variability (e.g., NAO, AO). The strongest AMT into the Arctic generally occurs in the North Atlantic sector, where cyclones and ARs are frequent and often more intense than other regions of the Arctic (Bengtsson et al., 2011). Because of this, modes of climate variability, such as the NAO and AO, that affect the orientation and strength of the polar jet stream are fundamental in determining the distribution of extreme precipitation in the Arctic.

Several previous studies have investigated how thermodynamic and dynamic factors influence precipitation changes in terms of mean precipitation (e.g., Bintanja & Selten, 2014; Seager et al., 2010; Yettella & Kay, 2017) and extremes (e.g., Norris et al., 2019; Pfahl et al., 2017; Yu & Zhong, 2021). These studies unanimously found that thermodynamic increases in atmospheric moisture explain most of the precipitation increases, while the dynamic factors lead to more complex changes. Evaporation tied to sea ice loss is thought to be the largest driver of winter precipitation increases in the Arctic, whereas AMT changes are more important in the summer and autumn (Bintanja & Selten, 2014). Precipitation associated with cyclones and ARs is projected to increase due to higher atmospheric moisture availability, enhancing the risk of extreme precipitation (e.g., Nellikkattil et al., 2023; Yettella & Kay, 2017), although storm tracks may shift or become more variable as a result of Arctic warming (e.g., Kolbe, Sonnemans, et al., 2023; Priestley & Catto, 2022).

It is challenging to completely separate the effects of thermodynamic and dynamic drivers as they are inherently connected. For example, thermodynamic moisture increases can enhance the magnitude of AMT even if circulation patterns do not change, and altered circulation patterns can lead to different regions where temperatures rise more quickly, affecting the thermodynamic increase in moisture-holding capacity. Uncertainties also exist based on a limited understanding of the drivers of extreme precipitation and the imperfect representation of such processes in climate models.

Extreme precipitation and all the factors driving its changes can lead to impacts on the mass balance of land ice. Intense precipitation events can add mass to a glacier and lead to an overall positive impact on the mass balance, particularly if heavy snowfall occurs during the melt season (e.g., Oerlemans & Klok, 2004). However, a shift from snowfall towards rainfall is expected as the climate warms. Intense rainfall events have been shown to be detrimental to mass balance,

particularly if they occur outside of the melt season, through processes including latent heat release, the creation of impermeable ice lenses in the firn layer, increasing ice velocities, and lowering the surface albedo (e.g., Box, Wehrlé, et al., 2022; Doyle et al., 2015; Harper et al., 2023).

The warming climate is also changing how ice may respond to future precipitation extremes. Factors influencing extreme precipitation, such as atmospheric circulation patterns and ARs, can influence long-term ice stability by affecting factors including winter accumulation and the availability of firn pore space (e.g., Auger et al., 2017; Bjørk et al., 2018; Chen et al., 1997; Mattingly et al., 2018). These elements can change the way that a glacier may respond to an extreme precipitation event, suggesting that events that are similar to those observed today may have more substantial impacts in the future.

2.6.2 Research Gaps

Substantial uncertainties still exist in the projection of climate extremes, particularly precipitation as it is considered to be a relatively poorly constrained variable in models (e.g., Nitu et al., 2018). Firstly, little work has been done to better understand how well climate models and/or reanalyses capture observed extreme precipitation characteristics in the Arctic. Some previous work has indicated that reanalyses struggle to match daily precipitation rates (e.g., Avila-Diaz et al., 2021; A. P. Barrett et al., 2020), but these analyses did not focus on extremes.

Another notable gap to address is the lack of detailed regional projections of changes to extreme precipitation in the eastern Canadian Arctic and Greenland. While projections of changes to extreme precipitation do exist, they are often global (e.g., Pfahl et al., 2017) or Arctic-wide (e.g., Yu & Zhong, 2021), meaning that there has not been a comprehensive exploration of potential changes in the region's extremes.

Finally, a variety of case studies have illustrated the varied impacts of extreme precipitation on the SMB of land ice (e.g., Bailey & Hubbard, 2025; Box et al., 2005; Box, Wehrlé, et al., 2022; Doyle et al., 2015; Harper et al., 2023; Oerlemans & Klok, 2004) that may either accelerate or decelerate the loss of land ice, contributing to global sea level rise. However, there has not been a quantification of the relative importance of these events to seasonal or long-term SMB. It is important to understand the role that these events have played historically, and how they may factor into land ice changes in the warming Arctic climate.

Literature cited

Adler, R. F., Huffman, G. J., Chang, A., Ferraro, R., Xie, P.-P., Janowiak, J., et al. (2003). The Version-2 Global Precipitation Climatology Project (GPCP) Monthly Precipitation Analysis (1979–Present). *Journal of Hydrometeorology*, *4*(6), 1147–1167. https://doi.org/10.1175/1525-7541(2003)004<1147:TVGPCP>2.0.CO;2

Adler, R. F., Sapiano, M. R. P., Huffman, G. J., Wang, J.-J., Gu, G., Bolvin, D., et al. (2018). The Global Precipitation Climatology Project (GPCP) Monthly Analysis (New Version 2.3) and a Review of 2017 Global Precipitation. *Atmosphere*, *9*(4), 138. https://doi.org/10.3390/atmos9040138

Akperov, M., Rinke, A., Mokhov, I. I., Matthes, H., Semenov, V. A., Adakudlu, M., et al. (2019). Trends of intense cyclone activity in the Arctic from reanalyses data and regional climate models (Arctic-CORDEX). *IOP Conference Series: Earth and Environmental Science*, *231*(1), 012003. https://doi.org/10.1088/1755-1315/231/1/012003

Allen, M. R., & Ingram, W. J. (2002). Constraints on future changes in climate and the hydrologic cycle. *Nature*, *419*(6903), 224–232. https://doi.org/10.1038/nature01092

Ashmore, D. W., Mair, D. W. F., & Burgess, D. O. (2020). Meltwater percolation, impermeable layer formation and runoff buffering on Devon Ice Cap, Canada. *Journal of Glaciology*, *66*(255), 61–73. https://doi.org/10.1017/jog.2019.80

Auger, J. D., Birkel, S. D., Maasch, K. A., Mayewski, P. A., & Schuenemann, K. C. (2017). Examination of precipitation variability in southern Greenland. *Journal of Geophysical Research: Atmospheres*, *122*(12), 6202–6216. https://doi.org/10.1002/2016JD026377

Avila-Diaz, A., Bromwich, D. H., Wilson, A. B., Justino, F., & Wang, S.-H. (2021). Climate Extremes across the North American Arctic in Modern Reanalyses. https://doi.org/10.1175/JCLI-D-20-0093.1

Baek, S. H., Battalio, J. M., & Lora, J. M. (2023). Atmospheric River Variability Over the Last Millennium Driven by Annular Modes. *AGU Advances*, *4*(1), e2022AV000834. https://doi.org/10.1029/2022AV000834

Bailey, H., & Hubbard, A. (2025). Snow Mass Recharge of the Greenland Ice Sheet Fueled by Intense Atmospheric River. *Geophysical Research Letters*, *52*(5), e2024GL110121. https://doi.org/10.1029/2024GL110121

Bao, J.-W., Michelson, S. A., Neiman, P. J., Ralph, F. M., & Wilczak, J. M. (2006). Interpretation of Enhanced Integrated Water Vapor Bands Associated with Extratropical Cyclones: Their Formation and Connection to Tropical Moisture. *Monthly Weather Review*, *134*(4), 1063–1080. https://doi.org/10.1175/MWR3123.1

Barrett, A. P., Stroeve, J. C., & Serreze, M. C. (2020). Arctic Ocean Precipitation From Atmospheric Reanalyses and Comparisons With North Pole Drifting Station Records. *Journal of Geophysical Research: Oceans*, *125*(1), 1–17. https://doi.org/10.1029/2019JC015415

Barrett, B. S., Henderson, G. R., McDonnell, E., Henry, M., & Mote, T. (2020). Extreme Greenland blocking and high-latitude moisture transport. *Atmospheric Science Letters*, *21*(11), e1002. https://doi.org/10.1002/asl.1002

Bartholomew, I., Nienow, P., Mair, D., Hubbard, A., King, M. A., & Sole, A. (2010). Seasonal evolution of subglacial drainage and acceleration in a Greenland outlet glacier. *Nature Geoscience*, *3*(6), 408–411. https://doi.org/10.1038/ngeo863

Bartholomew, I., Nienow, P., Sole, A., Mair, D., Cowton, T., & King, M. A. (2012). Short-term variability in Greenland Ice Sheet motion forced by time-varying meltwater drainage: Implications for the relationship between subglacial drainage system behavior and ice velocity. *Journal of Geophysical Research: Earth Surface*, *117*(F3). https://doi.org/10.1029/2011JF002220

Beckmann, J., & Winkelmann, R. (2022). Effects of extreme melt events on ice flow and sea level rise of the Greenland Ice Sheet. *The Cryosphere Discussions*, 1–23. https://doi.org/10.5194/tc-2022-145

Bengtsson, L., Hodges, K. I., & Keenlyside, N. (2009). Will Extratropical Storms Intensify in a Warmer Climate? *Journal of Climate*, *22*(9), 2276–2301. https://doi.org/10.1175/2008JCLI2678.1

Bengtsson, L., Hodges, K. I., Koumoutsaris, S., Zahn, M., & Keenlyside, N. (2011). The changing atmospheric water cycle in Polar Regions in a warmer climate. *Tellus A: Dynamic Meteorology and Oceanography*, *63*(5), 907–920. https://doi.org/10.1111/j.1600-0870.2011.00534.x

Berdahl, M., Rennermalm, A., Hammann, A., Mioduszweski, J., Hameed, S., Tedesco, M., et al. (2018). Southeast Greenland Winter Precipitation Strongly Linked to the Icelandic Low Position. *Journal of Climate*, *31*(11), 4483–4500. https://doi.org/10.1175/JCLI-D-17-0622.1

Binder, H., Boettcher, M., Joos, H., & Wernli, H. (2016). The Role of Warm Conveyor Belts for the Intensification of Extratropical Cyclones in Northern Hemisphere Winter. https://doi.org/10.1175/JAS-D-15-0302.1

Bintanja, R., & Andry, O. (2017). Towards a rain-dominated Arctic. *Nature Climate Change*, *7*(4), 263–267. https://doi.org/10.1038/nclimate3240

Bintanja, R., & Selten, F. M. (2014). Future increases in Arctic precipitation linked to local evaporation and sea-ice retreat. *Nature*, *509*(7501), 479–482. https://doi.org/10.1038/nature13259

Bintanja, R., Wiel, K. van der, Linden, E. C. van der, Reusen, J., Bogerd, L., Krikken, F., & Selten, F. M. (2020). Strong future increases in Arctic precipitation variability linked to poleward moisture transport. *Science Advances*, *6*(7), eaax6869. https://doi.org/10.1126/sciadv.aax6869

Bjørk, A. A., Aagaard, S., Lütt, A., Khan, S. A., Box, J. E., Kjeldsen, K. K., et al. (2018). Changes in Greenland's peripheral glaciers linked to the North Atlantic Oscillation. *Nature Climate Change*, *8*(1), 48–52. https://doi.org/10.1038/s41558-017-0029-1

Bochow, N., Poltronieri, A., & Boers, N. (2024). Projections of precipitation and temperatures in Greenland and the impact of spatially uniform anomalies on the evolution of the ice sheet. *The Cryosphere*, *18*(12), 5825–5863. https://doi.org/10.5194/tc-18-5825-2024

Boeke, R. C., Taylor, P. C., & Sejas, S. A. (2021). On the Nature of the Arctic's Positive Lapse-Rate Feedback. *Geophysical Research Letters*, *48*(1), e2020GL091109. https://doi.org/10.1029/2020GL091109

Boer, G. J. (2009). Changes in Interannual Variability and Decadal Potential Predictability under Global Warming. *Journal of Climate*, *22*(11), 3098–3109. https://doi.org/10.1175/2008JCLI2835.1

Boers, N., & Rypdal, M. (2021). Critical slowing down suggests that the western Greenland Ice Sheet is close to a tipping point. *Proceedings of the National Academy of Sciences*, *118*(21), e2024192118. https://doi.org/10.1073/pnas.2024192118

Boisvert, L. N., & Stroeve, J. C. (2015). The Arctic is becoming warmer and wetter as revealed by the Atmospheric Infrared Sounder. *Geophysical Research Letters*, *42*(11), 4439–4446. https://doi.org/10.1002/2015GL063775

Boisvert, L. N., Webster, M. A., Petty, A. A., Markus, T., Bromwich, D. H., & Cullather, R. I. (2018). Intercomparison of Precipitation Estimates over the Arctic Ocean and Its Peripheral Seas from Reanalyses. *Journal of Climate*, *31*(20), 8441–8462. https://doi.org/10.1175/JCLI-D-18-0125.1

Box, J. E., Yang, L., Rogers, J., Bromwich, D., Bai, L. -s, Steffen, K., et al. (2005). Extreme Precipitation Events Over Greenland: Consequences to Ice Sheet Mass Balance (p. 5.2). Presented at the Eighth Conference on Polar Meteorology and Oceanography, San Diego, CA: American Meteorological Society. Retrieved from http://citeseerx.ist.psu.edu/viewdoc/download?doi=10.1.1.535.5897&rep=rep1&type=pdf

Box, J. E., Hubbard, A., Bahr, D. B., Colgan, W. T., Fettweis, X., Mankoff, K. D., et al. (2022). Greenland ice sheet climate disequilibrium and committed sea-level rise. *Nature Climate Change*, *12*(9), 808–813. https://doi.org/10.1038/s41558-022-01441-2

Box, J. E., Wehrlé, A., van As, D., Fausto, R. S., Kjeldsen, K. K., Dachauer, A., et al. (2022). Greenland Ice Sheet Rainfall, Heat and Albedo Feedback Impacts From the Mid-August 2021 Atmospheric River. *Geophysical Research Letters*, *49*(11), e2021GL097356. https://doi.org/10.1029/2021GL097356

Box, J. E., Nielsen, K. P., Yang, X., Niwano, M., Wehrlé, A., van As, D., et al. (2023). Greenland ice sheet rainfall climatology, extremes and atmospheric river rapids. *Meteorological Applications*, *30*(4), e2134. https://doi.org/10.1002/met.2134

Bromwich, D. H., Chen, Q., Li, Y., & Cullather, R. I. (1999). Precipitation over Greenland and its relation to the North Atlantic Oscillation. *Journal of Geophysical Research: Atmospheres*, *104*(D18), 22103–22115. https://doi.org/10.1029/1999JD900373

Brown, O. L. I. (1951). The Clausius-Clapeyron equation. *Journal of Chemical Education*, *28*(8), 428. https://doi.org/10.1021/ed028p428

Browning, K. A., & Pardoe, C. W. (1973). Structure of low-level jet streams ahead of mid-latitude cold fronts. *Quarterly Journal of the Royal Meteorological Society*, *99*(422), 619–638. https://doi.org/10.1002/qj.49709942204

Cai, L., Alexeev, V. A., Arp, C. D., Jones, B. M., Liljedahl, A. K., & Gädeke, A. (2018). The Polar WRF Downscaled Historical and Projected Twenty-First Century Climate for the Coast and Foothills of Arctic Alaska. *Frontiers in Earth Science*, *5*. https://doi.org/10.3389/feart.2017.00111

Catto, J. L. (2016). Extratropical cyclone classification and its use in climate studies. *Reviews of Geophysics*, *54*(2), 486–520. https://doi.org/10.1002/2016RG000519

Chen, Q., Bromwich, D. H., & Bai, L. (1997). Precipitation over Greenland Retrieved by a Dynamic Method and Its Relation to Cyclonic Activity. *Journal of Climate*, *10*(5), 839–870. https://doi.org/10.1175/1520-0442(1997)010<0839:POGRBA>2.0.CO;2

Cogley, J. G., Hock, R., Rasmussen, L. A., Arendt, A. A., Bauder, A., Braithwaite, R. J., et al. (2011). *Glossary of Glacier Mass Balance and Related Terms* (IHP-VII Technical Documents in Hydrology No. No. 86, IACS Contribution No. 2) (p. 124). Paris, France: UNESCO-IHP. Retrieved from https://wgms.ch/downloads/Cogley_etal_2011.pdf

Collier, C. G. (2000). *Precipitation estimation and forecasting* (Vol. 46). Geneva, Switzerland: Secretariat of the World Meteorological Organization.

Crawford, A. D., Lukovich, J. V., McCrystall, M. R., Stroeve, J. C., & Barber, D. G. (2022). Reduced Sea Ice Enhances Intensification of Winter Storms over the Arctic Ocean. *Journal of Climate*, *35*(11), 3353–3370. https://doi.org/10.1175/JCLI-D-21-0747.1

Crawford, A. D., McCrystall, M. R., Lukovich, J. V., & Stroeve, J. C. (2023). The Response of Extratropical Cyclone Propagation in the Northern Hemisphere to Global Warming. *Journal of Climate*, *36*(20), 7123–7142. https://doi.org/10.1175/JCLI-D-23-0082.1

Cuffey, K. M., & Paterson, W. S. B. (2010). *The Physics of Glaciers*. Academic Press.

Curry, J. A., Schramm, J. L., & Ebert, E. E. (1995). Sea Ice-Albedo Climate Feedback Mechanism. *Journal of Climate*, *8*(2), 240–247. https://doi.org/10.1175/1520-0442(1995)008<0240:SIACFM>2.0.CO;2

Dacre, H. F., Clark, P. A., Martinez-Alvarado, O., Stringer, M. A., & Lavers, D. A. (2015). How Do Atmospheric Rivers Form? *Bulletin of the American Meteorological Society*, *96*(8), 1243–1255. https://doi.org/10.1175/BAMS-D-14-00031.1

Dacre, H. F., Martínez-Alvarado, O., & Mbengue, C. O. (2019). Linking Atmospheric Rivers and Warm Conveyor Belt Airflows. https://doi.org/10.1175/JHM-D-18-0175.1

Diaconescu, E. P., Mailhot, A., Brown, R., & Chaumont, D. (2018). Evaluation of CORDEX-Arctic daily precipitation and temperature-based climate indices over Canadian Arctic land areas. *Climate Dynamics*, *50*(5), 2061–2085. https://doi.org/10.1007/s00382-017-3736-4

Dietrich, L. J., Steen-Larsen, H. C., Wahl, S., Faber, A.-K., & Fettweis, X. (2024). On the importance of the humidity flux for the surface mass balance in the accumulation zone of the Greenland Ice Sheet. *The Cryosphere*, *18*(1), 289–305. https://doi.org/10.5194/tc-18-289-2024

Diro, G. T., & Sushama, L. (2019). Simulating Canadian Arctic Climate at Convection-Permitting Resolution. *Atmosphere*, *10*(8), 430. https://doi.org/10.3390/atmos10080430

Dou, T., Xiao, C., Liu, J., Han, W., Du, Z., Mahoney, A. R., et al. (2019). A key factor initiating surface ablation of Arctic sea ice: earlier and increasing liquid precipitation. *The Cryosphere*, *13*(4), 1233–1246. https://doi.org/10.5194/tc-13-1233-2019

Dowdeswell, J., Hagen, J., Björnsson, H., Glazovsky, A., Harrison, W., Holmlund, P., et al. (1997). The Mass Balance of Circum-Arctic Glaciers and Recent Climate Change. *Quaternary Research*, *48*, 1–14. https://doi.org/10.1006/qres.1997.1900

Doyle, S. H., Hubbard, A., van de Wal, R. S. W., Box, J. E., van As, D., Scharrer, K., et al. (2015). Amplified melt and flow of the Greenland ice sheet driven by late-summer cyclonic rainfall. *Nature Geoscience*, *8*(8), 647–653. https://doi.org/10.1038/ngeo2482

Dufour, A., Zolina, O., & Gulev, S. K. (2016). Atmospheric Moisture Transport to the Arctic: Assessment of Reanalyses and Analysis of Transport Components. *Journal of Climate*, *29*(14), 5061–5081. https://doi.org/10.1175/JCLI-D-15-0559.1

Eady, E. T. (1949). Long Waves and Cyclone Waves. *Tellus*, *1*(3), 33–52. https://doi.org/10.3402/tellusa.v1i3.8507

Edel, L., Claud, C., Genthon, C., Palerme, C., Wood, N., L'Ecuyer, T., & Bromwich, D. (2020). Arctic Snowfall from CloudSat Observations and Reanalyses. https://doi.org/10.1175/JCLI-D-19-0105.1

Fausto, R. S., van As, D., Box, J. E., Colgan, W., & Langen, P. L. (2016). Quantifying the Surface Energy Fluxes in South Greenland during the 2012 High Melt Episodes Using In-situ Observations. *Frontiers in Earth Science*, *4*. https://doi.org/10.3389/feart.2016.00082

Fearon, M. G., Doyle, J. D., Ryglicki, D. R., Finocchio, P. M., & Sprenger, M. (2021). The Role of Cyclones in Moisture Transport into the Arctic. *Geophysical Research Letters*, *48*(4), e2020GL090353. https://doi.org/10.1029/2020GL090353

Federer, M., Papritz, L., Sprenger, M., Grams, C. M., & Wenta, M. (2024). On the Local Available Potential Energy Perspective of Baroclinic Wave Development. https://doi.org/10.1175/JAS-D-23-0138.1

Fischer, E. M., & Knutti, R. (2016). Observed heavy precipitation increase confirms theory and early models. *Nature Climate Change*, *6*(11), 986–991. https://doi.org/10.1038/nclimate3110

Ford, J. D., Bell, T., & St-Hilaire-Gravel, D. (2010). Vulnerability of Community Infrastructure to Climate Change in Nunavut: A Case Study From Arctic Bay. In G. K. Hovelsrud & B. Smit (Eds.), *Community Adaptation and Vulnerability in Arctic Regions* (pp. 107–130). Dordrecht: Springer Netherlands. https://doi.org/10.1007/978-90-481-9174-1_5

Forster, R. R., Box, J. E., van den Broeke, M. R., Miège, C., Burgess, E. W., van Angelen, J. H., et al. (2014). Extensive liquid meltwater storage in firn within the Greenland ice sheet. *Nature Geoscience*, *7*(2), 95–98. https://doi.org/10.1038/ngeo2043

Gallagher, M. R., Chepfer, H., Shupe, M. D., & Guzman, R. (2020). Warm Temperature Extremes Across Greenland Connected to Clouds. *Geophysical Research Letters*, *47*(9), e2019GL086059. https://doi.org/10.1029/2019GL086059

Gascon, G., Stewart, R. E., & Henson, W. (2010). Major Cold-Season Precipitation Events at Iqaluit, Nunavut. *Arctic*, *63*(3), 327–337.

Gettelman, A., & Rood, R. B. (2016). Essence of a Climate Model. In A. Gettelman & R. B. Rood (Eds.), *Demystifying Climate Models: A Users Guide to Earth System Models* (pp. 37–58). Berlin, Heidelberg: Springer. https://doi.org/10.1007/978-3-662-48959-8_4

Gillett, N. P., & Fyfe, J. C. (2013). Annular mode changes in the CMIP5 simulations. *Geophysical Research Letters*, *40*(6), 1189–1193. https://doi.org/10.1002/grl.50249

Goodison, B. E., Louie, P. Y. T., & Yang, D. (1998). *WMO Solid Precipitation Measurement Intercomparison--Final Report* (Instruments and Observing Methods No. WMO/TD-No. 872) (p. 318). World Meteorological Organization.

Goosse, H., Kay, J. E., Armour, K. C., Bodas-Salcedo, A., Chepfer, H., Docquier, D., et al. (2018). Quantifying climate feedbacks in polar regions. *Nature Communications*, *9*(1), 1919. https://doi.org/10.1038/s41467-018-04173-0

Groisman, P. Y., & Legates, D. R. (1994). The Accuracy of United States Precipitation Data. *Bulletin of the American Meteorological Society*, *75*(2), 215–228. https://doi.org/10.1175/1520-0477(1994)075<0215:TAOUSP>2.0.CO;2

Hall, R., Erdélyi, R., Hanna, E., Jones, J. M., & Scaife, A. A. (2014). Drivers of North Atlantic Polar Front jet stream variability. *International Journal of Climatology*, *35*(8), 1697–1720. https://doi.org/10.1002/joc.4121

Hanesiak, J. M., & Wang, X. L. (2005). Adverse-Weather Trends in the Canadian Arctic. *Journal of Climate*, *18*(16), 3140–3156. https://doi.org/10.1175/JCLI3505.1

Hanna, E., McConnell, J., Das, S., Cappelen, J., & Stephens, A. (2006). Observed and Modeled Greenland Ice Sheet Snow Accumulation, 1958–2003, and Links with Regional Climate Forcing. *Journal of Climate*, *19*(3), 344–358. https://doi.org/10.1175/JCLI3615.1

Hanna, E., Fettweis, X., Mernild, S. H., Cappelen, J., Ribergaard, M. H., Shuman, C. A., et al. (2014). Atmospheric and oceanic climate forcing of the exceptional Greenland ice sheet surface melt in summer 2012. *International Journal of Climatology*, *34*(4), 1022–1037. https://doi.org/10.1002/joc.3743

Hanna, E., Cropper, T. E., Hall, R. J., & Cappelen, J. (2016). Greenland Blocking Index 1851–2015: a regional climate change signal. *International Journal of Climatology*, *36*(15), 4847–4861. https://doi.org/10.1002/joc.4673

Hanna, E., Fettweis, X., & Hall, R. J. (2018). Brief communication: Recent changes in summer Greenland blocking captured by none of the CMIP5 models. *The Cryosphere*, *12*(10), 3287–3292. https://doi.org/10.5194/tc-12-3287-2018

Hanna, E., Cappelen, J., Fettweis, X., Mernild, S. H., Mote, T. L., Mottram, R., et al. (2021). Greenland surface air temperature changes from 1981 to 2019 and implications for ice-sheet melt and mass-balance change. *International Journal of Climatology*, *41*(S1), E1336–E1352. https://doi.org/10.1002/joc.6771

Hansen, J., Sato, M., & Ruedy, R. (1997). Radiative forcing and climate response. *Journal of Geophysical Research: Atmospheres*, *102*(D6), 6831–6864. https://doi.org/10.1029/96JD03436

Harper, J., Humphrey, N., Pfeffer, W. T., Brown, J., & Fettweis, X. (2012). Greenland ice-sheet contribution to sea-level rise buffered by meltwater storage in firn. *Nature*, *491*(7423), 240–243. https://doi.org/10.1038/nature11566

Harper, J., Saito, J., & Humphrey, N. (2023). Cold Season Rain Event Has Impact on Greenland's Firn Layer Comparable to Entire Summer Melt Season. *Geophysical Research Letters*, *50*(14), e2023GL103654. https://doi.org/10.1029/2023GL103654

Hawcroft, M. K., Shaffrey, L. C., Hodges, K. I., & Dacre, H. F. (2012). How much Northern Hemisphere precipitation is associated with extratropical cyclones? *Geophysical Research Letters*, *39*(24). https://doi.org/10.1029/2012GL053866

Hay, S., Kushner, P. J., Blackport, R., McCusker, K. E., Oudar, T., Sun, L., et al. (2022). Separating the Influences of Low-Latitude Warming and Sea Ice Loss on Northern Hemisphere Climate Change. https://doi.org/10.1175/JCLI-D-21-0180.1

Hay, S., Priestley, M. D. K., Yu, H., Catto, J. L., & Screen, J. A. (2023). The Effect of Arctic Sea-Ice Loss on Extratropical Cyclones. *Geophysical Research Letters*, *50*(17), e2023GL102840. https://doi.org/10.1029/2023GL102840

Heitmann, K., Sprenger, M., Binder, H., Wernli, H., & Joos, H. (2024). Warm conveyor belt characteristics and impacts along the life cycle of extratropical cyclones: case studies and climatological analysis based on ERA5. *Weather and Climate Dynamics*, *5*(2), 537–557. https://doi.org/10.5194/wcd-5-537-2024

Held, I. M., & Soden, B. J. (2006). Robust Responses of the Hydrological Cycle to Global Warming. *Journal of Climate*, *19*(21), 5686–5699. https://doi.org/10.1175/JCLI3990.1

Hermann, M., Papritz, L., & Wernli, H. (2020). A Lagrangian analysis of the dynamical and thermodynamic drivers of large-scale Greenland melt events during 1979–2017. *Weather and Climate Dynamics*, *1*(2), 497–518. https://doi.org/10.5194/wcd-1-497-2020

Holton, J. R. (2004). *An Introduction to Dynamic Meteorology*. Academic Press.

Hudson, H. R. (1971). On the Relationship Between Horizontal Moisture Convergence and Convective Cloud Formation. *Journal of Applied Meteorology (1962-1982)*, *10*(4), 755–762.

Hugonnet, R., McNabb, R., Berthier, E., Menounos, B., Nuth, C., Girod, L., et al. (2021). Accelerated global glacier mass loss in the early twenty-first century. *Nature*, *592*(7856), 726–731. https://doi.org/10.1038/s41586-021-03436-z

Hurrell, J. W. (1995). Decadal Trends in the North Atlantic Oscillation: Regional Temperatures and Precipitation. *Science*, *269*(5224), 676–679. https://doi.org/10.1126/science.269.5224.676

Hurrell, J. W., Kushnir, Y., Ottersen, G., & Visbeck, M. (2003). An Overview of the North Atlantic Oscillation. In *The North Atlantic Oscillation: Climatic Significance and Environmental Impact* (pp. 1–35). American Geophysical Union (AGU). https://doi.org/10.1029/134GM01

Iken, A., & Bindschadler, R. A. (1986). Combined measurements of Subglacial Water Pressure and Surface Velocity of Findelengletscher, Switzerland: Conclusions about Drainage System and Sliding Mechanism. *Journal of Glaciology*, *32*(110), 101–119. https://doi.org/10.3189/S0022143000006936

Intihar, M. R., & Stewart, R. E. (2005). Extratropical Cyclones and Precipitation within the Canadian Archipelago during the Cold Season. *Arctic*, *58*(2), 162–174.

Jennings, K. S., Kittel, T. G. F., & Molotch, N. P. (2018). Observations and simulations of the seasonal evolution of snowpack cold content and its relation to snowmelt and the snowpack energy budget. *The Cryosphere*, *12*(5), 1595–1614. https://doi.org/10.5194/tc-12-1595-2018

Jolliffe, I. T. (Ed.). (2002). Introduction. In *Principal Component Analysis* (pp. 1–9). New York, NY: Springer. https://doi.org/10.1007/0-387-22440-8_1

Jonassen, M. O., Chechin, D., Karpechko, A., Lüpkes, C., Spengler, T., Tepstra, A., et al. (2020). Dynamical Processes in the Arctic Atmosphere. In *Physics and Chemistry of the Arctic Atmosphere* (pp. 1–51). Springer, Cham. https://doi.org/10.1007/978-3-030-33566-3_1

Joos, H., Sprenger, M., Binder, H., Beyerle, U., & Wernli, H. (2023). Warm conveyor belts in present-day and future climate simulations – Part 1: Climatology and impacts. *Weather and Climate Dynamics*, *4*(1), 133–155. https://doi.org/10.5194/wcd-4-133-2023

van Kampenhout, L., Rhoades, A. M., Herrington, A. R., Zarzycki, C. M., Lenaerts, J. T. M., Sacks, W. J., & van den Broeke, M. R. (2019). Regional grid refinement in an Earth system model: impacts on the simulated Greenland surface mass balance. *The Cryosphere*, *13*(6), 1547–1564. https://doi.org/10.5194/tc-13-1547-2019

Kay, J. E., & Gettelman, A. (2009). Cloud influence on and response to seasonal Arctic sea ice loss. *Journal of Geophysical Research: Atmospheres*, *114*(D18). https://doi.org/10.1029/2009JD011773

Kellogg, W. W. (1983). Feedback mechanisms in the climate system affecting future levels of carbon dioxide. *Journal of Geophysical Research: Oceans*, *88*(C2), 1263–1269. https://doi.org/10.1029/JC088iC02p01263

Kolbe, M., Sonnemans, J. P. J., Bintanja, R., van der Linden, E. C., van der Wiel, K., Whan, K., & Benedict, I. (2023). Impact of Atmospheric Rivers on Future Poleward Moisture Transport and Arctic Climate in EC-Earth2. *Journal of Geophysical Research: Atmospheres*, e2023JD038926. https://doi.org/10.1029/2023JD038926

Kolbe, M., Bintanja, R., & van der Linden, E. C. (2023). Seasonal and regional contrasts of future trends in interannual arctic climate variability. *Climate Dynamics*, *61*(7), 3673–3706. https://doi.org/10.1007/s00382-023-06766-y

Komatsu, K. K., Alexeev, V. A., Repina, I. A., & Tachibana, Y. (2018). Poleward upgliding Siberian atmospheric rivers over sea ice heat up Arctic upper air. *Scientific Reports*, *8*(1), 2872. https://doi.org/10.1038/s41598-018-21159-6

Konstali, K., Spensberger, C., Spengler, T., & Sorteberg, A. (2024). Global Attribution of Precipitation to Weather Features. https://doi.org/10.1175/JCLI-D-23-0293.1

Kopec, B. G., Feng, X., Michel, F. A., & Posmentier, E. S. (2016). Influence of sea ice on Arctic precipitation. *Proceedings of the National Academy of Sciences of the United States of America*, *113*(1), 46–51. https://doi.org/10.1073/pnas.1504633113

Koyama, T., Stroeve, J., Cassano, J., & Crawford, A. (2017). Sea Ice Loss and Arctic Cyclone Activity from 1979 to 2014. *Journal of Climate*, *30*(12), 4735–4754. https://doi.org/10.1175/JCLI-D-16-0542.1

Lauer, M., Rinke, A., Gorodetskaya, I., Sprenger, M., Mech, M., & Crewell, S. (2023). Influence of atmospheric rivers and associated weather systems on precipitation in the Arctic. *Atmospheric Chemistry and Physics*, *23*(15), 8705–8726. https://doi.org/10.5194/acp-23-8705-2023

Legras, B., & Ghil, M. (1985). Persistent Anomalies, Blocking and Variations in Atmospheric Predictability. *Journal of the Atmospheric Sciences*, *42*(5), 433–471. https://doi.org/10.1175/1520-0469(1985)042<0433:PABAVI>2.0.CO;2

Lenaerts, J. T. M., Camron, M. D., Wyburn-Powell, C. R., & Kay, J. E. (2020). Present-day and future Greenland Ice Sheet precipitation frequency from CloudSat observations and the Community Earth System Model. *The Cryosphere*, *14*(7), 2253–2265. https://doi.org/10.5194/tc-14-2253-2020

Levermann, A., & Winkelmann, R. (2016). A simple equation for the melt elevation feedback of ice sheets. *The Cryosphere*, *10*(4), 1799–1807. https://doi.org/10.5194/tc-10-1799-2016

Levizzani, V., Laviola, S., & Cattani, E. (2011). Detection and Measurement of Snowfall from Space. *Remote Sensing*, *3*(1), 145–166. https://doi.org/10.3390/rs3010145

Lindsay, R., Wensnahan, M., Schweiger, A., & Zhang, J. (2014). Evaluation of Seven Different Atmospheric Reanalysis Products in the Arctic. *Journal of Climate*, *27*(7), 2588–2606. https://doi.org/10.1175/JCLI-D-13-00014.1

Little, K., Kingston, D. G., Cullen, N. J., & Gibson, P. B. (2019). The Role of Atmospheric Rivers for Extreme Ablation and Snowfall Events in the Southern Alps of New Zealand. *Geophysical Research Letters*, *46*(5), 2761–2771. https://doi.org/10.1029/2018GL081669

Liu, C., & Barnes, E. A. (2015). Extreme moisture transport into the Arctic linked to Rossby wave breaking. *Journal of Geophysical Research: Atmospheres*, *120*(9), 3774–3788. https://doi.org/10.1002/2014JD022796

Liu, G., & Curry, J. A. (1997). Precipitation characteristics in Greenland-Iceland-Norwegian Seas determined by using satellite microwave data. *Journal of Geophysical Research: Atmospheres*, *102*(D12), 13987–13997. https://doi.org/10.1029/96JD03090

Liu, J., Wu, D., Xu, X., Ji, M., Chen, Q., & Wang, X. (2021). Projection of extreme precipitation induced by Arctic amplification over the Northern Hemisphere. *Environmental Research Letters*, *16*(7), 074012. https://doi.org/10.1088/1748-9326/ac0acc

Lopez, P. (2007). Cloud and Precipitation Parameterizations in Modeling and Variational Data Assimilation: A Review. *Journal of the Atmospheric Sciences*, *64*(11), 3766–3784. https://doi.org/10.1175/2006JAS2030.1

Lorenz, E. N. (1951). SEASONAL AND IRREGULAR VARIATIONS OF THE NORTHERN HEMISPHERE SEA-LEVEL PRESSURE PROFILE. *Journal of the Atmospheric Sciences*, *8*(1), 52–59. https://doi.org/10.1175/1520-0469(1951)008<0052:SAIVOT>2.0.CO;2

Loriaux, J. M., Lenderink, G., & Siebesma, A. P. (2017). Large-Scale Controls on Extreme Precipitation. *Journal of Climate*, *30*(3), 955–968. https://doi.org/10.1175/JCLI-D-16-0381.1

MacFerrin, M., Machguth, H., As, D. van, Charalampidis, C., Stevens, C. M., Heilig, A., et al. (2019). Rapid expansion of Greenland's low-permeability ice slabs. *Nature*, *573*(7774), 403–407. https://doi.org/10.1038/s41586-019-1550-3

Machguth, H., MacFerrin, M., van As, D., Box, J. E., Charalampidis, C., Colgan, W., et al. (2016). Greenland meltwater storage in firn limited by near-surface ice formation. *Nature Climate Change*, *6*(4), 390–393. https://doi.org/10.1038/nclimate2899

Manabe, S., & Wetherald, R. T. (1975). The Effects of Doubling the CO2 Concentration on the climate of a General Circulation Model. Retrieved from https://journals.ametsoc.org/view/journals/atsc/32/1/1520-0469_1975_032_0003_teodtc_2_0_co_2.xml

Mattingly, K. S., Mote, T. L., & Fettweis, X. (2018). Atmospheric River Impacts on Greenland Ice Sheet Surface Mass Balance. *Journal of Geophysical Research: Atmospheres*, *123*(16), 8538–8560. https://doi.org/10.1029/2018JD028714

Mattingly, K. S., Turton, J. V., Wille, J. D., Noël, B., Fettweis, X., Rennermalm, Å. K., & Mote, T. L. (2023). Increasing extreme melt in northeast Greenland linked to foehn winds and atmospheric rivers. *Nature Communications*, *14*(1), 1743. https://doi.org/10.1038/s41467-023-37434-8

McCrystall, M. R., Stroeve, J., Serreze, M., Forbes, B. C., & Screen, J. A. (2021). New climate models reveal faster and larger increases in Arctic precipitation than previously projected. *Nature Communications*, *12*(1), 6765. https://doi.org/10.1038/s41467-021-27031-y

McLeod, J. T., & Mote, T. L. (2016). Linking interannual variability in extreme Greenland blocking episodes to the recent increase in summer melting across the Greenland ice sheet. *International Journal of Climatology*, *36*(3), 1484–1499. https://doi.org/10.1002/joc.4440

Medley, B., Neumann, T. A., Zwally, H. J., Smith, B. E., & Stevens, C. M. (2022). Simulations of firn processes over the Greenland and Antarctic ice sheets: 1980–2021. *The Cryosphere*, *16*(10), 3971–4011. https://doi.org/10.5194/tc-16-3971-2022

Mekis, É., Donaldson, N., Reid, J., Zucconi, A., Hoover, J., Li, Q., et al. (2018). An Overview of Surface-Based Precipitation Observations at Environment and Climate Change Canada. *Atmosphere-Ocean*, *56*(2), 71–95. https://doi.org/10.1080/07055900.2018.1433627

Metcalfe, J. R., & Goodison, B. E. (1993). A Corrected Precipitation Archive for the Northwest Territories of Canada. In *Proceedings of the Eigth Symposium on Meteorological Observations and Instrumentation* (pp. 338–343). Anaheim, California: American Meteorological Society. Retrieved from https://www.usask.ca/geography/MAGS/Data/Public_Data/precip_corr/pcpncor_e.htm

Morrison, H., de Boer, G., Feingold, G., Harrington, J., Shupe, M. D., & Sulia, K. (2012). Resilience of persistent Arctic mixed-phase clouds. *Nature Geoscience*, *5*(1), 11–17. https://doi.org/10.1038/ngeo1332

Mortin, J., Svensson, G., Graversen, R. G., Kapsch, M.-L., Stroeve, J. C., & Boisvert, L. N. (2016). Melt onset over Arctic sea ice controlled by atmospheric moisture transport. *Geophysical Research Letters*, *43*(12), 6636–6642. https://doi.org/10.1002/2016GL069330

Mosley-Thompson, E., Readinger, C. R., Craigmile, P., Thompson, L. G., & Calder, C. A. (2005). Regional sensitivity of Greenland precipitation to NAO variability. *Geophysical Research Letters*, *32*(24). https://doi.org/10.1029/2005GL024776

Mote, T. L. (2007). Greenland surface melt trends 1973–2007: Evidence of a large increase in 2007. *Geophysical Research Letters*, *34*(22). https://doi.org/10.1029/2007GL031976

Myhre, G., Alterskjær, K., Stjern, C. W., Hodnebrog, Ø., Marelle, L., Samset, B. H., et al. (2019). Frequency of extreme precipitation increases extensively with event rareness under global warming. *Scientific Reports*, *9*(1), 16063. https://doi.org/10.1038/s41598-019-52277-4

Naakka, T., Nygård, T., Vihma, T., Sedlar, J., & Graversen, R. (2019). Atmospheric moisture transport between mid-latitudes and the Arctic: Regional, seasonal and vertical distributions. *International Journal of Climatology*, *39*(6), 2862–2879. https://doi.org/10.1002/joc.5988

Neff, W. (2018). Atmospheric rivers melt Greenland. *Nature Climate Change*, *8*(10), 857–858. https://doi.org/10.1038/s41558-018-0297-4

Nellikkattil, A. B., Lee, J.-Y., Guan, B., Timmermann, A., Lee, S.-S., Chu, J.-E., & Lemmon, D. (2023). Increased amplitude of atmospheric rivers and associated extreme precipitation in ultra-high-resolution greenhouse warming simulations. *Communications Earth & Environment*, *4*(1), 1–11. https://doi.org/10.1038/s43247-023-00963-7

Nitu, R., Roulet, Y. A., Wolff, M., Rasmussen, R., Lanzinger, E., Smith, C., et al. (2018). *WMO Solid Precipitation Intercomparison Experiment (SPICE)(2012-2015)* (SPICE Final Report No. 131) (p. 1445). World Meteorological Organization. Retrieved from https://library.wmo.int/doc_num.php?explnum_id=5686

Noël, B., van de Berg, W. J., Machguth, H., Lhermitte, S., Howat, I., Fettweis, X., & van den Broeke, M. R. (2016). A daily, 1 km resolution data set of downscaled Greenland ice sheet surface mass balance (1958–2015). *The Cryosphere*, *10*(5), 2361–2377. https://doi.org/10.5194/tc-10-2361-2016

Noël, B., van de Berg, W. J., Lhermitte, S., Wouters, B., Machguth, H., Howat, I., et al. (2017). A tipping point in refreezing accelerates mass loss of Greenland's glaciers and ice caps. *Nature Communications*, *8*(1), 14730. https://doi.org/10.1038/ncomms14730

Noël, B., van de Berg, W. J., Lhermitte, S., Wouters, B., Schaffer, N., & van den Broeke, M. R. (2018). Six Decades of Glacial Mass Loss in the Canadian Arctic Archipelago. *Journal of Geophysical Research: Earth Surface*, *123*(6), 1430–1449. https://doi.org/10.1029/2017JF004304

Noël, B., van Kampenhout, L., van de Berg, W. J., Lenaerts, J. T. M., Wouters, B., & van den Broeke, M. R. (2020). Brief communication: CESM2 climate forcing (1950–2014) yields realistic Greenland ice sheet surface mass balance. *The Cryosphere*, *14*(4), 1425–1435. https://doi.org/10.5194/tc-14-1425-2020

Noël, B., Lenaerts, J. T. M., Lipscomb, W. H., Thayer-Calder, K., & van den Broeke, M. R. (2022). Peak refreezing in the Greenland firn layer under future warming scenarios. *Nature Communications*, *13*(1), 6870. https://doi.org/10.1038/s41467-022-34524-x

Norin, L., Devasthale, A., L'Ecuyer, T. S., Wood, N. B., & Smalley, M. (2015). Intercomparison of snowfall estimates derived from the CloudSat Cloud Profiling Radar and the ground-based weather radar network over Sweden. *Atmospheric Measurement Techniques*, *8*(12), 5009–5021. https://doi.org/10.5194/amt-8-5009-2015

Norris, J., Chen, G., & Neelin, J. D. (2019). Thermodynamic versus Dynamic Controls on Extreme Precipitation in a Warming Climate from the Community Earth System Model Large Ensemble. *Journal of Climate*, *32*(4), 1025–1045. https://doi.org/10.1175/JCLI-D-18-0302.1

O'Brien, T. A., Wehner, M. F., Payne, A. E., Shields, C. A., Rutz, J. J., Leung, L.-R., et al. (2022). Increases in Future AR Count and Size: Overview of the ARTMIP Tier 2 CMIP5/6 Experiment. *Journal of Geophysical Research: Atmospheres*, *127*(6), e2021JD036013. https://doi.org/10.1029/2021JD036013

Oerlemans, J., & Klok, E. J. L. (2004). Effect of summer snowfall on glacier mass balance. *Annals of Glaciology*, *38*, 97–100. https://doi.org/10.3189/172756404781815158

Otto, F. (2019). Attribution of extreme weather events: how does climate change affect weather? *Weather*, *74*(9), 325–326. https://doi.org/10.1002/wea.3610

Panetta, R. L., & Held, I. M. (1988). Baroclinic Eddy Fluxes in a One-Dimensional Model of Quasi-geostrophic Turbulence. *Journal of the Atmospheric Sciences*, *45*(22), 3354–3365. https://doi.org/10.1175/1520-0469(1988)045<3354:BEFIAO>2.0.CO;2

Parker, C. L., Mooney, P. A., Webster, M. A., & Boisvert, L. N. (2022). The influence of recent and future climate change on spring Arctic cyclones. *Nature Communications*, *13*(1), 6514. https://doi.org/10.1038/s41467-022-34126-7

Payne, A., Demory, M.-E., Leung, L., Ramos, A., Shields, C., Rutz, J., et al. (2020). Responses and impacts of atmospheric rivers to climate change. *Nature Reviews Earth & Environment*, *1*, 143–157. https://doi.org/10.1038/s43017-020-0030-5

van Pelt, W. J. J., Pohjola, V. A., & Reijmer, C. H. (2016). The Changing Impact of Snow Conditions and Refreezing on the Mass Balance of an Idealized Svalbard Glacier. *Frontiers in Earth Science*, *4*. Retrieved from https://www.frontiersin.org/articles/10.3389/feart.2016.00102

Pendergrass, A. G. (2018). What precipitation is extreme? *Science*, *360*(6393), 1072–1073. https://doi.org/10.1126/science.aat1871

Pendergrass, A. G., & Hartmann, D. L. (2014). The Atmospheric Energy Constraint on Global-Mean Precipitation Change. *Journal of Climate*, *27*(2), 757–768. https://doi.org/10.1175/JCLI-D-13-00163.1

Pendergrass, A. G., Knutti, R., Lehner, F., Deser, C., & Sanderson, B. M. (2017). Precipitation variability increases in a warmer climate. *Scientific Reports*, *7*(1), 17966. https://doi.org/10.1038/s41598-017-17966-y

Peterson, T. C., Folland, C., Gruza, G., Hogg, W., Mokssit, A., & Plummer, N. (2001). *Report on the Activities of the Working Group on Climate Change Detection and Related Rapporteurs 1998-2001* (pp. 1–143). Retrieved from https://etccdi.pacificclimate.org/docs/wgccd.2001.pdf

Pfahl, S., & Wernli, H. (2012). Quantifying the relevance of atmospheric blocking for co-located temperature extremes in the Northern Hemisphere on (sub-)daily time scales. *Geophysical Research Letters*, *39*(12). https://doi.org/10.1029/2012GL052261

Pfahl, S., Madonna, E., Boettcher, M., Joos, H., & Wernli, H. (2014). Warm Conveyor Belts in the ERA-Interim Dataset (1979–2010). Part II: Moisture Origin and Relevance for Precipitation. https://doi.org/10.1175/JCLI-D-13-00223.1

Pfahl, S., O'Gorman, P. A., & Fischer, E. M. (2017). Understanding the regional pattern of projected future changes in extreme precipitation. *Nature Climate Change*, *7*(6), 423–427. https://doi.org/10.1038/nclimate3287

Pithan, F., & Jung, T. (2021). Arctic Amplification of Precipitation Changes—The Energy Hypothesis. *Geophysical Research Letters*, *48*(21), e2021GL094977. https://doi.org/10.1029/2021GL094977

Priestley, M. D. K., & Catto, J. L. (2022). Future changes in the extratropical storm tracks and cyclone intensity, wind speed, and structure. *Weather and Climate Dynamics*, *3*(1), 337–360. https://doi.org/10.5194/wcd-3-337-2022

Ralph, F. M., Dettinger, M. D., Cairns, M. M., Galarneau, T. J., & Eylander, J. (2018). Defining "Atmospheric River": How the Glossary of Meteorology Helped Resolve a Debate. *Bulletin of the American Meteorological Society*, *99*(4), 837–839. https://doi.org/10.1175/BAMS-D-17-0157.1

Rapaić, M., Brown, R., Markovic, M., & Chaumont, D. (2015). An Evaluation of Temperature and Precipitation Surface-Based and Reanalysis Datasets for the Canadian Arctic, 1950–2010. *Atmosphere-Ocean*, *53*(3), 283–303. https://doi.org/10.1080/07055900.2015.1045825

Rasmussen, R., Baker, B., Kochendorfer, J., Meyers, T., Landolt, S., Fischer, A. P., et al. (2012). How Well Are We Measuring Snow: The NOAA/FAA/NCAR Winter Precipitation Test Bed. *Bulletin of the American Meteorological Society*, *93*(6), 811–829. https://doi.org/10.1175/BAMS-D-11-00052.1

Rawlins, M. A., Steele, M., Holland, M. M., Adam, J. C., Cherry, J. E., Francis, J. A., et al. (2010). Analysis of the Arctic System for Freshwater Cycle Intensification: Observations and Expectations. *Journal of Climate*, *23*(21), 5715–5737. https://doi.org/10.1175/2010JCLI3421.1

Rhoades, A. M., Jones, A. D., O'Brien, T. A., O'Brien, J. P., Ullrich, P. A., & Zarzycki, C. M. (2020). Influences of North Pacific Ocean Domain Extent on the Western U.S. Winter Hydroclimatology in Variable-Resolution CESM. *Journal of Geophysical Research: Atmospheres*, *125*(14), e2019JD031977. https://doi.org/10.1029/2019JD031977

Riddaway, B. (2014). Climate reanalysis. Reading, England: European Centre for Medium-Range Weather Forecasts. https://doi.org/10.21957/QNREH9T5

Rind, D., Chiou, E.-W., Chu, W., Larsen, J., Oltmans, S., Lerner, J., et al. (1991). Positive water vapour feedback in climate models confirmed by satellite data. *Nature*, *349*(6309), 500–503. https://doi.org/10.1038/349500a0

Schuenemann, K. C., & Cassano, J. J. (2010). Changes in synoptic weather patterns and Greenland precipitation in the 20th and 21st centuries: 2. Analysis of 21st century atmospheric changes using self-organizing maps. *Journal of Geophysical Research: Atmospheres*, *115*(D5). https://doi.org/10.1029/2009JD011706

Schuenemann, K. C., Cassano, J. J., & Finnis, J. (2009). Synoptic Forcing of Precipitation over Greenland: Climatology for 1961–99. *Journal of Hydrometeorology*, *10*(1), 60–78. https://doi.org/10.1175/2008JHM1014.1

Schweiger, A. J., Lindsay, R. W., Vavrus, S., & Francis, J. A. (2008). Relationships between Arctic Sea Ice and Clouds during Autumn. *Journal of Climate*, *21*(18), 4799–4810. https://doi.org/10.1175/2008JCLI2156.1

Scoccimarro, E., & Gualdi, S. (2020). Heavy Daily Precipitation Events in the CMIP6 Worst-Case Scenario: Projected Twenty-First-Century Changes. *Journal of Climate*, *33*(17), 7631–7642. https://doi.org/10.1175/JCLI-D-19-0940.1

Screen, J. A., & Simmonds, I. (2010). The central role of diminishing sea ice in recent Arctic temperature amplification. *Nature*, *464*(7293), 1334–1337. https://doi.org/10.1038/nature09051

Seager, R., Naik, N., & Vecchi, G. A. (2010). Thermodynamic and Dynamic Mechanisms for Large-Scale Changes in the Hydrological Cycle in Response to Global Warming. *Journal of Climate*, *23*(17), 4651–4668. https://doi.org/10.1175/2010JCLI3655.1

Serreze, M. C., Carse, F., Barry, R. G., & Rogers, J. C. (1997). Icelandic Low Cyclone Activity: Climatological Features, Linkages with the NAO, and Relationships with Recent Changes in the Northern Hemisphere Circulation. *Journal of Climate*, *10*(3), 453–464. https://doi.org/10.1175/1520-0442(1997)010<0453:ILCACF>2.0.CO;2

Serreze, M. C., Barrett, A. P., Stroeve, J. C., Kindig, D. N., & Holland, M. M. (2009). The emergence of surface-based Arctic amplification. *The Cryosphere*, *3*(1), 11–19. https://doi.org/10.5194/tc-3-11-2009

Serreze, M. C., Barrett, A. P., & Stroeve, J. (2012). Recent changes in tropospheric water vapor over the Arctic as assessed from radiosondes and atmospheric reanalyses. *Journal of Geophysical Research: Atmospheres*, *117*(D10). https://doi.org/10.1029/2011JD017421

Serreze, M. C., Crawford, A. D., & Barrett, A. P. (2015). Extreme daily precipitation events at Spitsbergen, an Arctic Island. *International Journal of Climatology*, *35*(15), 4574–4588. https://doi.org/10.1002/joc.4308

Serreze, M. C., Voveris, J., Barrett, A. P., Fox, S., Blanken, P. D., & Crawford, A. (2022). Characteristics of extreme daily precipitation events over the Canadian Arctic. *International Journal of Climatology*, *42*(16), 10353–10372. https://doi.org/10.1002/joc.7907

Sevruk, B., & Klemm, S. (1989). *Catalogue of National Standard Precipitation Gauges* (WMO/TD- No. 313 No. IOM Report-No. 39) (p. 50). World Meteorological Organization. Retrieved from https://library.wmo.int/index.php?lvl=notice_display&id=11246#.YF35IGRudB0

Shaw, T. A., Baldwin, M., Barnes, E. A., Caballero, R., Garfinkel, C. I., Hwang, Y.-T., et al. (2016). Storm track processes and the opposing influences of climate change. *Nature Geoscience*, *9*(9), 656–664. https://doi.org/10.1038/ngeo2783

Shea, J. M., Anslow, F. S., & Marshall, S. J. (2005). Hydrometeorological relationships on Haig Glacier, Alberta, Canada. *Annals of Glaciology*, *40*, 52–60. https://doi.org/10.3189/172756405781813465

Skific, N., Francis, J. A., & Cassano, J. J. (2009). Attribution of Seasonal and Regional Changes in Arctic Moisture Convergence. *Journal of Climate*, *22*(19), 5115–5134. https://doi.org/10.1175/2009JCLI2829.1

Smith, D. M., Eade, R., Andrews, M. B., Ayres, H., Clark, A., Chripko, S., et al. (2022). Robust but weak winter atmospheric circulation response to future Arctic sea ice loss. *Nature Communications*, *13*(1), 727. https://doi.org/10.1038/s41467-022-28283-y

Stroeve, J., & Notz, D. (2018). Changing state of Arctic sea ice across all seasons. *Environmental Research Letters*, *13*(10), 103001. https://doi.org/10.1088/1748-9326/aade56

Stroeve, J., Holland, M. M., Meier, W., Scambos, T., & Serreze, M. C. (2007). Arctic sea ice decline: Faster than forecast. *Geophysical Research Letters*, *34*(9). https://doi.org/10.1029/2007GL029703

Stroeve, J., Serreze, M. C., Barrett, A., & Kindig, D. N. (2011). Attribution of recent changes in autumn cyclone associated precipitation in the Arctic. *Tellus A: Dynamic Meteorology and Oceanography*, *63*(4), 653–663. https://doi.org/10.1111/j.1600-0870.2011.00515.x

Strong, C., & Magnusdottir, G. (2008). Tropospheric Rossby Wave Breaking and the NAO/NAM. *Journal of the Atmospheric Sciences*, *65*(9), 2861–2876. https://doi.org/10.1175/2008JAS2632.1

Stull, R. (2017). Water Vapor. In *Practical Meteorology An Algebra-based Survey of Atmospheric Science* (1.02b, pp. 87–118). University of British Columbia. Retrieved from https://www.eoas.ubc.ca/books/Practical_Meteorology/

Talagrand, O. (2010). Variational Assimilation. In *Data Assimilation* (pp. 41–67). Berlin, Heidelberg: Springer. Retrieved from https://indico.fysik.su.se/event/2654/attachments/1559/1708/Talagrand.2010.pdf

Teng, X., Ding, M., Sun, W., Wang, L., Wang, Y., Kang, L., & Huai, B. (2025). Summer Extreme Rainfall Events Intensify Southern Greenland Ice Sheet Melt. *Journal of Geophysical Research: Atmospheres*, *130*(13), e2025JD043953. https://doi.org/10.1029/2025JD043953

Thompson, D. W. J., & Wallace, J. M. (1998). The Arctic oscillation signature in the wintertime geopotential height and temperature fields. *Geophysical Research Letters*, *25*(9), 1297–1300. https://doi.org/10.1029/98GL00950

Thompson, D. W. J., & Wallace, J. M. (2001). Regional Climate Impacts of the Northern Hemisphere Annular Mode. *Science*, *293*(5527), 85–89. https://doi.org/10.1126/science.1058958

Thompson-Munson, M., Kay, J. E., Markle, B. R., Bertrand, L., & Gallagher, M. R. (2025). An Observational Constraint for Future Greenland Rain in a Warmer Atmosphere. *Geophysical Research Letters*, *52*(5), e2025GL114710. https://doi.org/10.1029/2025GL114710

Trenberth, K. E., Dai, A., Rasmussen, R. M., & Parsons, D. B. (2003). The Changing Character of Precipitation. *Bulletin of the American Meteorological Society*, *84*(9), 1205–1218. https://doi.org/10.1175/BAMS-84-9-1205

Valkonen, E., Cassano, J., & Cassano, E. (2021). Arctic Cyclones and Their Interactions With the Declining Sea Ice: A Recent Climatology. *Journal of Geophysical Research: Atmospheres*, *126*(12), e2020JD034366. https://doi.org/10.1029/2020JD034366

Vavrus, S. (2004). The Impact of Cloud Feedbacks on Arctic Climate under Greenhouse Forcing. *Journal of Climate*, *17*(3), 603–615.

Vavrus, S. J. (2013). Extreme Arctic cyclones in CMIP5 historical simulations. *Geophysical Research Letters*, *40*(23), 6208–6212. https://doi.org/10.1002/2013GL058161

Vihma, T., Screen, J., Tjernström, M., Newton, B., Zhang, X., Popova, V., et al. (2016). The atmospheric role in the Arctic water cycle: A review on processes, past and future changes, and their impacts. *Journal of Geophysical Research: Biogeosciences*, *121*(3), 586–620. https://doi.org/10.1002/2015JG003132

Villamil-Otero, G. A., Zhang, J., He, J., & Zhang, X. (2018). Role of extratropical cyclones in the recently observed increase in poleward moisture transport into the Arctic Ocean. *Advances in Atmospheric Sciences*, *35*(1), 85–94. https://doi.org/10.1007/s00376-017-7116-0

de Vries, A. J. (2021). A global climatological perspective on the importance of Rossby wave breaking and intense moisture transport for extreme precipitation events. *Weather and Climate Dynamics*, *2*(1), 129–161. https://doi.org/10.5194/wcd-2-129-2021

Wagner, D. N., Shupe, M. D., Persson, O. G., Uttal, T., Frey, M. M., Kirchgaessner, A., et al. (2021). Snowfall and snow accumulation processes during the MOSAiC winter and spring season. *The Cryosphere Discussions*, 1–48. https://doi.org/10.5194/tc-2021-126

Walsh, J. E., Ballinger, T. J., Euskirchen, E. S., Hanna, E., Mård, J., Overland, J. E., et al. (2020). Extreme weather and climate events in northern areas: A review. *Earth-Science Reviews*, *209*, 103324. https://doi.org/10.1016/j.earscirev.2020.103324

Wang, H.-R., Li, F.-F., Grigorev, G. V., Yao, Z.-Y., Ge, D., Wang, G.-Q., & Qiu, J. (2024). Occurrence Frequency of Global Atmospheric River (AR) Events: A Data Fusion Analysis of 12 Identification Data Sets. *Journal of Geophysical Research: Atmospheres*, *129*(5), e2023JD039730. https://doi.org/10.1029/2023JD039730

Warren, S. G. (1982). Optical properties of snow. *Reviews of Geophysics*, *20*(1), 67–89. https://doi.org/10.1029/RG020i001p00067

WCRP. (2021). Expert Team on Climate Change Detection and Indices (ETCCDI). Retrieved July 6, 2025, from https://www.wcrp-climate.org/etccdi

Wei, T., Noël, B., Ding, M., & Yan, Q. (2022). Spatiotemporal variations of extreme events in surface mass balance over Greenland during 1958–2019. *International Journal of Climatology*. https://doi.org/10.1002/joc.7689

Wernli, H., & Davies, H. C. (1997). A Lagrangian-based analysis of extratropical cyclones. I: The method and some applications. *Quarterly Journal of the Royal Meteorological Society*, *123*(538), 467–489. https://doi.org/10.1002/qj.49712353811

Wille, J. D., Favier, V., Gorodetskaya, I. V., Agosta, C., Baiman, R., Barrett, J. E., et al. (2025). Atmospheric rivers in Antarctica. *Nature Reviews Earth & Environment*, 1–15. https://doi.org/10.1038/s43017-024-00638-7

Wood, N. B. (2011). *ESTIMATION OF SNOW MICROPHYSICAL PROPERTIES WITH APPLICATION TO MILLIMETER-WAVELENGTH RADAR RETRIEVALS FOR SNOWFALL RATE* (Dissertation). Colorado State University, Fort Collins, CO, USA. Retrieved from https://mountainscholar.org/handle/10217/48170

Woods, C., Caballero, R., & Svensson, G. (2013). Large-scale circulation associated with moisture intrusions into the Arctic during winter. *Geophysical Research Letters*, *40*(17), 4717–4721. https://doi.org/10.1002/grl.50912

Yang, D., Goodison, B. E., Metcalfe, J. R., Golubev, V. S., Elomaa, E., Gunther, T., et al. (1995). Accuracy of Tretyakov Precipitation Gauge: Result of WMO Intercomparison. *Hydrological Processes*, *9*(8), 877–895. https://doi.org/10.1002/hyp.3360090805

Yang, D., Kane, D. L., Hinzman, L. D., Goodison, B. E., Metcalfe, J. R., Louie, P. Y. T., et al. (2000). An evaluation of the Wyoming Gauge System for snowfall measurement. *Water Resources Research*, *36*(9), 2665–2677. https://doi.org/10.1029/2000WR900158

Yettella, V., & Kay, J. E. (2017). How will precipitation change in extratropical cyclones as the planet warms? Insights from a large initial condition climate model ensemble. *Climate Dynamics*, *49*(5), 1765–1781. https://doi.org/10.1007/s00382-016-3410-2

Yu, L., & Zhong, S. (2021). Trends in Arctic seasonal and extreme precipitation in recent decades. *Theoretical and Applied Climatology*, *145*(3), 1541–1559. https://doi.org/10.1007/s00704-021-03717-7

Zahn, M., Akperov, M., Rinke, A., Feser, F., & Mokhov, I. I. (2018). Trends of Cyclone Characteristics in the Arctic and Their Patterns From Different Reanalysis Data. *Journal of Geophysical Research: Atmospheres*, *123*(5), 2737–2751. https://doi.org/10.1002/2017JD027439

Zhang, P., Chen, G., Ma, W., Ming, Y., & Wu, Z. (2021). Robust Atmospheric River Response to Global Warming in Idealized and Comprehensive Climate Models. *Journal of Climate*, *34*(18), 7717–7734. https://doi.org/10.1175/JCLI-D-20-1005.1

Zwally, H. J., & Jun, L. (2002). Seasonal and interannual variations of firn densification and ice-sheet surface elevation at the Greenland summit. *Journal of Glaciology*, *48*(161), 199–207. https://doi.org/10.3189/172756502781831403

Chapter 3 Extreme Precipitation in the Eastern Canadian Arctic and Greenland: An Evaluation of Atmospheric Reanalyses

Nicole A. Loeb[1,2], Alex Crawford[1], Julienne C. Stroeve[1,3,4], John Hanesiak[1,2]

[1]Centre for Earth Observation Science, Clayton H. Riddell Faculty of Environment, Earth, and Resources, University of Manitoba, Winnipeg, Manitoba, Canada

[2]Department of Environment and Geography, Clayton H. Riddell Faculty of Environment, Earth, and Resources, University of Manitoba, Winnipeg, Manitoba, Canada

[3]Department of Earth Sciences, University College London, London, United Kingdom

[4]National Snow and Ice Data Center, Cooperative Institute for Research in Environmental Sciences, University of Colorado Boulder, Boulder, Colorado, USA

This chapter was published in Frontiers in Environmental Science.

Loeb, N. A., Crawford, A., Stroeve, J. C., & Hanesiak, J. (2022). Extreme Precipitation in the Eastern Canadian Arctic and Greenland: An Evaluation of Atmospheric Reanalyses. *Frontiers in Environmental Science*, *10*. https://www.doi.org/10.3389/fenvs.2022.866929

Abstract

Extreme precipitation events are becoming more common in the Arctic as the climate warms, but characterizing these events is notoriously challenging. Atmospheric reanalyses have become popular tools for climate studies in data-sparse regions such as the Arctic. While modern reanalyses have been shown to perform reasonably well at reproducing Arctic climate, their ability to represent extreme precipitation events has not been investigated in depth. In this study, three of the most recent reanalyses, ERA-5, MERRA-2, and CFSR, are compared to surface precipitation observations in the Eastern Canadian Arctic and Greenland from 1980-2016 to assess how well they represent the most intense observed events. Overall, the reanalyses struggled to match observed accumulations from individual events ($-0.11 \leq r \leq 0.47$) but matched the observed seasonality of precipitation extremes. The region with the strongest match between observations and reanalyses was Southwest Greenland. Performance varies by event, and the best match between reanalyses and station observations may have a spatial/temporal offset (up to one grid cell or one day). The three products saw similar performance in general; however, ERA-5 tends to see slightly higher correlations and lower biases than MERRA-2 or CFSR. Considering the limitations of in situ observations, these results suggest that the reanalyses are capable of representing aggregate extreme precipitation (e.g., seasonal or annual time scales), but struggle to consistently match the timing and location of specific observed events.

3.1 Introduction

In situ precipitation measurements are notoriously difficult to obtain in the Arctic. Factors that increase their uncertainty include systematic errors due to instrument design and specifications

(e.g., Collier 2000; Jain and Singh 2003), gauge undercatch (e.g., Goodison, Louie, and Yang 1998; Wagner et al. 2021), and wetting loss (e.g., Collier 2000; Groisman and Legates 1994), along with a relatively sparse observational network (Serreze and Barry 2011). Satellite-based precipitation retrieval methods have been developed since the 1990s (Levizzani, Laviola, and Cattani 2011), providing a broader spatial estimate of precipitation patterns, yet uncertainty remains due in part to microphysical assumptions and lack of ground truth (e.g., Levizzani, Laviola, and Cattani 2011; Liu and Curry 1997). In addition to uncertainties associated with measurement methods, precipitation has low spatial autocorrelation (Jones 2013). These issues combined with a generally sparse surface observational network (Mekis and Vincent 2011; Xie and Arkin 1997) make it challenging to obtain spatially and temporally continuous datasets that are representative of the Arctic region via interpolation. Because of this, atmospheric retrospective analyses, or reanalyses, have become a very popular tool for climate studies in the Arctic where observations are lacking.

Atmospheric reanalyses are produced by numerical models run over a specified historical time-period that assimilate observations at regular intervals to ensure that the model remains close to observed conditions (Riddaway 2014). These products are designed to provide a more spatially and temporally homogeneous record of atmospheric variables (Riddaway 2014). The use of a model means that many observations can be used, sometimes numbering in the millions, and ensures that observations will be incorporated and interpreted consistently (Parker 2016). Spatial and temporal gaps are filled on a physical and dynamical basis rather than interpolation alone, which can help maintain realistic patterns (Parker 2016).

Given the general paucity of observational networks, reanalyses are commonly used to assess precipitation patterns and amounts in the Arctic and Antarctic (Bengtsson et al. 2011; Boisvert et al. 2018; Koyama and Stroeve 2019; Rapaić et al. 2015). Several studies have evaluated the veracity of various reanalysis data products (e.g., Barrett, Stroeve, and Serreze 2020; Boisvert et al. 2018). In terms of precipitation, there is generally more spread between reanalyses in total precipitation and snowfall amounts than other variables, such as air temperature, because of limited observations for data assimilation and thus more dependence on model setup in addition to the high variability seen in precipitation patterns. Several studies have found that most reanalyses exhibit a warm and wet bias in the Arctic, producing rain rather than snow and more precipitation overall (e.g., Barrett, Stroeve, and Serreze 2020; Boisvert et al. 2018; Lindsay et al. 2014; Rapaić et al. 2015). While reanalyses can help to fill in observational gaps, they produce accumulations representing the average over an area, meaning they are not expected to match point observations and may lose representation of sub-grid resolution extremes.

While previous studies have assessed the general performance of reanalyses in the Arctic, how well these products reproduce observed extreme precipitation events remains unknown. It is vital to understand how well current products represent extreme precipitation events because slight changes in mean precipitation conditions can cause a more significant shift in the intensity and frequency of extreme events an area receives (e.g., Pendergrass 2018). Reanalyses are commonly used as forcing datasets for regional climate models, so their performance can directly impact the quality of climate projections. With shrinking Arctic sea ice cover, the potential for extreme precipitation in the Arctic may increase substantially (Landrum & Holland, 2020; McCrystall et al., 2021). However, climate models currently produce less realistic extreme precipitation in the Arctic than the mid-latitudes (Abdelmoaty et al., 2021). This amplifies the need to better understand and represent extreme precipitation in atmospheric reanalyses.

The eastern Canadian Arctic and Greenland region is particularly vulnerable to changes in extreme events because of the risk they pose to the Indigenous communities of the region and the substantial amount of land ice nearby. Changes to these events could have substantial impacts on the physical climate system and severe implications for local communities through increased flooding and degradation of permafrost (Rinke et al. 2012), which can threaten infrastructure (Ford et al., 2010) and access to both traditional and western food sources (Ford, 2009). Additionally, these events can cause abrupt increases or decreases in the surface mass balance (SMB) of the region's land ice. Doyle et al. (2015) suggested that the late-summer timing of an extreme precipitation event in Western Greenland led to widespread ice flow acceleration and a more substantial mass loss from the Greenland Ice Sheet. On the other hand, Oerlemans and Klok (2004) illustrated how a heavy summer snowfall event dramatically reduced melt due to the increased albedo of the fresh snow cover on a glacier in Switzerland. As such, the difference in the timing, intensity, or frequency of extreme events can substantially impact the SMB of glaciers and ice caps. Given the Greenland Ice Sheet and glaciers and ice caps of the eastern Canadian Arctic account for approximately 11% of global land ice mass (Bamber et al., 2018), understanding SMB changes in response to a warming Arctic is essential. Recent projections estimate that Greenland Ice Sheet melt will contribute 10.2 ± 4.8 cm (Hofer et al., 2020) over the 21st century under a moderate warming scenario, with the Canadian Arctic contributing an additional 0.35 ± 0.24 mm yr^{-1} (Lenaerts et al., 2013).

In this paper, the most recent reanalyses from the European Centre for Medium-Range Weather Forecasts (ECMWF), the National Aeronautics and Space Administration (NASA), and the National Centers for Environmental Prediction (NCEP) are compared to station precipitation observations in the Eastern Canadian Arctic Archipelago and Greenland for 1980-2016 to assess agreement in extreme precipitation events. The selected products do not assimilate surface precipitation observations. Similarities and differences between reanalyses regarding seasonal and spatial variability of extreme precipitation are investigated. Finally, a case study details performance of these reanalyses during the event highlighted in Doyle et al. (2015).

3.2 Materials and Methods

3.2.1 Reanalyses

3.2.1.1 ERA-5

ERA-5 is the fifth-generation reanalysis product from the ECMWF (Hersbach et al., 2020). Hourly data is available from 1979 to 2021 on a 0.25° × 0.25° grid (Hersbach et al., 2020). ERA-5 provides improved spatial and temporal resolution and an increase in the number of observations assimilated relative to its predecessor, ERA-Interim (Hersbach et al., 2020). The most notable change with respect to the previous generation is the increase in vertical atmospheric layers represented in the model from 60 to 137 (Hersbach et al., 2020). This increase in vertical resolution has been shown to improve the representation of processes in the upper atmosphere (Barrett et al., 2020). Other changes include improvements to the 4D-Var data assimilation system and more observations assimilated into the model (Hennermann & Giusti, 2021). ERA-5 has also been shown to produce a more realistic representation of the near-surface climate of Greenland than ERA-Interim, though the differences between the two were not substantial (Delhasse et al., 2020).

3.2.1.2 MERRA-2

MERRA-2 is the second-generation version of NASA's Modern-Era Retrospective analysis for Research and Applications (Gelaro et al., 2017). Data is provided on a 0.5° × 0.625° grid with 72 hybrid-eta vertical levels and version 5.12.4. of the Goddard Earth Observing System data assimilation system (Bosilovich et al., 2015; Gelaro et al., 2017). MERRA-2 was designed to build upon shortcomings of the first-generation product, namely, to decrease imbalances in the water cycle, reduce erroneous abrupt changes in precipitation, and incorporate new satellite observations (Gelaro et al., 2017). Previous analysis of MERRA-2 precipitation in the Arctic showed that it is often wetter than observations, particularly producing too much light precipitation (e.g., Barrett, Stroeve, and Serreze 2020; Boisvert et al. 2018).

3.2.1.3 CFSR

The NCEP Climate Forecast System Reanalysis (CFSR) was developed to improve upon the first version of the Climate Forecast System (Saha et al., 2010). CFSR covers the period of 1979-2009 with a 0.5° × 0.5° spatial resolution poleward of 30° (Saha et al., 2010). While it works as a stand-alone data product, it was designed to provide consistent and stable calibration for the second version of the Climate Forecast System (CFSv2), which became operational in 2011 (Saha et al., 2014). Both CFSR and CFSv2 are spectral models with 64 sigma-pressure hybrid levels (Saha et al., 2014). While some slight differences exist between CFSR and CFSv2, discontinuities are minimal (Barrett et al., 2020; Saha et al., 2014), so they are used in concert to provide a continuous record from 1979-2009 and will be referred to collectively as CFSR for simplicity.

3.2.1.4 Observations

Canadian observations were retrieved from the Second Generation Adjusted Daily Precipitation Dataset, detailed in Mekis & Vincent (2011). Data is available from station installation until 2016. This dataset includes daily rainfall gauge and snowfall ruler observations for 464 stations that have been adjusted manually to account for common issues. Most of the selected stations are protected, meaning that they cannot be closed in the near future. Rainfall observations were corrected for wind undercatch, evaporation, and retention with unique corrections applied to each type of rain gauge used (copper MSC, plastic MSC, and Type B gauges). Snow-water equivalent (SWE) was calculated using spatially-varied fresh snow density values determined based on concurrent Nipher gauge and snow ruler observations from 175 climatological stations with over 20 years of data (Mekis & Brown, 2010). Stations were selected to be included in the dataset based on the availability of manual snowfall and rainfall measurements and the length of observational records. No observations from automated gauges were included in the dataset.

Synoptic station precipitation observations for Greenland were retrieved from the Danish Meteorological Institute (Cappelen et al., 2014). This dataset provides observations from 88 surface stations across Greenland for 1958-2013. The temporal resolution varies between stations from hourly to daily. Most included stations are automated. Quality control was performed

manually to ensure the removal of erroneous data from issues such as frozen instrumentation or calibration errors (Boas & Wang, 2011). Raw 24 h accumulations were corrected for wind-induced undercatch following the Yang et al. (1999) method, which factors precipitation phase and windspeed into the calculation of bias. Precipitation phase is not explicitly included in the observations so a simple temperature-based threshold is used to determine phase, as in Koyama and Stroeve (2019). If all the day's observations are above (below) 0°C, it is designated as rain (snow); otherwise, it is mixed precipitation.

In this study, 18 stations are used from the Canadian dataset and 21 stations from Greenland. Details of each station included in the analysis are shown in Table A.1. It must be noted that because the corrections applied to the two datasets differ, it is not possible to make direct comparison of reanalysis biases between Canada and Greenland. However, relative comparisons of performance can still be made.

3.2.2 Methodology

The study region was split into subregions to help illustrate spatial differences in performance (Figure 3.1). Baffin and Ellesmere Islands were selected as subregions of interest in the Canadian Arctic Archipelago. Greenland was divided into subregions following glacier regimes and surface mass balance characteristics (Rignot et al., 2011; Rignot & Mouginot, 2012). These basins were introduced in the European Space Agency's 2016 Ice sheet Mass Balance Intercomparison Exercise. Since the observational network is relatively sparse, some regions have little data available. The northern (NO) Greenland subregion has no stations and was not included in the analysis. All other subregions were included; however, several subregions have few stations available (particularly, NW and SE Greenland), meaning that the analysis performed may be less robust.

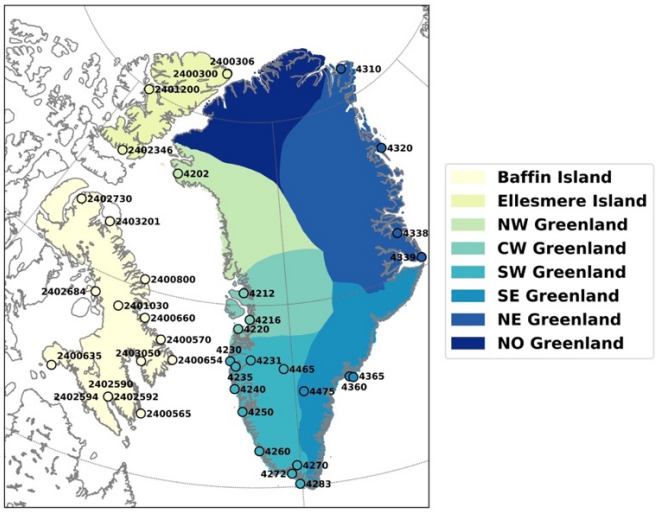

Figure 3.1. Map of the study region. Coloured circles show station locations within each subregion.

In this study, an extreme event is defined as the top 5% of daily precipitation totals where at least 1 mm of accumulation occurred, which is one of the definitions outlined in Pendergrass

(2018). Extreme event occurrence is compared between products and subregions using a normalized event frequency (f_e);

$$f_e = \frac{N_e}{N_o} \times 365 = \frac{\sum_i n_{e,i}}{\sum_i n_{o,i}} \times 365 \quad (3.1)$$

where N_e and N_o represent the total number of extreme events and daily observations, respectively, in a subregion. The extreme event threshold for each station (i) is calculated relative to the observations and then applied to the corresponding grid cell in each reanalysis product to find the local number of extreme events. Each subregion's normalized event frequency (f_e) is then calculated as a weighted average: the sum of station event frequency (n_e) divided by the sum of station observations (n_o). Values of N_e and N_o used in Equation 3.1 can be found in Table 3.1.

Table 3.1. Number of stations (N_s), observations (N_o), and extreme events (N_e) within each subregion.

Region	N_s [stations]	N_o [days]	N_e [days]
Baffin Island	14	74888	843
Ellesmere Island	4	33870	219
NW Greenland	1	8325	41
CW Greenland	3	16343	152
SW Greenland	10	65068	750
NE Greenland	4	30055	241
SE Greenland	3	13659	175

Extreme events are, by definition, rare, and fewer than 20% of all stations in this region have timeseries exceeding thirty years. To obtain sufficient data, stations were combined within subregions for statistical comparisons. However, observations from nearby stations are not entirely independent, so any statistical error is likely an underestimate. Statistical comparisons are performed for the days with accumulations greater than the extreme threshold at each station and its corresponding grid cell in each product. Again, the threshold for extremes at each station is defined using only the observations. Taylor diagrams are created that show the Pearson correlation coefficient, root-mean-square error (RMSE) between each reanalysis and the observations, and the standard deviation of each product (Taylor, 2001).

To assess potential spatial offsetting, a three-by-three cell group centered on each station is analyzed. Similarly, three-day running accumulations are examined to account for single-day offsets in the timing of events. Details of these tests can be found in the Figures A.1-3. The extreme threshold of each product is also compared to the observations to illustrate differences in the distributions. The Heidke skill score (HSS) is used to compare the occurrence of extreme days between the reanalyses and observations (Doswell et al., 1990). The HSS is a skill score for categorical forecasts with correct results that occur due to chance taken into account. It is calculated based on a 2 x 2 contingency table (Table 3.2) and the following equation;

$$HSS = \frac{2(AD - BC)}{(A + B)(B + D) + (A + C)(C + D)} \tag{3.2}$$

where the variables are those of the contingency table (Hyvärinen, 2014). For rare events, the contingency table is dominated by correct non-occurrences (D), causing the HSS to be artificially lowered. In this case, an approximation of the HSS can be used

$$HSS \approx \frac{2A}{2A + B + C} \tag{3.3}$$

which removes the bias due to the event's rarity (Doswell et al., 1990). This approximation is used for assessing reanalysis performance for extreme events since correct non-extreme detections comprise the vast majority of the dataset.

Table 3.2. 2 x 2 contingency table.

	Observations		
Reanalysis		Extreme	Non-extreme
	Extreme	A	B
	Non-extreme	C	D

Spatial comparisons are also performed to compare the performance of the reanalyses to each other and determine the relative importance of extreme events to overall precipitation across the domain. These comparisons are based on the extreme threshold of each product since observations are not available across much of the domain, so only relative comparisons can be made. Additionally, perfect matches with station observations are not expected due to the spatial averaging inherent to the reanalyses.

3.3 Results

3.3.1 Climatological Comparisons

Table 3.3 summarizes daily accumulations constituting an extreme event and f_e in each region. Threshold values in Table 3.3 represent the weighted mean of extreme accumulations at each station (thresholds for each station provided in Table A.2). Overall, the reanalyses reproduced extreme event thresholds similar to the observational data, generally within 5 mm. The normalized event frequency saw higher variability, particularly in SE Greenland, where the reanalyses produced higher frequencies. Here, two of the three stations see many more days with at least 1 mm of accumulation than observed, causing large differences in the calculated event frequency (Table A.2). While these frequencies provide an estimate of how often extreme events occur, it must be noted that the low sample size in some subregions adds uncertainty.

Table 3.3. Extreme daily accumulation thresholds and the event frequency for each subregion relative to the observational threshold. Extreme thresholds are the mean of the individual thresholds from each station in the region weighted by the station's number of observations.

	Extreme Threshold [mm]				f_e [events (yr)$^{-1}$]			
Subregion	*Obs.*	*ERA-5*	*MERRA-2*	*CFSR*	*Obs.*	*ERA-5*	*MERRA-2*	*CFSR*
Baffin Island	14.3	11.4	10.6	10.4	4.1	3.0	2.8	2.6
Ellesmere Island	10.0	7.0	8.4	8.1	2.4	0.9	2.5	3.1
NW Greenland	11.2	12.4	10.0	10.9	1.8	5.0	2.9	4.5
CW Greenland	14.2	11.0	11.5	12.4	4.0	2.0	3.0	4.4
SW Greenland	22.3	17.9	20.7	18.6	4.4	3.7	6.3	4.4
NE Greenland	15.4	17.4	15.6	14.5	3.0	6.3	5.2	4.8
SE Greenland	21.2	23.3	25.6	26.0	4.8	14.5	16.9	18.8

The relationship between reanalysis and station-measured accumulation for each subregion is summarized in Figure 3.2. In CW and SW Greenland, CFSR has a higher standard deviation and RMSE than the other reanalyses. On the other hand, ERA-5 tends to have a lower RMSE than the other reanalyses and similar standard deviations to observations, particularly in SW and SE Greenland. While some regions have considerable performance differences, NE Greenland saw an almost equivalent performance from all three reanalyses.

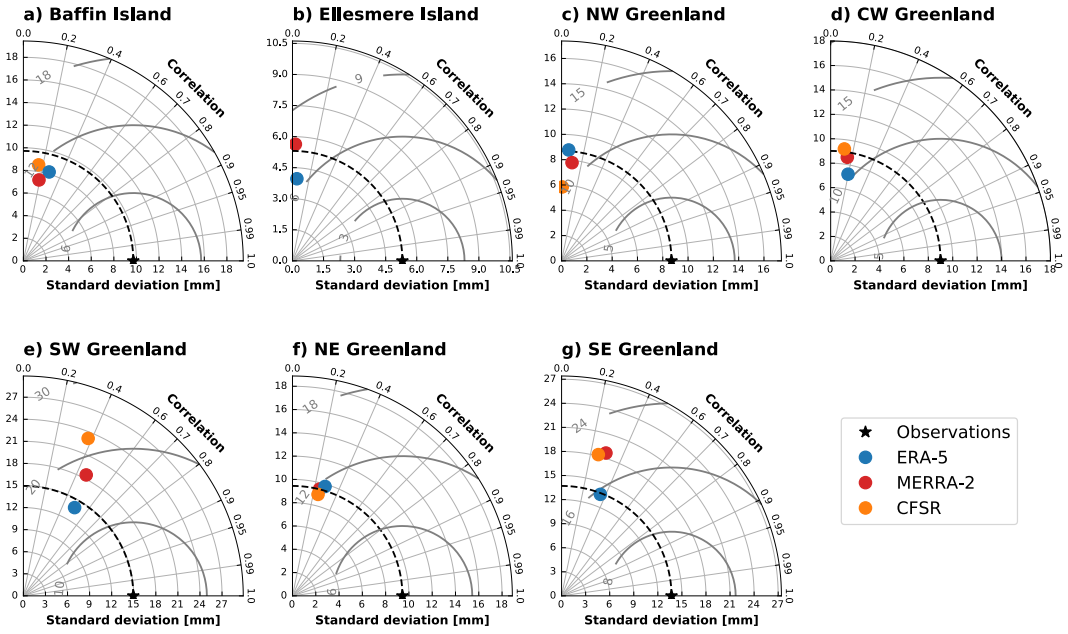

Figure 3.2. Taylor diagrams comparing accumulations for extreme events between products in each subregion. CFSR is not visible in b) due to the correlation falling below 0 and ERA-5 is overlain by MERRA-2 in f).

Correlations between reanalyses and the observations for extreme precipitation days were poor to moderate in each subregion (Table 3.4). The 95% confidence interval (CI) for each

subregion is provided in Table A.3. However, recall that because of how data are processed, these confidence intervals are likely underestimates. The highest correlations are seen in SW Greenland, with all products showing correlations between 0.34 and 0.47. While the correlations are relatively low, Table 3.4 shows that the correlations for all daily precipitation are typically 0.10-0.30 higher than that of extremes, with the smallest differences seen in SW Greenland. One notable exception is the substantial drop in correlation that each product exhibits for extremes over Ellesmere Island and NW Greenland; the correlation is moderate for all daily observations but becomes approximately zero when only extreme events are considered.

Table 3.4. Correlation coefficient between the reanalyses and observations for precipitation amounts in each subregion. Values in the overall column represent the correlations between the reanalyses and observations for all precipitation days with at least 1 mm of accumulation, while the extreme events column only includes days at or above the observed extreme threshold.

	Overall Correlation			**Extreme Event Correlation**		
Subregion	*ERA-5*	*MERRA-2*	*CFSR*	*ERA-5*	*MERRA-2*	*CFSR*
Baffin Island	0.48	0.43	0.36	0.23	0.14	0.13
Ellesmere Island	0.36	0.29	0.19	0.02	-0.01	-0.11
NW Greenland	0.27	0.26	0.29	-0.03	-0.05	-0.03
CW Greenland	0.46	0.37	0.41	0.20	0.17	0.12
SW Greenland	0.60	0.54	0.49	0.47	0.41	0.34
NE Greenland	0.42	0.38	0.37	0.23	0.23	0.21
SE Greenland	0.50	0.47	0.49	0.31	0.26	0.22

Table 3.5 shows the results of the HSS analysis. The HSS values for extreme events range from 0.15 to 0.58. While these results are generally higher than the correlations for extreme events, the agreement with observations generally remains poor. This indicates that the reanalyses struggle in reproducing events on the same days as observed. However, SW and SE Greenland produce relatively high HSS (> 0.50), which is notably higher than any of the other subregions (HSS ≤ 0.32). Here, the HSS of extreme events is almost equal to that of all precipitation events. It can also be noted that the HSS of extreme events in the other subregions was roughly half that of the broader precipitation days shown in Table 3.5, suggesting that the reanalyses particularly struggle with matching dates of extreme events, rather than all precipitation.

Table 3.5. HSS for the reanalyses in each subregion. $HSS_{\geq 1mm}$ refers to that of all precipitation days with at least 1 mm of accumulation (Equation 3.2), and ($HSS_{extreme}$) refers to extreme events using (Equation 3.3).

	$HSS_{\geq 1mm}$			**$HSS_{extreme}$**		
Subregion	*ERA-5*	*MERRA-2*	*CFSR*	*ERA-5*	*MERRA-2*	*CFSR*
Baffin Island	0.50	0.45	0.45	0.30	0.24	0.21
Ellesmere Island	0.46	0.40	0.35	0.22	0.16	0.14
NW Greenland	0.36	0.33	0.32	0.17	0.15	0.19
CW Greenland	0.52	0.51	0.53	0.28	0.22	0.32
SW Greenland	0.55	0.50	0.52	0.58	0.53	0.55
NE Greenland	0.59	0.54	0.53	0.25	0.21	0.19
SE Greenland	0.55	0.49	0.51	0.53	0.51	0.50

Figure 3.3 demonstrates the seasonality of extremes by subregion seen in each product normalized by the number of events. While the HSS showed that the reanalyses failed to match event days accurately, the seasonality of events matches quite well between the products and observations. Some subregions have almost perfect agreement, such as SW Greenland. The most notable differences are a negative bias in SE Greenland during the winter that becomes positive in spring, and a positive bias in Baffin and Ellesmere Islands during the summer and early autumn months.

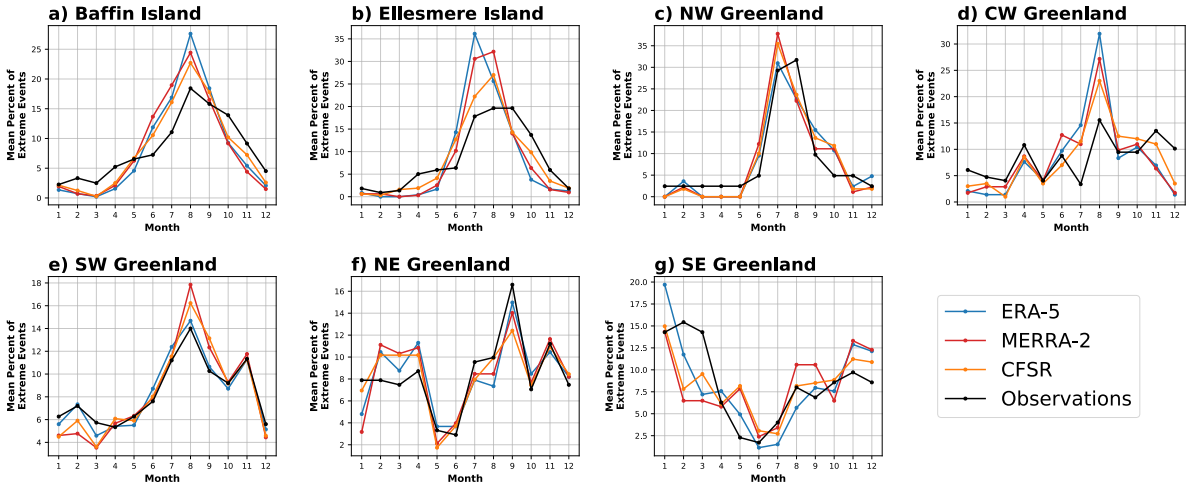

Figure 3.3. Percent of all extreme events in each product occurring in each month for all subregions.

The distribution of the mean percentage of annual precipitation attributed to extreme events across the domain is shown in Figure 3.4. Here, values are relative to the extreme threshold for each grid cell rather than that of station observations. It also should be noted that the observational record at each station is generally shorter than the length of the reanalyses, so the fraction attributed to extreme events is not expected to match perfectly. Overall, the patterns seen from each product are very similar, with coastal regions generally seeing higher dependence on extreme events than further inland. Generally, the southern coastal regions have the highest dependence on extremes, with lower dependence inland and at higher altitudes.

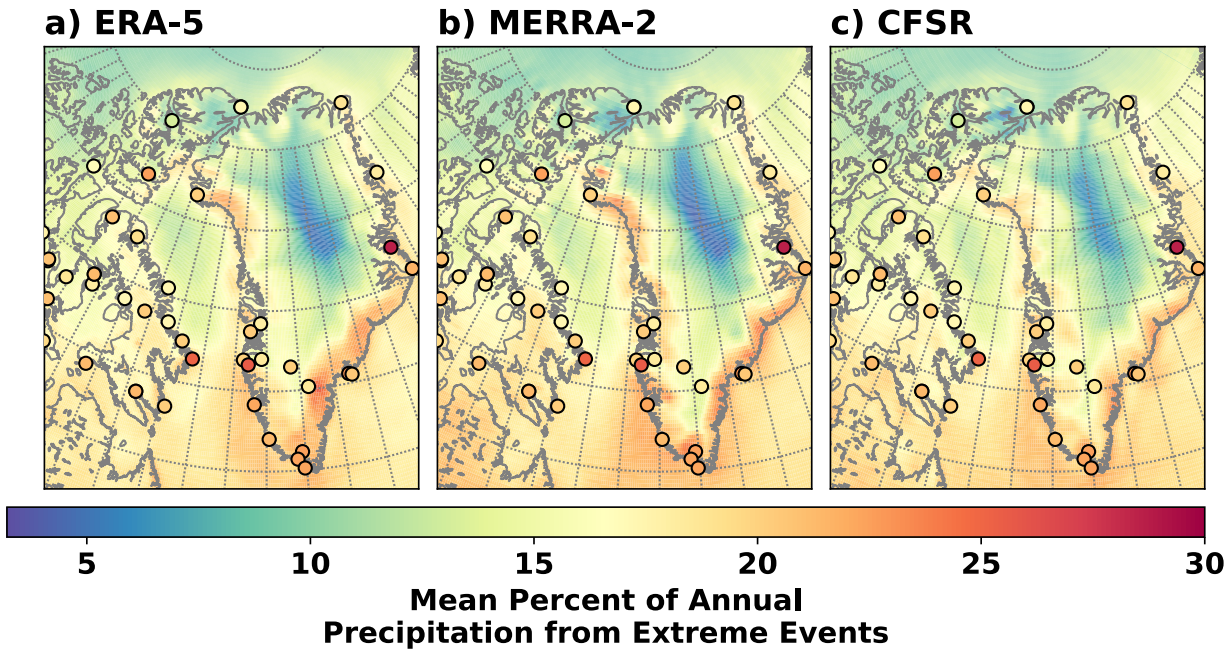

Figure 3.4. Mean percent of annual precipitation attributed to extreme events based on a) ERA-5, b) MERRA-2, and c) CFSR. Circles show the relative contribution of extremes to annual precipitation for each station with at least 4 years of data.

3.3.2 Case Study

In the late summer of 2011, a low-pressure system brought extended heavy precipitation across much of southern Greenland. Doyle et al. (2015) illustrated how this event caused enhanced melt and increased ice flow along the lower ablation zone of the Kangerlussuaq sector of the Greenland Ice Sheet. A meteorological overview of the event was produced using data from the National Centers for Environmental Prediction/National Centre for Atmospheric Research reanalysis. The low-pressure system moved across Baffin Bay with a minimum surface pressure of 992 hPa, bringing warm and moist southwesterly winds to the west coast of Greenland. As the warm air moves inland, substantial orographic lift occurs and can cause a dramatic increase in precipitation (Schuenemann et al., 2009). During this event, some regions along the central west coast saw over 100 mm of precipitation in less than one week. While Doyle et al. (2015) presented some analysis from a single reanalysis, it was mainly used as context for the melt event rather than focusing on the product's performance. Here, the performance of the three reanalyses is investigated for the period of 26-28 August 2011, which were the days of heaviest precipitation during this event.

Figure 3.5 shows daily accumulations from each reanalysis and any stations that recorded precipitation that day. The reanalyses showed similar patterns overall, but with some notable differences. Firstly, ERA-5 produced a broader area of maximum precipitation near Nuuk on 26 August. There are no surface stations close to the precipitation maximum, making it difficult to speculate on whether ERA-5 overproduced precipitation or if the other reanalyses underproduced precipitation. The maximum produced by CFSR on 27 August was much larger than the other products near the Qaqortoq station at the southern tip of Greenland. While 77 mm was observed

at the station, making it an extreme event, CFSR exceeded 100 mm. Additionally, MERRA-2 saw broader light precipitation; the light precipitation region reached further inland on all three days. This aligns with the drizzle bias previously observed in MERRA-2 and its predecessor in the Arctic (e.g., Boisvert et al., 2018; Lindsay et al., 2014; Rapaić et al., 2015).

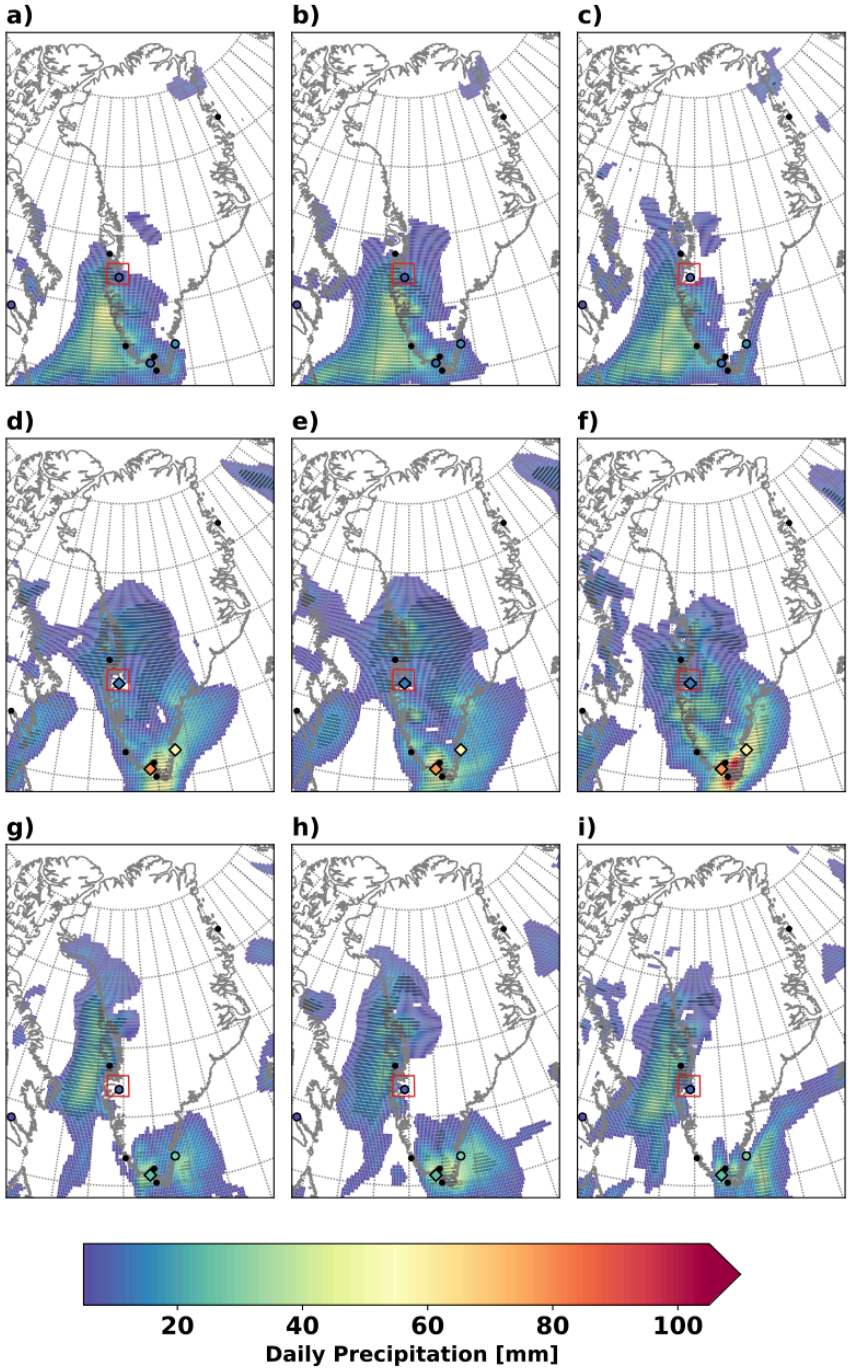

Figure 3.5. Daily precipitation (≥ 5 mm) for 26-28 August 2011 from ERA-5 (a,d,g), MERRA-2 (b,e,h), and CFSR (c,f,i). The rows show data for 26 (a-c), 27 (d-f), and 28 (g-i) August 2011. Stippling indicates grid cells with daily accumulations above the extreme threshold. Stations are shown with black dots, filled circles, and filled diamonds if no precipitation, non-extreme precipitation, or extreme precipitation were observed, respectively. The color of filled station markers indicates the daily precipitation accumulation. The red square highlights the Kangerlussuaq region.

3.4 Discussion and Conclusion

Most previous work assessing Arctic precipitation in reanalyses has focused on averages rather than extremes, but the presented results support some previous conclusions. Previous studies investigating daily and annual precipitation in the Arctic have demonstrated that many reanalyses are biased low for short-term, intense precipitation (e.g., Koyama and Stroeve 2019; Boisvert et al. 2018). Over the Arctic Ocean, MERRA-2 and CFSR were shown to produce monthly/annual accumulations that were notably higher than other reanalyses (Barrett et al., 2020; Boisvert et al., 2018). Here, MERRA-2 and CFSR have higher biases than ERA-5 across most of the domain, but the difference in performance is reduced compared to that seen in previous studies. The little work that has been done assessing Arctic precipitation fields of ERA-5 (the newest product) shows that ERA-5 slightly outperforms other reanalyses over the Arctic Ocean (Barrett et al., 2020) and adequately matches the timing of observed events during the MOSAiC Expedition (Wagner et al., 2021). Our results suggest that ERA-5 is the most successful in representing observed precipitation extremes over Greenland, Baffin and Ellesmere Islands, but the timing of events often differs from observations.

While the presented analysis showed that the reanalyses struggled to reproduce observed extreme events across the domain, several factors contribute to the disagreement. Firstly, reanalysis accumulation represents the average over the grid cell, which may remove the highest precipitation values. Many of the surface stations in the domain are near complex topography, and there is likely a high degree of variability in local precipitation (Gascon et al., 2010; Ohmura & Reeh, 1991). The spatial resolution of the analyzed products is too low to adequately represent much of the local topographic effects that may lead to extreme precipitation. Additionally, surface precipitation observations suffer from a variety of biases, as discussed in Section 3.1, that may not be accounted for in quality control measures (e.g., Yang et al. 2005; Adam and Lettenmaier 2003; Ye et al. 2021; Mekis and Vincent 2011). This suggests that the observations may be quite different than the average of a larger area.

Conversely, the reanalyses performed well in a relative sense. With the low HSS, it is evident that the event days are not always the same, but the reanalyses accurately reproduce the seasonality of observed extremes. This presents problems for analyzing specific events but optimism for climatological studies. Previous studies have shown much higher correlations, particularly for ERA-5 and MERRA-2, when looking at monthly or annual accumulations (e.g., Barrett, Stroeve, and Serreze 2020; Boisvert et al. 2018). Since extreme precipitation accounts for up to ~25% of annual totals across parts of the domain (Figure 3.4) and

Table 3.3 shows that most regions see higher event frequencies than the observations, it can be inferred that the extreme precipitation events are accounted for at seasonal, annual, and longer timescales.

Spatial lag analysis shows that most stations produce higher correlations with one of the surrounding cells rather than the cell containing the station (Figures A.1-2). Most subregions see slight correlation increases (increase in $r \leq 0.10$) when the surrounding cells are considered. Baffin Island improved the most with spatial lag, with the correlation improving by 0.18. Ellesmere Island and NW Greenland, which have virtually no correlation with the observations, do not improve substantially with spatial offsetting but Ellesmere Island does see improvements in temporal lag

tests (Figure A.3), suggesting that single-day offsets are a major contribution to the low correlations in the region.

In general, the products better agreed with observations in the regions with the best data availability. The best agreement was found in SW Greenland, which had six stations with observational records exceeding 20 years long (Table A.1) and the second-most observations overall (Table 3.1). Contrarily, the fewest observations were available for Ellesmere Island and the Northern Greenland subregions, both of which saw poorer agreement with observations.

Based on the presented analysis, ERA-5 slightly outperforms MERRA-2 and CFSR in representing extremes in our domain of interest. ERA-5 seems to be the most consistent, with standard deviations lower than or close to observations and with higher correlations in most regions. It is hypothesized that a major factor in the differences between products is spatial resolution. The higher resolution of ERA-5 allows for better representation of regional topography, as well as the pivotal topographic effects influencing precipitation (e.g., Gascon, Stewart, and Henson 2010; Ohmura and Reeh 1991). This may be seen in Figure 3.4, where ERA-5 yields higher dependence on extremes along the coast of SE Greenland, where there is dramatic topography. This agrees with previous studies that have found that increased spatial resolution improves agreement with precipitation observations, particularly in regions of complex topography (e.g., van Kampenhout et al. 2019; Bacmeister et al. 2014). Notably, ERA-5 produces a lower event frequency than the other reanalyses in the region (Table 3.3). This may be explained by the other reanalyses producing more light precipitation, which has been documented for MERRA-2 in the Arctic (e.g., Boisvert et al. 2018; Barrett, Stroeve, and Serreze 2020). While the presented results are not particularly positive, the newer products (particularly ERA-5) show promise in representing extreme precipitation and may be further improved using dynamical downscaling.

Author Contributions

Conceptualization and methodology: NAL, AC, JCS, and JH. Data processing and analysis: NAL. Writing: NAL. Editing/reviewing: AC, JCS, and JH. Supervision: JCS and JH. All authors contributed to the article and approved the submitted version.

Funding

This research was undertaken, in part, thanks to funding from the Canada 150 Research Chairs Program.

Literature cited

Abdelmoaty, H. M., Papalexiou, S. M., Rajulapati, C. R., & AghaKouchak, A. (2021). Biases Beyond the Mean in CMIP6 Extreme Precipitation: A Global Investigation. *Earth's Future*, *9*(10), e2021EF002196. https://doi.org/10.1029/2021EF002196

Adam, J. C., & Lettenmaier, D. P. (2003). Adjustment of global gridded precipitation for systematic bias. *Journal of Geophysical Research: Atmospheres*, *108*(D9). https://doi.org/10.1029/2002JD002499

Bacmeister, J. T., Wehner, M. F., Neale, R. B., Gettelman, A., Hannay, C., Lauritzen, P. H., et al. (2014). Exploratory High-Resolution Climate Simulations using the Community Atmosphere Model (CAM). *Journal of Climate*, *27*(9), 3073–3099. https://doi.org/10.1175/JCLI-D-13-00387.1

Bamber, J. L., Westaway, R. M., Marzeion, B., & Wouters, B. (2018). The land ice contribution to sea level during the satellite era. *Environmental Research Letters*, *13*(6), 063008. https://doi.org/10.1088/1748-9326/aac2f0

Barrett, A. P., Stroeve, J. C., & Serreze, M. C. (2020). Arctic Ocean Precipitation From Atmospheric Reanalyses and Comparisons With North Pole Drifting Station Records. *Journal of Geophysical Research: Oceans*, *125*(1), 1–17. https://doi.org/10.1029/2019JC015415

Bengtsson, L., Hodges, K. I., Koumoutsaris, S., Zahn, M., & Keenlyside, N. (2011). The changing atmospheric water cycle in Polar Regions in a warmer climate. *Tellus A: Dynamic Meteorology and Oceanography*, *63*(5), 907–920. https://doi.org/10.1111/j.1600-0870.2011.00534.x

Boas, L., & Wang, P. R. (2011). *Quality control of Greenlandic weather and climate data series 1958-2010* (Technical Report No. Technical Report 11-16) (p. 14). Copenhagen, Denmark: Danish Meteorological Institute. Retrieved from https://www.dmi.dk/fileadmin/Rapporter/TR/tr11-16.pdf

Boisvert, L. N., Webster, M. A., Petty, A. A., Markus, T., Bromwich, D. H., & Cullather, R. I. (2018). Intercomparison of Precipitation Estimates over the Arctic Ocean and Its Peripheral Seas from Reanalyses. *Journal of Climate*, *31*(20), 8441–8462. https://doi.org/10.1175/JCLI-D-18-0125.1

Bosilovich, M., Akella, S., Coy, L., Cullather, R., Draper, C., Gelaro, R., et al. (2015). *MERRA-2: Initial Evaluation of the Climate* (Technical Report No. NASA/TM-2015-104606/Vol.43) (p. 145). Greenbelt, Maryland: Goddard Space Flight Center. Retrieved from https://gmao.gsfc.nasa.gov/pubs/docs/Bosilovich803.pdf

Cappelen, J., Laursen, E. V., Kern-Hansen, C., Boas, L., Wang, P., Jørgensen, B. V., & Carstensen, L. S. (2014). *Weather observations from Greenland 1958-2013 - Observation data with description* (Technical Report No. Technical Report 14-08) (p. 24). Copenhagen, Denmark: Danish Meteorological Institute. Retrieved from https://www.dmi.dk/fileadmin/user_upload/Rapporter/TR/2014/tr14-08.pdf

Collier, C. G. (2000). *Precipitation estimation and forecasting* (Vol. 46). Geneva, Switzerland: Secretariat of the World Meteorological Organization.

Delhasse, A., Kittel, C., Amory, C., Hofer, S., van As, D., S. Fausto, R., & Fettweis, X. (2020). Brief communication: Evaluation of the near-surface climate in ERA5 over the Greenland Ice Sheet. *The Cryosphere*, *14*(3), 957–965. https://doi.org/10.5194/tc-14-957-2020

Doswell, C. A., Davies-Jones, R., & Keller, D. L. (1990). On Summary Measures of Skill in Rare Event Forecasting Based on Contingency Tables. *Weather and Forecasting*, *5*(4), 576–585. https://doi.org/10.1175/1520-0434(1990)005<0576:OSMOSI>2.0.CO;2

Doyle, S. H., Hubbard, A., van de Wal, R. S. W., Box, J. E., van As, D., Scharrer, K., et al. (2015). Amplified melt and flow of the Greenland ice sheet driven by late-summer cyclonic rainfall. *Nature Geoscience*, *8*(8), 647–653. https://doi.org/10.1038/ngeo2482

Ford, J. D. (2009). Vulnerability of Inuit food systems to food insecurity as a consequence of climate change: a case study from Igloolik, Nunavut. *Regional Environmental Change*, *9*(2), 83–100. https://doi.org/10.1007/s10113-008-0060-x

Ford, J. D., Bell, T., & St-Hilaire-Gravel, D. (2010). Vulnerability of Community Infrastructure to Climate Change in Nunavut: A Case Study From Arctic Bay. In G. K. Hovelsrud & B. Smit (Eds.), *Community Adaptation and Vulnerability in Arctic Regions* (pp. 107–130). Dordrecht: Springer Netherlands. https://doi.org/10.1007/978-90-481-9174-1_5

Gascon, G., Stewart, R. E., & Henson, W. (2010). Major Cold-Season Precipitation Events at Iqaluit, Nunavut. *Arctic*, *63*(3), 327–337.

Gelaro, R., McCarty, W., Suárez, M. J., Todling, R., Molod, A., Takacs, L., et al. (2017). The Modern-Era Retrospective Analysis for Research and Applications, Version 2 (MERRA-2). *Journal of Climate*, *30*(14), 5419–5454. https://doi.org/10.1175/JCLI-D-16-0758.1

Goodison, B. E., Louie, P. Y. T., & Yang, D. (1998). *WMO Solid Precipitation Measurement Intercomparison--Final Report* (Instruments and Observing Methods No. WMO/TD-No. 872) (p. 318). World Meteorological Organization.

Groisman, P. Y., & Legates, D. R. (1994). The Accuracy of United States Precipitation Data. *Bulletin of the American Meteorological Society*, *75*(2), 215–228. https://doi.org/10.1175/1520-0477(1994)075<0215:TAOUSP>2.0.CO;2

Hennermann, K., & Giusti, M. (2021). What are the changes from ERA-Interim to ERA5 and ERA5-Land? Retrieved October 27, 2021, from https://confluence.ecmwf.int//pages/viewpage.action?pageId=74764925

Hersbach, H., Bell, B., Berrisford, P., Hirahara, S., Horányi, A., Muñoz-Sabater, J., et al. (2020). The ERA5 global reanalysis. *Quarterly Journal of the Royal Meteorological Society*, *146*(730), 1999–2049. https://doi.org/10.1002/qj.3803

Hofer, S., Lang, C., Amory, C., Kittel, C., Delhasse, A., Tedstone, A., & Fettweis, X. (2020). Greater Greenland Ice Sheet contribution to global sea level rise in CMIP6. *Nature Communications*, *11*(1), 6289. https://doi.org/10.1038/s41467-020-20011-8

Hyvärinen, O. (2014). A Probabilistic Derivation of Heidke Skill Score. *Weather and Forecasting*, *29*(1), 177–181. https://doi.org/10.1175/WAF-D-13-00103.1

Jain, S. K., & Singh, V. P. (2003). Chapter 2 - Acquisition and Processing of Water Resources Data. In S. K. Jain & V. P. Singh (Eds.), *Developments in Water Science* (Vol. 51, pp. 47–121). Elsevier. https://doi.org/10.1016/S0167-5648(03)80056-4

Jones, P. D. (2013). Greenhouse Effect and Climate Data. In *Reference Module in Earth Systems and Environmental Sciences*. Elsevier. https://doi.org/10.1016/B978-0-12-409548-9.05365-3

van Kampenhout, L., Rhoades, A. M., Herrington, A. R., Zarzycki, C. M., Lenaerts, J. T. M., Sacks, W. J., & van den Broeke, M. R. (2019). Regional grid refinement in an Earth system model: impacts on the simulated Greenland surface mass balance. *The Cryosphere*, *13*(6), 1547–1564. https://doi.org/10.5194/tc-13-1547-2019

Koyama, T., & Stroeve, J. (2019). Greenland monthly precipitation analysis from the Arctic System Reanalysis (ASR): 2000–2012. *Polar Science*, *19*, 1–12. https://doi.org/10.1016/j.polar.2018.09.001

Landrum, L., & Holland, M. M. (2020). Extremes become routine in an emerging new Arctic. *Nature Climate Change*, *10*(12), 1108–1115. https://doi.org/10.1038/s41558-020-0892-z

Lenaerts, J. T. M., Angelen, J. H. van, Broeke, M. R. van den, Gardner, A. S., Wouters, B., & Meijgaard, E. van. (2013). Irreversible mass loss of Canadian Arctic Archipelago glaciers. *Geophysical Research Letters*, *40*(5), 870–874. https://doi.org/10.1002/grl.50214

Levizzani, V., Laviola, S., & Cattani, E. (2011). Detection and Measurement of Snowfall from Space. *Remote Sensing*, *3*(1), 145–166. https://doi.org/10.3390/rs3010145

Lindsay, R., Wensnahan, M., Schweiger, A., & Zhang, J. (2014). Evaluation of Seven Different Atmospheric Reanalysis Products in the Arctic. *Journal of Climate*, *27*(7), 2588–2606. https://doi.org/10.1175/JCLI-D-13-00014.1

Liu, G., & Curry, J. A. (1997). Precipitation characteristics in Greenland-Iceland-Norwegian Seas determined by using satellite microwave data. *Journal of Geophysical Research: Atmospheres*, *102*(D12), 13987–13997. https://doi.org/10.1029/96JD03090

McCrystall, M. R., Stroeve, J., Serreze, M., Forbes, B. C., & Screen, J. A. (2021). New climate models reveal faster and larger increases in Arctic precipitation than previously projected. *Nature Communications*, *12*(1), 6765. https://doi.org/10.1038/s41467-021-27031-y

Mekis, É., & Brown, R. (2010). Derivation of an adjustment factor map for the estimation of the water equivalent of snowfall from ruler measurements in Canada. *Atmosphere-Ocean*, *48*(4), 284–293. https://doi.org/10.3137/AO1104.2010

Mekis, É., & Vincent, L. A. (2011). An Overview of the Second Generation Adjusted Daily Precipitation Dataset for Trend Analysis in Canada. *Atmosphere-Ocean*, *49*(2), 163–177. https://doi.org/10.1080/07055900.2011.583910

Oerlemans, J., & Klok, E. J. L. (2004). Effect of summer snowfall on glacier mass balance. *Annals of Glaciology*, *38*, 97–100. https://doi.org/10.3189/172756404781815158

Ohmura, A., & Reeh, N. (1991). New precipitation and accumulation maps for Greenland. *Journal of Glaciology*, *37*(125), 140–148. https://doi.org/10.3189/S0022143000042891

Parker, W. S. (2016). Reanalyses and Observations: What's the Difference? *Bulletin of the American Meteorological Society*, *97*(9), 1565–1572. https://doi.org/10.1175/BAMS-D-14-00226.1

Pendergrass, A. G. (2018). What precipitation is extreme? *Science*, *360*(6393), 1072–1073. https://doi.org/10.1126/science.aat1871

Rapaić, M., Brown, R., Markovic, M., & Chaumont, D. (2015). An Evaluation of Temperature and Precipitation Surface-Based and Reanalysis Datasets for the Canadian Arctic, 1950–2010. *Atmosphere-Ocean*, *53*(3), 283–303. https://doi.org/10.1080/07055900.2015.1045825

Riddaway, B. (2014). Climate reanalysis. Reading, England: European Centre for Medium-Range Weather Forecasts. https://doi.org/10.21957/QNREH9T5

Rignot, E., & Mouginot, J. (2012). Ice flow in Greenland for the International Polar Year 2008–2009. *Geophysical Research Letters*, *39*(11). https://doi.org/10.1029/2012GL051634

Rignot, E., Velicogna, I., van den Broeke, M. R., Monaghan, A., & Lenaerts, J. T. M. (2011). Acceleration of the contribution of the Greenland and Antarctic ice sheets to sea level rise. *Geophysical Research Letters*, *38*(5). https://doi.org/10.1029/2011GL046583

Rinke, A., Matthes, H., Christensen, J. H., Kuhry, P., Romanovsky, V. E., & Dethloff, K. (2012). Arctic RCM simulations of temperature and precipitation derived indices relevant to future frozen ground conditions. *Global and Planetary Change*, *80–81*, 136–148. https://doi.org/10.1016/j.gloplacha.2011.10.011

Saha, S., Moorthi, S., Pan, H.-L., Wu, X., Wang, J., Nadiga, S., et al. (2010). The NCEP Climate Forecast System Reanalysis. *Bulletin of the American Meteorological Society*, *91*(8), 1015–1058. https://doi.org/10.1175/2010BAMS3001.1

Saha, S., Moorthi, S., Wu, X., Wang, J., Nadiga, S., Tripp, P., et al. (2014). The NCEP Climate Forecast System Version 2. *Journal of Climate*, *27*(6), 2185–2208. https://doi.org/10.1175/JCLI-D-12-00823.1

Schuenemann, K. C., Cassano, J. J., & Finnis, J. (2009). Synoptic Forcing of Precipitation over Greenland: Climatology for 1961–99. *Journal of Hydrometeorology*, *10*(1), 60–78. https://doi.org/10.1175/2008JHM1014.1

Taylor, K. E. (2001). Summarizing multiple aspects of model performance in a single diagram. *Journal of Geophysical Research: Atmospheres*, *106*(D7), 7183–7192. https://doi.org/10.1029/2000JD900719

Wagner, D. N., Shupe, M. D., Persson, O. G., Uttal, T., Frey, M. M., Kirchgaessner, A., et al. (2021). Snowfall and snow accumulation processes during the MOSAiC winter and spring season. *The Cryosphere Discussions*, 1–48. https://doi.org/10.5194/tc-2021-126

Xie, P., & Arkin, P. A. (1997). Global Precipitation: A 17-Year Monthly Analysis Based on Gauge Observations, Satellite Estimates, and Numerical Model Outputs. *Bulletin of the American Meteorological Society*, *78*(11), 2539–2558. https://doi.org/10.1175/1520-0477(1997)078<2539:GPAYMA>2.0.CO;2

Yang, D., Ishida, S., Goodison, B. E., & Gunther, T. (1999). Bias correction of daily precipitation measurements for Greenland. *Journal of Geophysical Research: Atmospheres*, *104*(D6), 6171–6181. https://doi.org/10.1029/1998JD200110

Yang, D., Kane, D., Zhang, Z., Legates, D., & Goodison, B. (2005). Bias corrections of long-term (1973–2004) daily precipitation data over the northern regions. *Geophysical Research Letters*, *32*(19). https://doi.org/10.1029/2005GL024057

Ye, H., Yang, D., Behrangi, A., Stuefer, S. L., Pan, X., Mekis, E., et al. (2021). Precipitation Characteristics and Changes. In D. Yang & D. L. Kane (Eds.), *Arctic Hydrology, Permafrost and Ecosystems* (pp. 25–59). Cham, Switzerland: Springer International Publishing. Retrieved from https://books.google.ca/books?id=l_75DwAAQBAJ&pg=PA24&source=gbs_toc_r&cad=3#v=onepage&q&f=false

Chapter 4 Projections and Physical Drivers of Extreme Precipitation in Greenland & Baffin Bay

Nicole A. Loeb[1,2], Alex Crawford[1,2], Adam Herrington[3], Michelle McCrystall[4], Julienne Stroeve[1,2,5,6], John Hanesiak[1,2]

[1] Department of Environment & Geography, University of Manitoba, Winnipeg, MB, Canada

[2] Centre for Earth Observation Science, University of Manitoba, Winnipeg, MB, Canada

[3] Climate and Global Dynamics Laboratory, National Center for Atmospheric Research, Boulder, CO, USA

[4] Faculty of Physics, University of Auckland, Auckland, New Zealand

[5] Department of Earth Sciences, University College London, London, United Kingdom

[6] National Snow and Ice Data Center, Cooperative Institute for Research in Environmental Science, University of Colorado Boulder, Boulder, Colorado

An edited version of this chapter was published by AGU in Journal of Geophysical Research: Atmospheres. Published 2024 American Geophysical Union.

Loeb, N. A., Crawford, A., Herrington, A., McCrystall, M., Stroeve, J., & Hanesiak, J. (2024). Projections and Physical Drivers of Extreme Precipitation in Greenland & Baffin Bay. *Journal of Geophysical Research: Atmospheres*, *129*(22), e2024JD041375. https://doi.org/10.1029/2024JD041375

Key Points:

- Extreme precipitation increases (and accounts for a higher portion of total annual precipitation) for most subregions by 2100, but decreases in SE Greenland
- Most extreme precipitation is associated with cyclones, but the role of cyclones does not appear to change in future projections
- Increasing AR frequency facilitates increased extreme precipitation in SW Greenland, particularly during the summer

Abstract

Extreme precipitation events can have substantial impacts on communities and the climate system in the warming Arctic, but their changes are not well understood. In this study, characteristics of extreme precipitation days in the Eastern Canadian Arctic and Greenland are examined in historical (1980-1999) and future (2080-2099, SSP5-8.5) Variable-Resolution Community Earth System Model (VR-CESM) simulations. Comparisons between the simulations illustrate potential changes in the frequency and intensity of these events in the region. Extreme precipitation is expected to increase broadly across the region. The frequency of the most intense daily precipitation rates is projected to rise, particularly in the northernmost areas. The seasonality of extremes does not shift substantially in the future simulation, with most areas receiving the highest accumulations and increases during the summer. However, southeastern Greenland is projected to see decreases in extreme precipitation. Algorithms detecting atmospheric rivers and cyclones are employed to assess how their changes may factor into changes in extreme precipitation. Cyclone frequency remains largely consistent with slight decreases near southeastern Greenland which may explain decreased extreme precipitation seen in the region. Atmospheric rivers are projected to become more frequent across the domain, largely during the summer. While the majority of the region's extreme precipitation is associated with cyclones, this suggests that atmospheric rivers become more important in a warming climate. These results provide insight into potential changes in impactful precipitation events in the region and how the processes driving them may change.

Plain Language Summary

Extreme precipitation events can have significant impacts on Arctic communities and the climate system. As the climate changes, extreme precipitation may bring about different impacts, but we still don't fully understand how these events are changing as temperatures increase. In this study, we use simulations from two different climate models to examine changes in the occurrence and characteristics of extreme precipitation days in Greenland and Baffin Bay between the historical period (1980-1999) and the future (2080-2099) under a high emissions scenario. We also use tracking algorithms to investigate the connection between these events and the occurrence of extratropical cyclones and atmospheric rivers. Extreme precipitation is shown to increase across the region except for in southeastern Greenland, where minor decreases are expected. This decrease is likely tied to a slight reduction in cyclone occurrence in the area. Most of the region sees the strongest extreme precipitation increases in the summer when atmospheric rivers are also expected to become more common. Historically, almost all extreme precipitation was associated with cyclones, but their role does not appear to change in the future simulation, whereas atmospheric rivers become associated with a higher fraction of extreme precipitation.

4.1 Introduction

The warming Arctic amplifies the hydrological cycle, which leads to higher precipitation totals and rates across the region (Bengtsson et al., 2011; Rawlins et al., 2010). Precipitation is also expected to see higher interannual variability (e.g., Bintanja et al., 2020; Pendergrass et al., 2017) and a shift from snowfall towards rain (e.g., Bintanja & Andry, 2017; McCrystall et al.,

2021). Observations have shown that even slight changes in mean precipitation can lead to a more substantial shift in the most intense events (e.g., Fischer & Knutti, 2016; Myhre et al., 2019; Pendergrass et al., 2017). Extreme precipitation events are important to consider because of the strong impacts they can have on community infrastructure (e.g., Ford et al., 2010) and the mass balance of glaciers (e.g., Doyle et al., 2015; Harper et al., 2023; Oerlemans & Klok, 2004). The Baffin Bay region and Greenland are of particular interest due to the presence of many communities vulnerable to change, as well as large quantities of land ice undergoing dramatic changes in the warming climate (e.g., Bjørk et al., 2018; Gardner et al., 2011; Hugonnet et al., 2021).

To accurately predict changes in precipitation extremes, it is essential to understand the processes causing them. In general, a large portion of Arctic precipitation is driven by extratropical cyclones, referred to as "cyclones" (e.g., Bintanja & Selten, 2014; Chen et al., 1997; Schuenemann et al., 2009). Cyclones are synoptic low-pressure systems in which air converges toward the centre, driving upward motion and precipitation (Catto, 2016). These systems are transient eddies in the background circulation that transport energy and moisture as they propagate (Seager et al., 2010). Certain regions of the Arctic tend to experience higher cyclone activity, such as southeastern Greenland and Iceland along the north Atlantic storm track (Vavrus, 2013). Baffin Bay is a region where cyclones often become occluded and slow-moving, bringing about intense, prolonged precipitation to eastern Baffin Island (Bintanja et al., 2020; Intihar & Stewart, 2005). Because of this, cyclones are pivotal in the precipitation patterns across the study region.

Another precipitation-generating feature is atmospheric rivers (ARs). An AR is a narrow corridor of intense atmospheric water vapour transport (Dacre et al., 2015). They are often associated with the warm conveyor belt of a cyclone, bringing warm, moist air poleward (Bao et al., 2006; Browning & Pardoe, 1973). The majority of ARs, particularly strong ARs, occur associated with a cyclone, but they can occur independently (Guo et al., 2020; Zhang et al., 2019). ARs can have a variety of notable hydrological impacts in the study region, such as increasing rainfall fraction (Mattingly et al., 2018) and bringing intense precipitation rates (Box et al., 2022).

Extreme precipitation is generally localized in nature, often enhanced by complex topography. In the Arctic, a sparse observational network (e.g., Nitu et al., 2018) and the coarse resolution of climate models (e.g., Cai et al., 2018) presents challenges for accurately representing intense precipitation. Several methodologies have been developed to improve the spatial resolution of gridded climate datasets, such as statistical downscaling (e.g., Noël et al., 2016), dynamically downscaling a dataset with a regional climate model (e.g., Cai et al., 2018), and regional grid refinement within a global model where higher-resolution grids are nested in a global simulation (e.g., Herrington et al., 2022).

While all these methods have shown success in improving the prediction of precipitation rates in the Arctic (e.g., Cai et al., 2018; Noël et al., 2018), there are a number of benefits of using the variable-resolution nested grid approach, such as the two-way interaction between the global and refined grid. Regional climate models require boundary conditions, which means that the conditions at the edges of the domain are prescribed by another dataset, whereas a nested grid can freely evolve with the rest of the global simulation without needing external boundary conditions (e.g., Herrington et al., 2022). Another benefit is having consistent model physics for the entire simulation, rather than forcing one model with output from another that has a different setup (Herrington et al., 2022; van Kampenhout et al., 2019). One example of a model with regional grid

refinement is the Variable Resolution Community Earth System Model (VR-CESM; Herrington et al., 2022).

The main questions to be addressed in this study are as follows;

1) What are the projected changes of extreme precipitation by the end of the 21st century in the Greenland and Baffin Bay region in novel high-resolution climate model projections?
2) Are there changes in cyclone and AR occurrence in the region?
3) How do cyclones and ARs influence the changes in extreme precipitation seen in the projections?

To address these questions, future VR-CESM simulations are produced for the first time in the region and explored to assess extreme precipitation occurrence over the recent historical time-period and at the end of the 21st century under a high emissions scenario. The final two questions are addressed using detection and tracking algorithms to identify cyclones and ARs and relate their presence to the occurrence of daily precipitation extremes.

4.2 Data and Methods

4.2.1 VR-CESM Simulations

The Community Earth System Model, version 2.2, (CESM2) is a global earth system model from the National Center for Atmospheric Research that can simulate land, atmosphere, ocean, and cryospheric systems and their interactions (Danabasoglu et al., 2020; Herrington et al. 2022). Each component (e.g., land surface, atmosphere, ocean, sea ice, and land ice) can be fully coupled with each other component, actively modelled, or be partially coupled. The default atmospheric grid of CESM2 is a 1° x 1° latitude-longitude grid (Danabasoglu et al., 2020).

The atmospheric model component is the sixth version of the Community Atmosphere Model (CAM6). The CAM6 physical parameterization package (Gettelman et al., 2019) is implemented which improves cloud and turbulence representation over previous versions of CAM. Cloud macrophysics, shallow convection, and PBL mixing are simulated by the Cloud Layers Unified by Bi-Normals (CLUBB; Golaz et al. 2002). The two-moment MG2 bulk microphysical scheme (Gettelman et al., 2015; Gettelman & Morrison, 2015) is used, providing prognostic precipitation (meaning that it is carried across time steps). The land model, Community Land Model version 5 (CLM5), includes hydrological and snow processes, including surface mass balance components for grid cells containing land ice (Danabasoglu et al., 2020). However, mass balance processes such as calving (ice breaking off from the end of a glacier into icebergs) are not active if the ocean component is not actively modelled.

Recently, spectral-element dynamical cores have been implemented that allow for quasi-uniform grid spacing to provide greater detail over areas of interest more efficiently than the previous finite-element dynamical core (Herrington et al., 2022; Lauritzen et al., 2018). A variable-resolution version of CESM2 (VR-CESM) with 0.25° x 0.25° grid refinement over the Arctic, referred to as the ARCTIC grid (Herrington et al., 2022), shown in Figure B.1, has been developed to dynamically downscale the global 1° x 1° CESM2 and better resolve small-scale features.

Two 20-year ARCTIC VR-CESM simulations covering 2080-2100 and forced using the Shared Socioeconomic Pathway 5-8.5 (SSP5-8.5; O'Neill et al., 2016) emission scenario were completed with coupled atmosphere and land components and prescribed monthly ocean and sea ice conditions. This partial coupling follows the procedure used in the Atmospheric Model Intercomparison Project (Hurrell et al., 2008). Monthly ocean and sea ice conditions are retrieved from existing 1° x 1° resolution CESM2 SSP5-8.5 CMIP6 simulations (Danabasoglu et al., 2020; Meehl et al., 2020).

The new future simulations were designed for comparison to an existing VR-CESM ARCTIC historical simulation (Herrington et al., 2022) to estimate changes over time. In this paper, the historical simulation (HIST) for 1980-1999 is compared to one of the new future simulations (FUT, SST and sea ice forced by simulation 101, Figure B.2) of 2080-2099. Results from the second future simulation are provided in the Supplementary Information (Figures B.5, S7-S10, S15-S17), but the difference between the two forcing simulations are minor. HIST is also compared to a native 1° SSP5-8.5 CMIP6 simulation of CESM2 (Danabasoglu, 2019) to illustrate changes due to regional refinement.

4.2.2 ERA5

To assess how well VR-CESM simulates historical extreme precipitation days, it is compared to the fifth-generation reanalysis product from the European Centre for Medium-Range Weather Forecasts (ERA5). ERA5 provides hourly data from 1979 to present on a 0.25° × 0.25° grid with 137 vertical levels and a 4D-Var data assimilation system (Hennermann & Giusti, 2021; Hersbach et al., 2020). ERA5 has been shown to effectively reproduce the historical climate of Greenland (e.g., Delhasse et al., 2020) and the broader Arctic (e.g., Barrett et al., 2020; Graham et al., 2019). More specifically, ERA5 is better able to reproduce the climatological statistics (e.g., the seasonality of event frequency and seasonal accumulations) of extreme precipitation in the study area than the other atmospheric reanalyses (Loeb et al., 2022).

4.2.3 Cyclone Tracking

The Lagrangian cyclone tracking algorithm used in this study is outlined in Crawford et al. (2021). To identify cyclone centers, sea level pressure (SLP) data are interpolated to a 25 km, pole-centered, Lambert azimuthal equal-area grid, and local SLP minima are identified using a 200 km kernel size. Minima must be below 1500 m altitude and the SLP difference within a 1000 km radius must be greater than 7.5 hPa. The cyclone area is identified as the area within the outermost closed isobar (meaning no cyclone centers from other storms, nor any local maxima in SLP, are encompassed by the isobar). This algorithm can also detect the presence of multi-center cyclones, which are identified if there is a secondary SLP minimum within 1200 km of the main center, and if including the secondary center at least doubles the area of the system. Cyclone centers are tracked through time using two steps. First, a prediction of each cyclone center's future location is made based on its previous motion. Second, a cyclone track is continued to the cyclone center in the subsequent SLP field that is closest to its predicted location, provided the resulting propagation speed is no greater than 150 km h^{-1}. If no center is identified that satisfies these conditions,

cyclolysis is assumed. The parameter values used in the cyclone tracking algorithm are shown in Table B.1.

To assess the changes in cyclone occurrence and characteristics, variables including track length, lifespan, depth, and pressure gradient in the 1000 km surrounding the cyclone center are investigated. Changes in average and maximum conditions between the historical and future periods are assessed. The cyclone tracking algorithm was applied to both ERA5 and VR-CESM from 1980 to 1999 to assess agreement for historical conditions. Precipitation is considered to be cyclone-associated precipitation (CAP) if it occurs within 1200 km of a cyclone center. This distance was selected following Crawford et al. (2019), and because it is the radius used to specify separate cyclone centers in the tracking algorithm. The 1200 km radius to identify cyclone-associated precipitation surrounding centers is applied after detection, meaning that it is possible for precipitation to be considered cyclone-associated over all landmasses in the domain. However, the results may underestimate CAP over high altitudes of Greenland because of the elevation mask applied to cyclone center detection. Extreme precipitation identified using a 600 km CAP radius is shown in Figure B.11, and does not result in different patterns of changes associated with cyclones.

4.2.4 AR Tracking

The detection and tracking of ARs was done using TempestExtremes v2.1, which uses the Laplacian of integrated water vapour transport (IVT) to identify features based on specified thresholds (Ullrich et al., 2021). Using the Laplacian of IVT to identify ARs means that the feature must contain IVT that is substantially higher than its surroundings, therefore making the detection agnostic to background changes in IVT that are expected in a warming climate.

ARs were identified as regions where the Laplacian of IVT was $< -50{,}000$ kg m^{-2} s^{-1} rad^{-2} and areal extent greater than 566,666 km^2, which is two-thirds of the average AR spatial extent (Waling et al., 2024). The Laplacian of IVT threshold of -50,000 kg m^{-2} s^{-1} rad^{-2} is slightly higher than previous studies (Ullrich et al., 2021; Waling et al., 2024), but was selected to only include strong Arctic ARs. The algorithm is applied to the 6-hourly IVT field on the native model grid, to identify and track ARs using the DetectBlobs and StitchBlobs functions of TempestExtremes v2.1, respectively (Ullrich et al., 2021).

4.2.5 Assessment of extreme precipitation

Extreme precipitation is defined as daily precipitation totals exceeding the 95th percentile of days where at least 1 mm of accumulation occurs (Pendergrass, 2018). This definition was chosen as it removes the frequent drizzle/light precipitation that occurs in reanalyses across many Arctic regions (e.g., Barrett et al., 2020). The threshold is calculated for each grid cell in the historical simulation. The same threshold is applied to the future simulation to show changes in an absolute precipitation level. Hourly ERA5 and six-hourly VR-CESM and CESM2 precipitation rate data are converted to accumulation and summed to produce daily precipitation accumulations. VR-CESM HIST provides six-hourly instantaneous precipitation rate, as opposed to the averages

provided by the other datasets used. This means that the daily precipitation rates in HIST may be biased slightly high compared to other datasets.

All differences between historical and future simulations are tested for statistical significance using a two-sided Mann-Whitney U test, and differences are only shown where statistically significant ($p < 0.05$). Significance of the difference in extreme precipitation threshold between ERA5 and HIST is calculated using bootstrapping analysis, whereby 1000 random resamplings without replacement of daily precipitation amounts are conducted for each grid cell. The domain is split into subregions for assessment of event seasonality and changes in precipitation distribution, following Loeb et al. (2022). The subregions in the eastern Canadian Arctic are divided by islands, and Greenland is split following glacier regimes and surface mass balance characteristics (Rignot et al., 2011; Rignot & Mouginot, 2012). The representation of topography in each dataset and the Greenland subregion divisions are illustrated in Figure 4.1.

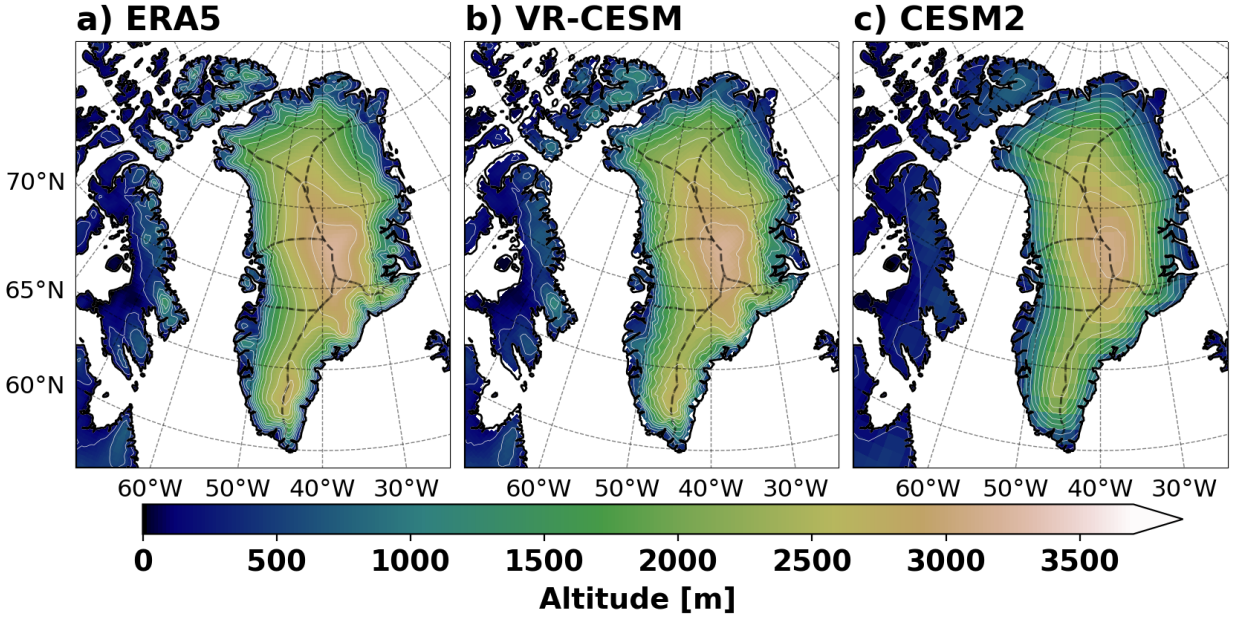

Figure 4.1. Maps showing surface topography from (a) ERA5, (b) VR-CESM, and (c) CESM2. Light contours are shown every 250 m and black dashed lines show the division of the subregions.

4.3 Extreme precipitation events

4.3.1 Validation of historical simulations

To evaluate how well VR-CESM reproduces historical climate, Figure 4.2 shows comparisons of HIST to ERA5. Overall, VR-CESM matches the mean annual precipitation from ERA5 well, producing slightly higher totals in southwestern and northeastern Greenland. Both products have 0.25° × 0.25° grid spacing, which may contribute to the observed similarities. However, a similar difference pattern has also been shown when comparing ERA5 to a higher-resolution regional climate model (Herrington et al., 2022). The extreme daily precipitation threshold follows the mean annual precipitation pattern closely; thresholds are highest where annual precipitation is highest, such as SE Greenland. Again, VR-CESM matches the thresholds

produced by ERA5 closely. Larger fractional differences exist when looking at mean annual extreme precipitation accumulation (Figure 4.2i-l). VR-CESM produces higher extreme precipitation accumulation over southeastern Greenland as it tends to have more positively skewed precipitation distributions in the region (see Section 4.3.2), producing more intense precipitation days even though the extreme threshold is similar to that of ERA5.

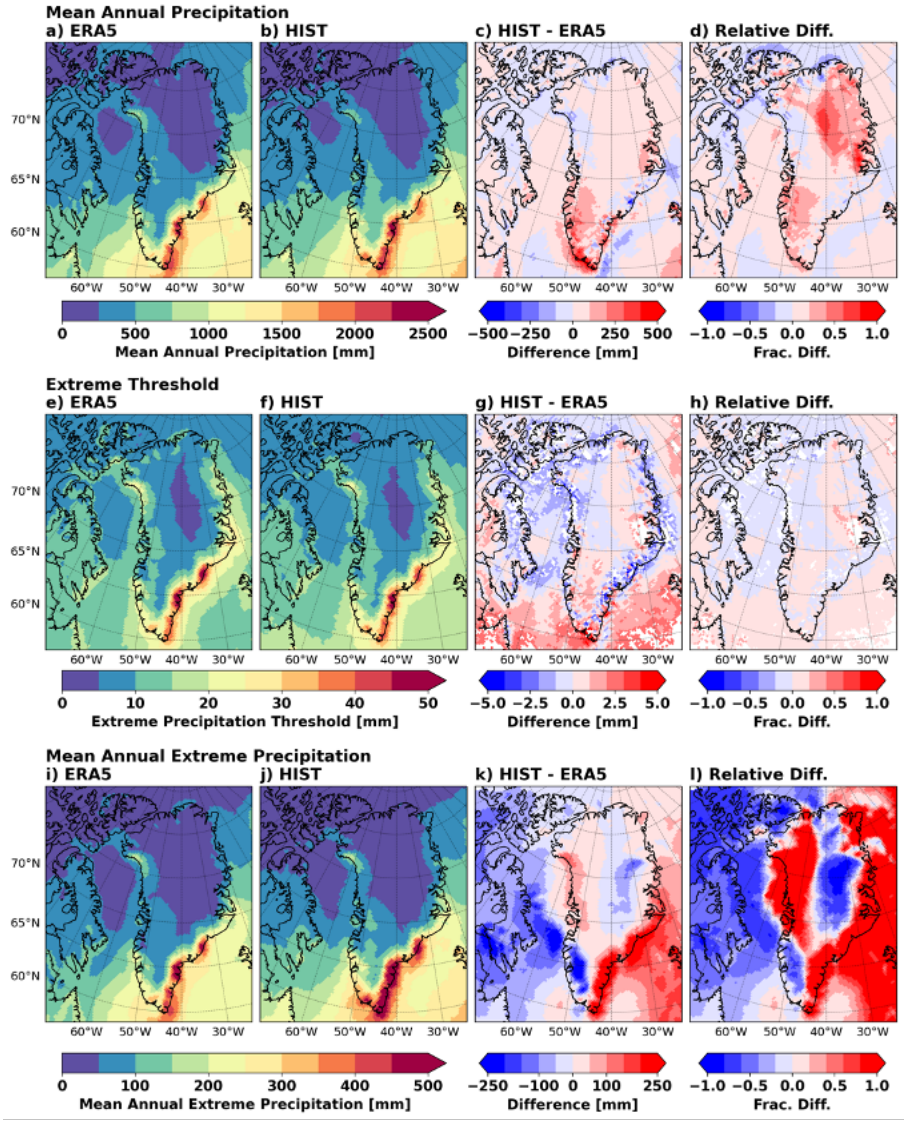

Figure 4.2. Comparisons of ERA5 to HIST for (a-d) mean annual precipitation, (e-h) extreme precipitation threshold, and (i-l) mean annual extreme precipitation. The third (c, g, k) and fourth (d, h, l) columns show the absolute and fractional differences between the products, respectively. The relative difference is the fractional difference relative to ERA5 (i.e., (HIST-ERA5)/ERA5).

Figure 4.3 illustrates mean annual precipitation and extreme precipitation thresholds in the native resolution CESM2 versus VR-CESM HIST to illustrate the differences. These changes are brought about by representing physical processes with finer detail as well as representing statistics on the higher-resolution grid. The largest differences exist in regions of complex topography, such as southeastern Greenland, where the extreme thresholds tend to be higher and more regionally refined in HIST along the coast (Figure 4.3g). HIST also reduces annual precipitation in southern

Greenland (Figure 4.3c), aligning more closely with ERA5 than CESM2, agreeing with similar annual comparisons in Herrington et al. (2022) and van Kampenhout et al. (2019). In general, HIST provides refinement of the patterns seen in the 1° CESM2 simulation.

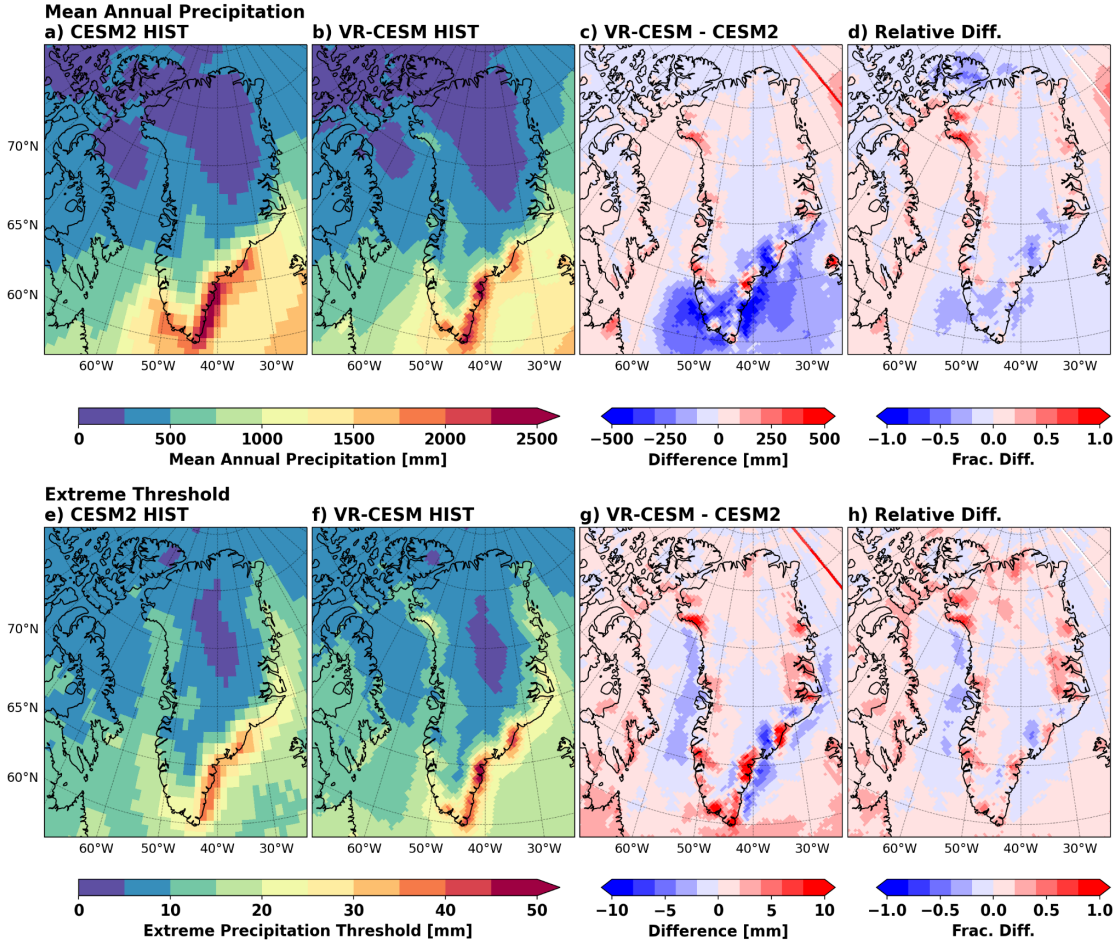

Figure 4.3. Comparisons of the native resolution CESM2-HIST to VR-CESM HIST for (a-d) mean annual precipitation and (e-h) extreme precipitation threshold. The relative difference is the fractional difference relative to CESM2 (i.e., (HIST-CESM2)/CESM2).

4.3.2 Future changes in extreme precipitation

Figure 4.4 shows the mean annual extreme precipitation totals and percent of annual precipitation that is attributed to extreme precipitation days in the historical and future periods. In the historical period, the highest portion of annual precipitation attributed to extremes is approximately 20%, with local maxima in low-lying coastal regions, agreeing with the results of the same analysis on reanalyses (Loeb et al., 2022). By 2100 under SSP5-8.5, broad increases are expected across the domain (Figure 4.4c,g). VR-CESM produces smaller-magnitude changes (especially in southeastern Greenland) that are more spatially refined than those seen in CESM2 (Figure B.6). Much of northern and central Greenland and Ellesmere Island see very little precipitation from extreme days (< 50 mm) in the historical period. In the future simulation, only the highest altitudes of the Greenland Ice Sheet see less than 50 mm of extreme precipitation

annually, with dramatic increases in extreme accumulations in the coastal regions of the northern edge of the domain. Considerable increases in the percent of annual precipitation attributed to extreme events occurs in western Greenland.

The only region shown to experience a decrease in the percent of annual precipitation attributed to extreme events is southeastern Greenland, which historically sees the highest amount of extreme precipitation owing to cyclone activity and orographic precipitation enhancement from steep coastal topography (Chen et al., 1997; Vavrus, 2013). Here, the future projection shows slight decreases in the amount of precipitation attributed to extremes at the end of the century.

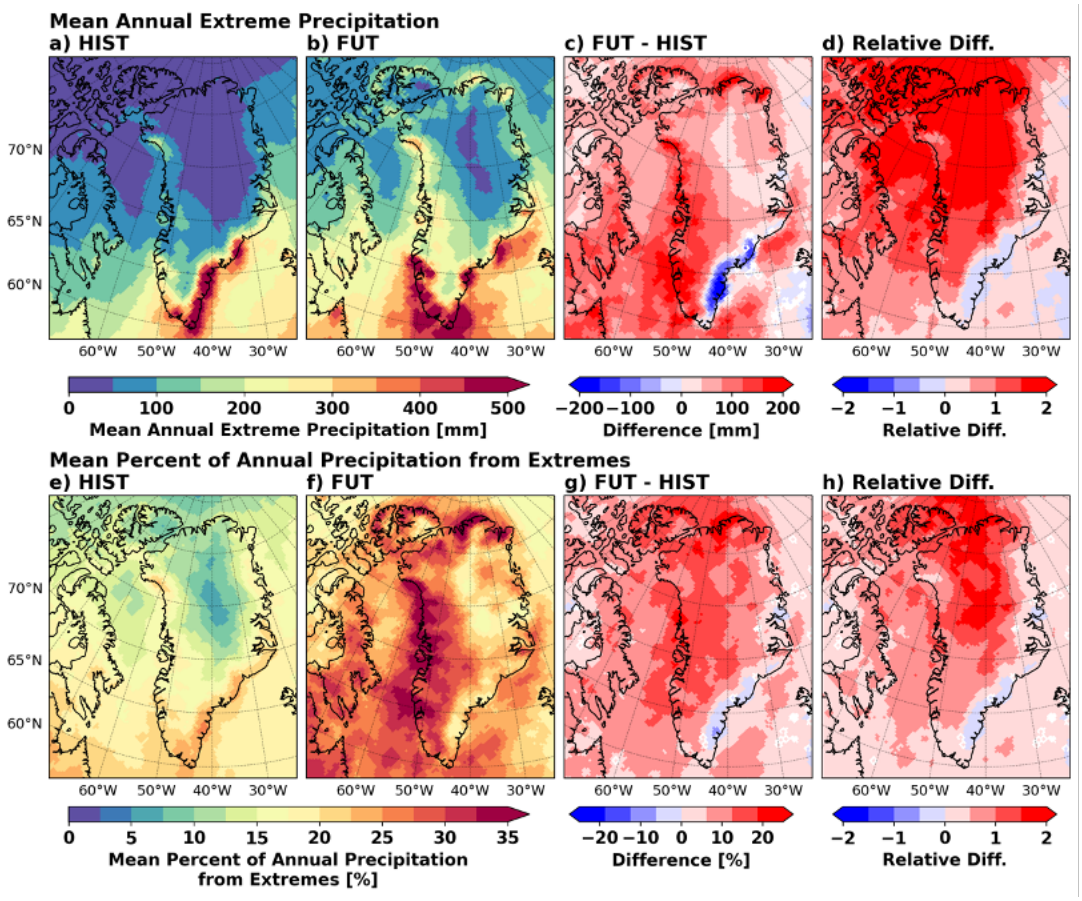

Figure 4.4. Mean (a-d) annual extreme precipitation and (e-h) percent of annual precipitation from extreme precipitation days in (a,e) HIST (1980-1999), (b,f) FUT (2080-2099) , (c,g) the difference between the two (FUT – HIST), and (d, h) the fractional difference relative to HIST (i.e., (FUT – HIST)/HIST). Only differences that are statistically significant ($p < 0.05$) are shown.

Figure 4.5 shows daily precipitation distributions across the domain from ERA5, HIST, and FUT. HIST tends to have lower occurrences of moderate and high precipitation totals than ERA5 in the northernmost subregions (NE/NO/NW Greenland, Ellesmere and Devon Islands). In these regions, FUT shows precipitation distributions comparable to ERA5, but with an extension towards even higher precipitation accumulations. Agreement between ERA5 and HIST for the lower and mid-range extreme events is closer in the southern subregions (SE/SW Greenland and Baffin Island), but HIST tends to produce higher frequencies of the most intense precipitation. The largest increases in FUT in SW Greenland and Baffin Island are seen around 75-125 mm and 30-60 mm, respectively, rather than the most extreme end of the distribution (in contrast to the

northernmost subregions). In SE Greenland and Baffin Island, there is a clear decrease in the most extreme precipitation accumulations, with FUT falling below HIST at daily accumulations close to or above 100 mm. However, Baffin Island shows an increase in the lower- and mid-range events, allowing for overall extreme precipitation to still increase in FUT (as seen in Figure 4.4).

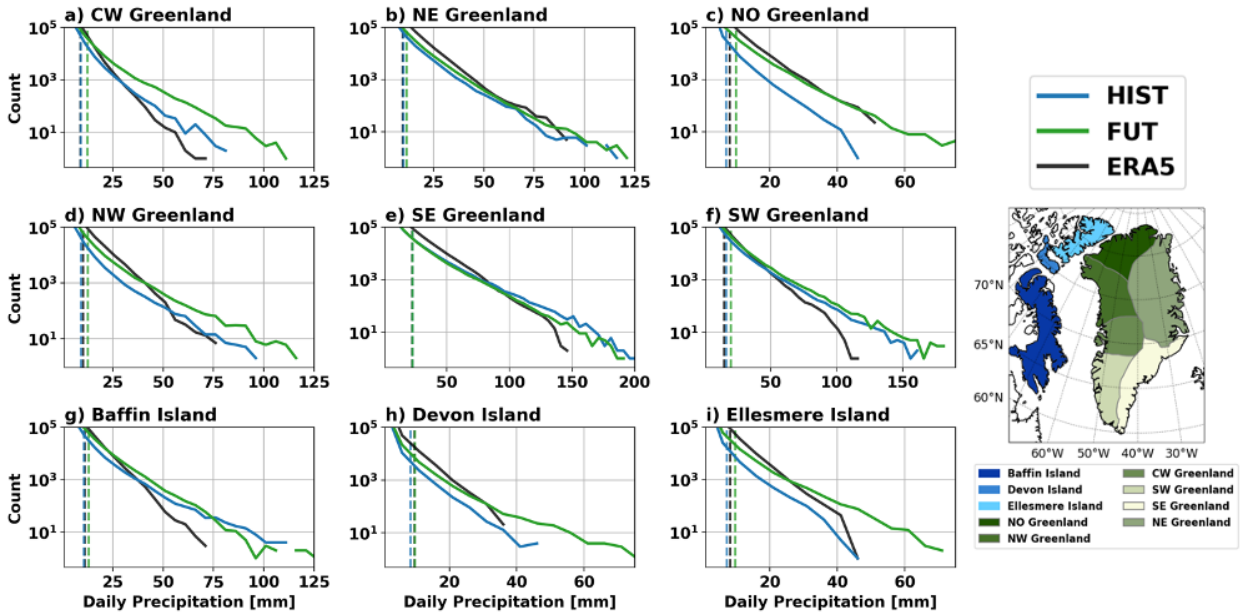

Figure 4.5. Daily precipitation distribution for all grid cells in each subregion (a-i, shown in the map) from ERA5 (1980-1999, black), HIST (1980-1999, blue), and FUT (2080-2099, green). Daily precipitation totals counts are binned every 5 mm. Vertical dashed lines indicate the mean extreme precipitation threshold in the subregion from each of ERA5 (black), HIST (blue), and FUT (green).

The seasonality of extreme precipitation is illustrated in Figure 4.6. In the historical period, ERA5 and HIST typically agree well except in Baffin and Devon Islands and SE Greenland, where VR-CESM fails to capture higher extreme accumulations in the winter (Figure 4.6g-h). In the future, most subregions experience more extreme precipitation accumulation during the warm season (particularly in July to September). The largest increases in future extreme precipitation occur in the summer and early autumn in the future simulation, particularly in western and northern Greenland. However, almost all subregions see little to no increase in future extreme precipitation during the cold season. This suggests that there is little change to the timing of extreme precipitation in the future. One region seeing different changes is SE Greenland, where there is a slight decrease in extreme precipitation during the cold season, agreeing with the results of Pfahl et al. (2017).

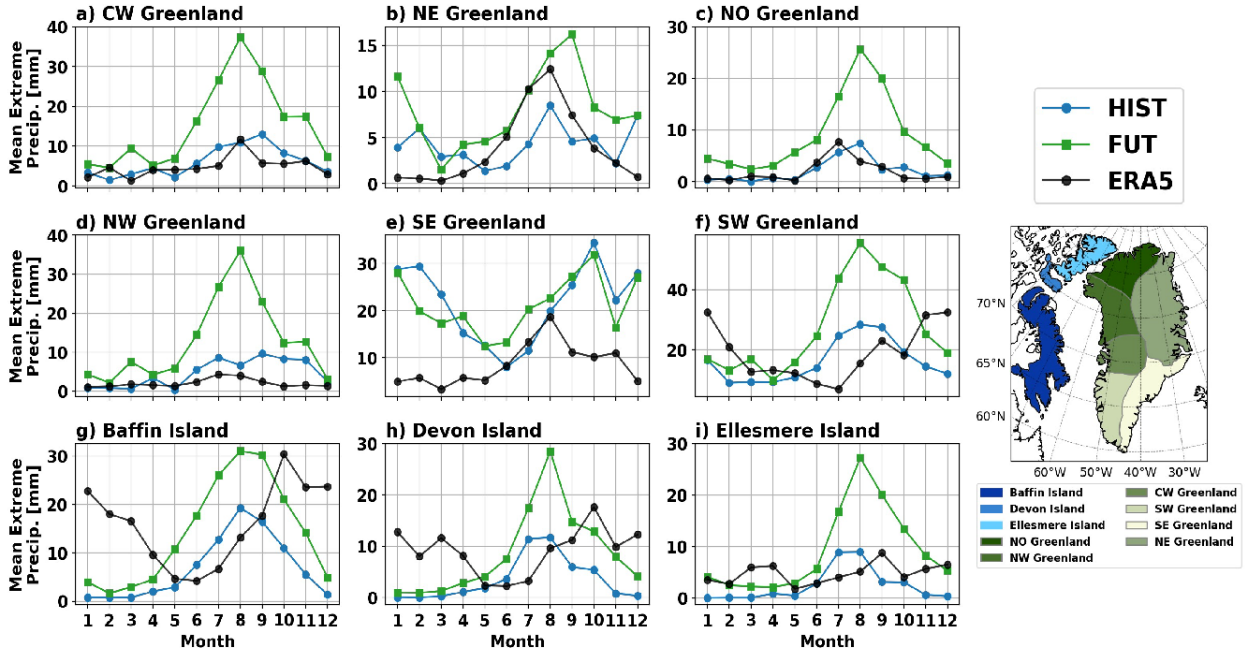

Figure 4.6. Mean total extreme precipitation accumulation in each in ERA5 (1980-1999, black), HIST (1980-1999, blue), and FUT (2080-2099, green) in each subregion (a-i). The map shows the location of each subregion.

4.4 Drivers of extremes

4.4.1 Changes in cyclones and ARs

The changes in cyclone characteristics when comparing the historical and future periods are relatively small overall. Figure 4.7 shows annual and seasonal cyclone track density in ERA5, HIST, and FUT. Note that the algorithm cannot detect cyclone centers above 1500 m ASL, so conclusions cannot be drawn about cyclone changes over inland regions of the Greenland Ice Sheet. The periods of JFM for winter and JAS for summer were selected to best align with the timing of changes shown in Figure 4.6. Overall, VR-CESM captures the pattern of track density, except for generating a higher density of tracks southeast of Greenland than is seen in ERA5. Comparing HIST and FUT, only relatively small changes are seen outside of a decrease in storm frequency predicted in the North Atlantic storm track (southeast of Greenland) throughout the year. This agrees with previous studies suggesting a weakening of the North Atlantic storm track under future warming scenarios including SSP5-8.5 (e.g., Crawford et al., 2023; Priestley & Catto, 2022). There is also a minor statistically significant increase in cyclone track density in northern Baffin Bay during the summer (Figure 4.7n). Cyclones entering Baffin Bay tend to move towards the north leading to cyclolysis in the region, rather than propagating over Greenland (Crawford et al., 2023).

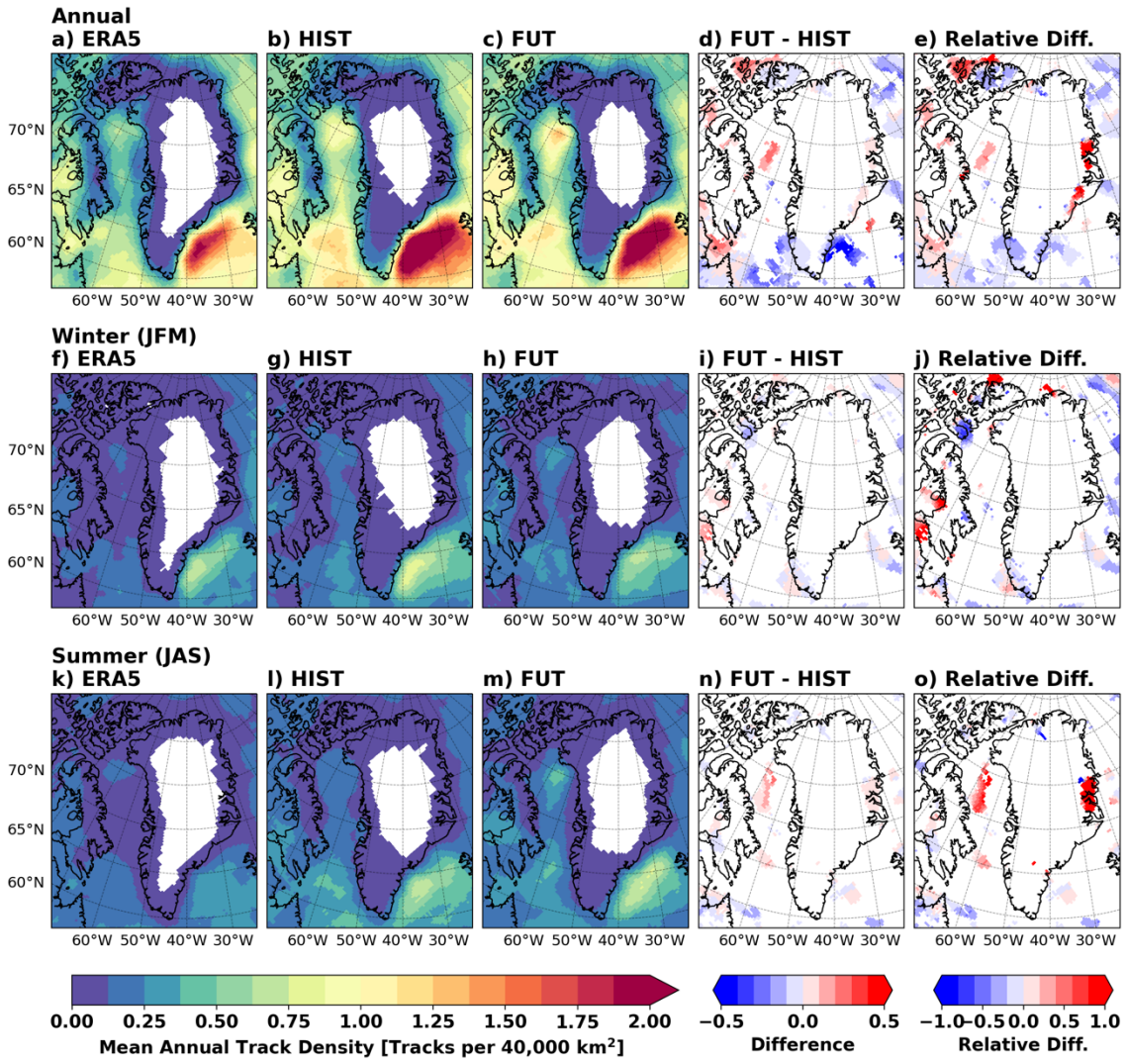

Figure 4.7. Cyclone track densities from (a) ERA5 (1980-1999), (B) HIST (1980-1999), and (c) FUT (2080-2099). The differences between the future and historical conditions are shown in (c), with fractional differences (relative to HIST) shown in (e). Only differences that are statistically significant ($p < 0.05$) are shown.

The number of days the region was impacted by an AR in ERA5 and the VR-CESM simulations are shown in Figure 4.8. Again, VR-CESM agrees quite well with ERA5, except that VR-CESM produces a few AR days reaching further north into Baffin Bay and west of Ellesmere Island. This agrees with Waling et al. (2024), who also found that reanalyses did not produce ARs as far north as several CESM2 and VR-CESM simulations. In the historical period, ARs occurred almost exclusively over the Labrador Sea and along the North Atlantic storm track toward Iceland, with the core of the AR generally dissipating quickly once reaching land within the domain. It is hypothesized that ARs often do not penetrate far inland on Greenland due to steep topography forcing orographic uplift and precipitation as the AR makes landfall (Waling et al., 2024). The highest frequency of ARs reaching Greenland occurred in the warm season and is most common along the southwestern coast, consistent with previous studies (e.g., Waling et al., 2024). The future simulation shows northward expansion of the area impacted by ARs, into Baffin Bay and near the southeastern coast of Greenland. Unlike cyclone frequency, AR occurrence either remains constant

or increases everywhere in the region. The strongest increases occur during the summer in the north Atlantic, agreeing with the findings of Kolbe et al. (2023).

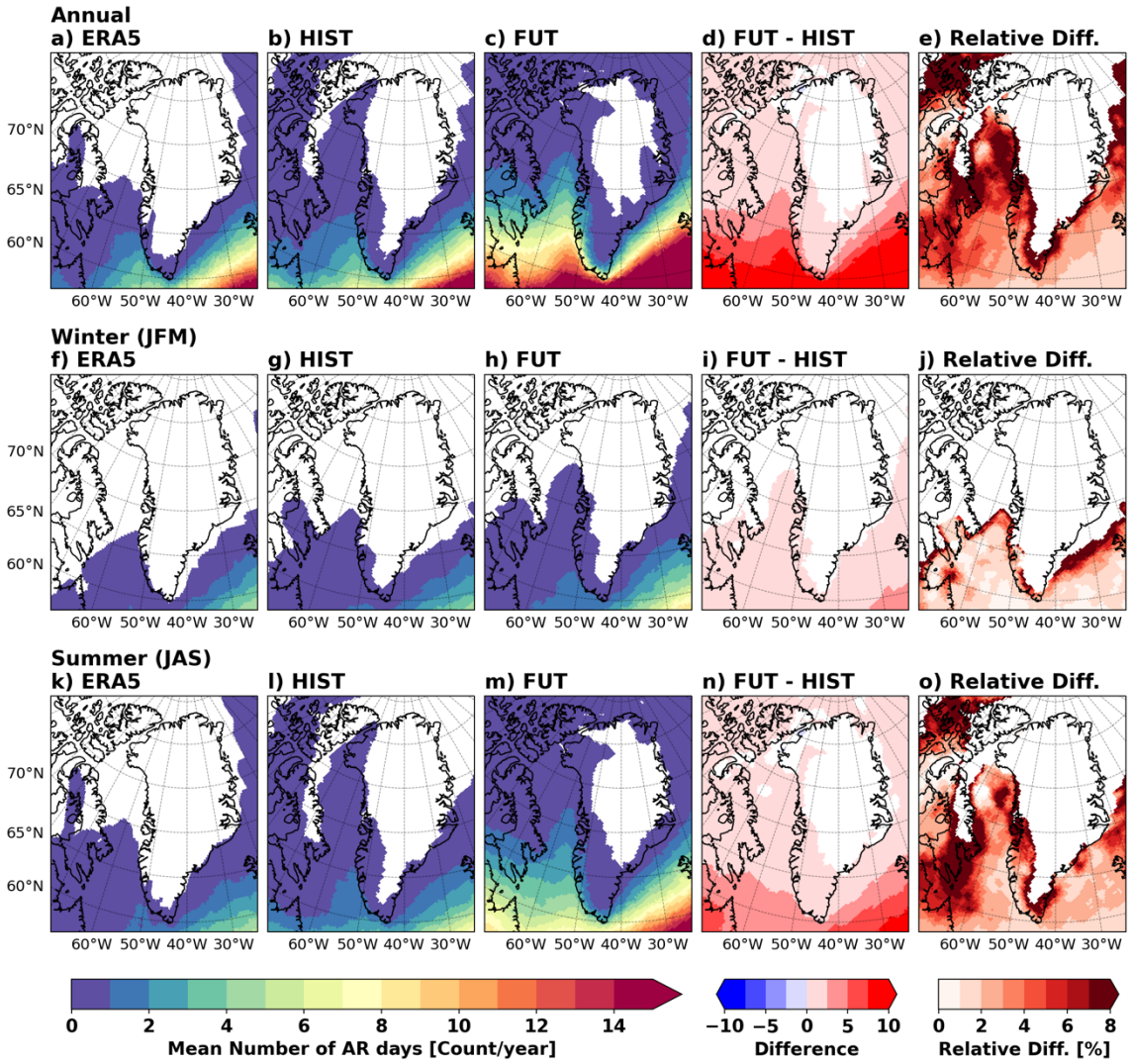

Figure 4.8. As in Figure 4.7, but for number of AR days in each grid cell.

Several factors are theorized to contribute to the changes in cyclone and AR frequency. One major consideration is the reduction in sea ice cover and Arctic amplification. Strong Arctic warming and sea ice loss can result in a weakening of geopotential thickness gradients, leading to slower upper-level wind speeds and changes to the polar jet stream (Crawford et al., 2023). This, in turn, alters the distribution of precipitation features such as cyclones and ARs. Some projections have shown a southeastward shift of the North Atlantic storm track (e.g., Priestley & Catto, 2022; Yettella & Kay, 2017), bringing fewer cyclones toward SE Greenland. This agrees with the slight reduction in cyclone track density seen in our projections (Figure 4.7). Strong ARs are generally associated with cyclones (e.g., Guo et al., 2020), meaning that the factors influencing cyclones are likely to produce similar results in AR frequency. These changes in cyclone and AR distribution in the warming climate can impact the occurrence of extreme precipitation as the events typically

rely on strong forcing to occur. This means that the distribution and occurrence of extreme precipitation days is likely closely tied to changes in cyclone frequency.

Other factors, such as the intensity of cyclones, can also play a role in the changing precipitation distribution. For example, SE Greenland is expected to see less cyclone-associated precipitation in the winter, but the change has been attributed to lower accumulations from a similar number of cyclones due to a dynamic weakening of storms in the region (Yettella & Kay, 2017). In general, the reduction of the pole-to-equator temperature (or geopotential thickness) gradient reduces the strength of the polar jet stream, resulting in fewer, weaker storms (Crawford et al., 2023; Harvey et al., 2020; Priestley and Catto, 2022). The future VR-CESM run shows a slight weakening of pressure gradients associated with cyclone centers, particularly in the summer (Figure B.8). This agrees with the minor summer weakening trend shown in previous studies (e.g., Crawford & Serreze, 2017; Priestley & Catto, 2022).

4.4.2 Relation of cyclones and ARs to extreme precipitation

Figure 4.9 shows the mean annual fraction of extreme precipitation days that are associated with extratropical cyclones or ARs in the historical and future periods. Historically, the vast majority of extreme precipitation days are associated with cyclones (Figure 4.9a-b), while ARs only bring extreme precipitation over water in the southern half of the domain (Figure 4.9e-f). ERA5 shows a lower fraction of extreme precipitation days associated with cyclones than HIST, but this is likely related to the lower cyclone track densities found in ERA5 (Figure 4.7a-b).

Overall, the future projection shows only relatively small changes in cyclone frequency (Figure 4.7), yielding only minor influence on the changes seen in extreme precipitation days. This suggests that changing precipitation rates within cyclones play a more important role in extreme precipitation occurrence than changes in cyclone frequency. Even the significant decrease in track density southeast of Greenland (Figure 4.7) is associated with only a slight decrease in extreme precipitation along the southeastern coast of Greenland. Note that this lack of notable cyclone-driven extreme precipitation change is robust to the radius used for identifying CAP. Using a 600 km radius (instead of 1200 km) results in a lower fraction of extreme precipitation associated with cyclones (< 80%), but results in almost identical patterns of change between the historical and future runs (Figure B.14).

Since ARs are most frequent in the southern edge of the domain, they are present on extreme precipitation days most commonly in the south. However, their importance in extreme precipitation days reaches further north into Baffin Bay in the future period. It should also be noted that the vast majority of ARs are associated with cyclones, particularly those reaching furthest north (Figure 4.9f-g, j-k). In general, outside of tropical or subtropical moisture source regions, the majority of ARs are associated with cyclones (e.g., Zhang et al., 2019).

The fraction of extreme precipitation days with a cyclone present decreases across most of the domain, with small regions of increase in western and northeastern Greenland (Figure 4.9d). The largest decrease is seen in northwestern Greenland, where the fraction of extreme precipitation days coinciding with cyclones decreases by approximately 15%. Conversely, increases in the importance of ARs for extreme precipitation are seen in the southern edge of the domain and along the southwestern coast of Greenland, where some of the largest increases in extreme precipitation

occur. In this region, the fraction of extreme precipitation days associated with ARs reaches up to 30% in FUT. Nellikkattil et al. (2023) found an increased probability of extreme precipitation associated with ARs in a warming climate in much of the Arctic, with some of the strongest increases in western Greenland and Baffin Bay, consistent with the increased portion of extreme precipitation days associated with ARs in our results.

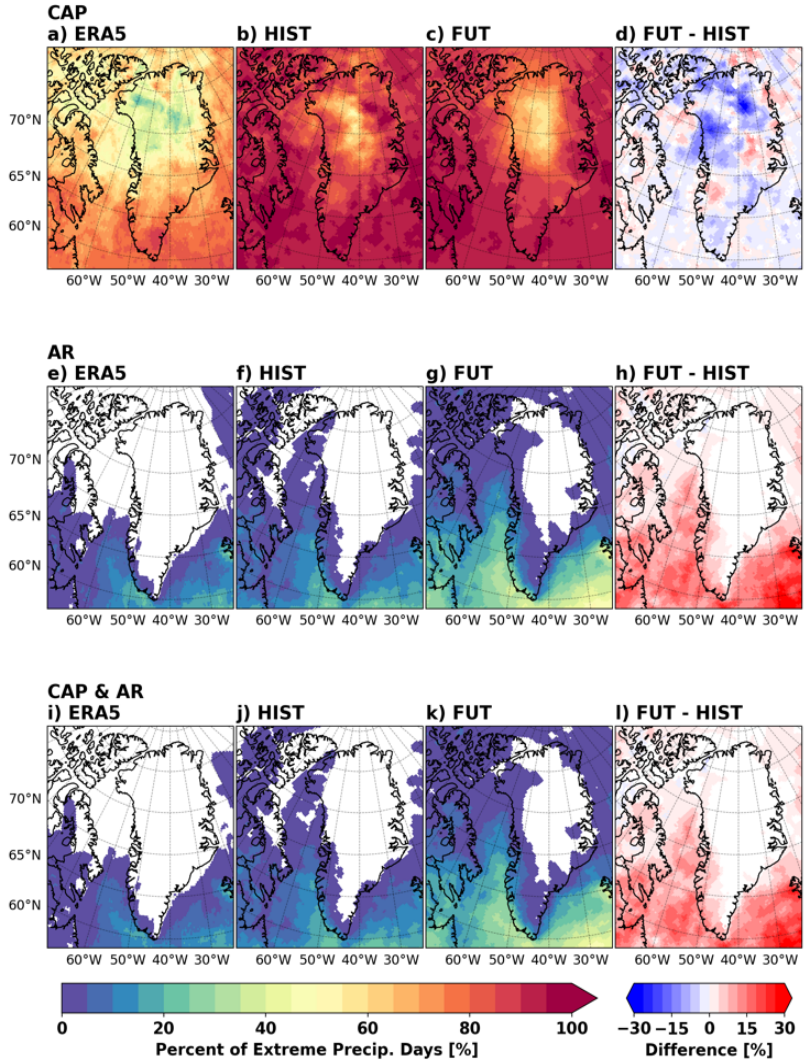

Figure 4.9. Fraction of all extreme precipitation days that are (a-d) cyclone-associated precipitation (CAP), (e-h) AR-associated, and (i-l) associated with both a cyclone and AR. Results are shown for (a,e,i) ERA5 (1980-1999), (b,f,j) HIST (1980-1999), (c,g,k) FUT (2080-2099) runs, and differences (FUT – HIST) are shown in (d,h,l). Only statistically significant differences ($p < 0.05$) are shown in (d,h,l).

The importance of cyclones and ARs to extreme precipitation days in the winter (JFM) and summer (JAS) is shown in Figures B.12 and B.13, respectively. In the winter, there is little to no change for most of the region outside of the increased importance of ARs in the north Atlantic and southern tip of Greenland. Changes are more substantial during the summer, particularly with ARs accounting for a higher portion of extreme precipitation days. This is likely due to the large increase in AR frequency during the summer shown in Figure 4.8.

Cyclones and ARs are expected to have increased precipitation rates as atmospheric moisture rises thermodynamically following the Clausius-Clapeyron relationship in a warming climate (e.g., Bengtsson et al., 2011). This means that extreme precipitation is likely to increase despite relatively minor changes to system frequency or intensity. Additionally, loss of sea ice allows for more open water in high latitudes, which can augment tropospheric moisture content and enhance precipitation associated with cyclones and ARs (e.g., Crawford et al., 2022; Kopec et al., 2016). With a warmer atmosphere carrying more moisture, moisture transport exceeding the threshold for ARs is expected to become more common (Dacre et al., 2015), as seen in Figure 4.8. The thermodynamic moisture increase is hypothesized to be the main factor driving increasing precipitation amounts in both cyclones (e.g., Cassano et al., 2007; Crawford & Serreze, 2017; Yettella & Kay, 2017) and ARs (e.g., Kolbe et al., 2023; Nellikkattil et al., 2023). The increase in the fraction of extreme precipitation days associated with ARs, along with the lack of difference in future changes in the second VR-CESM simulation with higher sea ice cover (Figures B.15-17), suggests that moisture convergence is likely contributing more to the increasing extreme precipitation than local evaporation in the region, as has been suggested by previous studies for the Arctic overall (e.g., Naakka et al., 2019; Nygård et al., 2020).

4.5 Conclusions

In this study, the occurrence of extreme precipitation in historical and future VR-CESM simulations was investigated. There are three key conclusions:

Firstly, future projections of VR-CESM show broad increases in extreme precipitation across the domain. In general, the seasonality of extreme precipitation remains consistent, with the highest accumulations occurring during the warm season. The exception to these increases is southeastern Greenland, where the amount of extreme precipitation and its contribution to annual precipitation is projected to decline. The projected decrease is hypothesized to be associated with a slight decrease in cyclone track density near southeastern Greenland.

Secondly, cyclones have been associated with the vast majority of intense precipitation in the study domain historically, but the role of cyclones in extreme precipitation shows only minor changes in future projections. There are slight decreases in the percent of extreme precipitation associated with cyclones (≈ -10%) in some regions, such as southeastern Greenland where a small decrease in cyclone track density is seen.

Finally, ARs become more frequent during the summer and are likely associated with the rise in extreme precipitation accumulations. ARs are projected to occur almost everywhere in the domain during the summer in the future period, including Ellesmere Island and northeastern Greenland, where HIST showed no ARs. This is associated with increased occurrence of AR-associated extreme precipitation days. Over land, the largest increases are seen in Baffin Island and southwestern Greenland, where the fraction of extremes associated with ARs increases by upwards of 15%.

While the results of this study provide insight into potential changes to extreme precipitation, there are some limitations that must be acknowledged. Firstly, extremes are rare by nature so there are limited quality observations to verify if VR-CESM agrees well with the overall patterns and statistics of historical extremes. VR-CESM agrees fairly well with ERA5 in the

overall statistics of extremes, but there are uncertainties in how well ERA5 represents precipitation extremes (e.g., Loeb et al., 2022). Finally, the use of only one model introduces uncertainty. The use of a multi-model ensemble where available can better capture internal variability that may be missed in a single simulation. Future work performing similar analyses with a variety of climate models can help to increase confidence in the results presented here.

Author Contributions

Conceptualization and methodology: NAL, AC, JS, and JH. Main data processing and analysis: NAL. TempestExtremes algorithm setup: AH. CMIP6 CESM comparison: MM. Writing: NAL. Editing/reviewing: AC, AH, MM, JS, and JH. Supervision: AC, JS and JH. All authors contributed to the article and approved the submitted version.

Open Research

Processed data is available on the Canadian Watershed Information Network (CanWIN, https://canwin-datahub.ad.umanitoba.ca/data/project/extreme-precipitation-events-in-greenland-baffin-bay, https://doi.org/10.34992/ebnw-s681). ERA5 data is retrieved from Copernicus (Hersbach et al., 2023; https://doi.org/10.24381/cds.adbb2d47). TempestExtremes v2.1 release is available from ZENODO at https://doi.org/10.5281/zenodo.4385656. The Crawford et al. (2021) cyclone-tracking algorithm can be accessed at https://doi.org/10.5281/zenodo.7562953.

Literature cited

Bao, J.-W., Michelson, S. A., Neiman, P. J., Ralph, F. M., & Wilczak, J. M. (2006). Interpretation of Enhanced Integrated Water Vapor Bands Associated with Extratropical Cyclones: Their Formation and Connection to Tropical Moisture. *Monthly Weather Review*, *134*(4), 1063–1080. https://doi.org/10.1175/MWR3123.1

Barrett, A. P., Stroeve, J. C., & Serreze, M. C. (2020). Arctic Ocean Precipitation From Atmospheric Reanalyses and Comparisons With North Pole Drifting Station Records. *Journal of Geophysical Research: Oceans*, *125*(1), 1–17. https://doi.org/10.1029/2019JC015415

Bengtsson, L., Hodges, K. I., Koumoutsaris, S., Zahn, M., & Keenlyside, N. (2011). The changing atmospheric water cycle in Polar Regions in a warmer climate. *Tellus A: Dynamic Meteorology and Oceanography*, *63*(5), 907–920. https://doi.org/10.1111/j.1600-0870.2011.00534.x

Bintanja, R., & Andry, O. (2017). Towards a rain-dominated Arctic. *Nature Climate Change*, *7*(4), 263–267. https://doi.org/10.1038/nclimate3240

Bintanja, R., & Selten, F. M. (2014). Future increases in Arctic precipitation linked to local evaporation and sea-ice retreat. *Nature*, *509*(7501), 479–482. https://doi.org/10.1038/nature13259

Bintanja, R., Wiel, K. van der, Linden, E. C. van der, Reusen, J., Bogerd, L., Krikken, F., & Selten, F. M. (2020). Strong future increases in Arctic precipitation variability linked to poleward moisture transport. *Science Advances*, *6*(7), eaax6869. https://doi.org/10.1126/sciadv.aax6869

Bjørk, A. A., Aagaard, S., Lütt, A., Khan, S. A., Box, J. E., Kjeldsen, K. K., et al. (2018). Changes in Greenland's peripheral glaciers linked to the North Atlantic Oscillation. *Nature Climate Change, 8*(1), 48–52. https://doi.org/10.1038/s41558-017-0029-1

Box, J. E., Wehrlé, A., van As, D., Fausto, R. S., Kjeldsen, K. K., Dachauer, A., et al. (2022). Greenland Ice Sheet Rainfall, Heat and Albedo Feedback Impacts From the Mid-August 2021 Atmospheric River. *Geophysical Research Letters, 49*(11), e2021GL097356. https://doi.org/10.1029/2021GL097356

Browning, K. A., & Pardoe, C. W. (1973). Structure of low-level jet streams ahead of mid-latitude cold fronts. *Quarterly Journal of the Royal Meteorological Society, 99*(422), 619–638. https://doi.org/10.1002/qj.49709942204

Cai, L., Alexeev, V. A., Arp, C. D., Jones, B. M., Liljedahl, A. K., & Gädeke, A. (2018). The Polar WRF Downscaled Historical and Projected Twenty-First Century Climate for the Coast and Foothills of Arctic Alaska. *Frontiers in Earth Science, 5*. https://doi.org/10.3389/feart.2017.00111

Catto, J. L. (2016). Extratropical cyclone classification and its use in climate studies. *Reviews of Geophysics, 54*(2), 486–520. https://doi.org/10.1002/2016RG000519

Chen, Q., Bromwich, D. H., & Bai, L. (1997). Precipitation over Greenland Retrieved by a Dynamic Method and Its Relation to Cyclonic Activity. *Journal of Climate, 10*(5), 839–870. https://doi.org/10.1175/1520-0442(1997)010<0839:POGRBA>2.0.CO;2

Crawford, A. D., & Serreze, M. C. (2017). Projected Changes in the Arctic Frontal Zone and Summer Arctic Cyclone Activity in the CESM Large Ensemble. *Journal of Climate, 30*(24), 9847–9869. https://doi.org/10.1175/JCLI-D-17-0296.1

Crawford, A. D., Schreiber, E. A. P., Sommer, N., Serreze, M. C., Stroeve, J. C., & Barber, D. G. (2021). Sensitivity of Northern Hemisphere Cyclone Detection and Tracking Results to Fine Spatial and Temporal Resolution Using ERA5. *Monthly Weather Review*, *149*(8), 2581–2598. https://doi.org/10.1175/MWR-D-20-0417.1

Crawford, A. D., McCrystall, M. R., Lukovich, J. V., & Stroeve, J. C. (2023). The Response of Extratropical Cyclone Propagation in the Northern Hemisphere to Global Warming. *Journal of Climate, 36*(20), 7123–7142. https://doi.org/10.1175/JCLI-D-23-0082.1

Dacre, H. F., Clark, P. A., Martinez-Alvarado, O., Stringer, M. A., & Lavers, D. A. (2015). How Do Atmospheric Rivers Form? *Bulletin of the American Meteorological Society, 96*(8), 1243–1255. https://doi.org/10.1175/BAMS-D-14-00031.1

Danabasoglu, G. (2019). NCAR CESM2 model output prepared for CMIP6 ScenarioMIP ssp585 [Data set]. Earth System Grid Federation. https://doi.org/10.22033/ESGF/CMIP6.7768

Danabasoglu, G., Lamarque, J.-F., Bacmeister, J., Bailey, D. A., DuVivier, A. K., Edwards, J., et al. (2020). The Community Earth System Model Version 2 (CESM2). *Journal of Advances in Modeling Earth Systems*, *12*, e2019MS001916. https://doi.org/10.1029/2019MS001916

Delhasse, A., Kittel, C., Amory, C., Hofer, S., van As, D., S. Fausto, R., & Fettweis, X. (2020). Brief communication: Evaluation of the near-surface climate in ERA5 over the Greenland Ice Sheet. *The Cryosphere, 14*(3), 957–965. https://doi.org/10.5194/tc-14-957-2020

Doyle, S. H., Hubbard, A., van de Wal, R. S. W., Box, J. E., van As, D., Scharrer, K., et al. (2015). Amplified melt and flow of the Greenland ice sheet driven by late-summer cyclonic rainfall. *Nature Geoscience, 8*(8), 647–653. https://doi.org/10.1038/ngeo2482

Fischer, E. M., & Knutti, R. (2016). Observed heavy precipitation increase confirms theory and early models. *Nature Climate Change, 6*(11), 986–991. https://doi.org/10.1038/nclimate3110

Ford, J. D., Bell, T., & St-Hilaire-Gravel, D. (2010). Vulnerability of Community Infrastructure to Climate Change in Nunavut: A Case Study From Arctic Bay. In G. K. Hovelsrud & B. Smit (Eds.), *Community Adaptation and Vulnerability in Arctic Regions* (pp. 107–130). Dordrecht: Springer Netherlands. https://doi.org/10.1007/978-90-481-9174-1_5

Gardner, A. S., Moholdt, G., Wouters, B., Wolken, G. J., Burgess, D. O., Sharp, M. J., et al. (2011). Sharply increased mass loss from glaciers and ice caps in the Canadian Arctic Archipelago. Nature, 473(7347), 357–360. https://doi.org/10.1038/nature10089

Gettelman, A., & Morrison, H. (2015). Advanced Two-Moment Bulk Microphysics for Global Models. Part I: Off-Line Tests and Comparison with Other Schemes. Journal of Climate, 28(3), 1268–1287. https://doi.org/10.1175/JCLI-D-14-00102.1

Gettelman, A., Morrison, H., Santos, S., Bogenschutz, P., & Caldwell, P. M. (2015). Advanced Two-Moment Bulk Microphysics for Global Models. Part II: Global Model Solutions and Aerosol–Cloud Interactions. *Journal of Climate, 28*(3), 1288–1307. https://doi.org/10.1175/JCLI-D-14-00103.1

Golaz, J.-C., Larson, V. E., & Cotton, W. R. (2002). A PDF-Based Model for Boundary Layer Clouds. Part I: Method and Model Description. *Journal of the Atmospheric Sciences, 59*(24), 3540–3551. https://doi.org/10.1175/1520-0469(2002)059<3540:APBMFB>2.0.CO;2

Graham, R. M., Hudson, S. R., & Maturilli, M. (2019). Improved Performance of ERA5 in Arctic Gateway Relative to Four Global Atmospheric Reanalyses. *Geophysical Research Letters, 46*(11), 6138–6147. https://doi.org/10.1029/2019GL082781

Guo, Y., Shinoda, T., Guan, B., Waliser, D. E., & Chang, E. K. M. (2020). Statistical Relationship between Atmospheric Rivers and Extratropical Cyclones and Anticyclones. *Journal of Climate, 33*(18), 7817–7834. https://doi.org/10.1175/JCLI-D-19-0126.1

Harper, J., Saito, J., & Humphrey, N. (2023). Cold Season Rain Event Has Impact on Greenland's Firn Layer Comparable to Entire Summer Melt Season. *Geophysical Research Letters, 50*(14), e2023GL103654. https://doi.org/10.1029/2023GL103654

Hennermann, K., & Giusti, M. (2021). What are the changes from ERA-Interim to ERA5 and ERA5-Land? Retrieved October 27, 2021, from https://confluence.ecmwf.int//pages/viewpage.action?pageId=74764925

Herrington, A. R., Lauritzen, P. H., Lofverstrom, M., Lipscomb, W. H., Gettelman, A., & Taylor, M. A. (2022). Impact of grids and dynamical cores in CESM2.2 on the surface mass balance of the Greenland Ice Sheet. J*ournal of Advances in Modeling Earth Systems*, e2022MS003192. https://doi.org/10.1029/2022MS003192

Hersbach, H., Bell, B., Berrisford, P., Hirahara, S., Horányi, A., Muñoz-Sabater, J., et al. (2020). The ERA5 global reanalysis. *Quarterly Journal of the Royal Meteorological Society, 146*(730), 1999–2049. https://doi.org/10.1002/qj.3803

Hersbach, H., Bell, B., Berrisford, P., Biavati, G., Horányi, A., Muñoz Sabater, J., Nicolas, J., Peubey, C., Radu, R., Rozum, I., Schepers, D., Simmons, A., Soci, C., Dee, D., Thépaut, J-N. (2023): ERA5 hourly data on single levels from 1940 to present. Copernicus Climate Change Service (C3S) Climate Data Store (CDS), https://www.doi.org/10.24381/cds.adbb2d47

Hugonnet, R., McNabb, R., Berthier, E., Menounos, B., Nuth, C., Girod, L., et al. (2021). Accelerated global glacier mass loss in the early twenty-first century. *Nature, 592*(7856), 726–731. https://doi.org/10.1038/s41586-021-03436-z

Intihar, M. R., & Stewart, R. E. (2005). Extratropical Cyclones and Precipitation within the Canadian Archipelago during the Cold Season. *Arctic, 58*(2), 162–174.

van Kampenhout, L., Rhoades, A. M., Herrington, A. R., Zarzycki, C. M., Lenaerts, J. T. M., Sacks, W. J., & van den Broeke, M. R. (2019). Regional grid refinement in an Earth system model: impacts on the simulated Greenland surface mass balance. *The Cryosphere, 13*(6), 1547–1564. https://doi.org/10.5194/tc-13-1547-2019

Kolbe, M., Sonnemans, J. P. J., Bintanja, R., van der Linden, E. C., van der Wiel, K., Whan, K., & Benedict, I. (2023). Impact of Atmospheric Rivers on Future Poleward Moisture Transport and Arctic Climate in EC-Earth2. *Journal of Geophysical Research: Atmospheres*, e2023JD038926. https://doi.org/10.1029/2023JD038926

Loeb, N. A., Crawford, A., Stroeve, J. C., & Hanesiak, J. (2022). Extreme Precipitation in the Eastern Canadian Arctic and Greenland: An Evaluation of Atmospheric Reanalyses. *Frontiers in Environmental Science, 10*. Retrieved from https://www.frontiersin.org/articles/10.3389/fenvs.2022.866929

Mattingly, K. S., Mote, T. L., & Fettweis, X. (2018). Atmospheric River Impacts on Greenland Ice Sheet Surface Mass Balance. *Journal of Geophysical Research: Atmospheres, 123*(16), 8538–8560. https://doi.org/10.1029/2018JD028714

McCrystall, M. R., Stroeve, J., Serreze, M., Forbes, B. C., & Screen, J. A. (2021). New climate models reveal faster and larger increases in Arctic precipitation than previously projected. *Nature Communications, 12*(1), 6765. https://doi.org/10.1038/s41467-021-27031-y

Myhre, G., Alterskjær, K., Stjern, C. W., Hodnebrog, Ø., Marelle, L., Samset, B. H., et al. (2019). Frequency of extreme precipitation increases extensively with event rareness under global warming. *Scientific Reports, 9*(1), 16063. https://doi.org/10.1038/s41598-019-52277-4

Nellikkattil, A. B., Lee, J.-Y., Guan, B., Timmermann, A., Lee, S.-S., Chu, J.-E., & Lemmon, D. (2023). Increased amplitude of atmospheric rivers and associated extreme precipitation in ultra-high-resolution greenhouse warming simulations. *Communications Earth & Environment, 4*(1), 1–11. https://doi.org/10.1038/s43247-023-00963-7

Nitu, R., Roulet, Y. A., Wolff, M., Rasmussen, R., Lanzinger, E., Smith, C., et al. (2018). WMO Solid Precipitation Intercomparison Experiment (SPICE)(2012-2015) (SPICE Final Report No. 131) (p. 1445). World Meteorological Organization. Retrieved from https://library.wmo.int/doc_num.php?explnum_id=5686

Noël, B., van de Berg, W. J., Machguth, H., Lhermitte, S., Howat, I., Fettweis, X., & van den Broeke, M. R. (2016). A daily, 1 km resolution data set of downscaled Greenland ice sheet surface mass balance (1958–2015). *The Cryosphere, 10*(5), 2361–2377. https://doi.org/10.5194/tc-10-2361-2016

Noël, B., van de Berg, W. J., van Wessem, J. M., van Meijgaard, E., van As, D., Lenaerts, J. T. M., et al. (2018). Modelling the climate and surface mass balance of polar ice sheets using RACMO2 – Part 1: Greenland (1958–2016). *The Cryosphere, 12*(3), 811–831. https://doi.org/10.5194/tc-12-811-2018

Oerlemans, J., & Klok, E. J. L. (2004). Effect of summer snowfall on glacier mass balance. *Annals of Glaciology, 38*, 97–100. https://doi.org/10.3189/172756404781815158

O'Neill, B. C., Tebaldi, C., van Vuuren, D. P., Eyring, V., Friedlingstein, P., Hurtt, G., et al. (2016). The Scenario Model Intercomparison Project (ScenarioMIP) for CMIP6. *Geoscientific Model Development, 9*(9), 3461–3482. https://doi.org/10.5194/gmd-9-3461-2016

Pendergrass, A. G. (2018). What precipitation is extreme? *Science, 360*(6393), 1072–1073. https://doi.org/10.1126/science.aat1871

Pendergrass, A. G., Knutti, R., Lehner, F., Deser, C., & Sanderson, B. M. (2017). Precipitation variability increases in a warmer climate. *Scientific Reports, 7*(1), 17966. https://doi.org/10.1038/s41598-017-17966-y

Pfahl, S., O'Gorman, P. A., & Fischer, E. M. (2017). Understanding the regional pattern of projected future changes in extreme precipitation. *Nature Climate Change, 7*(6), 423–427. https://doi.org/10.1038/nclimate3287

Priestley, M. D. K., & Catto, J. L. (2022). Future changes in the extratropical storm tracks and cyclone intensity, wind speed, and structure. *Weather and Climate Dynamics, 3*(1), 337–360. https://doi.org/10.5194/wcd-3-337-2022

Rawlins, M. A., Steele, M., Holland, M. M., Adam, J. C., Cherry, J. E., Francis, J. A., et al. (2010). Analysis of the Arctic System for Freshwater Cycle Intensification: Observations and Expectations. *Journal of Climate, 23*(21), 5715–5737. https://doi.org/10.1175/2010JCLI3421.1

Rignot, E., & Mouginot, J. (2012). Ice flow in Greenland for the International Polar Year 2008–2009. *Geophysical Research Letters, 39*(11). https://doi.org/10.1029/2012GL051634

Rignot, E., Velicogna, I., van den Broeke, M. R., Monaghan, A., & Lenaerts, J. T. M. (2011). Acceleration of the contribution of the Greenland and Antarctic ice sheets to sea level rise. *Geophysical Research Letters, 38*(5). https://doi.org/10.1029/2011GL046583

Schuenemann, K. C., Cassano, J. J., & Finnis, J. (2009). Synoptic Forcing of Precipitation over Greenland: Climatology for 1961–99. *Journal of Hydrometeorology, 10*(1), 60–78. https://doi.org/10.1175/2008JHM1014.1

Seager, R., Naik, N., & Vecchi, G. A. (2010). Thermodynamic and Dynamic Mechanisms for Large-Scale Changes in the Hydrological Cycle in Response to Global Warming. *Journal of Climate, 23*(17), 4651–4668. https://doi.org/10.1175/2010JCLI3655.1

Ullrich, P. A., Zarzycki, C. M., McClenny, E. E., Pinheiro, M. C., Stansfield, A. M., & Reed, K. A. (2021). TempestExtremes v2.1: a community framework for feature detection, tracking, and analysis in large datasets. *Geoscientific Model Development, 14*(8), 5023–5048. https://doi.org/10.5194/gmd-14-5023-2021

Vavrus, S. J. (2013). Extreme Arctic cyclones in CMIP5 historical simulations. *Geophysical Research Letters, 40*(23), 6208–6212. https://doi.org/10.1002/2013GL058161

Waling, A. (2023, May). Using Variable-Resolution Grids to Model Precipitation from Atmospheric Rivers Around the Greenland Ice Sheet - ProQuest (Masters Thesis). University of New Hampshire. Retrieved from https://www.proquest.com/openview/bfa453a3af5a977574c51bdeec469956/1?pq-origsite=gscholar&cbl=18750&diss=y

Yettella, V., & Kay, J. E. (2017). How will precipitation change in extratropical cyclones as the planet warms? *Insights from a large initial condition climate model ensemble. Climate Dynamics, 49*(5), 1765–1781. https://doi.org/10.1007/s00382-016-3410-2

Zhang, Z., Ralph, F. M., & Zheng, M. (2019). The Relationship Between Extratropical Cyclone Strength and Atmospheric River Intensity and Position. *Geophysical Research Letters, 46*(3), 1814–1823. https://doi.org/10.1029/2018GL079071

Chapter 5 Modelling the Impacts of Historical and Future Extreme Precipitation Days on Seasonal Surface Mass Balance in the Eastern Canadian Arctic and Greenland

Nicole A. Loeb[1], Alex Crawford[1], Brice Noël[2], Julienne Stroeve[1,3,4]

[1]Department of Environment & Geography and Centre for Earth Observation Science, University of Manitoba, Winnipeg, MB, Canada
[2] Laboratory of Climatology, Department of Geography, SPHERES research unit, University of Liège, Liège, Belgium
[3] Department of Earth Sciences, University College London, London, United Kingdom
[4] National Snow and Ice Data Center, Cooperative Institute for Research in Environmental Sciences, University of Colorado Boulder, Boulder, CO, United States

This chapter is under review in *The Cryosphere*.

Loeb, N. A., Crawford, A., Noël, B., & Stroeve, J. (in review). Modelling the Impacts of Historical and Future Extreme Precipitation Days on Seasonal Surface Mass Balance in the Eastern Canadian Arctic and Greenland. *EGUsphere*, 1–30. https://doi.org/10.5194/egusphere-2025-995

Abstract

Land ice in the Arctic is losing mass as temperatures increase, contributing to global sea level rise. While this loss is largely driven by melt induced by atmospheric warming, precipitation can alter the rate at which loss occurs depending on its intensity and phase. Case studies have illustrated varied potential impacts of extreme precipitation events on the surface mass balance (SMB) of land ice, but the importance of extreme precipitation to seasonal SMB has not been investigated. In this study, simulations from the Regional Atmospheric Climate Model (RACMO) and Variable-Resolution Community Earth System Model (VR-CESM) are explored over historical (1980-1998) and future (2080-2098, SSP5-8.5) periods to reconstruct and further project seasonal SMB for the Greenland Ice Sheet and ice caps of the Eastern Canadian Arctic. Historically, extreme precipitation days consistently had higher SMB than non-extreme precipitation days throughout the study area in both the cold season (DJFM) and warm season (JJAS). In future simulations, this relationship persists for the cold season. However, for the warm season, projections indicate a shift towards less positive and more variable SMB responses to extreme precipitation days in the future, accounting for a larger portion of cumulative seasonal positive and negative SMB. Mass loss during extreme precipitation days becomes more common, particularly in SW Greenland and Baffin Island. This likely occurs in part because of a shift toward more rainfall during extreme precipitation events. In other words, in a strong warming scenario, extreme warm season precipitation may no longer reliably yield mass gain for the Greenland Ice Sheet and surrounding ice caps.

5.1 Introduction

Arctic land ice, including the Greenland Ice Sheet (GrIS) and glacier and ice caps of the eastern Canadian Arctic, has been losing mass at an accelerated rate as the climate has warmed (e.g., Hugonnet et al. 2021; Constable et al. 2022). This mass loss is contributing to global sea level rise (e.g., Bamber et al., 2018; Hofer et al., 2020; Jacob et al., 2012) and triggers further warming via the ice-albedo feedback (e.g., Ryan et al., 2023). The ice-albedo feedback is one of the main drivers of "Arctic amplification", which refers to the Arctic region warming up to four times faster than the global average (Rantanen et al., 2022), in turn enhancing the rate of ice loss. The GrIS has been one of the largest contributors to global sea level rise since 1900 (van den Broeke et al., 2016; Fettweis et al., 2013; Frederikse et al., 2020; Hofer et al., 2020). A key driver of Greenland's contribution to global sea level rise is increased surface ice melt and runoff (e.g., Box, 2013; Fettweis et al., 2017). Annual and seasonal surface mass balance (SMB) of the GrIS has been extensively studied through observations (e.g., Bolch et al., 2013; Box, 2013; Cogley, 2004) and modelling (e.g., van Kampenhout et al., 2020; Noël et al., 2018a). The smaller ice caps and glaciers in the eastern Canadian Arctic Archipelago (CAA) have experienced accelerated mass loss in recent decades (Noël et al., 2018b). Lenaerts et al. (2013) showed that 18% of the land ice in the eastern CAA may be lost by 2100, even under a moderate warming scenario.

In models, the SMB is often quantified as

$$SMB = PR - RU - SU - ER \tag{5.1}$$

where PR refers to precipitation, RU is runoff, SU is loss due to sublimation/phase change, and ER represents wind-driven erosion (Noël et al., 2017, 2018b). The SMB neglects dynamic processes leading to ice loss, such as calving. In general, precipitation is expected to increase in most glaciated regions due to increased water vapour holding capacity as a result of atmospheric warming (e.g., Bengtsson et al., 2011; Norris et al., 2019; Skific et al., 2009). Surface melt has historically been the dominant factor driving land ice mass loss across much of the Arctic, largely due to rapid temperature increases and relatively low interannual variability in precipitation (Koerner, 2005; Van As et al., 2014). However, as the climate continues to warm, precipitation variability is expected to increase (Pendergrass et al., 2017), suggesting that precipitation may have a more critical impact on the variability of SMB in the future.

The SMB response to precipitation may change as the structure of the firn layer evolves with atmospheric warming. Firn is made up of snow that has lasted at least one melt season but has not yet compacted into glacial ice (Cogley et al., 2011). It is important when considering melt water and liquid precipitation, as it contains interconnected pore spaces that allow for liquid infiltration and freezing/refreezing, resulting in internal accumulation and reducing the amount of mass lost during melt (Forster et al., 2014; van Pelt and Kohler, 2015). However, the firn pore space is limited, and less may be available for retention as more melt and liquid precipitation occur (Machguth et al., 2016; Noël et al., 2022; van Pelt and Kohler, 2015). Noël et al. (2018b) noted how glaciers in the southern CAA are already experiencing decreased refreezing due to the filling of pore spaces, which has also been observed on the GrIS (MacFerrin et al., 2019). In addition to filling firn pore space, intense rainfall events can cause the densification of existing firn and prevent further firn growth (Machguth et al., 2016; Noël et al., 2017), meaning that more surface mass loss may occur due to rainfall in the future.

Another important factor when considering how precipitation may affect SMB is the rate of precipitation. Historical case studies have illustrated how extreme precipitation events can have different impacts depending on the timing and phase of precipitation. During the warm season, intense rainfall events have been shown to dramatically increase runoff and ice discharge (e.g., Doyle et al., 2015), causing the development of ice lenses that prevent infiltration and (re)freezing of liquid water in firn (e.g., Box et al., 2022). Increased surface melt warms the firn as refreezing releases latent heat at depth during infiltration (e.g., Harper et al., 2023). Doyle et al. (2015) examined rainfall associated with a late summer extratropical cyclone over Western Greenland. The Kangerlussuaq region received approximately 20% of its annual precipitation in a period of seven days, which is very uncommon for the area. This caused a dramatic increase in melt water runoff and acceleration of ice flow. While the cyclone brought warmer temperatures that promoted surface melt, latent heat was released as the rainfall froze to the ice surface, and surface albedo decreased. This caused melt production well into the accumulation region of impacted glaciers. Conversely, a heavy snowfall event can increase the albedo and reduce summer melt (e.g., Noël et al., 2015). Bailey & Hubbard (2025) presented an analysis of a March 2022 atmospheric river event impacting the southeastern GrIS. Temperatures remained near 0°C, resulting in heavy snowfall across the region. The fresh snowfall increased surface albedo, delaying the onset of the melt season by 11 days. The effect of the reduced melt and added snow mass from the event was found to offset seasonal mass loss by approximately 8% during the following melt season. While extreme precipitation events can cause dramatic short-term SMB changes, either positive or negative, their importance in a seasonal context has not been explicitly studied.

Climate model simulations project that extreme precipitation events will shift in the future. While mean precipitation is slowly changing, observations have shown that precipitation extremes have shifted more quickly than mean conditions (Fischer and Knutti, 2016; Myhre et al., 2019; Pendergrass et al., 2017). Loeb et al. (2024) showed how extreme precipitation increases across much of the Baffin Bay and Greenland region in simulations of warming scenarios in the Variable-Resolution Community Earth System Model (VR-CESM). Climate model simulations project that a higher portion of annual precipitation will originate from extreme events. One of the factors driving this increase is atmospheric rivers occurring farther north than historically observed (Li & Ding, 2024; Loeb et al., 2024), which can bring high temperatures and extreme precipitation (e.g., Bao et al., 2006; Browning and Pardoe, 1973; Mattingly et al., 2018). Conversely, southeastern Greenland is projected to experience a decrease in the amount of extreme precipitation, likely related to reduced cyclone frequency and intensity in the region (Crawford et al., 2023; Loeb et al., 2024; Priestley and Catto, 2022).

Changing precipitation extremes will impact the rate at which mass loss occurs from the GrIS and ice caps of the eastern Canadian Arctic and therefore may accelerate or decelerate their contributions to sea level rise. While case studies have illustrated the complex impacts of individual extreme precipitation events on the short-term SMB of land ice, the overall importance of extreme events at seasonal time scales has not been investigated. In this study, two climate models are used to investigate the contributions of extreme precipitation events to seasonal SMB of the GrIS and neighbouring ice caps of the eastern Canadian Arctic, and how those contributions differ between historical simulations and climate projections under a high emissions scenario.

5.2 Data & Methodology

5.2.1 Model Simulations

5.2.1.1 Regional Atmospheric Climate Model (RACMO)

The polar version of the Regional Atmospheric Climate Model (RACMO; van Meijgaard et al., 2008) is widely used to investigate the SMB of polar ice sheets (e.g., Lenaerts et al., 2013; Noël et al., 2017, 2018a). It contains a multi-layer snow module (40 layers) that reproduces processes within the snow column, including melt, percolation, refreezing, and runoff (Ettema et al., 2010). The amount of liquid water retention by capillary forces, or irreducible water saturation threshold, is set to 2% in RACMO2.3p2 (Glaude et al., 2024). Parameterization of snow surface albedo is based on prognostic snow-grain size, solar zenith angle, cloud optical thickness, and snow impurities (Kuipers Munneke et al., 2011).

The simulation used here is that of Noël et al. (2020, 2021); RACMO version 2.3p2 is used to dynamically downscale a Coupled Model Intercomparison Project (CMIP6) historical simulation of the Community Earth System Model (CESM) in 1950-2014, followed by a simulation of the SSP5-8.5 scenario in 2015-2100 with a spatial resolution of 11 km. Forcing of atmospheric temperature, pressure, specific humidity, wind speed and direction, sea ice, and sea surface temperature are prescribed at 6-hourly intervals (Noël et al., 2020, 2021).

5.2.1.2 Variable-resolution Community Earth System Model (VR-CESM)

The National Center for Atmospheric Research's Community Earth System Model (CESM), version 2.2, is a global earth system model that contains component models for the atmosphere, land, ocean, and cryospheric systems (Danabasoglu et al., 2020). The default spatial resolution of CESM is 1° × 1° latitude-longitude (Danabasoglu et al., 2020), but variable-resolution grids have been developed to downscale CESM simulations over areas of interest (Herrington et al., 2022). The Arctic VR-CESM grid is refined to 0.25° × 0.25° latitude-longitude over the entire Arctic nested within the 1° × 1° global simulation (Herrington et al., 2022).

The land component, the Community Land Model, version 5 (CLM5), simulates hydrological and snow processes, including SMB components for grid cells containing land ice (Danabasoglu et al., 2020; Lawrence et al., 2019). To account for the complex topography in glaciated areas, each glaciated grid cell is divided into 10 elevation classes to adjust atmospheric surface temperature, potential temperature, specific humidity, density, and pressure over ice surfaces (Lawrence et al., 2019). Along the periphery of ice caps and the GrIS, grid cells are also sub-divided into different land types to account for surface heterogeneity. CLM5 also redistributes precipitation produced by the atmospheric component model, the Community Atmosphere Model, version 6 (CAM6) over glaciers. Precipitation is assumed to be snow below -2°C and rainfall above 0°C, with a mix occurring between the two thresholds (Lawrence et al., 2019).

The SMB in CLM5 is calculated as in Eq. 5.1, except that ER is not explicitly modelled and is therefore not considered (van Kampenhout et al., 2020). Melt is determined based on the surface energy balance calculated over the top few centimeters of snow or ice (van Kampenhout et al., 2020). The snow model within CLM5 contains up to 12 layers, representing up to 10 m water equivalent (w.e.) of firn or snow (van Kampenhout et al., 2017; Lawrence et al., 2019). This allows

for representation of processes such as compaction and liquid water percolation and retention within the column, with an irreducible water saturation threshold of 3.3% in CLM5 (van Kampenhout et al., 2020). Further details of the calculation of SMB in CLM5 are provided in van Kampenhout et al. (2020). The downscaling of CLM5 within VR-CESM has been shown to improve precipitation rates in the Arctic (Herrington et al., 2022; Loeb et al., 2024) and SMB of the GrIS (van Kampenhout et al., 2019).

Historical (1 Jan 1980 - 31 Dec 1998; Herrington et al., 2022) and future (1 Jan 2080 – 31 Dec 2098; Loeb et al., 2024) simulations were completed following the procedure of the Atmospheric Model Intercomparison Project (Hurrell et al., 2008), where the land (CLM5) and atmosphere (CAM6) components are actively modelled and coupled and sea surface temperatures and sea ice conditions are prescribed monthly. Monthly sea ice and sea surface temperatures are retrieved from existing CESM CMIP6 simulations (Danabasoglu et al., 2020; Meehl et al., 2020). The future simulation follows SSP5-8.5.

5.2.2 Methods

The study domain is divided into nine subregions (Figure 5.1): Canadian subregions are split by island. Greenland is divided into six regions based on glacier regime and SMB characteristics (Rignot et al., 2011; Rignot & Mouginot, 2012). The historical period (HIST) used is 1980-1998 and the future period (FUT) is 2080-2098, limited by the availability of VR-CESM data. Mean annual temperature in the study region rises in FUT relative to HIST by 6.1°C and 7.4°C in RACMO and VR-CESM, respectively. Two seasons are included for analysis: the warm season (JJAS) and cold season (DJFM). Four-month seasons are used, rather than three, to increase the number of extreme precipitation days that can be included for analysis and increase signal-to-noise ratio.

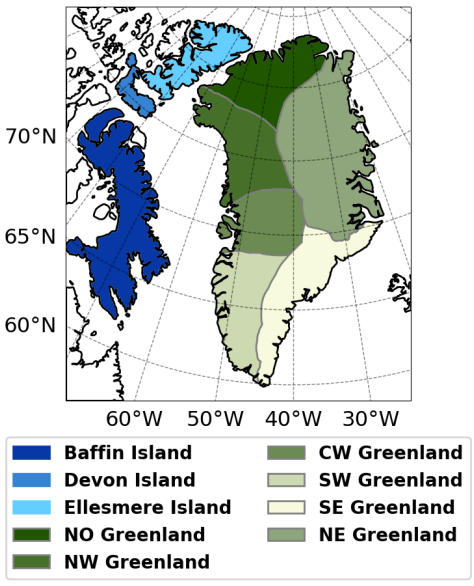

Figure 5.1. Study domain map showing subregions used for analysis.

Extreme precipitation is defined in two ways for this study: by individual grid cell, which highlights spatial gradients in extreme precipitation and its impacts, and by subregion, which facilitates the analysis of events that are extreme over an entire drainage basin or island. Extreme precipitation days in each grid cell (mm w.e./day) are those for which total daily precipitation is at or above the 95th percentile of days with at least 1 mm of precipitation, following Loeb et al. (2022, 2024). At the subregion level, extreme precipitation days are defined as the days at or above the 95th percentile of total daily precipitation volume (m^3/day) in the subregion, calculated by summing the product of precipitation multiplied by grid cell area for all glaciated grid cells in a subregion. To compare SMB on extreme precipitation days to non-extreme days, non-extreme precipitation days are defined as days where at least half of a region's grid cells receive at least 1 mm of precipitation, but the total amount is less than the extreme threshold for the subregion. In both cases, the historical threshold is used for both periods to assess changes in impacts resulting from precipitation at or above the same threshold. Historical extreme precipitation accumulations are compared to the 5th generation reanalysis product from the European Centre for Medium-Range Weather Forecasts (ERA5; Hersbach et al., 2020) to contextualize historical performance of RACMO and VR-CESM, following Loeb et al. (2024).

Short term anomalies in SMB-related variables for each extreme precipitation day were calculated relative to a window of ±15 days centred on the extreme precipitation day. We selected a 31-day period as the baseline instead of a climatology to focus on the within-season anomaly. This removes effects of background changes in mean seasonal/annual SMB conditions but will underestimate anomalies when the extreme events' impacts on SMB variables last for several days, which is likely most common for the albedo anomalies (e.g., Bailey and Hubbard, 2025; Oerlemans and Klok, 2004).

Next, the difference between historical and future (FUT minus HIST) interquartile range (IQR_{diff}) of SMB anomalies on extreme precipitation days was calculated. The IQR represents the difference between the first quartile (25th percentile) and third quartile (75th percentile) of the data. To assess statistical significance of this difference, a bootstrapping method was employed in which all years were randomly sorted into two groups and the IQR_{diff} was calculated. Repetitions were performed 1000 times, and if the real IQR_{diff} was greater than (respectively less than) 975 of the tests, this indicated a statistically significant increase (respectively decrease) in IQR in the future simulation, yielding a two-tailed confidence interval of 95%. Note that some of the anomalies from VR-CESM are presented in the supplementary information.

To assess the relative importance of extreme precipitation days to seasonal SMB, we first grouped each day (i) of SMB in each season into positive SMB (SMB_i^+) or negative SMB (SMB_i^-). Second, we calculated the cumulative positive (SMB_{all}^+) and negative SMB (SMB_{all}^-) during a season:

$$SMB_{all}^+ = \sum SMB_i^+ \tag{5.2}$$

$$SMB_{all}^- = \sum SMB_i^- \tag{5.3}$$

Third, the same metric was calculated only including extreme precipitation days with positive (negative) SMB for SMB_{ex}^{+} (SMB_{ex}^{-}). Finally, the mean fraction of seasonal positive and negative SMB was calculated as

$$SMB_{ex\,frac}^{+} = \frac{SMB_{ex}^{+}}{SMB_{all}^{+}} \tag{5.4}$$

$$SMB_{ex\,frac}^{-} = \frac{SMB_{ex}^{-}}{SMB_{all}^{-}} \tag{5.5}$$

5.3 Extreme precipitation

To understand the impacts of extreme precipitation on SMB, we first investigate the occurrence of extreme precipitation and its seasonal and long-term changes. The mean monthly extreme precipitation accumulation in each subregion is shown in Figure 5.2 to illustrate historical and future conditions across the domain. VR-CESM and RACMO generally agree well with ERA5 in the annual cycle of extreme precipitation over the historical time-period. One exception to this occurs in the winter months in Baffin and Devon Islands, where the models produce lower extreme precipitation amounts than seen in ERA5 or RACMO. Conversely, they produce higher winter extreme precipitation amounts than ERA5 in SE Greenland. The models also agree well on the annual cycle of extreme precipitation when the volumetric definition (m^3/day) of extreme precipitation is used (Figure C.1).

Outside of SE Greenland, the mean extreme precipitation either remains consistent or increases in the future in all months and for both models, with increases to extreme precipitation being most acute in the warm season. Although the two models generally agree about the seasonality of changes, they disagree in SE Greenland, where VR-CESM simulations exhibit little change in any month, but RACMO simulations exhibit a marked increase in warm season extreme precipitation.

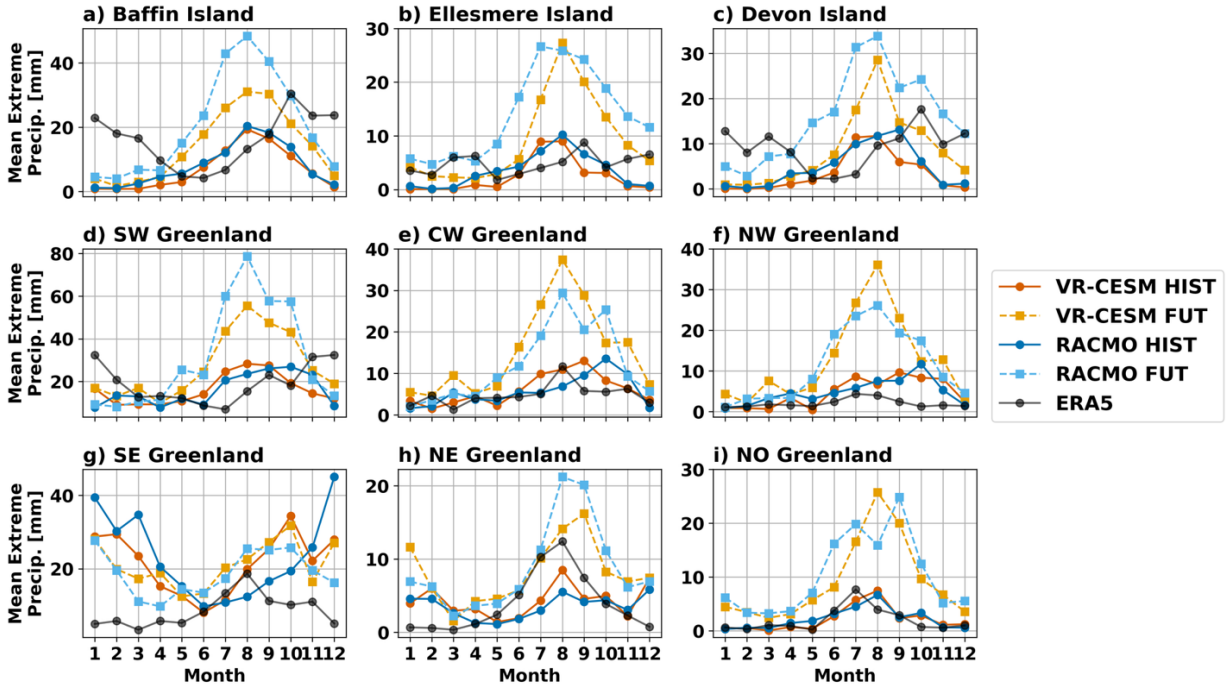

Figure 5.2. Mean monthly accumulation per grid cell from extreme precipitation in RACMO (blue lines), VR-CESM (orange lines), and ERA5 (black line) for the historical (1980-1998; solid lines) and future (2080-2098; dashed lines) in each subregion.

As outlined in Section 5.1, whether extreme precipitation falls as rain or snow has major impacts on SMB. Figure 5.3 shows mean monthly rain fraction of extreme and non-extreme precipitation in each model for the historical and future periods. All subregions show increases in rain fraction in the future, most of which occurs in the warm season. A sharp increase in the rain fraction in June is projected in the Canadian subregions and SW Greenland. Historically, the rain fraction was very similar between extreme and non-extreme precipitation in most subregions. This changes in the future, when several subregions show higher rain fractions on extreme precipitation days than on non-extreme days in the warm season (such as SW, CW, and NW Greenland). Historically, SE Greenland experienced a slightly lower rain fraction for extreme precipitation days than for non-extreme precipitation days in the warm season, but that difference becomes smaller in the future.

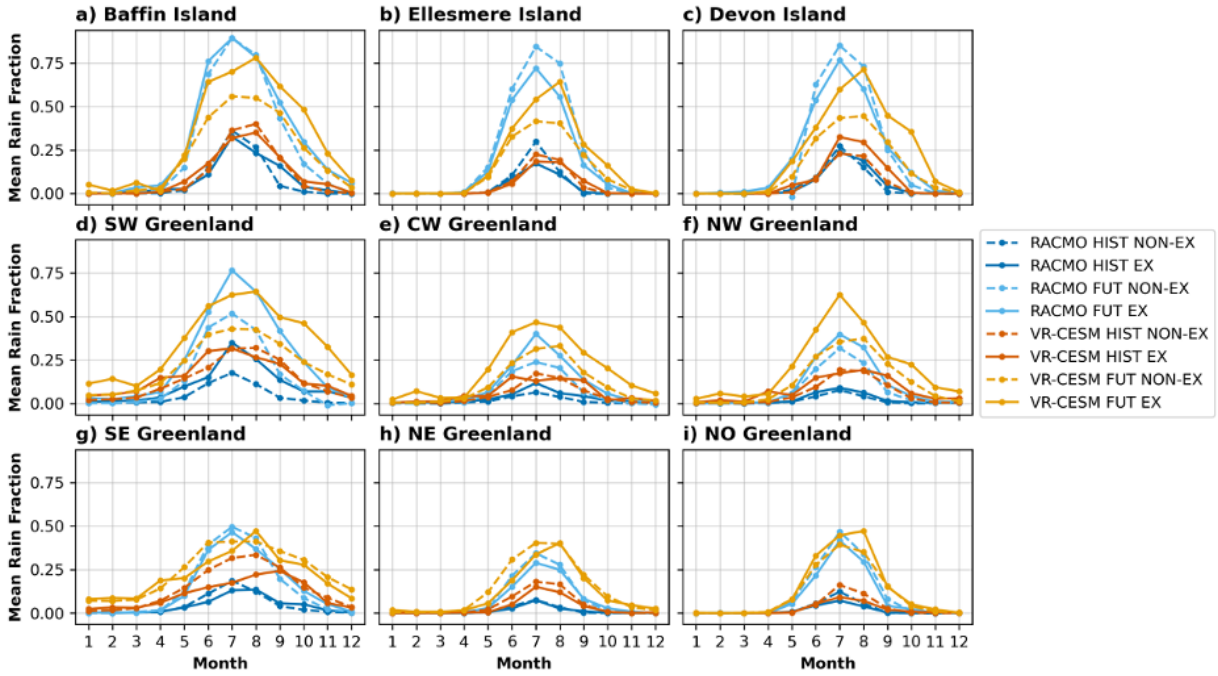

Figure 5.3. Mean monthly rain fraction for extreme precipitation days (solid lines, "EX") and non-extreme days (dashed lines, "NON-EX") in each subregion (a-i) from RACMO (blue lines) and VR-CESM (orange lines). The darker colours show the historical averages, and the lighter colours show the future projections.

5.4 SMB Response to Extreme Precipitation

5.4.1 Mean SMB Responses

Before exploring the impact of extreme precipitation on SMB, we first consider mean seasonal SMB in the historical and future simulations (Figure 5.4; future values shown in Figure C.2). Historically, the cold season (December-March) shows positive SMB across the domain with the highest values in SE Greenland. The two models agree well on cold season SMB, showing minimal changes in the future simulations except for a decrease in SE Greenland. However, SE Greenland still has the highest cold season SMB in the future projections. In the warm season historically, some low-lying and coastal regions show negative seasonal SMB across the domain, but the negative net SMB is limited to narrow margins along the edge of ice masses. In the future projections, the negative seasonal SMB expands to much wider margins of the GrIS, as well as the entirety of the eastern Canadian Arctic. The models agree on overall patterns of SMB, but larger differences exist during the warm season (Figure C.3). The higher spatial resolution of RACMO refines SMB patterns near complex topography, producing larger decreases in the eastern Canadian Arctic and GrIS margins. RACMO also shows strong decreases in SMB reaching further inland than VR-CESM. Both models showed the ablation zone similar altitudes historically (1742 m and 1830 m in RACMO and VR-CESM, respectively), though the ablation zone in RACMO covers ~17.7% of the GrIS compared to only 9.4% in VR-CESM. However, in the future, both models show the ablation zone expanding to cover an additional ~28% of GrIS area. RACMO shows expansion of the ablation zone to altitudes up to 2658 m, compared to only 2297 m in VR-CESM. These differences between RACMO and VR-CESM are consistent with those found by van

Kampenhout et al. (2019), which also showed the largest differences in the ablation zone with VR-CESM producing higher SMB than RACMO.

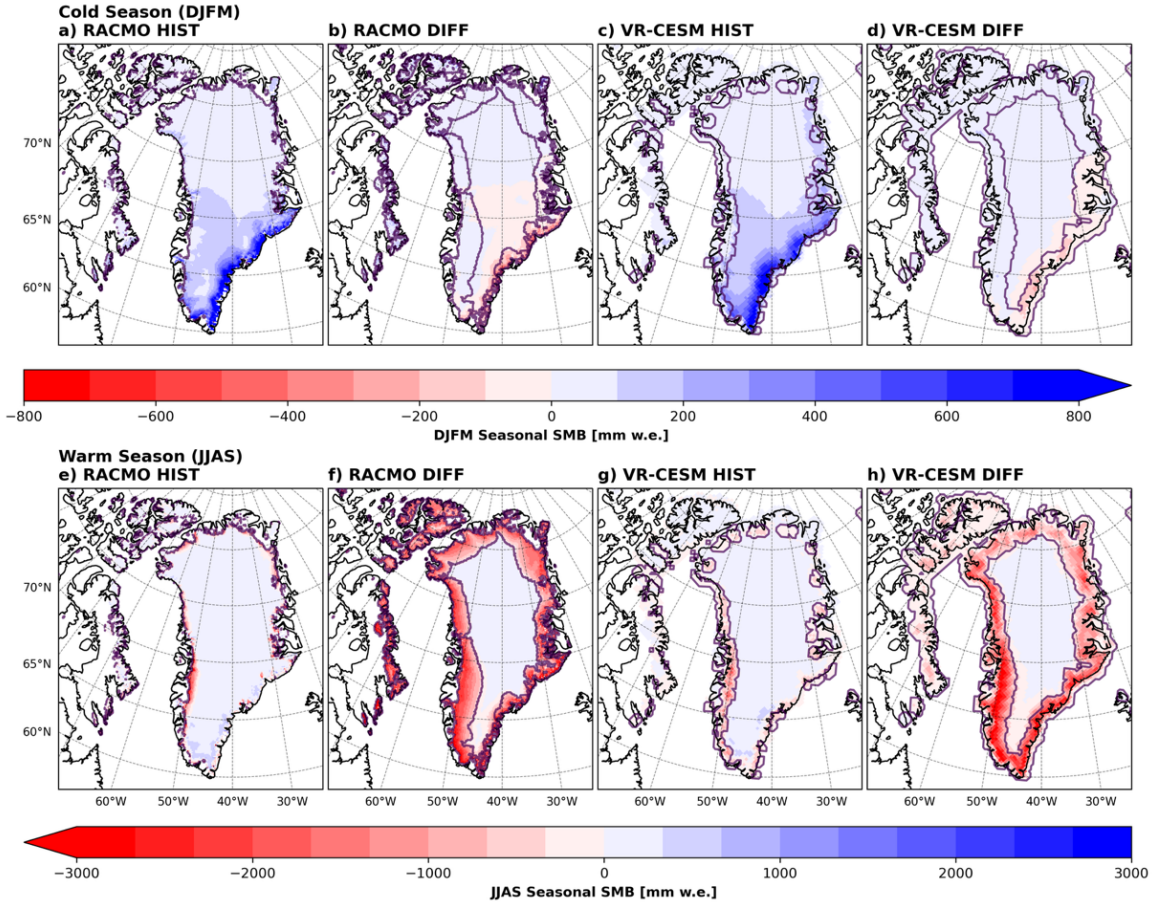

Figure 5.4. Mean seasonal SMB in the region for the (a-d) cold season (DJFM) and (e-h) warm season (JJAS) for the historical period (1980-1998; a,c,e,g), and the difference between historical and future (2080-2098) periods (FUT – HIST; b,d,f,h) in RACMO (a-b, e-f) and VR-CESM (c-d, g-h). The solid purple line denotes the top of the ablation zone for the full simulation period.

The average daily SMB on extreme and non-extreme precipitation days in the cold season in each subregion is shown in Figure 5.5 to understand how extreme precipitation days differ from the average conditions. For all sub-regions, the points for every year lie above the 1:1 line, indicating that SMB is higher on extreme precipitation days than on non-extreme precipitation days. This occurs because the rain fraction is near-zero during the cold season across the domain (Figure 5.3), so extreme precipitation days represent those when the most mass is added via snowfall. The largest differences between the SMB on extreme and non-extreme precipitation days are found in SW and SE Greenland which have the highest magnitude of extreme precipitation over the cold season (Figure 5.2).

Most subregions show little consistent change between HIST and FUT in the cold season. VR-CESM shows some general SMB increases on extreme precipitation days, particularly in NO Greenland. This is likely due to the increase in the magnitude of extreme precipitation events, as warmer air can hold more moisture (e.g., Bengtsson et al., 2011; Norris et al., 2019; Skific et al., 2009), which may be further enhanced by the loss of Arctic sea ice (e.g., Bintanja and Selten, 2014;

Hartmuth et al., 2023; Kopec et al., 2016). This difference between HIST and FUT is not as evident in RACMO. There is further disagreement between the models in that VR-CESM produces higher SMB than RACMO in most subregions. Much of this difference may be related to the different spatial resolution of the two models. The slightly coarser resolution of VR-CESM (~ 25 km) compared to RACMO (~ 11 km) allows precipitation to penetrate further inland and affect a larger area. VR-CESM has also been shown to produce higher historical annual SMB for the GrIS compared to RACMO (van Kampenhout et al., 2020), consistent with the differences shown in Figure 5.5.

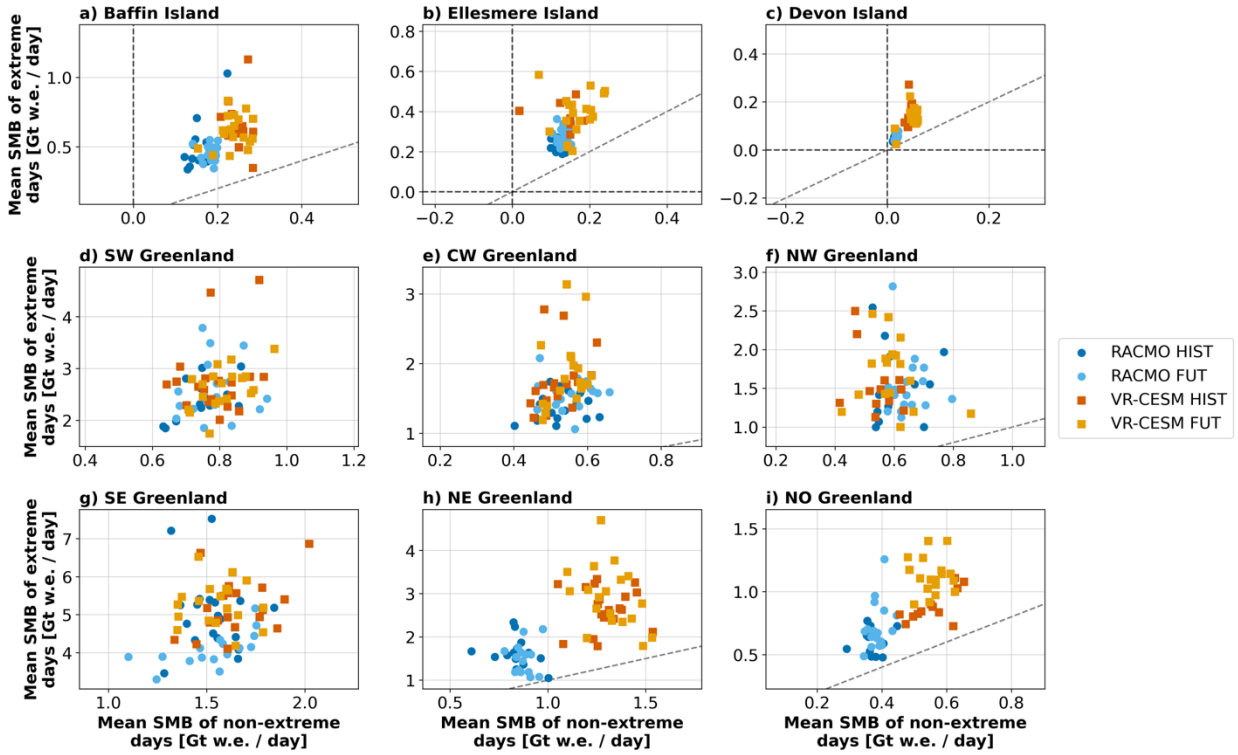

Figure 5.5. Average DJFM Daily mean SMB on extreme days vs. non-extreme days for all subregions (a-i). Each point represents one year. RACMO is shown in blue circles and VR-CESM is represented by orange/red squares, with the darker (lighter) colour showing historical (future) means. Dashed black lines show x = 0, y = 0, and x = y.

Larger changes in SMB on both extreme and non-extreme precipitation days are projected across the domain during the warm season (Figure 5.6). Historically, non-extreme precipitation days tended to have SMB near zero or weakly positive, and extreme precipitation days showed positive SMB in all subregions, with strong agreement between the two models. As in the cold season, regional SMB on warm season extreme precipitation days was greater than that of non-extreme days. Historical rain fractions remained near or below 0.25 in the warm season (Figure 5.3), meaning that most extreme precipitation events resulted in mass gain via snowfall.

However, unlike the cold season, there is a large shift between the historical and future periods in the warm season. In the future projections, the SMB of both extreme and non-extreme days becomes largely negative and more variable as temperatures rise. The difference between the SMB on extreme versus non-extreme days within each season shifts in many subregions as well. Most subregions show at least some years in the future where the seasonal SMB of extreme precipitation days becomes even more negative than that of non-extreme days. The projections

show that this is commonly becoming the case in regions such as SW Greenland, Baffin Island, and Ellesmere Island. Even in cases where the SMB is more positive on extreme precipitation days than non-extreme days, it is more common in the future for the SMB to be negative, with only NW and SE Greenland usually producing positive SMB on extreme precipitation days. Conversely, SW Greenland and Baffin Island shift more strongly towards extreme precipitation consistently associated with more negative SMB than its non-extreme counterparts, particularly in RACMO.

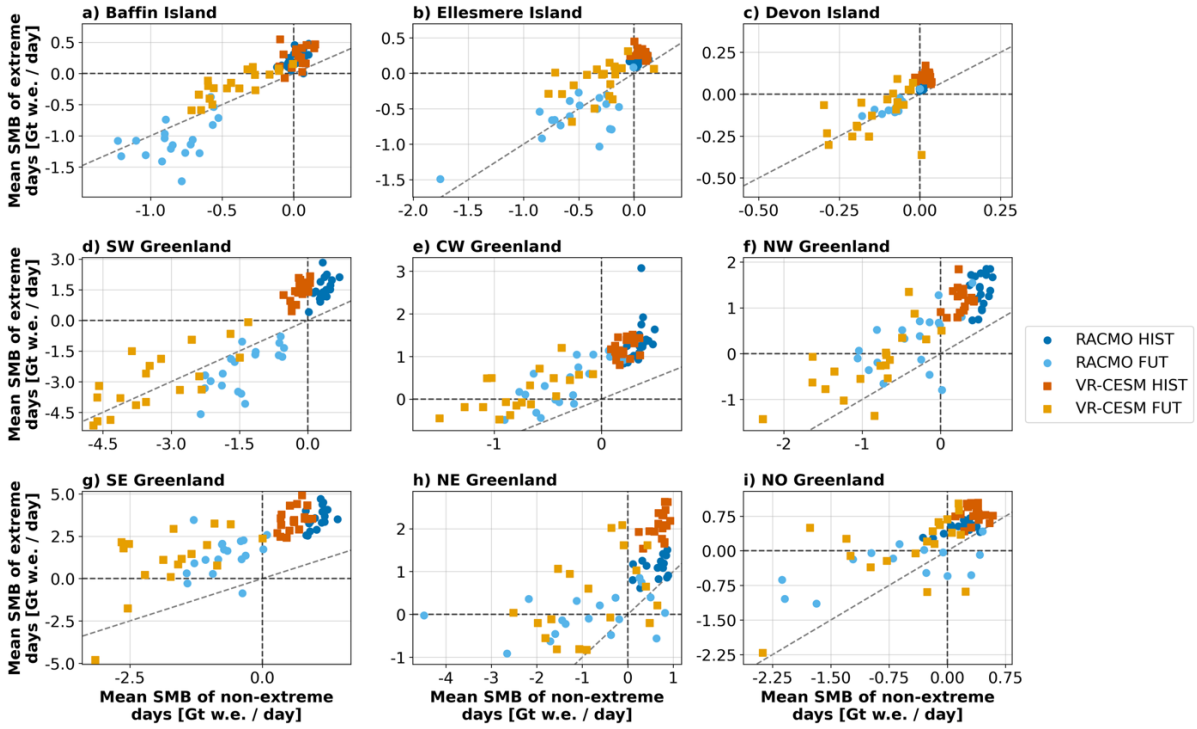

Figure 5.6. As in Figure 5.5, but for JJAS.

Historically, the mean SMB of extreme and non-extreme precipitation days were relatively consistent, particularly in the warm season. In the future projections, SMB responses to warm season extreme precipitation days exhibit greater spread and variability (Figure 5.6). Table 5.1 and Table 5.2 show the results of bootstrapping performed on IQR_{diff} in each subregion for the warm and cold seasons, respectively. Both RACMO and VR-CESM show a statistically significant increase in IQR in all subregions except SE Greenland in the warm season. In the cold season, VR-CESM shows an increase in IQR in NW and NE Greenland. Conversely, there is an increase in NO Greenland in RACMO, as well as a decrease in NW and SE Greenland, highlighting the disagreement between the models in the cold season. Despite these differences, both models show little overall change in the cold season SMB for extreme or non-extreme precipitation days.

Table 5.1. DJFM IQR bootstrapping results for each subregion. The number of events indicates the total number of extreme precipitation days in DJFM in HIST and FUT. Actual interquartile range (IQR) is the IQR of SMB anomalies on extreme precipitation days in the period and Difference indicates the difference in IQR between the two time periods. Bold indicates a statistically significant change in IQR as determined by the bootstrapping methodology outlined in Section 5.2.2.

	Subregion	Number of events		Actual IQR *[Gt]*		Difference (FUT-HIST) *[Gt]*
		HIST	FUT	HIST	FUT	
VR-CESM	Baffin Island	23	86	0.239	0.284	0.045
	Ellesmere Island	14	166	0.105	0.193	0.088
	Devon Island	10	107	0.089	0.056	-0.033
	SW Greenland	75	135	0.923	0.957	0.034
	CW Greenland	60	126	0.540	0.797	0.257
	NW Greenland	43	105	0.481	0.748	**0.267**
	SE Greenland	150	137	1.905	2.088	0.183
	NE Greenland	131	163	0.982	1.398	**0.415**
	NO Greenland	28	139	0.205	0.415	0.210
RACMO	Baffin Island	31	106	0.166	0.157	-0.009
	Ellesmere Island	16	185	0.061	0.105	0.044
	Devon Island	19	141	0.011	0.027	0.016
	SW Greenland	59	66	0.602	0.976	0.374
	CW Greenland	76	83	0.355	0.584	0.229
	NW Greenland	49	119	0.802	0.366	**-0.436**
	SE Greenland	189	107	2.072	1.121	**-0.951**
	NE Greenland	127	150	0.495	0.607	0.112
	NO Greenland	33	157	0.157	0.308	**0.151**

Table 5.2. As in Table 5.1, but for JJAS.

	Subregion	Number of events		Actual IQR *[Gt]*		Difference (FUT-HIST) *[Gt]*
		HIST	FUT	HIST	FUT	
VR-CESM	Baffin Island	207	388	0.349	0.455	**0.106**
	Ellesmere Island	261	466	0.212	0.463	**0.251**
	Devon Island	233	330	0.068	0.174	**0.106**
	SW Greenland	176	311	1.274	3.521	**2.247**
	CW Greenland	163	333	0.590	1.034	**0.444**
	NW Greenland	184	418	0.726	1.137	**0.411**
	SE Greenland	76	89	1.436	1.852	0.416
	NE Greenland	136	273	1.010	1.593	**0.584**
	NO Greenland	236	520	0.415	0.880	**0.466**
RACMO	Baffin Island	194	428	0.236	0.516	**0.280**
	Ellesmere Island	226	531	0.130	0.409	**0.279**
	Devon Island	218	398	0.020	0.084	**0.064**
	SW Greenland	167	358	0.960	2.947	**1.987**
	CW Greenland	129	271	0.547	0.950	**0.403**
	NW Greenland	145	372	0.598	1.280	**0.682**
	SE Greenland	57	88	0.914	1.180	0.266
	NE Greenland	140	407	0.623	1.549	**0.926**
	NO Greenland	203	476	0.395	0.950	**0.555**

Overall, the IQR changes shown in Table 5.1 and Table 5.2 confirm that the impact of extreme precipitation on SMB changes more in response to warming during the warm season than the cold season. In addition to the increased variability, it becomes more common for extreme precipitation to be associated with a negative SMB response in the future (Figure 5.6). In some subregions, such as NW and CW Greenland, this means that the increased accumulation simply cannot overcome the strongly negative seasonal SMB. In other regions, such as SW Greenland and Baffin and Ellesmere Islands, this results in extreme precipitation days that are associated with more negative SMB than that of non-extreme days in the future, suggesting that the extreme precipitation days may become particularly detrimental to SMB in the future. These regions also show some of the largest increases in rain fraction (Figure 5.3). This may help explain the shift towards more negative SMB associated with extreme precipitation, as rainwater directly runs-off on bare ice in ablation zones or progressively saturates firn in accumulation areas. This means that one can no longer assume that extreme precipitation directly leads to mass gain in the future climate.

5.4.2 Seasonal Context & Change

To contextualize the importance of these events on the seasonal cumulative SMB, seasonal SMB is split into days with positive SMB (SMB^{+}_{all}) and negative SMB (SMB^{-}_{all}), and the fraction of cumulative positive SMB ($SMB^{+}_{ex\ frac}$) and negative SMB ($SMB^{-}_{ex\ frac}$) that occurs on extreme precipitation days is calculated. The number of extreme precipitation days that occur with positive or negative SMB in each season are shown in Figure C.4.

5.4.2.1 Cold Season

The change in $SMB^{+}_{ex\ frac}$ for DJFM in RACMO is shown in Figure 5.7 (future values shown in Figure C.5). Over the historical period, most of the domain received a small fraction of positive SMB (<10%) from extreme precipitation days in the cold season, except for SE Greenland. The $SMB^{+}_{ex\ frac}$ increases slightly in the future across the majority of the domain as extreme precipitation increases (as seen in Figure 5.2 and Loeb et al., 2024) with the largest $SMB^{+}_{ex\ frac}$ increases occurring at the northernmost areas of Ellesmere Island and NO Greenland. However, SE Greenland shows the opposite: $SMB^{+}_{ex\ frac}$ decreases by approximately 20% in the future projections. This region had the highest historical $SMB^{+}_{ex\ frac}$ due to high extreme precipitation accumulations that peaked in the cold season, but shows decreasing accumulations in the future (Loeb et al., 2024). This is hypothesized to be due to a reduction in extratropical cyclone activity in the region, bringing fewer intense precipitation events to SE Greenland coast (e.g., Crawford et al., 2023; Loeb et al., 2024). The reduction in $SMB^{+}_{ex\ frac}$ in SE Greenland results in most of the domain showing ~5-10% of seasonal SMB coming from extreme precipitation days in the future. The patterns of changes agree well between RACMO and VR-CESM, although VR-CESM produces higher values of $SMB^{+}_{ex\ frac}$ in NW Greenland.

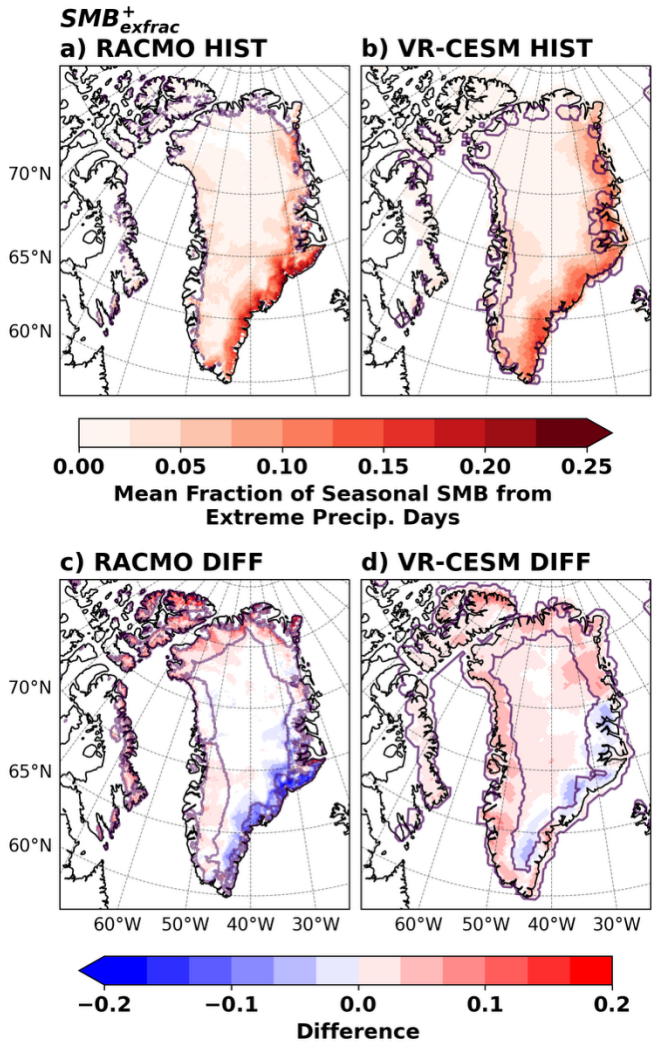

Figure 5.7. Mean DJFM $SMB^{+}_{ex\ frac}$ for HIST (1980-1998; a, c) and projected changes (FUT (2080-2098) - HIST; b, d) from RACMO (a-b) and VR-CESM (c-d). $SMB^{-}_{ex\ frac}$ is zero across the domain in both periods, and is therefore not shown. The solid purple line denotes the top of the ablation zone for the full simulation period, with the future ablation zone being shown on the DIFF panels (c-d).

5.4.2.2 Warm Season

More notable shifts are shown when considering changes in $SMB^{+}_{ex\ frac}$ and $SMB^{-}_{ex\ frac}$ in the warm season (Figure 5.8, Figure C.6). Historically, $SMB^{-}_{ex\ frac}$ is at or near zero across the domain, with only a small strip of coastal SW Greenland showing ≤ 7% of the negative seasonal SMB coming from extreme precipitation days. Conversely, the entire domain shows 5-20% of positive SMB during the season coming from extreme precipitation days. In the future projections, most of Greenland and northern Ellesmere Island experience an increase in $SMB^{+}_{ex\ frac}$, with extreme precipitation days contributing 10-20% more to the positive SMB in the warm season than in the historical period. The opposite occurs in SW Greenland and Baffin Island, where $SMB^{-}_{ex\ frac}$ increases at the expense of $SMB^{+}_{ex\ frac}$. This suggests a shift in the region, with extreme

precipitation days becoming more likely to contribute to seasonal mass loss than mass gain with continued warming. This aligns with the shift towards more negative SMB associated with extreme precipitation shown in Figure 5.6. This analysis cannot quantify the extent to which this shift results specifically from the precipitation itself versus other factors, such as increased temperatures on extreme precipitation days. Historical case studies have estimated the direct effects of rainfall on ice to account for < 20% of total mass loss in studied events (e.g., Box et al., 2023; Doyle et al., 2015; Fausto et al., 2016a, b). While full surface energy balance analysis is required to assess the direct precipitation-related effects, changes, such as those shown in Figure 5.8, illustrate the potential that even days with the highest precipitation may not yield positive SMB in the future. In general, RACMO and VR-CESM agree well on the distribution and changes. The increase in $SMB^{-}_{ex\,frac}$ in much of the southern or low altitude regions of the domain illustrates how future extreme precipitation days may have more negative contributions to seasonal SMB than shown in the historical period (Figure 5.8).

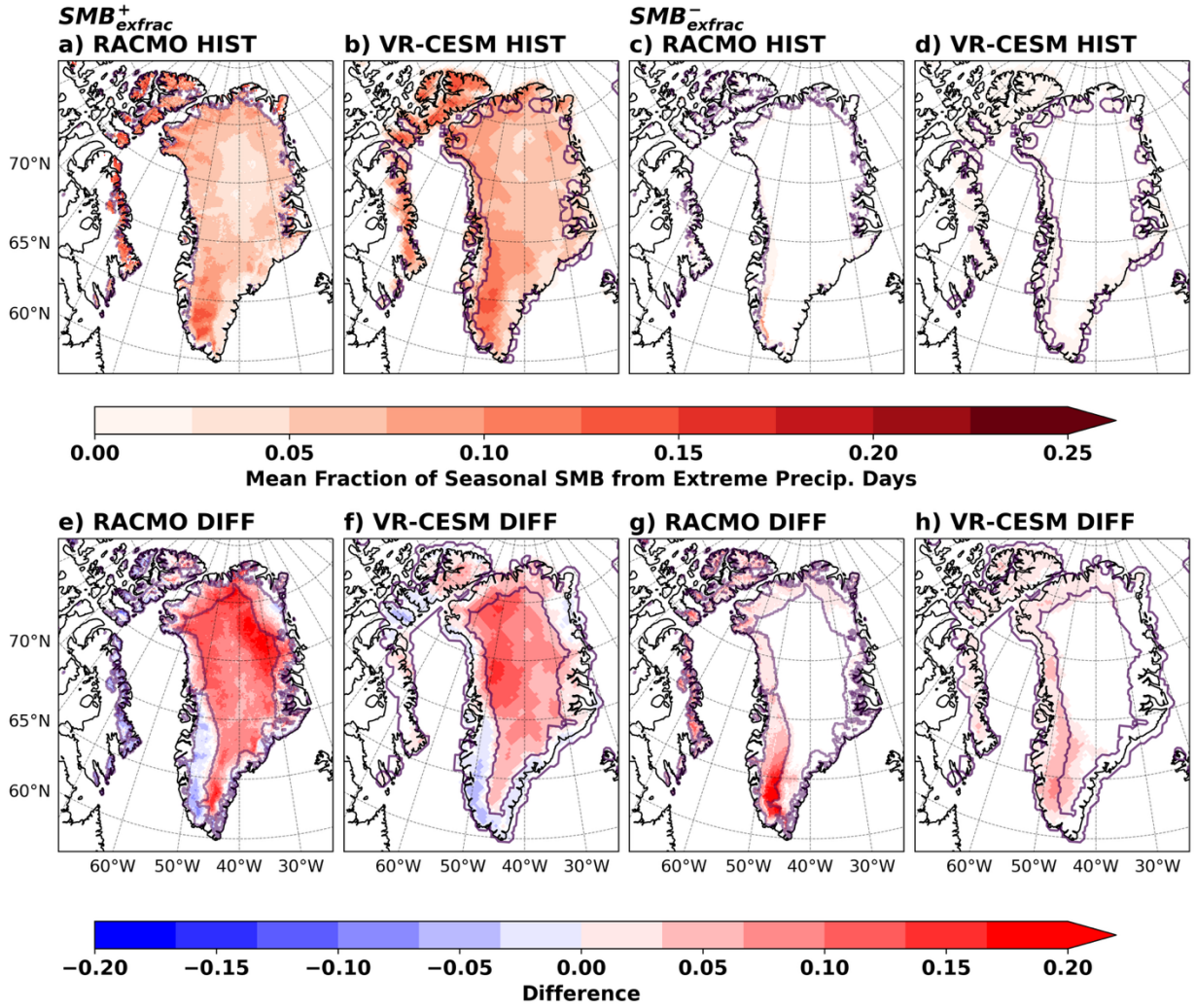

Figure 5.8. Mean JJAS $SMB^{+}_{ex\,frac}$ (a-b, e-f) and $SMB^{-}_{ex\,frac}$ (c-d, g-h) for HIST (1980-1998; a-d) and projected changes (FUT (2080-2098) - HIST; e-h) from RACMO (a, c, e, g) and VR-CESM (b, d, f, h). The solid purple line denotes the top of the ablation zone for the full simulation period, with the future ablation zone being shown on the DIFF panels (e-h).

To better understand the impacts of extreme precipitation on SMB components associated with the changes in SMB_{ex}^{-} and SMB_{ex}^{+}, we explore the mean anomalies associated with warm season extreme precipitation in Figures 5.9-5.11 (recall that the anomalies shown are calculated relative to a 31-day period centred on the extreme precipitation day, rather than the climatology, as described in Section 5.2.2). Mean extreme precipitation amounts and rain fraction for SMB_{ex}^{+} and SMB_{ex}^{-} from RACMO and VR-CESM are illustrated in Figure C.7 and Figure C.8, respectively. Historically, the positive SMB extreme precipitation days (SMB_{ex}^{+}) generally occur with positive temperature anomalies (~3-4 K) and modest anomalies in melt, runoff, and albedo (Figure 5.9). While positive temperature anomalies may usually contribute to melt, the warmer air can hold more moisture and feed heavy precipitation, which is likely to fall as snow in high latitude/altitude regions during the warm season. VR-CESM (Figure C.9) shows a slight increase in refreezing occurring on positive SMB extreme precipitation days in SW Greenland. Overall, the models agree on patterns of anomalies, except for albedo, where VR-CESM shows only very small changes.

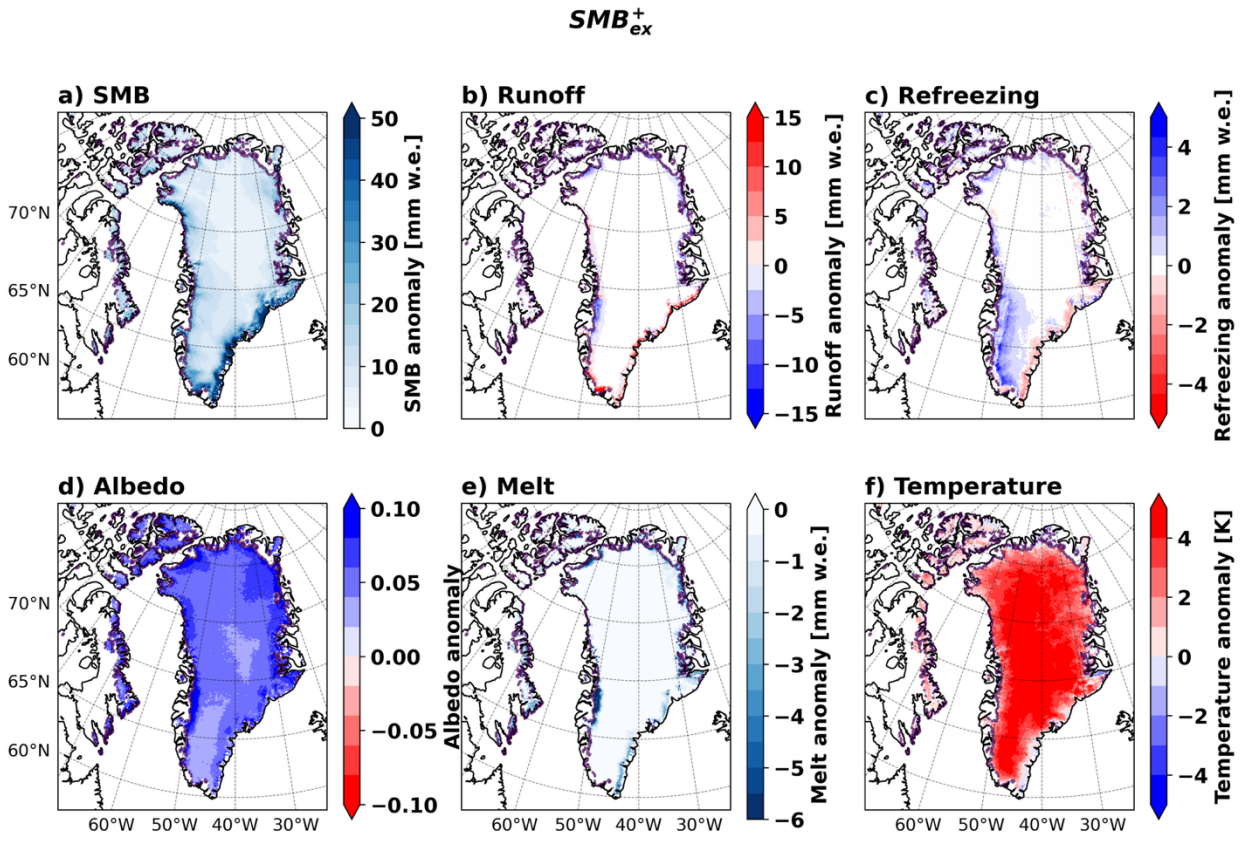

Figure 5.9. Mean anomalies on positive SMB JJAS extreme precipitation days in the historical period (1980-1998) from RACMO. Anomalies are calculated for the extreme precipitation day relative to ±15 days surrounding the extreme precipitation day. The solid purple line denotes the top of the ablation zone for the full simulation period. Blue colours in each panel indicate anomalies that act to increase SMB.

Next, the mean anomalies in future positive SMB extreme precipitation days (SMB_{ex}^{+}) are illustrated in Figure 5.10 and Figure C.10 for RACMO and VR-CESM, respectively. The models agree well on the patterns of anomalies. One notable change seen in both models is that most inland regions have positive temperature anomalies historically of 2-4 K, but future projections show

small negative temperature anomalies (-1 K) in some low-lying and coastal areas. This reduction in temperature anomaly associated with SMB_{ex}^{+} is likely due to the background increase in temperature, meaning the air can hold more moisture without requiring strong temperature anomalies. Some areas in the ablation zone show a negative future temperature anomaly associated with SMB_{ex}^{+} as a negative anomaly is required to bring the relatively warm summer temperatures towards freezing point, allowing for snowfall and favouring positive SMB anomalies. Both models show positive runoff anomalies of approximately 10 mm w.e. on positive SMB extreme precipitation days in SE Greenland. VR-CESM shows modest positive runoff anomalies in Ellesmere and Baffin Islands, disagreeing with the negative anomalies shown in RACMO. However, the largest differences between the models are again seen in the albedo anomalies. RACMO shows relatively large positive albedo anomalies (0.05-0.10) throughout much of the domain with decreased melt whereas VR-CESM shows very low albedo anomalies in general (anomalies below 0.025).

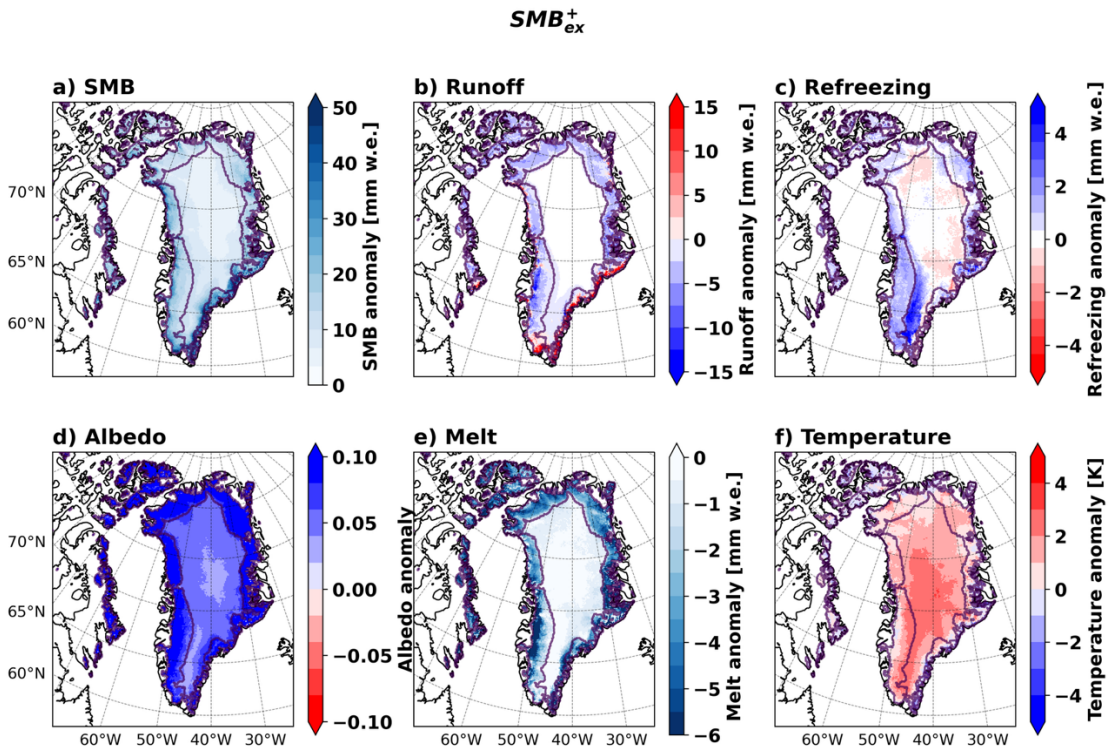

Figure 5.10. As in Figure 5.9, but for future (2080-2098) positive SMB JJAS extreme precipitation days from RACMO.

Some of the most notable changes exist in the negative SMB extreme precipitation days (SMB_{ex}^{-}), which go from contributing virtually 0% of the SMB^{-} mass loss historically to approximately 20% in the future period in coastal and southern regions of the domain in RACMO (Figure 5.8g). VR-CESM also shows an increase, though of smaller magnitude (approximately 10%, Figure 5.8h). The mean anomalies associated with future events are explored in Figure 5.11 and Figure C.13 for RACMO and VR-CESM, respectively (historical period anomalies are shown in Figure C.11-Figure C.12 as there are few occurrences, as shown in Figure C.4). While the historical simulations had limited events, one notable difference between historical and future simulations is that the temperature anomalies in the historical period (> 4 K; Figure C.7f) tended

to be larger than those in the future period (< 2-3 K, and sometimes slightly negative in SE Greenland and Ellesmere Island; Figure 5.11f).

The anomalies illustrated in Figure 5.11 show some of the mechanisms by which extreme precipitation days result in negative SMB throughout the ablation zone. In western Greenland and Baffin Island, there are large increases in melt (Figure 5.11e), which are collocated with reductions in albedo (Figure 5.11d) and increased temperature (Figure 5.11f). While we cannot quantify the drivers of the change in albedo, heavy rainfall may darken the surface and be a strong contributor to the negative albedo anomaly. These regions see a modest increase in refreezing (Figure 5.11c), but it does not offset the increase in melt, leading to a large increase in runoff (Figure 5.11b) and negative SMB anomaly (Figure 5.11a).

Both models show relatively modest SMB anomalies across most of the domain (~ -15 mm w.e.), but larger negative anomalies in southern Greenland, occurring with large runoff increases (upwards of 30 mm w.e.). The pattern of refreezing anomalies in each model differs slightly but are relatively small (< 3 mm w.e.). Larger differences exist in albedo anomalies, where VR-CESM is near-zero across the domain and RACMO shows larger negative anomalies in SW Greenland (~ -0.10) and positive anomalies along the eastern coast of Greenland (~0.05). RACMO produces much larger positive melt anomalies, which may contribute to the larger decrease in albedo, whereas VR-CESM only shows very localized increases in melt along the coast of SW Greenland. Another notable difference is that the extreme precipitation tends to reach further inland in VR-CESM than RACMO (e.g., Figure 5.8g-h), likely owing to the lower resolution producing weaker topography gradients and allowing precipitation to move further inland, as found by van Kampenhout et al. (2020).

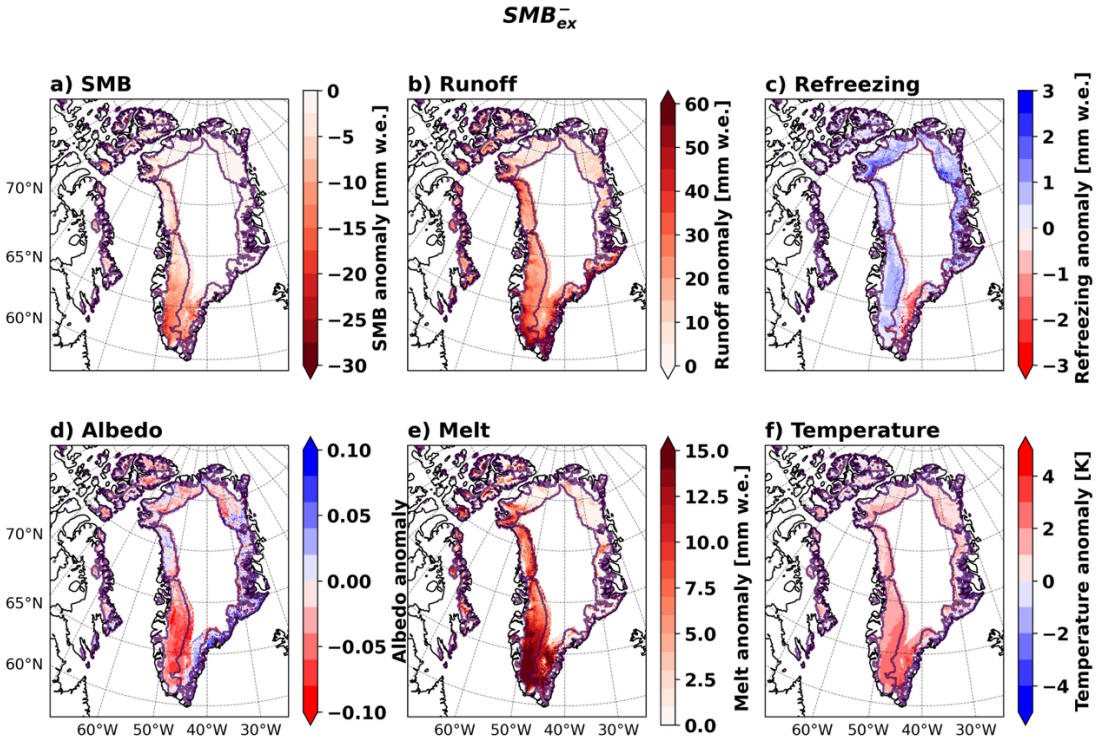

Figure 5.11. As in Figure 5.9, but for future negative SMB JJAS extreme precipitation days from RACMO.

In general, the differences in positive SMB extreme precipitation day anomalies between the two time periods are modest. Conversely, the negative SMB extreme precipitation days cause notable anomalies in the future, particularly decreasing the surface albedo in SW Greenland driving prominent increases in melt. In fact, heavy rainfall may alter snow metamorphism to darken the surface, and decreased snowfall increases the period when dark, bare ice is exposed on the surface.

5.5 Discussion & Limitations

5.5.1 Connection to previous case studies

As discussed in Section 5.1, the effects of extreme precipitation on land ice SMB have not been investigated in a climatological context but have been explored in case studies, which can help to contextualize the results found here. Historical positive SMB extreme precipitation days are tied to increases in albedo and refreezing, with less melt occurring, similar to the effect seen by Oerlemans and Klok (2004) in the Swiss Alps. Unlike the case study presented by Oerlemans and Klok (2004), the temperature anomaly associated with warm season positive SMB extreme precipitation days in our study region remains positive during historical positive SMB extreme precipitation days, which is likely due to local climatological factors. The majority of intense precipitation events in the domain are associated with extratropical cyclones that approach from the south through Baffin Bay or along the North Atlantic Storm Track, bringing warmer air with heavy precipitation (Crawford et al., 2023; Loeb et al., 2024). Because of the high latitude, snowfall can still occur with the warmer air temperatures (Figure 5.3), leading to overall mass gains. The largest positive temperature anomalies associated with extreme precipitation tend to be at higher altitudes for both positive and negative SMB events.

While historically, there were few negative SMB extreme precipitation days in the warm season, the future impacts align with those seen in recent case studies. Several case studies have noted large runoff anomalies associated with increased melt associated with extreme liquid precipitation in the warm season (e.g., Box et al., 2022; Doyle et al., 2015), as seen in Figure 5.11. Projections suggest that refreezing will begin to decline in the future due to a lack of available firn pore space (Noël et al., 2022), which may contribute to the very modest refreezing anomalies, leading to more liquid water runoff.

5.5.2 Model albedo differences

Comparing albedo anomalies between RACMO and VR-CESM highlights large differences; RACMO produces anomalies on the order of 0.05-0.1 during extreme precipitation days, whereas those seen in VR-CESM are only ~0.01. These disparities are tied to large differences in the amount of melt that occur, suggesting that the different albedo parameterizations used may be important in understanding the responses. Both models use parts of the Snow, Ice, and Aerosol Radiative (SNICAR) model (Flanner and Zender, 2006) for snow aging metamorphism (van Dalum et al., 2022; Lawrence et al., 2018). However, other aspects of the treatment of albedo differ between the models.

One difference, for example, is the treatment of bare ice. RACMO bases the bare ice albedo on the 500 m MODerate-resolution Imaging Spectroradiometer (MODIS) albedo product, ranging between 0.30 and 0.55 (Noël et al., 2020), whereas VR-CESM assumes bare ice is constant at 0.50 for the visible spectrum (van Kampenhout et al., 2020). Another notable difference is the complexity of the snow module; RACMO can represent a deep snowpack of (up to ~100 m) containing 40 layers (Noël et al., 2020) compared to the maximum depth of ~10 m made up of 12 layers in CLM5 (van Kampenhout et al., 2017, 2020).

Additionally, van Kampenhout et al. (2019) investigated the differences between native resolution CESM and VR-CESM in reproducing historical GrIS SMB and noted several potential biases related to albedo representation. One such issue is that CLM5 repartitions precipitation phase from CAM based on temperature, which does not allow for supercooled rainfall that darkens surface albedo, particularly for the northern GrIS. The downscaling also redistributes clouds within the simulation, which was found to delay summer melt. Additionally, CLM5 does not account for changes in snow properties due to pooling water on the surface, which can lead to darkening being missed by the model. Each of these factors can lead to higher albedos and reduced melt in CLM5, reducing the melt-albedo feedback. This would lead to small albedo changes, as seen in Fig. C.9-C.10 and C.12-C.13.

Further differences in albedo may arise from the difference in the irreducible water saturation thresholds between the models. While the difference is relatively minor (2% versus 3.3% in RACMO and VR-CESM, respectively), a higher threshold can result in slightly lower runoff occurrence. Even a modest change in simulated runoff can have a variety of impacts, since liquid water at the surface can alter snow metamorphism, albedo, and melt. Glaude et al. (2024) hypothesized this to be a factor in major differences in GrIS SMB projections found from three commonly used regional climate models, including RACMO.

5.5.3 Limitations

The results presented here help to illustrate the impacts and importance of extreme precipitation events on seasonal SMB, but there are several notable limitations. Firstly, across the domain, it is common for extreme precipitation to occur with warm air advection, driven by features such as atmospheric rivers (e.g., Box et al., 2022; Loeb et al., 2024). Increased air temperature alone can cause increased melt and drive some of the anomalies seen in Section 5.4. Because of this, it is difficult to disentangle the effects of other climate variables from the effects of extreme precipitation. Indeed, the changes illustrated here are likely small contributors to the total decrease in SMB from melt due to rising temperatures but can still provide a better understanding of processes impacting the SMB. Future work analysing the surface energy balance would allow for a more detailed understanding of the magnitude of the impacts associated with the precipitation itself versus other factors on extreme precipitation days.

Additionally, this analysis only considers impacts on the day of each extreme precipitation event, but the impacts may extend beyond. For example, extreme precipitation events can have direct effects on SMB that last for several days, such as albedo changes (e.g., Bailey and Hubbard, 2025; Oerlemans and Klok, 2004), which may lead to differing seasonal-scale impacts. The calculation of anomalies relative to $\pm$ 15 days centred on the extreme precipitation day means that

these multi-day impacts are included in the background mean, suggesting that the anomalies shown in Figures 5.9-5.11 may be slightly underestimated. This likely has the largest impact on the albedo anomalies. We also only consider impacts within the area experiencing extreme precipitation, but it is also possible for the precipitation to affect SMB beyond the precipitation area. For example, increased runoff from rainfall and melt can lead to increased melt or refreezing downslope, which would not be accounted for in the current analysis. Future work investigating these extended impacts is necessary to better quantify the true importance of extreme precipitation events.

Finally, only two simulations with relatively short time periods are analyzed in this study, although agreement between the two separate models helps increase confidence in the conclusions. Glaude et al. (2024) illustrated large differences in annual GrIS SMB from three commonly used polar regional climate models using the same forcing data, including the RACMO simulation used in this study. Even though the same CESM2 forcing dataset is used, the three regional models yielded annual SMB that differed by a factor of two, highlighting the importance of looking at a range of projections to understand potential outcomes. RACMO produced the highest future SMB of the three simulations, suggesting that the impacts seen in this study may be more intense in simulations from different polar climate models. Repetition of this assessment with a larger ensemble of high-resolution models with longer simulation periods would be valuable to further substantiate results. It would be particularly insightful to explore models with differing albedo parameterizations to further explore the albedo-related differences seen between RACMO and VR-CESM. Additionally, using higher spatial resolution models may better resolve extreme precipitation events (Ali and Tandon, 2024; Cai et al., 2018) and SMB processes (e.g., Noël et al., 2016).

5.6 Conclusions

Through the presented analysis of the impacts and importance of extreme precipitation days on the SMB of land ice in Greenland and the Eastern Canadian Arctic, we come to three main conclusions:

Firstly, the changes that occur during the warm season (JJAS) are more prominent than those of the cold season (DJFM), having the potential for larger implications for seasonal SMB. Historically, precipitation days in the warm season had positive average SMB in virtually all years and subregions except for SW Greenland and Baffin Island. However, as the climate warms, much of the domain shifts to almost all precipitation days being associated with negative SMB. Even extreme precipitation days are projected to always result in a mean negative seasonal SMB in SW Greenland and the Canadian subregions in the future. There is also a shift in the role that extreme precipitation days play in these subregions in the future. In the historical period, the mean SMB of extreme days was always higher (more positive) than on non-extreme precipitation days. The future projections indicate that this may no longer be the case in SW Greenland and Baffin Island, where mean SMB on extreme days becomes even more negative than non-extreme days, particularly in RACMO. This likely results from the shift towards rainfall at the expense of snowfall as temperatures rise. In addition to the potential surface darkening, heavy rainfall can lead to dramatic runoff increases and pooling water that drives further melt. Overall, model projections suggest that extreme precipitation days shift from being consistent contributors of

warm season mass gain to a potential driver of sustained mass loss in the future in regions such as SW Greenland.

Secondly, the relative importance of extreme precipitation days to seasonal positive and negative SMB components is projected to increase in the across much of the domain. The warm season illustrates both positive and negative changes across the domain; extreme precipitation days account for a larger portion of warm season SMB^+ across inland regions and SMB^- in coastal regions in the ablation zone, particularly in SW Greenland where the contribution of extreme precipitation days to negative SMB increases from near-zero to approximately 20%. Future changes are generally smaller in the cold season, when the most notable change is a decrease in the contribution of extreme precipitation days to positive SMB in SE Greenland. Small increases across the northernmost regions of the domain reflect the increased water vapour holding capacity of warmer air, which allows for more cold season extreme precipitation, and may also be facilitated by sea ice loss and enhanced moisture availability. These changes result in most of the domain showing ~5-10% of cold season SMB coming from extreme precipitation days in the future

Finally, the SMB responses to warm season extreme precipitation are projected to become more variable in the future. Both models show increases in the IQR of SMB anomalies on extreme precipitation days everywhere except for SE Greenland, where cold season changes are more prominent. The warm season shows the largest projected shift in rainfall fraction. This can drive the more varied SMB impacts in the future since the effects of an extreme event can be dramatically different depending on the precipitation phase. Combined with the shift towards negative SMB, this suggests that one can no longer assume that extreme precipitation simply leads to a mass gain in the region.

This work provides a first estimate of the seasonal-scale impacts of extreme precipitation on the SMB of glaciers and ice caps in the eastern Canadian Arctic and Greenland and how that role may change in the future. While only two models are used in this analysis, it provides a framework for future studies using larger ensembles to further investigate the contribution of extreme precipitation to land ice SMB anomalies under climate warming.

Data Availability Statement

The CESM2-forced RACMO historical reconstruction and future projection under SSP5-8.5 are discussed in Noël et al. (2020), and can be freely accessed from Brice Noël (bnoel@uliege.be) upon request and without conditions. Processed VR-CESM data is available on the Canadian Watershed Information Network (CanWIN, DOI forthcoming).

Author contributions

NAL, AC, and JS developed the study and methodology. BN shared RACMO data and guidance on analysis. NAL performed analysis and prepared manuscript. All authors contributed to editing the manuscript.

Acknowledgments

This research was undertaken, in part, thanks to funding from the Canada 150 Research Chairs Program (Grant 50296), the Natural Sciences and Engineering Research Council of Canada (NSERC), and Horizon 2020 CRiceS (Grant 101003826). B. Noël is a Research Associate of the Fonds de la Recherche Scientifique de Belgique – F.R.S.-FNRS. The authors would like to thank Jan Lenaerts and the Land Ice Working Group at the National Center for Atmospheric Research for VR-CESM run support, and two anonymous reviewers for their constructive feedback.

Literature cited

Ali, S. M. A., & Tandon, N. F. (2024). Influence of Horizontal Model Resolution on the Horizontal Scale of Extreme Precipitation Events. *Journal of Geophysical Research: Atmospheres*, *129*(22), e2023JD040146. https://doi.org/10.1029/2023JD040146

Bailey, H., & Hubbard, A. (2025). Snow Mass Recharge of the Greenland Ice Sheet Fueled by Intense Atmospheric River. *Geophysical Research Letters*, *52*(5), e2024GL110121. https://doi.org/10.1029/2024GL110121

Bamber, J. L., Westaway, R. M., Marzeion, B., & Wouters, B. (2018). The land ice contribution to sea level during the satellite era. *Environmental Research Letters*, *13*(6), 063008. https://doi.org/10.1088/1748-9326/aac2f0

Bao, J.-W., Michelson, S. A., Neiman, P. J., Ralph, F. M., & Wilczak, J. M. (2006). Interpretation of Enhanced Integrated Water Vapor Bands Associated with Extratropical Cyclones: Their Formation and Connection to Tropical Moisture. *Monthly Weather Review*, *134*(4), 1063–1080. https://doi.org/10.1175/MWR3123.1

Bengtsson, L., Hodges, K. I., Koumoutsaris, S., Zahn, M., & Keenlyside, N. (2011). The changing atmospheric water cycle in Polar Regions in a warmer climate. *Tellus A: Dynamic Meteorology and Oceanography*, *63*(5), 907–920. https://doi.org/10.1111/j.1600-0870.2011.00534.x

Bintanja, R., & Selten, F. M. (2014). Future increases in Arctic precipitation linked to local evaporation and sea-ice retreat. *Nature*, *509*(7501), 479–482. https://doi.org/10.1038/nature13259

Bolch, T., Sandberg Sørensen, L., Simonsen, S. B., Mölg, N., Machguth, H., Rastner, P., & Paul, F. (2013). Mass loss of Greenland's glaciers and ice caps 2003–2008 revealed from ICESat laser altimetry data. *Geophysical Research Letters*, *40*(5), 875–881. https://doi.org/10.1002/grl.50270

Box, J. E. (2013). Greenland Ice Sheet Mass Balance Reconstruction. Part II: Surface Mass Balance (1840–2010). *Journal of Climate*, *26*(18), 6974–6989. https://doi.org/10.1175/JCLI-D-12-00518.1

Box, J. E., Wehrlé, A., van As, D., Fausto, R. S., Kjeldsen, K. K., Dachauer, A., et al. (2022). Greenland Ice Sheet Rainfall, Heat and Albedo Feedback Impacts From the Mid-August

2021 Atmospheric River. *Geophysical Research Letters*, *49*(11), e2021GL097356. https://doi.org/10.1029/2021GL097356

Box, J. E., Nielsen, K. P., Yang, X., Niwano, M., Wehrlé, A., van As, D., et al. (2023). Greenland ice sheet rainfall climatology, extremes and atmospheric river rapids. *Meteorological Applications*, *30*(4), e2134. https://doi.org/10.1002/met.2134

van den Broeke, M. R., Enderlin, E. M., Howat, I. M., Kuipers Munneke, P., Noël, B. P. Y., van de Berg, W. J., et al. (2016). On the recent contribution of the Greenland ice sheet to sea level change. *The Cryosphere*, *10*(5), 1933–1946. https://doi.org/10.5194/tc-10-1933-2016

Browning, K. A., & Pardoe, C. W. (1973). Structure of low-level jet streams ahead of mid-latitude cold fronts. *Quarterly Journal of the Royal Meteorological Society*, *99*(422), 619–638. https://doi.org/10.1002/qj.49709942204

Cai, L., Alexeev, V. A., Arp, C. D., Jones, B. M., Liljedahl, A. K., & Gädeke, A. (2018). The Polar WRF Downscaled Historical and Projected Twenty-First Century Climate for the Coast and Foothills of Arctic Alaska. *Frontiers in Earth Science*, *5*. https://doi.org/10.3389/feart.2017.00111

Cogley, J. G. (2004). Greenland accumulation: An error model. *Journal of Geophysical Research: Atmospheres*, *109*(D18). https://doi.org/10.1029/2003JD004449

Cogley, J. G., Hock, R., Rasmussen, L. A., Arendt, A. A., Bauder, A., Braithwaite, R. J., et al. (2011). *Glossary of Glacier Mass Balance and Related Terms* (IHP-VII Technical Documents in Hydrology No. No. 86, IACS Contribution No. 2) (p. 124). Paris, France: UNESCO-IHP. Retrieved from https://wgms.ch/downloads/Cogley_etal_2011.pdf

Constable, A., Harper, S., Dawson, J., Mustonen, T., Piepenburg, D., Rost, B., et al. (2022). Cross-Chapter Paper 6: Polar Regions. In H.-O. Pörtner, D. C. Roberts, M. Tignor, E. S. Poloczanska, K. Mintenbeck, A. Alegría, et al. (Eds.), *Climate Change 2022: Impacts, Adaptation, and Vulnerability.* (pp. CCP6-1–66). Intergovernmental Panel on Climate Change.

Crawford, A. D., McCrystall, M. R., Lukovich, J. V., & Stroeve, J. C. (2023). The Response of Extratropical Cyclone Propagation in the Northern Hemisphere to Global Warming. *Journal of Climate*, *36*(20), 7123–7142. https://doi.org/10.1175/JCLI-D-23-0082.1

Danabasoglu, G., Lamarque, J.-F., Bacmeister, J., Bailey, D. A., DuVivier, A. K., Edwards, J., et al. (2020). The Community Earth System Model Version 2 (CESM2). *Journal of Advances in Modeling Earth Systems*, *12*(2), e2019MS001916. https://doi.org/10.1029/2019MS001916

Doyle, S. H., Hubbard, A., van de Wal, R. S. W., Box, J. E., van As, D., Scharrer, K., et al. (2015). Amplified melt and flow of the Greenland ice sheet driven by late-summer cyclonic rainfall. *Nature Geoscience*, *8*(8), 647–653. https://doi.org/10.1038/ngeo2482

Ettema, J., van den Broeke, M. R., van Meijgaard, E., van de Berg, W. J., Box, J. E., & Steffen, K. (2010). Climate of the Greenland ice sheet using a high-resolution climate model – Part 1: Evaluation. *The Cryosphere*, *4*(4), 511–527. https://doi.org/10.5194/tc-4-511-2010

Fausto, R. S., van As, D., Box, J. E., Colgan, W., & Langen, P. L. (2016). Quantifying the Surface Energy Fluxes in South Greenland during the 2012 High Melt Episodes Using In-situ Observations. *Frontiers in Earth Science*, *4*. https://doi.org/10.3389/feart.2016.00082

Fausto, R. S., van As, D., Box, J. E., Colgan, W., Langen, P. L., & Mottram, R. H. (2016). The implication of nonradiative energy fluxes dominating Greenland ice sheet exceptional ablation area surface melt in 2012. *Geophysical Research Letters*, *43*(6), 2649–2658. https://doi.org/10.1002/2016GL067720

Fettweis, X., Franco, B., Tedesco, M., van Angelen, J. H., Lenaerts, J. T. M., van den Broeke, M. R., & Gallée, H. (2013). Estimating the Greenland ice sheet surface mass balance contribution to future sea level rise using the regional atmospheric climate model MAR. *The Cryosphere*, *7*(2), 469–489. https://doi.org/10.5194/tc-7-469-2013

Fettweis, X., Box, J. E., Agosta, C., Amory, C., Kittel, C., Lang, C., et al. (2017). Reconstructions of the 1900–2015 Greenland ice sheet surface mass balance using the regional climate MAR model. *The Cryosphere*, *11*(2), 1015–1033. https://doi.org/10.5194/tc-11-1015-2017

Fischer, E. M., & Knutti, R. (2016). Observed heavy precipitation increase confirms theory and early models. *Nature Climate Change*, *6*(11), 986–991. https://doi.org/10.1038/nclimate3110

Forster, R. R., Box, J. E., van den Broeke, M. R., Miège, C., Burgess, E. W., van Angelen, J. H., et al. (2014). Extensive liquid meltwater storage in firn within the Greenland ice sheet. *Nature Geoscience*, *7*(2), 95–98. https://doi.org/10.1038/ngeo2043

Frederikse, T., Landerer, F., Caron, L., Adhikari, S., Parkes, D., Humphrey, V. W., et al. (2020). The causes of sea-level rise since 1900. *Nature*, *584*(7821), 393–397. https://doi.org/10.1038/s41586-020-2591-3

Glaude, Q., Noel, B., Olesen, M., Van den Broeke, M., van de Berg, W. J., Mottram, R., et al. (2024). A Factor Two Difference in 21st-Century Greenland Ice Sheet Surface Mass Balance Projections From Three Regional Climate Models Under a Strong Warming Scenario (SSP5-8.5). *Geophysical Research Letters*, *51*(22), e2024GL111902. https://doi.org/10.1029/2024GL111902

Hartmuth, K., Papritz, L., Boettcher, M., & Wernli, H. (2023). Arctic Seasonal Variability and Extremes, and the Role of Weather Systems in a Changing Climate. *Geophysical Research Letters*, *50*(8), e2022GL102349. https://doi.org/10.1029/2022GL102349

Herrington, A. R., Lauritzen, P. H., Lofverstrom, M., Lipscomb, W. H., Gettelman, A., & Taylor, M. A. (2022). Impact of grids and dynamical cores in CESM2.2 on the surface mass balance of the Greenland Ice Sheet. *Journal of Advances in Modeling Earth Systems*, e2022MS003192. https://doi.org/10.1029/2022MS003192

Hersbach, H., Bell, B., Berrisford, P., Hirahara, S., Horányi, A., Muñoz-Sabater, J., et al. (2020). The ERA5 global reanalysis. *Quarterly Journal of the Royal Meteorological Society*, *146*(730), 1999–2049. https://doi.org/10.1002/qj.3803

Hofer, S., Lang, C., Amory, C., Kittel, C., Delhasse, A., Tedstone, A., & Fettweis, X. (2020). Greater Greenland Ice Sheet contribution to global sea level rise in CMIP6. *Nature Communications*, *11*(1), 6289. https://doi.org/10.1038/s41467-020-20011-8

Hugonnet, R., McNabb, R., Berthier, E., Menounos, B., Nuth, C., Girod, L., et al. (2021). Accelerated global glacier mass loss in the early twenty-first century. *Nature*, *592*(7856), 726–731. https://doi.org/10.1038/s41586-021-03436-z

Hurrell, J. W., Hack, J. J., Shea, D., Caron, J. M., & Rosinski, J. (2008). A New Sea Surface Temperature and Sea Ice Boundary Dataset for the Community Atmosphere Model. *Journal of Climate*, *21*(19), 5145–5153. https://doi.org/10.1175/2008JCLI2292.1

Jacob, T., Wahr, J., Pfeffer, W. T., & Swenson, S. (2012). Recent contributions of glaciers and ice caps to sea level rise. *Nature*, *482*(7386), 514–518. https://doi.org/10.1038/nature10847

van Kampenhout, L., Lenaerts, J. T. M., Lipscomb, W. H., Sacks, W. J., Lawrence, D. M., Slater, A. G., & van den Broeke, M. R. (2017). Improving the Representation of Polar Snow and Firn in the Community Earth System Model. *Journal of Advances in Modeling Earth Systems*, *9*(7), 2583–2600. https://doi.org/10.1002/2017MS000988

van Kampenhout, L., Rhoades, A. M., Herrington, A. R., Zarzycki, C. M., Lenaerts, J. T. M., Sacks, W. J., & van den Broeke, M. R. (2019). Regional grid refinement in an Earth system model: impacts on the simulated Greenland surface mass balance. *The Cryosphere*, *13*(6), 1547–1564. https://doi.org/10.5194/tc-13-1547-2019

van Kampenhout, L., Lenaerts, J. T. M., Lipscomb, W. H., Lhermitte, S., Noël, B., Vizcaíno, M., et al. (2020). Present-Day Greenland Ice Sheet Climate and Surface Mass Balance in CESM2. *Journal of Geophysical Research: Earth Surface*, *125*(2), e2019JF005318. https://doi.org/10.1029/2019JF005318

Kopec, B. G., Feng, X., Michel, F. A., & Posmentier, E. S. (2016). Influence of sea ice on Arctic precipitation. *Proceedings of the National Academy of Sciences of the United States of America*, *113*(1), 46–51. https://doi.org/10.1073/pnas.1504633113

Kuipers Munneke, P., van den Broeke, M. R., Lenaerts, J. T. M., Flanner, M. G., Gardner, A. S., & van de Berg, W. J. (2011). A new albedo parameterization for use in climate models over the Antarctic ice sheet. *Journal of Geophysical Research*, *116*(D5), D05114. https://doi.org/10.1029/2010JD015113

Lawrence, D. M., Fisher, R. A., Koven, C. D., Oleson, K. W., Swenson, S. C., Bonan, G., et al. (2019). The Community Land Model Version 5: Description of New Features, Benchmarking, and Impact of Forcing Uncertainty. *Journal of Advances in Modeling Earth Systems*, *11*(12), 4245–4287. https://doi.org/10.1029/2018MS001583

Lenaerts, J. T. M., Angelen, J. H. van, Broeke, M. R. van den, Gardner, A. S., Wouters, B., & Meijgaard, E. van. (2013). Irreversible mass loss of Canadian Arctic Archipelago glaciers. *Geophysical Research Letters*, *40*(5), 870–874. https://doi.org/10.1002/grl.50214

Li, Z., & Ding, Q. (2024). A global poleward shift of atmospheric rivers. *Science Advances*, *10*(41), eadq0604. https://doi.org/10.1126/sciadv.adq0604

Loeb, N. A., Crawford, A., Stroeve, J. C., & Hanesiak, J. (2022). Extreme Precipitation in the Eastern Canadian Arctic and Greenland: An Evaluation of Atmospheric Reanalyses. *Frontiers in Environmental Science*, *10*. https://doi.org/10.3389/fenvs.2022.866929

Loeb, N. A., Crawford, A., Herrington, A., McCrystall, M., Stroeve, J., & Hanesiak, J. (2024). Projections and Physical Drivers of Extreme Precipitation in Greenland & Baffin Bay. *Journal of Geophysical Research: Atmospheres*, *129*(22), e2024JD041375. https://doi.org/10.1029/2024JD041375

MacFerrin, M., Machguth, H., As, D. van, Charalampidis, C., Stevens, C. M., Heilig, A., et al. (2019). Rapid expansion of Greenland's low-permeability ice slabs. *Nature*, *573*(7774), 403–407. https://doi.org/10.1038/s41586-019-1550-3

Machguth, H., MacFerrin, M., van As, D., Box, J. E., Charalampidis, C., Colgan, W., et al. (2016). Greenland meltwater storage in firn limited by near-surface ice formation. *Nature Climate Change*, *6*(4), 390–393. https://doi.org/10.1038/nclimate2899

Mattingly, K. S., Mote, T. L., & Fettweis, X. (2018). Atmospheric River Impacts on Greenland Ice Sheet Surface Mass Balance. *Journal of Geophysical Research: Atmospheres*, *123*(16), 8538–8560. https://doi.org/10.1029/2018JD028714

Meehl, G. A., Arblaster, J. M., Bates, S., Richter, J. H., Tebaldi, C., Gettelman, A., et al. (2020). Characteristics of Future Warmer Base States in CESM2. *Earth and Space Science*, *7*(9), e2020EA001296. https://doi.org/10.1029/2020EA001296

van Meijgaard, E., van Ulft, L. H., van den Hurk, B. J. J. M., Lenderink, G., & Siebesma, A. P. (2008). *The KNMI regional atmospheric climate model RACMO, version 2.* (Technical Report No. TR-302) (p. 50). De Bilt. Retrieved from https://cdn.knmi.nl/knmi/pdf/bibliotheek/knmipubTR/TR302.pdf

Myhre, G., Alterskjær, K., Stjern, C. W., Hodnebrog, Ø., Marelle, L., Samset, B. H., et al. (2019). Frequency of extreme precipitation increases extensively with event rareness under global warming. *Scientific Reports*, *9*(1), 16063. https://doi.org/10.1038/s41598-019-52277-4

Noël, B., van de Berg, W. J., van Meijgaard, E., Kuipers Munneke, P., van de Wal, R. S. W., & van den Broeke, M. R. (2015). Evaluation of the updated regional climate model RACMO2.3: summer snowfall impact on the Greenland Ice Sheet. *The Cryosphere*, *9*(5), 1831–1844. https://doi.org/10.5194/tc-9-1831-2015

Noël, B., van de Berg, W. J., Machguth, H., Lhermitte, S., Howat, I., Fettweis, X., & van den Broeke, M. R. (2016). A daily, 1 km resolution data set of downscaled Greenland ice sheet surface mass balance (1958–2015). *The Cryosphere*, *10*(5), 2361–2377. https://doi.org/10.5194/tc-10-2361-2016

Noël, B., van de Berg, W. J., Lhermitte, S., Wouters, B., Machguth, H., Howat, I., et al. (2017). A tipping point in refreezing accelerates mass loss of Greenland's glaciers and ice caps. *Nature Communications*, *8*(1), 14730. https://doi.org/10.1038/ncomms14730

Noël, B., van de Berg, W. J., van Wessem, J. M., van Meijgaard, E., van As, D., Lenaerts, J. T. M., et al. (2018). Modelling the climate and surface mass balance of polar ice sheets using

RACMO2 – Part 1: Greenland (1958–2016). *The Cryosphere*, *12*(3), 811–831. https://doi.org/10.5194/tc-12-811-2018

Noël, B., van de Berg, W. J., Lhermitte, S., Wouters, B., Schaffer, N., & van den Broeke, M. R. (2018). Six Decades of Glacial Mass Loss in the Canadian Arctic Archipelago. *Journal of Geophysical Research: Earth Surface*, *123*(6), 1430–1449. https://doi.org/10.1029/2017JF004304

Noël, B., van Kampenhout, L., van de Berg, W. J., Lenaerts, J. T. M., Wouters, B., & van den Broeke, M. R. (2020). Brief communication: CESM2 climate forcing (1950–2014) yields realistic Greenland ice sheet surface mass balance. *The Cryosphere*, *14*(4), 1425–1435. https://doi.org/10.5194/tc-14-1425-2020

Noël, B., Kampenhout, L. van, Lenaerts, J. T. M., van de Berg, W. J., & van den Broeke, M. R. (2021). A 21st Century Warming Threshold for Sustained Greenland Ice Sheet Mass Loss. *Geophysical Research Letters*, *48*(5), e2020GL090471. https://doi.org/10.1029/2020GL090471

Noël, B., Lenaerts, J. T. M., Lipscomb, W. H., Thayer-Calder, K., & van den Broeke, M. R. (2022). Peak refreezing in the Greenland firn layer under future warming scenarios. *Nature Communications*, *13*(1), 6870. https://doi.org/10.1038/s41467-022-34524-x

Norris, J., Chen, G., & Neelin, J. D. (2019). Thermodynamic versus Dynamic Controls on Extreme Precipitation in a Warming Climate from the Community Earth System Model Large Ensemble. *Journal of Climate*, *32*(4), 1025–1045. https://doi.org/10.1175/JCLI-D-18-0302.1

Oerlemans, J., & Klok, E. J. L. (2004). Effect of summer snowfall on glacier mass balance. *Annals of Glaciology*, *38*, 97–100. https://doi.org/10.3189/172756404781815158

van Pelt, W., & Kohler, J. (2015). Modelling the long-term mass balance and firn evolution of glaciers around Kongsfjorden, Svalbard. *Journal of Glaciology*, *61*(228), 731–744. https://doi.org/10.3189/2015JoG14J223

Pendergrass, A. G., Knutti, R., Lehner, F., Deser, C., & Sanderson, B. M. (2017). Precipitation variability increases in a warmer climate. *Scientific Reports*, *7*(1), 17966. https://doi.org/10.1038/s41598-017-17966-y

Priestley, M. D. K., & Catto, J. L. (2022). Future changes in the extratropical storm tracks and cyclone intensity, wind speed, and structure. *Weather and Climate Dynamics*, *3*(1), 337–360. https://doi.org/10.5194/wcd-3-337-2022

Rantanen, M., Karpechko, A. Y., Lipponen, A., Nordling, K., Hyvärinen, O., Ruosteenoja, K., et al. (2022). The Arctic has warmed nearly four times faster than the globe since 1979. *Communications Earth & Environment*, *3*(1), 1–10. https://doi.org/10.1038/s43247-022-00498-3

Ryan, J. C., Medley, B., Stevens, C. M., Sutterley, T. C., & Siegfried, M. R. (2023). Role of Snowfall Versus Air Temperatures for Greenland Ice Sheet Melt-Albedo Feedbacks. *Earth and Space Science*, *10*(11), e2023EA003158. https://doi.org/10.1029/2023EA003158

Skific, N., Francis, J. A., & Cassano, J. J. (2009). Attribution of Seasonal and Regional Changes in Arctic Moisture Convergence. *Journal of Climate*, *22*(19), 5115–5134. https://doi.org/10.1175/2009JCLI2829.1

Chapter 6 Summary and Conclusions

6.1 Summary of major contributions

The work presented in Chapters 3-5 have advanced our understanding of extreme precipitation in the Arctic climate system and its potential changes in the eastern Canadian Arctic and Greenland, meeting the thesis objectives outlined in Section 1.2. In Chapter 3, I presented a detailed regional comparison of atmospheric reanalyses to surface observations of extreme precipitation and evaluated their ability to represent extreme events. Chapter 4 introduced novel, relatively high-resolution global climate simulations, allowing for an in-depth exploration of changes in extreme daily precipitation and the processes that drive it. The final paper, in Chapter 5, made the first approximation of the climatological-scale importance of extreme precipitation to the surface mass balance (SMB) of land ice in the region. While this work has yielded many interesting results, I would like to highlight four key contributions that this work has made to our understanding of Arctic precipitation extremes and its links to the climate system.

Contribution 1: Atmospheric reanalyses may struggle to exactly reproduce individual observed extreme precipitation events but can adequately represent the seasonality and event statistics.

Previous studies have investigated how well atmospheric reanalyses capture observed precipitation in the Arctic (e.g., Barrett et al., 2020; Boisvert et al., 2018; Lindsay et al., 2014; Rapaić et al., 2015; Wagner et al., 2021). However, limited comparisons focusing on extreme precipitation exist. For example, Avila-Diaz et al. (2021) investigated extreme temperature and precipitation indices in the Arctic in several modern reanalyses but the analysis of extreme precipitation was limited to a single figure and only included the North American Arctic as a one data point, with no inclusion of Greenland. The study presented in Chapter 3 provides a more in-depth exploration of the characteristics of extreme daily precipitation with a regional focus and a detailed comparison of three popular reanalyses to surface station observations.

The findings of this paper show that the reanalyses often did not capture the exact precipitation accumulations on the day of observed extreme precipitation, yielding low correlations between accumulations from observations and reanalyses. Some disagreement is expected as point observations and gridded datasets are inherently different. This is particularly true near complex topography (e.g, Gascon et al., 2010; Ohmura & Reeh, 1991), which includes most of the locations of observations in the study region. This finding agrees with previous work suggesting reanalyses struggle to reproduce observed short-term precipitation amounts (e.g., Boisvert et al., 2018; Koyama & Stroeve, 2019). However, the reanalyses were able to reproduce regional statistics of observed extreme precipitation, such as the seasonality and extreme precipitation thresholds. Additionally, correlations with station observations were slightly increased when spatial offsetting (including all of the surrounding grid cells to find the one with the highest correlation) and temporal offsetting (including the day before and after the event) was performed.

Because of this, we have found that atmospheric reanalyses may not be sufficient for studying an individual extreme precipitation event, but they can be a useful tool to look at the climatological statistics of extreme precipitation. Of the studied datasets, ERA5 was found to slightly outperform other products as it produced the smallest biases across the domain. This work has provided a justification for using reanalyses, specifically ERA5, to represent historical extreme precipitation climatological statistics in future work.

Contribution 2: There are broad projected increases in extreme precipitation in much of the study domain as ARs extend farther poleward throughout, but SE Greenland is projected to receive less extreme precipitation because of decreasing frequency of extratropical cyclones for that subregion.

Through assessment of our novel future VR-CESM simulations, we identify broad increases of extreme precipitation across the domain. The largest increases in extreme precipitation accumulations occur in SW Greenland and southern Baffin Bay, with increases of up to 200 mm $year^{-1}$. The northernmost and high-altitude areas of the domain are projected to see annual extreme precipitation accumulations increase by up to 200%. Along with the increase in extreme precipitation accumulations, extremes are projected to account for a higher portion of total annual precipitation. Historically, extremes accounted for ~15-20% of annual totals in the southern parts of the domain and < 10% in the northernmost and high-altitude areas. This increases by up to 20% across the domain, with much of Baffin and Ellesmere Islands and western and northern Greenland seeing 30-35% of annual precipitation received via extreme days in the future projections. The only region that differs from these increases is SE Greenland which historically received the highest annual extreme precipitation accumulations.

Further, we connect the changes in extreme precipitation to extratropical cyclone and AR activity to better understand why the changes occur. It is evident that the majority of extreme precipitation occurs with a cyclone present in both the historical and future simulations. This supports previous work suggesting that upwards of 75% of annual precipitation in the Arctic is cyclone-associated (Hawcroft et al., 2012). The future simulations suggest slight decreases in extreme precipitation in SE Greenland, which is hypothesized to be related to a decrease in cyclone occurrence in the region. This decline in cyclone frequency in the region has also been found by previous studies (e.g., Crawford et al., 2023; Joos et al., 2023; Yettella & Kay, 2017). However, cyclone changes are minor in the projections, suggesting that the role cyclones play in extreme precipitation days does not change drastically in the future, outside of the noted modest changes in SE Greenland. Conversely, there is evidence that the poleward expansion of AR occurrence is tied to increased extreme precipitation, particularly during the warm season.

This detailed analysis provides unique insight into not only the potential regional changes in extreme precipitation, but also how changes in the processes that drive the extremes factor in to said change. By investigating what changes are projected to occur along with why some of these changes may be happening, we can develop a more holistic understanding of extreme precipitation in the region.

Contribution 3: A new framework for examining the role of extreme precipitation in seasonal/climatological-scale SMB of land ice.

A number of previous studies have highlighted substantial impacts of historical extreme precipitation events on the SMB of land ice via observational case studies (e.g., Bailey & Hubbard, 2025; Box et al., 2022, 2023; Doyle et al., 2015; Harper et al., 2023; Oerlemans & Klok, 2004). However, no estimate of the impacts of these events to seasonal SMB previously existed. In Chapter 5, two models (RACMO and VR-CESM) are employed to explore this question and estimate the importance and impacts of extreme precipitation in the historical period and future projections during the cold season (DJFM) and warm season (JJAS). To achieve this, several novel analysis methods were developed:

1. *Comparing mean SMB on extreme precipitation days to that of non-extreme precipitation days*

   Here, the mean regional SMB of extreme precipitation days is compared to non-extreme precipitation days in the same season to highlight differences when extremes occur, yielding the results shown in Figures 5.5-5.6. This analysis highlights how extreme precipitation days differ from other precipitation days during the same season, providing insight into whether the region experiences more positive or negative SMB effects with extreme precipitation days. This comparison also helps to contextualize the SMB on extreme precipitation days while keeping the SMB on more average precipitation days in mind.

2. *Splitting seasonal SMB into positive and negative components based on daily SMB*

   One of the goals of this project is to estimate the relative importance of extreme precipitation days to seasonal SMB, but since extreme precipitation has been shown to be tied to both positive (e.g., Bailey & Hubbard, 2025; Oerlemans & Klok, 2004) and negative (e.g., Doyle et al., 2015) SMB impacts, simply calculating the seasonal cumulative SMB on extreme precipitation days and comparing to total seasonal SMB may quickly become biased depending on the type of extreme precipitation that occurs. To address this, the seasonal SMB was split into days with positive SMB and days with negative SMB and the relative importance of extreme precipitation days was calculated for each. Once split, the anomalies of SMB components were assessed to better understand the behaviour of each component in cases leading to positive and negative SMB outcomes. The anomalies were calculated relative to ± 15 days to contextualize how impactful the event day is relative to the time in which it occurs.

These novel methods applied to climate model simulations have allowed for an estimate of the importance and varied regional impacts of extreme precipitation events on the region's land ice. This work can provide a framework for future studies to continue to develop our understanding of these connections by applying these analyses to more simulations in various glaciated regions.

Contribution 4: Historical extreme precipitation consistently yielded positive SMB. Projections indicate this remains true at high altitudes, but low-lying areas see a shift toward negative SMB in the warmer future climate. Extreme precipitation days account for a larger portion of total warm season SMB in the future projections.

In the historical simulations, the mean contribution of extreme precipitation to seasonal SMB was consistently positive, even in the warm season. With the shift towards higher rain fractions in the warm season (e.g., Bintanja & Andry, 2017; McCrystall et al., 2021), this is shifting in the future bringing about more variable SMB on precipitation days in general. Both models investigated show that the SMB on extreme precipitation days in the future warm season is projected to become much more variable in future projections. Regions of high elevation, such as the central Greenland Ice Sheet, are projected to still see positive SMB anomalies associated with warm season extreme precipitation in the future as most precipitation still falls as snow. However, most subregions still see overall negative SMB on extreme and non-extreme precipitation days in the future as overall seasonal SMB becomes increasingly negative.

A different story emerges in the ablation zone: as more extreme precipitation falls as rain, anomalous mass loss begins to occur with intense precipitation. Some subregions even demonstrate more negative SMB on extreme than non-extreme precipitation days. This means that even though more precipitation falls, more mass may be lost on extreme days than non-extreme days in the warmer future climate. This is likely tied to increased melt and runoff associated with the presence of liquid precipitation and pooling of liquid at the surface, further promoting melt and decreasing albedo.

Another notable finding is the changes in the relative importance of extreme precipitation days to seasonal SMB. In the cold season, most regions display little change other than a decrease in the relative importance of extremes in SE Greenland. However, in the warm season, the relative contribution of extreme precipitation days to positive seasonal SMB increases from ~5-10% in the historical period to ~20% in most high elevation areas in the future projections. The most notable shift, though, is the negative SMB contribution increasing in the low-lying regions. The eastern Canadian Arctic and most of the periphery of the Greenland Ice Sheet sees ~5-10% of future negative seasonal SMB coming from extreme precipitation days, but SW Greenland sees an increase to > 20%, all of which saw virtually no negative contribution historically. This demonstrates the potential for a substantial shift in the dominant impacts of extreme precipitation days on the SMB of the region's land ice.

6.2 Limitations and recommendations for future work

While the analysis presented in this thesis provides a unique look into extreme precipitation in the eastern Canadian Arctic and Greenland and the impacts it has on land ice in a warming climate, several notable limitations exist. In this section, I will outline suggestions for future research to address these limitations and further develop our understanding of extreme precipitation and its connection to land ice in the Arctic.

6.2.1 Systematic study of extreme precipitation changes in the region with a larger amount of model data

One major limitation of the presented work is the relatively small number of simulations used for analysis. In this section, I will explore several methods that can help reduce the uncertainty that this introduces.

The use of a model ensemble could help to address this limitation. A model ensemble is a set of simulations that can be examined collectively. One type of ensemble is an initial condition ensemble, which refers to simulations from a particular climate/Earth system model that are produced by slightly varying initial conditions or parameters (e.g., Kay et al., 2015). By producing many simulations of the same time period with only slight variations in initial conditions, an estimation of natural climate variability can be achieved, increasing the certainty in the conditions found in the study.

Ensembles can also be generated by using a variety of models that contain different physical and dynamical characteristics (e.g., Eyring et al., 2016). This helps to reduce the uncertainty associated with the model characteristics, such as physical parameterizations and dynamics. Since each model uses different formulations, it produces a variety of outcomes that may better capture the uncertainty due to model choice. Since Chapter 5 illustrated notable differences in albedo between VR-CESM and RACMO, analysis of simulations from different models can help to understand whether one model tends to agree more closely with other comparable simulations.

A number of large ensembles exist that may be used for earth system studies in the Arctic. However, the study of extremes is found to greatly improve with higher spatial resolution (e.g., Ali & Tandon, 2024; Cai et al., 2018). Most currently available large ensembles are of coarse resolution (~1° latitude/longitude), such as data from phase 6 of the Coupled Model Intercomparison Project (CMIP6; Eyring et al., 2016) or the CESM2 large ensemble (Kay et al., 2015). While these datasets would provide more insight into the uncertainty and potential range of changes in extreme precipitation, valuable spatial detail would be lost, as seen in Figure 4.3. High resolution simulations require a great deal of computing resources to produce, therefore the availability of these simulations is currently limited. Because of this, the time coverage of simulations is also generally shorter compared to the lengthy coarse simulations available.

Finally, the datasets used in this analysis were limited in time coverage due to computing resources for the novel VR-CESM simulations and large storage allocations required to house high resolution climate datasets. The use of longer simulations (ideally at least 30 years) would allow for a better characterization of mean conditions in historical and future simulations, as shorter time periods risk interannual variability skewing the averages (World Meteorological Organization, 2017). However, this could also be achieved using an initial condition ensemble that helps to capture the interannual variability across the simulations.

The future development of ensembles of simulations with a similar resolution would be an excellent opportunity to perform similar analyses to assess agreement with the simulations used in the presented analysis. Further, the use of simulations with even higher resolution may be of benefit

in understanding local-scale changes in extreme precipitation occurrence and intensity in the future as computing resources allow for more detailed coupled simulations and ensembles.

6.2.2 Analyze potential timeline of changes in extreme precipitation

As discussed in Section 6.2.1, the simulation periods used for analysis in this thesis were limited due to computing resources. Since two discrete time periods were used, no insight is given into the rate of changes shown in Chapters 4 and 5. This raises the question: are the changes seen in these simulations relatively linear, or is there a tipping point at which the changes amplify?

Several studies have identified "tipping points" associated with the Greenland Ice Sheet related to refreezing capacity (Noël et al., 2017, 2022) and melt rates (Boers & Rypdal, 2021). Since previous studies have identified warming-based thresholds that lead to accelerating changes in the study domain, it would be insightful to understand whether extreme precipitation is changing linearly or displays similar behaviour. Specifically, understanding the timing of the shift to rainfall, particularly for extremes, would shed light onto when the impacts to land ice may shift towards the negative regime. Performing similar analyses on simulations that span from the historical period to the future period can help to answer this important question. Again, the use of an initial condition model ensemble could help in this analysis to increase confidence that natural variability is captured in the study.

6.2.3 Investigate connections between extreme precipitation and large-scale circulation

The study region's climate is largely tied to the behaviour of the North Atlantic Oscillation (NAO) and Arctic Oscillation (AO), as discussed in Section 2.3.2. Previous studies have highlighted the connections between general precipitation patterns and these indices (e.g., Berdahl et al., 2018; Bromwich et al., 1999; Hall et al., 2014; Villamil-Otero et al., 2018) as well as their connection to the SMB of the Greenland Ice Sheet (e.g., Bevis et al., 2019; Bjørk et al., 2018). However, no previous study has directly connected these indices to the occurrence and intensity of extreme precipitation events in the study region.

With the results presented in Chapter 4, we can hypothesize on what may be happening with the NAO and/or AO based on previous studies. The positive phase of the NAO has been tied to decreased winter precipitation in southern Greenland (Bromwich et al., 1999), which may help to describe the decreasing extreme precipitation in SE Greenland, and the weak cold season increases seen elsewhere. However, the relationship between the NAO and Greenland precipitation is not consistently agreed upon (e.g., Berdahl et al., 2018) and therefore not strong enough to draw conclusions since the NAO index was not explicitly investigated in this work. Future in depth analysis of the NAO/AO in the same simulations would provide insight into the relationship between extreme precipitation and large-scale circulation in the region.

6.2.4 Connection of extreme precipitation characteristics to cyclone and AR parameters

In Chapter 4, the occurrence of extreme precipitation was tied to the presence of extratropical cyclones and ARs. This provided valuable insight into the importance of cyclones for extreme precipitation in the region, and how ARs appear to be linked to the warm season extreme precipitation increases. Future work further developing the links between extreme precipitation characteristics with cyclone and AR characteristics would be insightful to develop our understanding of the relationships.

For example, in Figure 4.7 and Figure B.11, it is apparent that the frequency and pressure gradient associated with cyclones are not projected to change drastically in the future projections. Previous studies have indicated that precipitation rates are expected to increase within cyclones of similar intensities (e.g., Bailey & Hubbard, 2025; Box et al., 2022; Kodama et al., 2019; Sinclair & Catto, 2023), posing the question: do cyclone-associated extreme precipitation days become more intense in the future due to increases in cyclone intensity or are other factors responsible?

An exploration of the range of extremes associated with cyclones and ARs would provide insight into this relationship. For example, ARs provide some of the most intense moisture transport (Kolbe et al., 2023), so one may postulate that the majority of the most intense precipitation would be associated with ARs. Similarly, are the extremes that occur without a cyclone or AR less intense than extremes that occur with one or both present?

6.2.5 Investigate the longevity of impacts of extreme precipitation outside of the day and location/grid cell in which they occur, and how glacier dynamics are affected by these changes

One notable limitation of the study presented in Chapter 5 is that only the exact date of the extreme precipitation is included in the location in which it occurs. Case studies have indicated notable downstream effects that can last several days, or longer, after the intense precipitation occurs (e.g., Bailey & Hubbard, 2025; Doyle et al., 2015; Harper et al., 2023; Oerlemans & Klok, 2004). Because of this, it is possible that the impacts explored in Chapter 5 underestimate the true impact that extreme precipitation may have on land ice. Further exploration of these lasting and indirect impacts would help to address this uncertainty.

For example, cumulative seasonal SMB impacts may increase when considering the length of time after an event that impacts/anomalies persist. To address this, one may consider performing more detailed anomaly exploration for individual events to identify and track anomalies through time to better understand the longevity of impacts of intense precipitation. This may also be possible to explore the downstream effects, whereby anomalies in surrounding grid cells may be considered until reaching unaffected cells. The use of machine learning pattern recognition techniques may aid in identifying the spatial and temporal extent of the SMB impacts. This type of analysis would greatly benefit from increased spatial and temporal resolution to capture small-scale variations and better representation of the firn layer that is crucial for extreme precipitation impacts.

Employing complex ice sheet/glacier models to explore impacts associated with extreme precipitation could also provide a more detailed view of the changes that occur with different rates of precipitation and how they persist throughout a season. It may also facilitate a detailed analysis of the surface energy balance during/after extreme precipitation events; Teng et al. (2025) studied extreme rainfall events ($\geq 90^{th}$ percentile) at two observation sites in southern Greenland and found that radiative fluxes dominated the impacts at one site (e.g., albedo effect) but non-radiative fluxes were dominant at the other site (e.g., turbulent sensible and latent heat fluxes). Further study would allow for a better understanding of the direct effects of heavy precipitation and how it influences other parts of the energy balance. The use of detailed land ice models can also allow for the impacts on glacial dynamics to be explored; Doyle et al. (2015) found a dramatic increase in ice flow and discharge as a result of intense late summer rainfall, illustrating that understanding the impacts outside of the SMB is important to better characterize the importance of extreme precipitation to land ice changes.

6.3 Closing comments

The results presented in this thesis provide a deep exploration of projected changes to extreme precipitation in the eastern Canadian Arctic and Greenland and the potential impacts of these events on the region's land ice. Arctic temperatures are rising rapidly, and previous studies have highlighted how the associated loss of sea ice and increased moisture holding capacity of warmer air increase the potential for extreme precipitation events (e.g., Crawford et al., 2022; McCrystall et al., 2021; Pendergrass et al., 2017; Scoccimarro & Gualdi, 2020). While these changes have been investigated with coarse global climate models (e.g., McCrystall et al., 2021; Pfahl et al., 2017), little previous work has examined regional-scale changes in extreme precipitation in the Arctic.

The detailed examination of extreme daily precipitation events presented here provides valuable insight into the potential for substantial increases in extreme events in regions such as SW Greenland and Baffin Island, largely as summer rainfall rather than cold season accumulations. This increase in summer extreme precipitation with a high rain fraction brings increasingly negative SMB impacts on event days. For example, SW Greenland is projected to see >20% of seasonal negative SMB in the warm season resulting from extreme precipitation days. This shift suggests that warm season extreme precipitation is accelerating future mass loss, hastening contributions to sea level rise. However, this pattern was not shown to be consistent across the domain; SE Greenland is projected to see a decrease in extreme precipitation. Historical extremes in this region peaked during the winter, tied to extratropical cyclone occurrence. In the future projections, a slight decrease of cyclone activity leads to lower extreme precipitation accumulations in SE Greenland, reducing the large mass gains seen from these events historically.

This work also employs unique analyses that help to broaden our understanding of extreme precipitation and its connections to the Arctic climate system. The connection of extreme precipitation to extratropical cyclones and ARs provides valuable insight into their role in driving extremes, showing that cyclones are more commonly associated with extreme events but ARs become more important in future extremes. The novel seasonal SMB analysis methods developed here also allow for the first attempt at quantifying the overall climatological impacts of extreme

precipitation on the SMB of land ice, illustrating that the role of these events is becoming larger in the warmer future climate, both when considering positive and negative SMB impacts.

Ultimately, this work has yielded a unique and valuable view of the potential changes and connections of extreme precipitation with other aspects of the Arctic climate system. I hope that this work can act as a framework for future studies of other glaciated regions, and further in-depth assessments of the interactions between extreme precipitation and land ice. Developing our understanding of these processes and their interconnections will help to further illustrate the potential risks to local communities and acceleration, or deceleration, of the contribution of regional land ice mass to global sea level rise in the warming Arctic.

Literature cited

Ali, S. M. A., & Tandon, N. F. (2024). Influence of Horizontal Model Resolution on the Horizontal Scale of Extreme Precipitation Events. *Journal of Geophysical Research: Atmospheres*, *129*(22), e2023JD040146. https://doi.org/10.1029/2023JD040146

Avila-Diaz, A., Bromwich, D. H., Wilson, A. B., Justino, F., & Wang, S.-H. (2021). Climate Extremes across the North American Arctic in Modern Reanalyses. https://doi.org/10.1175/JCLI-D-20-0093.1

Bailey, H., & Hubbard, A. (2025). Snow Mass Recharge of the Greenland Ice Sheet Fueled by Intense Atmospheric River. *Geophysical Research Letters*, *52*(5), e2024GL110121. https://doi.org/10.1029/2024GL110121

Barrett, A. P., Stroeve, J. C., & Serreze, M. C. (2020). Arctic Ocean Precipitation From Atmospheric Reanalyses and Comparisons With North Pole Drifting Station Records. *Journal of Geophysical Research: Oceans*, *125*(1), 1–17. https://doi.org/10.1029/2019JC015415

Berdahl, M., Rennermalm, A., Hammann, A., Mioduszweski, J., Hameed, S., Tedesco, M., et al. (2018). Southeast Greenland Winter Precipitation Strongly Linked to the Icelandic Low Position. *Journal of Climate*, *31*(11), 4483–4500. https://doi.org/10.1175/JCLI-D-17-0622.1

Bevis, M., Harig, C., Khan, S. A., Brown, A., Simons, F. J., Willis, M., et al. (2019). Accelerating changes in ice mass within Greenland, and the ice sheet's sensitivity to atmospheric forcing. *Proceedings of the National Academy of Sciences*, *116*(6), 1934–1939. https://doi.org/10.1073/pnas.1806562116

Bintanja, R., & Andry, O. (2017). Towards a rain-dominated Arctic. *Nature Climate Change*, *7*(4), 263–267. https://doi.org/10.1038/nclimate3240

Bjørk, A. A., Aagaard, S., Lütt, A., Khan, S. A., Box, J. E., Kjeldsen, K. K., et al. (2018). Changes in Greenland's peripheral glaciers linked to the North Atlantic Oscillation. *Nature Climate Change*, *8*(1), 48–52. https://doi.org/10.1038/s41558-017-0029-1

Boers, N., & Rypdal, M. (2021). Critical slowing down suggests that the western Greenland Ice Sheet is close to a tipping point. *Proceedings of the National Academy of Sciences*, *118*(21), e2024192118. https://doi.org/10.1073/pnas.2024192118

Boisvert, L. N., Webster, M. A., Petty, A. A., Markus, T., Bromwich, D. H., & Cullather, R. I. (2018). Intercomparison of Precipitation Estimates over the Arctic Ocean and Its Peripheral Seas from Reanalyses. *Journal of Climate*, *31*(20), 8441–8462. https://doi.org/10.1175/JCLI-D-18-0125.1

Box, J. E., Wehrlé, A., van As, D., Fausto, R. S., Kjeldsen, K. K., Dachauer, A., et al. (2022). Greenland Ice Sheet Rainfall, Heat and Albedo Feedback Impacts From the Mid-August 2021 Atmospheric River. *Geophysical Research Letters*, *49*(11), e2021GL097356. https://doi.org/10.1029/2021GL097356

Box, J. E., Nielsen, K. P., Yang, X., Niwano, M., Wehrlé, A., van As, D., et al. (2023). Greenland ice sheet rainfall climatology, extremes and atmospheric river rapids. *Meteorological Applications*, *30*(4), e2134. https://doi.org/10.1002/met.2134

Bromwich, D. H., Chen, Q., Li, Y., & Cullather, R. I. (1999). Precipitation over Greenland and its relation to the North Atlantic Oscillation. *Journal of Geophysical Research: Atmospheres*, *104*(D18), 22103–22115. https://doi.org/10.1029/1999JD900373

Cai, L., Alexeev, V. A., Arp, C. D., Jones, B. M., Liljedahl, A. K., & Gädeke, A. (2018). The Polar WRF Downscaled Historical and Projected Twenty-First Century Climate for the Coast and Foothills of Arctic Alaska. *Frontiers in Earth Science*, *5*. https://doi.org/10.3389/feart.2017.00111

Crawford, A. D., Lukovich, J. V., McCrystall, M. R., Stroeve, J. C., & Barber, D. G. (2022). Reduced Sea Ice Enhances Intensification of Winter Storms over the Arctic Ocean. *Journal of Climate*, *35*(11), 3353–3370. https://doi.org/10.1175/JCLI-D-21-0747.1

Crawford, A. D., McCrystall, M. R., Lukovich, J. V., & Stroeve, J. C. (2023). The Response of Extratropical Cyclone Propagation in the Northern Hemisphere to Global Warming. *Journal of Climate*, *36*(20), 7123–7142. https://doi.org/10.1175/JCLI-D-23-0082.1

Doyle, S. H., Hubbard, A., van de Wal, R. S. W., Box, J. E., van As, D., Scharrer, K., et al. (2015). Amplified melt and flow of the Greenland ice sheet driven by late-summer cyclonic rainfall. *Nature Geoscience*, *8*(8), 647–653. https://doi.org/10.1038/ngeo2482

Eyring, V., Bony, S., Meehl, G. A., Senior, C. A., Stevens, B., Stouffer, R. J., & Taylor, K. E. (2016). Overview of the Coupled Model Intercomparison Project Phase 6 (CMIP6) experimental design and organization. *Geoscientific Model Development*, *9*(5), 1937–1958. https://doi.org/10.5194/gmd-9-1937-2016

Gascon, G., Stewart, R. E., & Henson, W. (2010). Major Cold-Season Precipitation Events at Iqaluit, Nunavut. *Arctic*, *63*(3), 327–337.

Hall, R., Erdélyi, R., Hanna, E., Jones, J. M., & Scaife, A. A. (2014). Drivers of North Atlantic Polar Front jet stream variability. *International Journal of Climatology*, *35*(8), 1697–1720. https://doi.org/10.1002/joc.4121

Harper, J., Saito, J., & Humphrey, N. (2023). Cold Season Rain Event Has Impact on Greenland's Firn Layer Comparable to Entire Summer Melt Season. *Geophysical Research Letters*, *50*(14), e2023GL103654. https://doi.org/10.1029/2023GL103654

Hawcroft, M. K., Shaffrey, L. C., Hodges, K. I., & Dacre, H. F. (2012). How much Northern Hemisphere precipitation is associated with extratropical cyclones? *Geophysical Research Letters*, *39*(24). https://doi.org/10.1029/2012GL053866

Joos, H., Sprenger, M., Binder, H., Beyerle, U., & Wernli, H. (2023). Warm conveyor belts in present-day and future climate simulations – Part 1: Climatology and impacts. *Weather and Climate Dynamics*, *4*(1), 133–155. https://doi.org/10.5194/wcd-4-133-2023

Kay, J. E., Deser, C., Phillips, A., Mai, A., Hannay, C., Strand, G., et al. (2015). The Community Earth System Model (CESM) Large Ensemble Project: A Community Resource for Studying Climate Change in the Presence of Internal Climate Variability. https://doi.org/10.1175/BAMS-D-13-00255.1

Kodama, C., Stevens, B., Mauritsen, T., Seiki, T., & Satoh, M. (2019). A New Perspective for Future Precipitation Change from Intense Extratropical Cyclones. *Geophysical Research Letters*, *46*(21), 12435–12444. https://doi.org/10.1029/2019GL084001

Kolbe, M., Sonnemans, J. P. J., Bintanja, R., van der Linden, E. C., van der Wiel, K., Whan, K., & Benedict, I. (2023). Impact of Atmospheric Rivers on Future Poleward Moisture Transport and Arctic Climate in EC-Earth2. *Journal of Geophysical Research: Atmospheres*, e2023JD038926. https://doi.org/10.1029/2023JD038926

Koyama, T., & Stroeve, J. (2019). Greenland monthly precipitation analysis from the Arctic System Reanalysis (ASR): 2000–2012. *Polar Science*, *19*, 1–12. https://doi.org/10.1016/j.polar.2018.09.001

Lindsay, R., Wensnahan, M., Schweiger, A., & Zhang, J. (2014). Evaluation of Seven Different Atmospheric Reanalysis Products in the Arctic. *Journal of Climate*, *27*(7), 2588–2606. https://doi.org/10.1175/JCLI-D-13-00014.1

McCrystall, M. R., Stroeve, J., Serreze, M., Forbes, B. C., & Screen, J. A. (2021). New climate models reveal faster and larger increases in Arctic precipitation than previously projected. *Nature Communications*, *12*(1), 6765. https://doi.org/10.1038/s41467-021-27031-y

Noël, B., van de Berg, W. J., Lhermitte, S., Wouters, B., Machguth, H., Howat, I., et al. (2017). A tipping point in refreezing accelerates mass loss of Greenland's glaciers and ice caps. *Nature Communications*, *8*(1), 14730. https://doi.org/10.1038/ncomms14730

Noël, B., Lenaerts, J. T. M., Lipscomb, W. H., Thayer-Calder, K., & van den Broeke, M. R. (2022). Peak refreezing in the Greenland firn layer under future warming scenarios. *Nature Communications*, *13*(1), 6870. https://doi.org/10.1038/s41467-022-34524-x

Oerlemans, J., & Klok, E. J. L. (2004). Effect of summer snowfall on glacier mass balance. *Annals of Glaciology*, *38*, 97–100. https://doi.org/10.3189/172756404781815158

Ohmura, A., & Reeh, N. (1991). New precipitation and accumulation maps for Greenland. *Journal of Glaciology*, *37*(125), 140–148. https://doi.org/10.3189/S0022143000042891

Pendergrass, A. G., Knutti, R., Lehner, F., Deser, C., & Sanderson, B. M. (2017). Precipitation variability increases in a warmer climate. *Scientific Reports*, *7*(1), 17966. https://doi.org/10.1038/s41598-017-17966-y

Pfahl, S., O'Gorman, P. A., & Fischer, E. M. (2017). Understanding the regional pattern of projected future changes in extreme precipitation. *Nature Climate Change*, *7*(6), 423–427. https://doi.org/10.1038/nclimate3287

Priestley, M. D. K., & Catto, J. L. (2022). Future changes in the extratropical storm tracks and cyclone intensity, wind speed, and structure. *Weather and Climate Dynamics*, *3*(1), 337–360. https://doi.org/10.5194/wcd-3-337-2022

Rapaić, M., Brown, R., Markovic, M., & Chaumont, D. (2015). An Evaluation of Temperature and Precipitation Surface-Based and Reanalysis Datasets for the Canadian Arctic, 1950–2010. *Atmosphere-Ocean*, *53*(3), 283–303. https://doi.org/10.1080/07055900.2015.1045825

Scoccimarro, E., & Gualdi, S. (2020). Heavy Daily Precipitation Events in the CMIP6 Worst-Case Scenario: Projected Twenty-First-Century Changes. *Journal of Climate*, *33*(17), 7631–7642. https://doi.org/10.1175/JCLI-D-19-0940.1

Sinclair, V. A., & Catto, J. L. (2023). The relationship between extra-tropical cyclone intensity and precipitation in idealised current and future climates. https://doi.org/10.5194/wcd-4-567-2023

Villamil-Otero, G. A., Zhang, J., He, J., & Zhang, X. (2018). Role of extratropical cyclones in the recently observed increase in poleward moisture transport into the Arctic Ocean. *Advances in Atmospheric Sciences*, *35*(1), 85–94. https://doi.org/10.1007/s00376-017-7116-0

Wagner, D. N., Shupe, M. D., Persson, O. G., Uttal, T., Frey, M. M., Kirchgaessner, A., et al. (2021). Snowfall and snow accumulation processes during the MOSAiC winter and spring season. *The Cryosphere Discussions*, 1–48. https://doi.org/10.5194/tc-2021-126

World Meteorological Organization. (2017). *WMO Guidelines on the Calculation of Climate Normals* (No. WMO-No. 1203) (p. 29). Retrieved from https://www.agroorbi.pt/livroagrometeorologia/DocsProg/Temas&Exerc%C3%ADciosExtraPorCap%C3%ADtulo/Cap1_Introdu%C3%A7%C3%A3o/Docs/WMO%20Guidelines%20on%20the%20Calculation%20of%20Climate%20Normals_en.pdf

Yettella, V., & Kay, J. E. (2017). How will precipitation change in extratropical cyclones as the planet warms? Insights from a large initial condition climate model ensemble. *Climate Dynamics*, *49*(5), 1765–1781. https://doi.org/10.1007/s00382-016-3410-2

Appendix A. Supplementary Material for Chapter 3

Table A.1. Details of each observation station analyzed.

Station ID	Long Name	Subregion	Latitude [°]	Longitude [°]	Start Date	End Date	Days of Data
2400565	Brevoort Island	Baffin Island	63.34	-64.15	1989-04-01	1993-03-30	1427
2400570	Broughton Island	Baffin Island	67.54	-63.79	1980-01-01	1991-06-30	4189
2400635	Cape Dorset A	Baffin Island	64.23	-76.53	1980-01-01	2010-12-30	10460
2400654	Cape Dyer A	Baffin Island	66.58	-61.62	1980-01-01	1993-03-30	4801
2400660	Cape Hooper	Baffin Island	68.47	-66.82	1980-01-01	1991-06-30	4174
2400800	Clyde A	Baffin Island	70.49	-68.52	1980-01-01	2002-06-30	7915
2401030	Dewar Lakes	Baffin Island	68.65	-71.17	1980-01-01	1993-05-12	4754
2402590	Iqaluit A	Baffin Island	63.75	-68.55	1980-01-01	2002-05-31	6629
2402592	Iqaluit Climate	Baffin Island	63.75	-68.54	2005-03-01	2007-11-30	866
2402594	Iqaluit Ua	Baffin Island	63.75	-68.55	1997-04-01	2016-02-15	5930
2402684	Longstaff Bluff	Baffin Island	68.90	-75.14	1980-01-01	1991-06-28	4191
2402730	Nanisivik A	Baffin Island	72.98	-84.62	1980-01-01	2010-12-30	9528
2403050	Pangnirtung 1925 Climate	Baffin Island	66.13	-65.73	1981-02-01	1983-08-31	209
2403201	Pond Inlet A	Baffin Island	72.69	-77.97	1980-01-01	2009-09-30	9815
2400300	Alert	Ellesmere Island	82.52	-62.28	1980-01-01	1999-12-31	7294
2400306	Alert Ua	Ellesmere Island	82.50	-62.33	2000-01-01	2014-12-31	5382
2401200	Eureka A	Ellesmere Island	79.98	-85.93	1980-01-01	2016-02-16	13080
2402346	Grise Fiord	Ellesmere Island	76.42	-82.90	1984-08-01	2010-06-25	8114
04202	Pituffik	NW Greenland	76.53	-68.75	1982-01-01	2006-11-27	8325
04212	Uummannaq Heli.	CW Greenland	70.67	-52.12	1980-01-03	1989-08-21	1691
04216	Ilulissat	CW Greenland	69.22	-51.05	1980-01-01	1991-10-11	3311
04220	Aasiaat	CW Greenland	68.70	-52.75	1980-01-01	2013-12-31	11341
04230	Sisimiut	SW Greenland	66.92	-53.67	1980-01-01	2001-05-15	5675
04231	Kangerlussuaq	SW Greenland	67.00	-50.80	1980-01-01	2013-12-31	12242
04235	DYE 1	SW Greenland	66.63	-52.87	1982-02-01	1989-09-18	2492
04240	Maniitsoq	SW Greenland	65.40	-52.87	1980-01-02	1987-01-30	1583
04250	Nuuk	SW Greenland	64.17	-51.75	1980-01-01	2006-12-05	9390
04260	Mitt. Paamiut	SW Greenland	62.02	-49.67	1980-01-01	2003-03-31	7232
04270	Mitt. Narsarsuaq	SW Greenland	61.17	-45.42	1980-01-01	2008-12-30	10364
04272	Qaqortoq	SW Greenland	60.72	-46.05	1980-01-01	2013-12-31	12201
04283	Nanortalik Heli.	SW Greenland	60.13	-45.23	1980-01-01	1985-11-02	1960
04465	DYE 2	SW Greenland	66.48	-46.28	1982-01-28	1988-10-06	1929
04310	Station Nord	NE Greenland	81.60	-16.65	1980-01-01	2007-07-09	9192

Appendix A: Supplementary Material for Chapter 3

Station ID	Long Name	Subregion	Latitude [°]	Longitude [°]	Start Date	End Date	Days of Data
04320	Danmarkshavn	NE Greenland	76.77	-18.67	1980-01-01	2008-12-31	10417
04338	Mestersvig	NE Greenland	72.25	-23.90	1980-01-01	1985-10-25	1993
04339	Ittoqqortoormiit	NE Greenland	70.48	-21.95	1980-11-02	2006-01-14	8453
04360	Tasiilaq	SE Greenland	65.60	-37.63	1980-01-01	2013-12-21	8737
04365	DYE 4	SE Greenland	65.52	-37.17	1981-02-04	1991-05-20	2587
04475	DYE 3	SE Greenland	65.18	-43.83	1982-07-18	1989-09-18	2335

Table A.2. Extreme event threshold accumulation, frequency (f_e), and number of days with at least 1 mm of accumulation for each station. Dashed lines separate the subregions. E, M, and C represent ERA-5, MERRA-2, and CFSR, respectively.

	Extreme Threshold [mm]				f_e [events (yr)-1]				Days with Accumulation ≥ 1 mm			
Station ID	*Obs.*	*E.*	*M.*	*C.*	*Obs.*	*E.*	*M.*	*C.*	*Obs.*	*E.*	*M.*	*C.*
2400565	25.3	17.3	16.8	15.1	4.9	1.3	1.5	0.3	366	414	403	412
2400570	12.0	11.1	10.4	9.3	3.6	3.6	3.6	2.2	777	910	1030	971
2400635	13.8	11.6	11.3	10.5	5.8	3.4	3.7	3.3	3321	2843	3262	3761
2400654	26.3	16.6	14.3	13.6	4.8	1.2	0.3	0.2	1223	1225	1291	1544
2400660	11.6	12.1	10.8	9.8	3.9	5.7	3.4	2.8	900	1169	949	1106
2400800	11.7	10.7	10.4	9.7	3.4	3.1	3.2	2.7	1438	1637	1987	1801
2401030	11.8	10.1	9.8	9.9	3.6	3.4	3.7	3.3	922	1243	1503	1309
2402590	14.9	12.7	10.9	10.2	4.6	4.1	2.3	2.0	1656	2072	2281	2107
2402592	14.5	13.9	12.3	9.7	4.6	6.7	3.0	2.5	203	332	354	334
2402594	16.0	13.8	11.8	19.3	4.6	4.1	3.1	9.2	1478	2024	2180	2342
2402684	10.3	10.8	10.7	9.7	3.0	4.8	5.9	3.6	663	992	1223	1059
2402730	13.7	8.7	8.6	6.2	3.7	1.0	1.9	0.3	1891	1888	2894	2143
2403050	17.9	13.4	13.8	10.7	5.2	5.2	5.2	3.5	55	85	96	87
2403201	13.4	9.5	8.6	8.7	3.2	1.6	1.6	1.4	1683	2232	3067	3255
2400300	9.4	7.1	6.1	6.0	3.1	1.5	0.9	0.9	1183	1254	1307	1098
2400306	8.3	6.3	5.0	10.2	3.5	1.0	0.5	5.1	951	903	749	968
2401200	7.8	6.3	9.0	9.1	1.5	0.9	4.6	5.4	1041	1246	2531	2980
2402346	15.2	8.6	11.8	7.0	2.4	0.4	1.8	0.2	1035	1309	1653	1222
04202	11.2	12.4	10.0	10.9	1.8	5.0	2.9	4.5	819	1700	1785	2202
04212	12.6	10.0	10.4	11.4	0.9	1.1	2.8	4.1	68	358	425	446
04216	16.9	10.3	13.0	11.8	3.3	1.0	2.1	1.7	566	638	770	671
04220	13.7	11.4	11.2	12.7	4.1	2.2	2.9	4.6	2366	2249	2687	3319
04230	17.4	14.2	14.1	9.0	4.2	3.4	3.5	0.8	1287	1846	2127	2126
04231	10.6	8.2	11.0	11.5	2.3	1.5	5.1	3.7	1552	2614	3174	2169
04235	9.2	10.9	10.1	8.7	2.2	7.8	7.8	5.5	267	675	792	898
04250	24.0	18.3	17.0	16.3	6.1	3.0	2.9	2.5	3053	3617	4145	4456

	Extreme Threshold [mm]				f_e [events (yr)-1]				Days with Accumulation ≥ 1 mm			
Station ID	*Obs.*	*E.*	*M.*	*C.*	*Obs.*	*E.*	*M.*	*C.*	*Obs.*	*E.*	*M.*	*C.*
04260	27.0	22.8	26.0	22.1	5.9	4.3	7.5	5.0	2340	2839	3335	3206
04270	28.1	22.1	25.6	20.5	4.2	4.4	6.4	3.2	2360	4809	4483	4027
04272	32.0	24.7	33.0	31.7	5.4	3.3	8.8	7.1	3413	4406	5168	4688
04283	26.4	22.2	22.7	21.7	4.7	3.6	5.5	5.7	348	619	658	706
04465	6.1	10.3	11.0	9.5	1.9	13.3	17.3	16.3	190	545	563	570
04310	13.8	12.4	10.4	9.4	3.2	3.2	1.9	1.2	1556	2232	2282	2257
04320	12.9	16.6	15.7	13.9	2.3	6.0	6.0	5.3	1311	1875	2089	2444
04338	28.3	23.4	22.4	21.2	2.7	1.3	1.9	1.1	278	387	451	417
04339	17.3	22.2	19.4	19.1	3.6	11.0	8.4	8.7	1645	2593	2720	2934
04360	27.9	25.5	29.8	29.5	6.0	5.4	9.6	9.5	2820	3371	3831	3764
04365	9.9	26.2	26.9	26.1	4.0	44.6	51.3	47.7	551	1027	1132	1119
04475	8.7	11.8	8.5	13.2	0.9	15.2	6.0	21.3	111	884	915	982

Table A.3. 95% Confidence interval (CI) for each subregion corresponding to the correlations provided in

Table 3.4. Regions whose correlation is not statistically significant ($p \geq 0.05$) are italicized.

	Overall Correlation (95% CI)			Extreme Event Correlation (95% CI)		
Subregion	*ERA-5*	*MERRA-2*	*CFSR*	*ERA-5*	*MERRA-2*	*CFSR*
Baffin Island	0.47-0.50	0.42-0.44	0.35-0.37	0.17-0.30	0.08-0.21	0.07-0.20
Ellesmere Island	0.34-0.39	0.26-0.31	0.16-0.22	*-0.12-0.15*	*-0.14-0.13*	*-0.24-0.03*
NW Greenland	0.20-0.33	0.20-0.32	0.22-0.35	*-0.33-0.28*	*-0.35-0.26*	*-0.33-0.28*
CW Greenland	0.43-0.48	0.34-0.40	0.37-0.43	0.03-0.34	*0.00-0.31*	*-0.05-0.26*
SW Greenland	0.59-0.61	0.52-0.55	0.47-0.50	0.41-0.52	0.35-0.47	0.27-0.40
NE Greenland	0.40-0.44	0.35-0.40	0.35-0.39	0.11-0.35	0.11-0.35	0.08-0.32
SE Greenland	0.47-0.52	0.44-0.49	0.47-0.52	0.17-0.44	0.12-0.40	0.08-0.35

Table A.4. 3-by-3 cell group used for spatial offsetting analysis. The cell with a star indicates the cell containing the station.

1	2	3
4	★	6
7	8	9

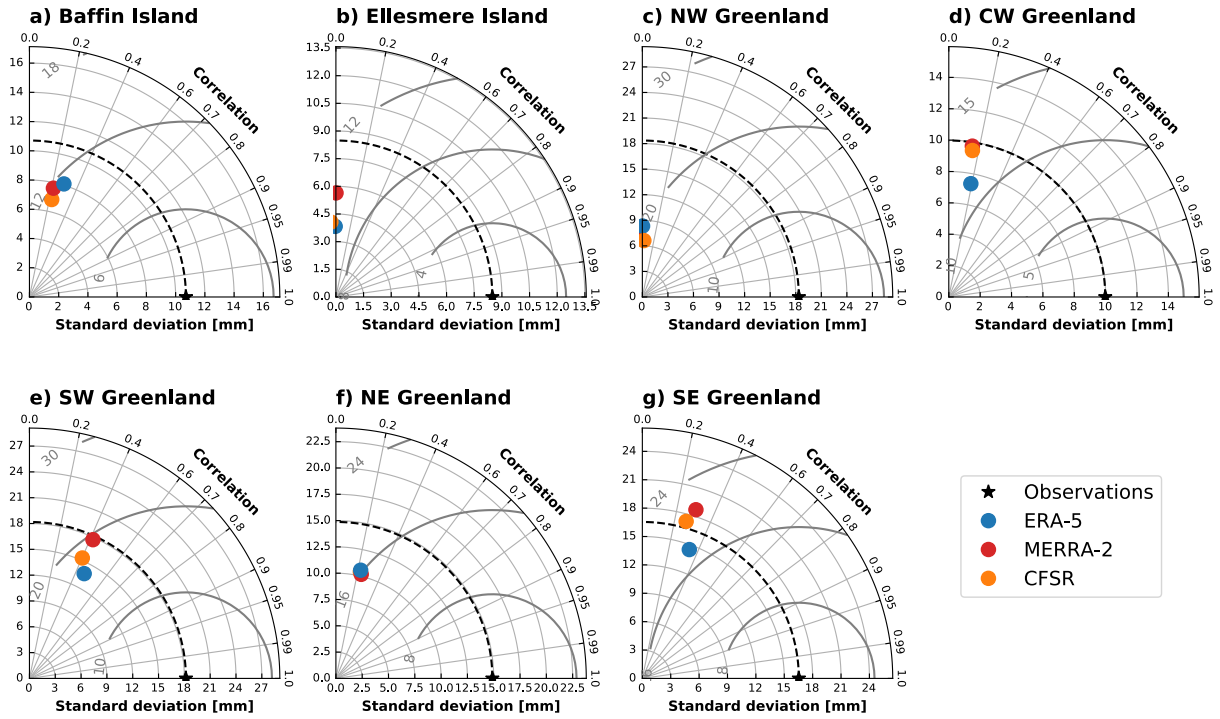

Figure A.1. Taylor diagrams comparing accumulations for extreme events between products in each subregion. The reanalysis accumulations are retrieved from the cell surrounding the station that produces the highest correlation with the station record to account for potential spatial offsets. CFSR is not visible in f) as it is overlain by ERA-5 and MERRA-2.

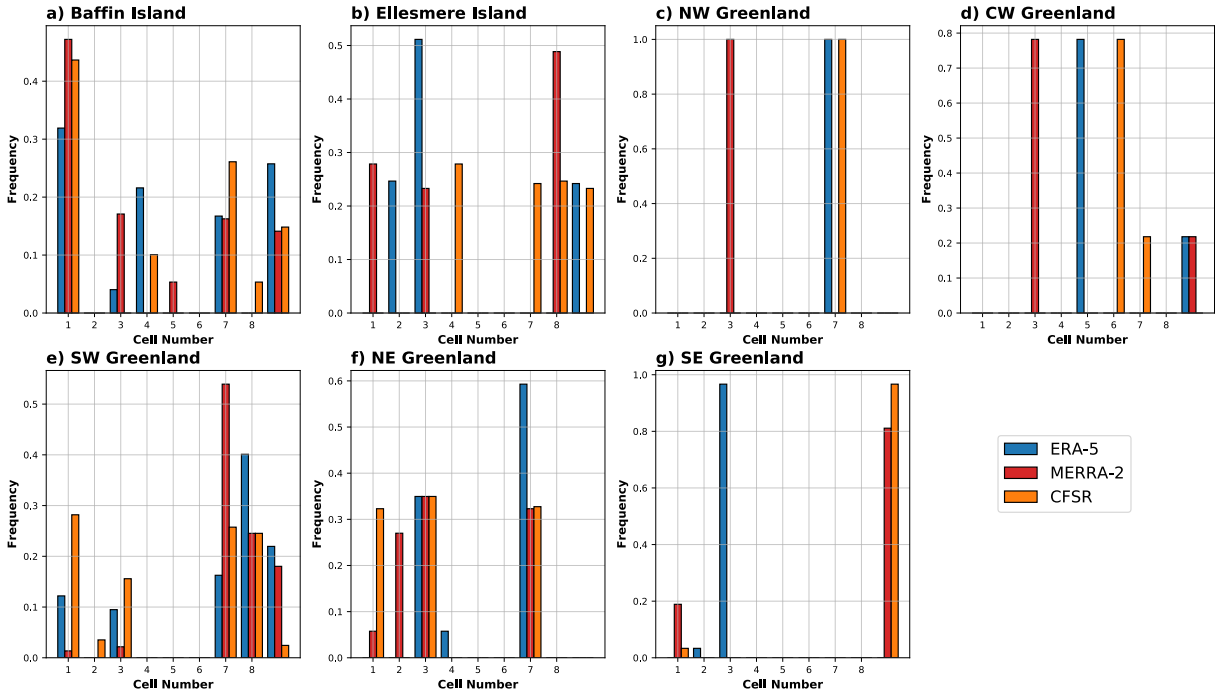

Figure A.2. Histograms showing the cell with the highest correlation between the reanalyses and observations in each subregion. The cell numbers are as shown in Table A.4.

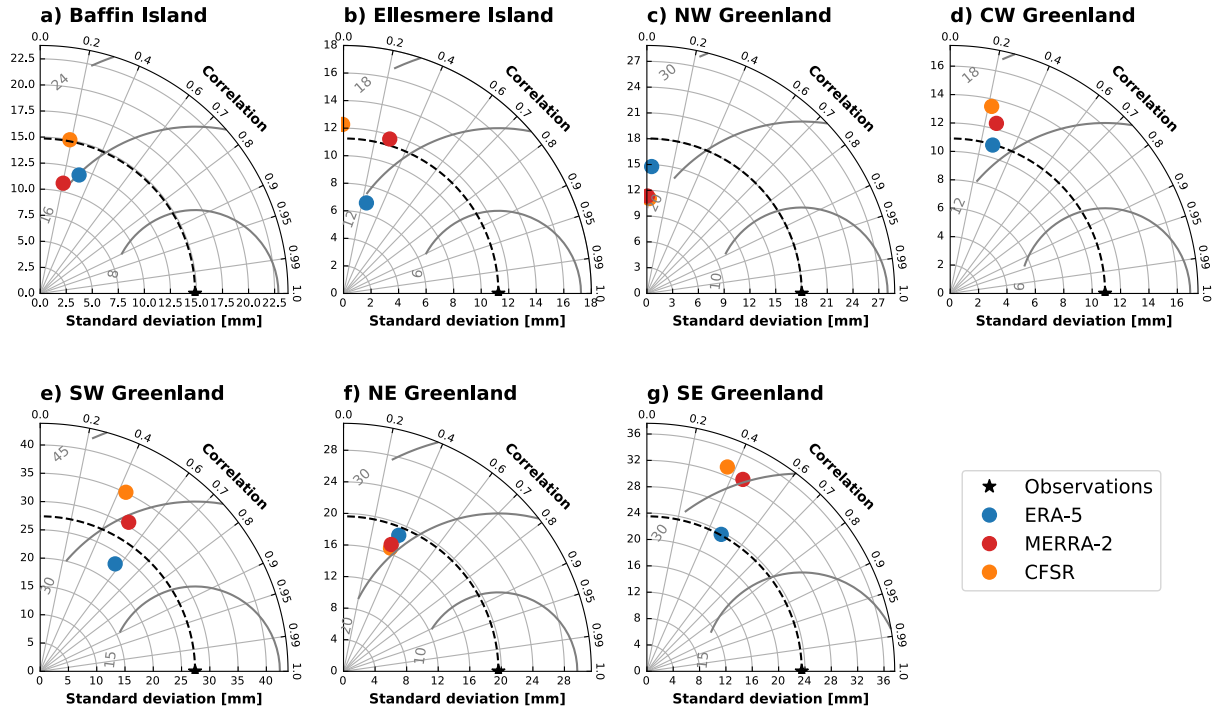

Figure A.3. Taylor diagrams comparing three-day accumulations for extreme events between products in each subregion to account for potential temporal offsets in the reanalyses. CFSR is not visible in c) due to the correlation falling below 0, and f) as it is overlain by MERRA-2.

Appendix B. Supplementary Material for Chapter 4

Journal of Geophysical Research: Atmospheres

Supporting Information for

Projections and Physical Drivers of Extreme Precipitation in Greenland & Baffin Bay

Nicole A. Loeb[1,2], Alex Crawford[1,2], Adam Herrington[3], Michelle McCrystall[4], Julienne Stroeve[1,2,5,6], John Hanesiak[1,2]

[1] Department of Environment & Geography, University of Manitoba, Winnipeg, MB, Canada

[2] Centre for Earth Observation Science, University of Manitoba, Winnipeg, MB, Canada

[3] Climate and Global Dynamics Laboratory, National Center for Atmospheric Research, Boulder, CO, USA

[4] Faculty of Physics, University of Auckland, Auckland, New Zealand

[5] Department of Earth Sciences, University College London, London, United Kingdom

[6] National Snow and Ice Data Center, Cooperative Institute for Research in Environmental Science, University of Colorado Boulder, Boulder, Colorado

Introduction

Figures B.1 and B.2 provide illustration of the ARCTIC VR-CESM grid and the forcing datasets used for the SSP5-8.5 future runs, respectively. The parameters used in the Crawford et al. (2021) algorithm are described in Table B.1.

Figures B.3 and B.4 reproduce results of comparisons of reanalyses (ERA5, CFSR, and MERRA-2) with surface station observations from Loeb et al. (2022) including VR-CESM.

Figures B.5, 7-10, 15-17 reproduce Figures 4.3-4.9 from the main text using the second future VR-CESM run (FUT-102), providing very similar results to those of FUT.

Figure B.6 shows the changes in extreme precipitation (as in Figure 4.4) from the future native-resolution CESM2 run.

Figure B.8 shows the changes in mean pressure gradient associated with detected cyclones to illustrate potential changes in the strength of cyclones.

Figure B.11 provides the results of using a 600 km radius around cyclone centers to identify cyclone-associated precipitation to compare to the 1200 km radius used in the main analysis. Figure B14 reproduces Figure 9 using the 600 km radius.

Figures B.12 and B.13 show the fraction of extreme precipitation days associated with cyclones and ARs in winter (JFM) and summer (JAS), respectively.

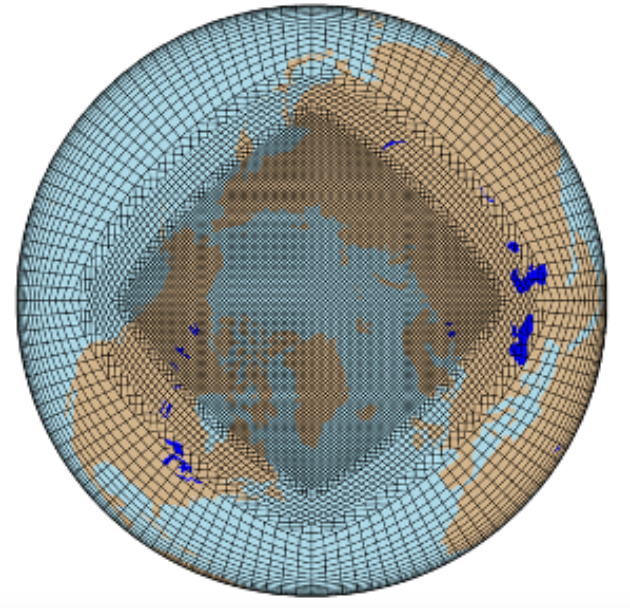

Figure B.1. ARCTIC VR-CESM grid (adapted from Herrington et al., 2022).

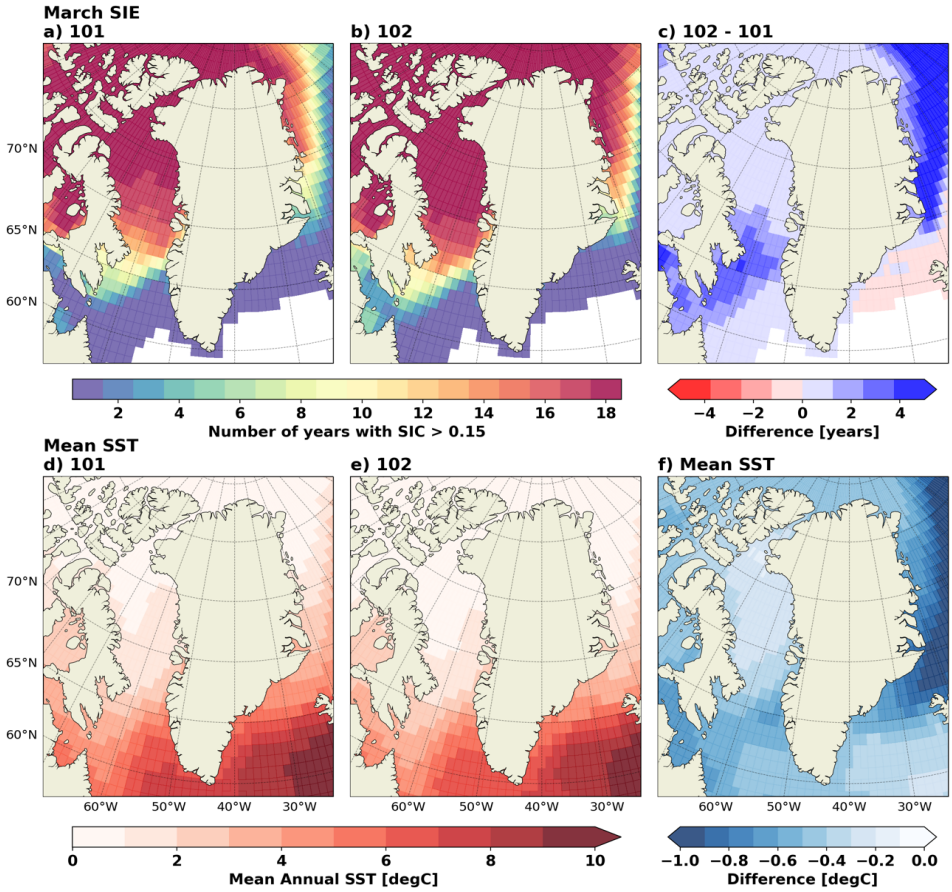

Figure B.2. (a-c) March sea ice extent (years in which each grid cell exceeds 0.15 sea ice concentration of 18-year record), and (d-f) mean annual sea surface temperatures used from forcing CESM CMIP6 runs. Run 101 (f09_g17.CMIP6-SSP5-8.5.101) results are shown in (a,d), 102 (f09_g17.CMIP6-SSP5-8.5.102) in (b,e), and differences are shown in (c,f).

Appendix B: Supplementary Material for Chapter 4

Table B.1. Parameters used in the Crawford et al. (2021) Lagrangian cyclone tracking algorithm.

Parameter Name	Description	Value
kSizekm	Size of kernel used to determine if grid cell is a local minimum	200 km
nanThres	Maximum fraction of neighbouring grid cells with no data allowed for a cell to be considered during minimum detection	0.4
d_slp	Minimum SLP gradient for identifying and removing weak minima	750 Pa
d_dist	Minimum distance in m for identifying and removing weak minima	1000 km
maxelev	Maximum elevation for masking out high elevation minima	1500 m
mcctol	Maximum ratio permitted between the number of unshared and total contours in a multi-centered cyclone. "Unshared" contours are only used by the primary center. "Shared" contours are used by both the primary and secondary centers	0.5
mccdist	Maximum distance two SLP minima can lie apart and still be considered part of the same cyclone system	1200 km
maxspeed	Maximum speed a cyclone can travel	150 km h^{-1}
red	Reduction parameter is a scaling of cyclone speed – When tracking, the algorithm uses the cyclone speed and direction from the last interval to estimate a "best guess" position. This parameter modifies that speed, making it slower. This reflects how cyclones tend to slow down as they mature	0.75

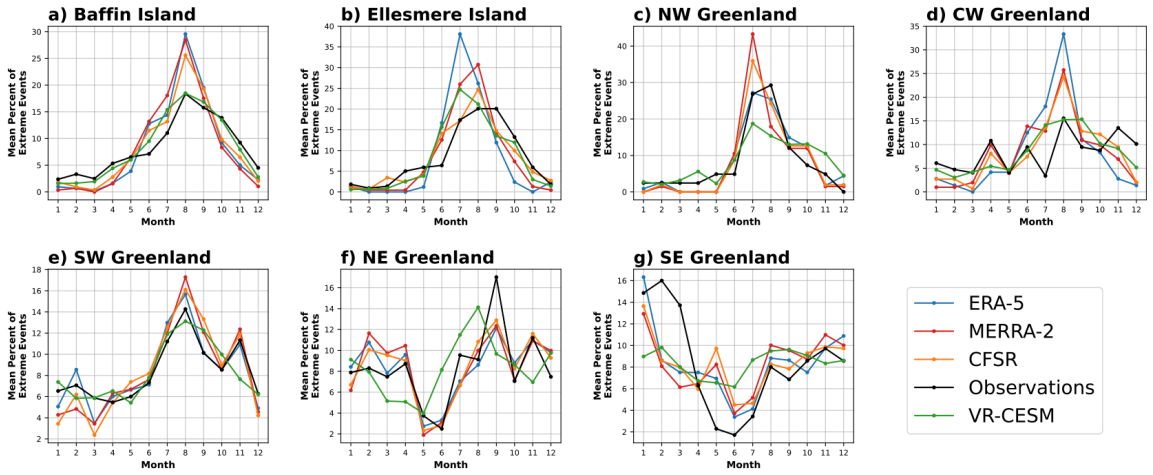

Figure B.3. Percent of all extreme events in reanalyses (ERA5, MERRA-2, CFSR) and VR-CESM HIST occurring in each month for all subregions (a-g), as in

Figure 3.3 (Figure 3 of Loeb et al. (2022)).

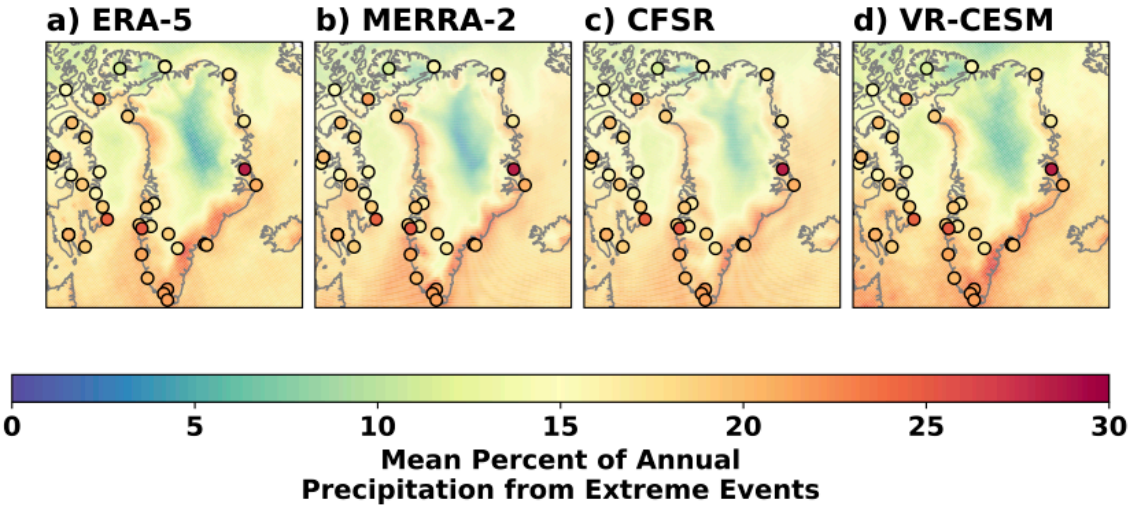

Figure B.4. Mean percent of annual precipitation attributed to extreme events based on (a) ERA-5, (b) MERRA-2, (c) CFSR, and (d) VR-CESM HIST, as in Figure 3.4 (Figure 4 of Loeb et al. (2022)). Circles show the relative contribution of extremes to annual precipitation for each station with at least 4 years of data from the Second Generation Adjusted Daily Precipitation Dataset for Canada and Danish Meteorological Institute synoptic stations for Greenland.

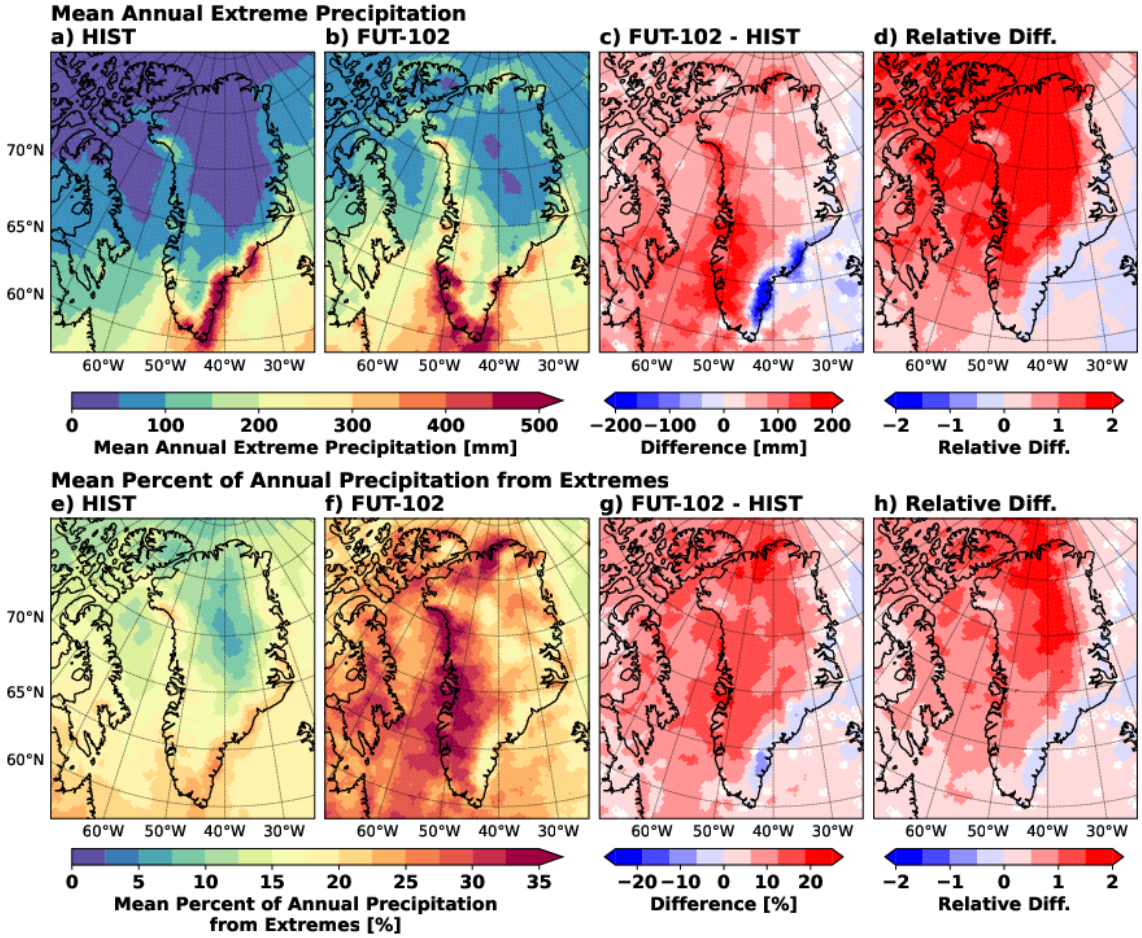

Figure B.5. As in Figure 4.4, but for the results of the second VR-CESM future run (FUT-102).

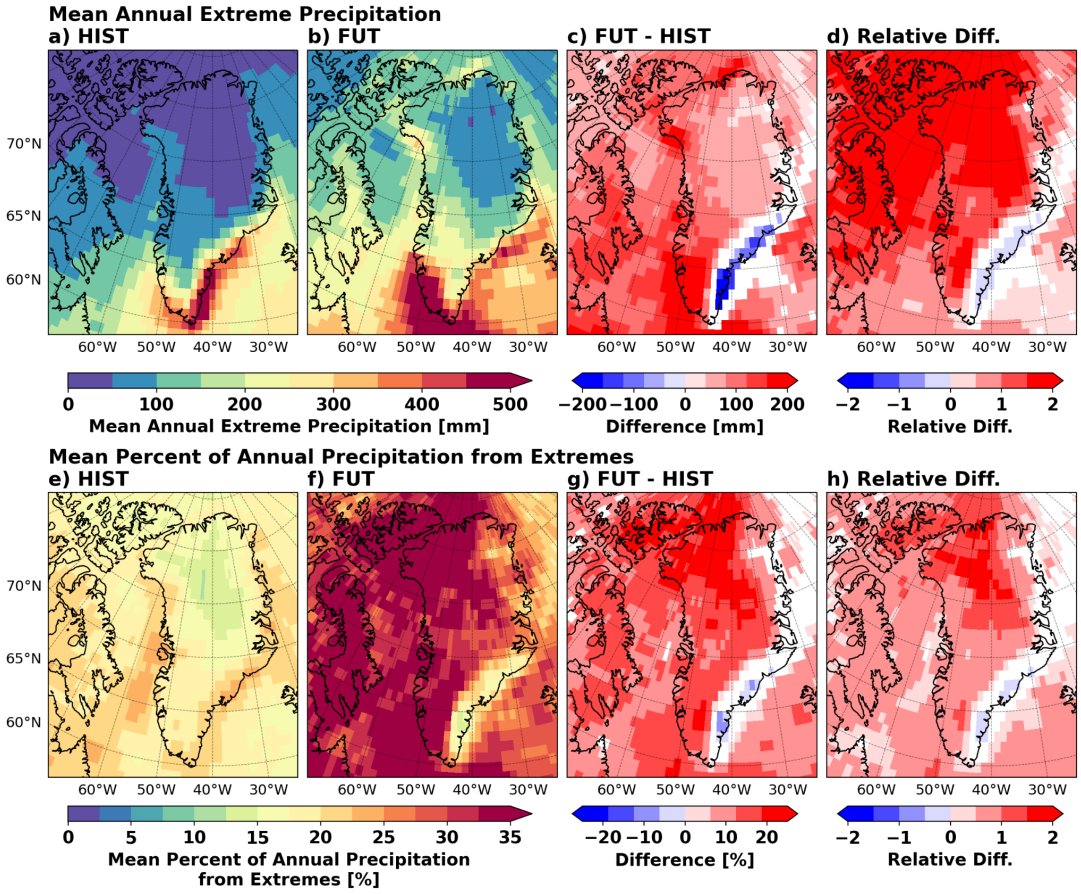

Figure B.6. As in Figure 4.4, but for the results of the future CESM2 run.

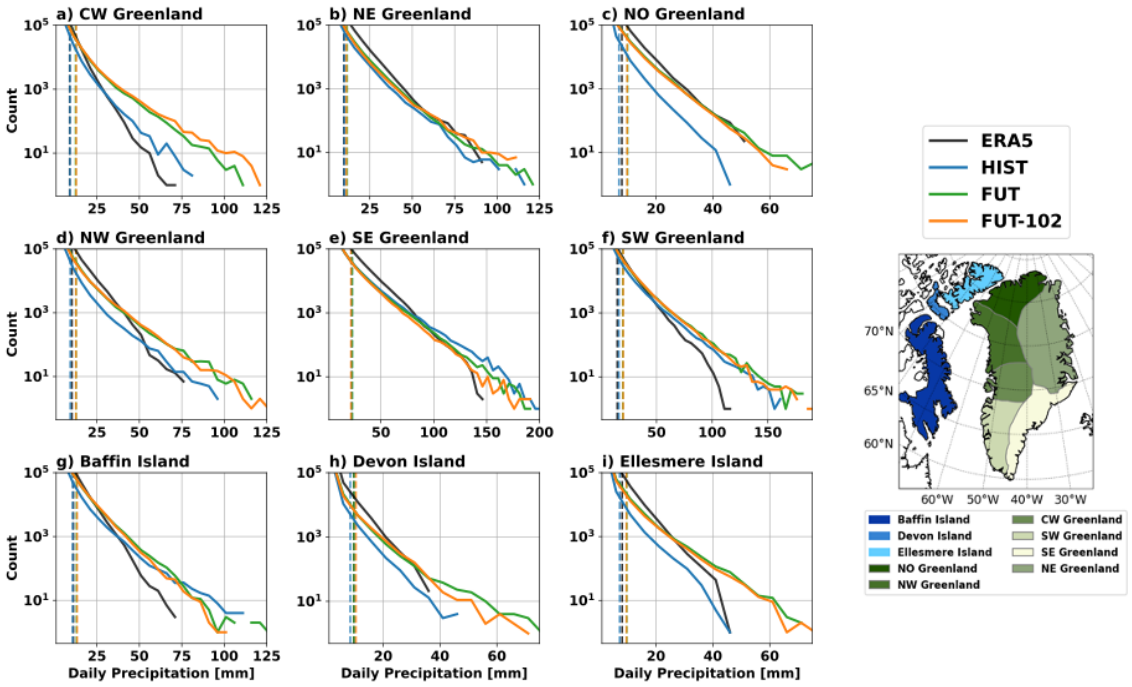

Figure B.7. As in Figure 4.5, but including the results of the second VR-CESM future run (FUT-102).

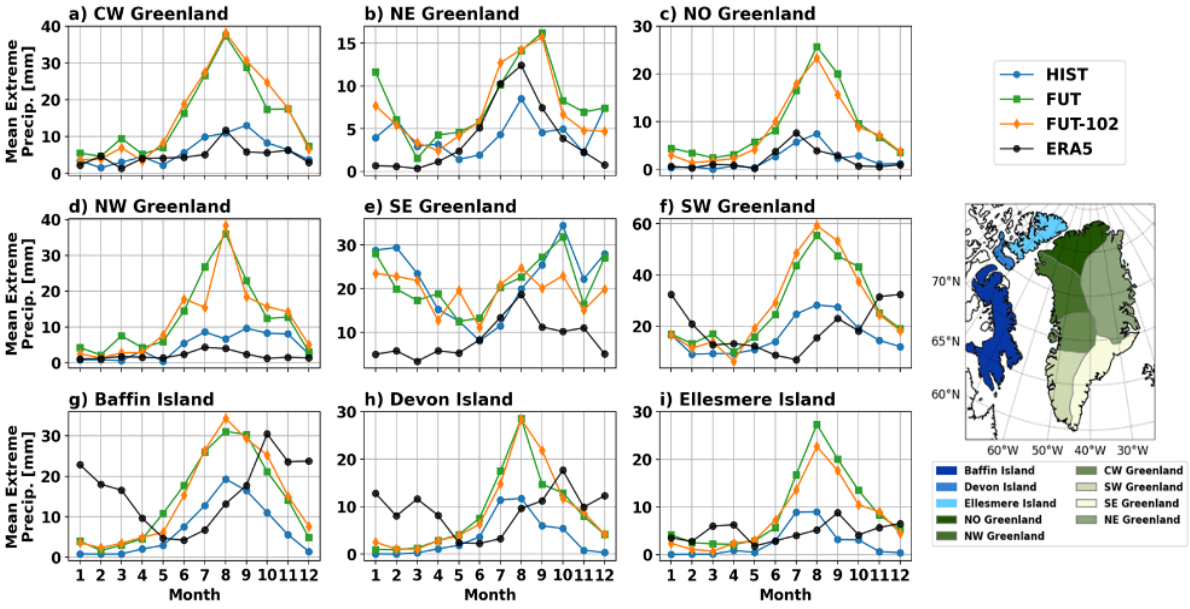

Figure B.8. As in Figure 4.6, but including the results of the second VR-CESM future run (FUT-102).

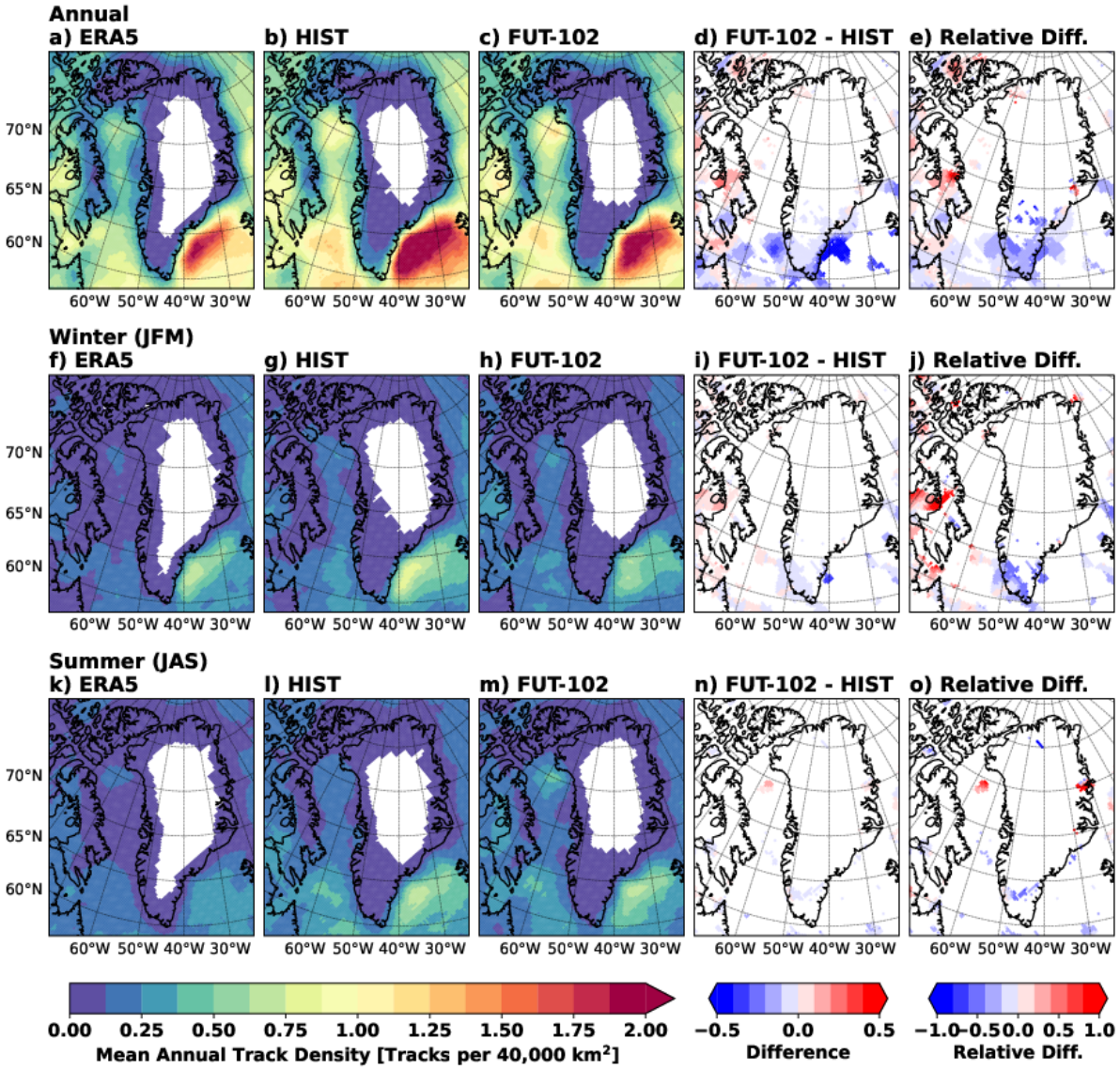

Figure B.9. As in Figure 4.7, but for the results of the second VR-CESM future run (FUT-102).

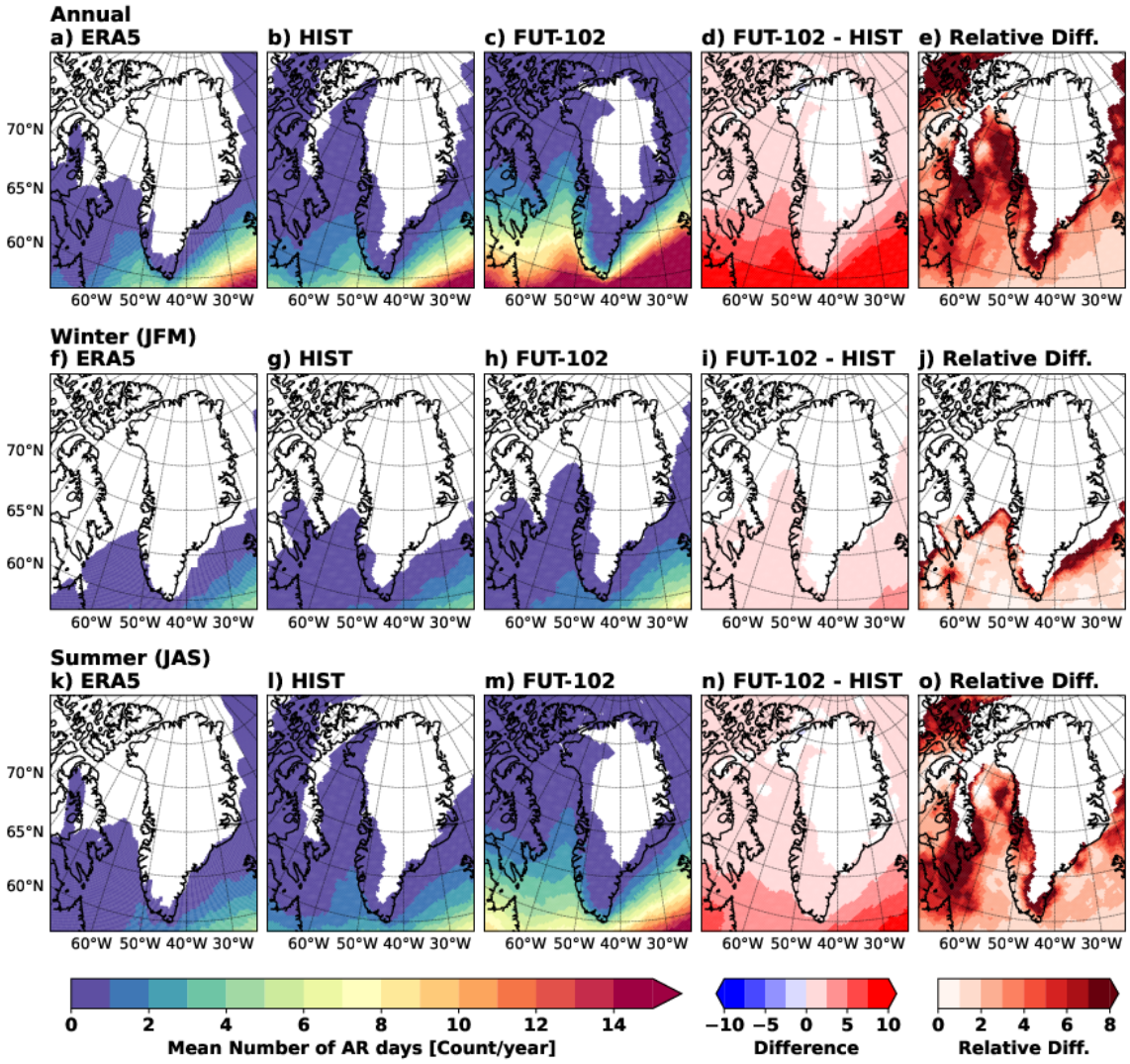

Figure B.10. As in Figure 4.8, but for the results of the second VR-CESM future run (FUT-102).

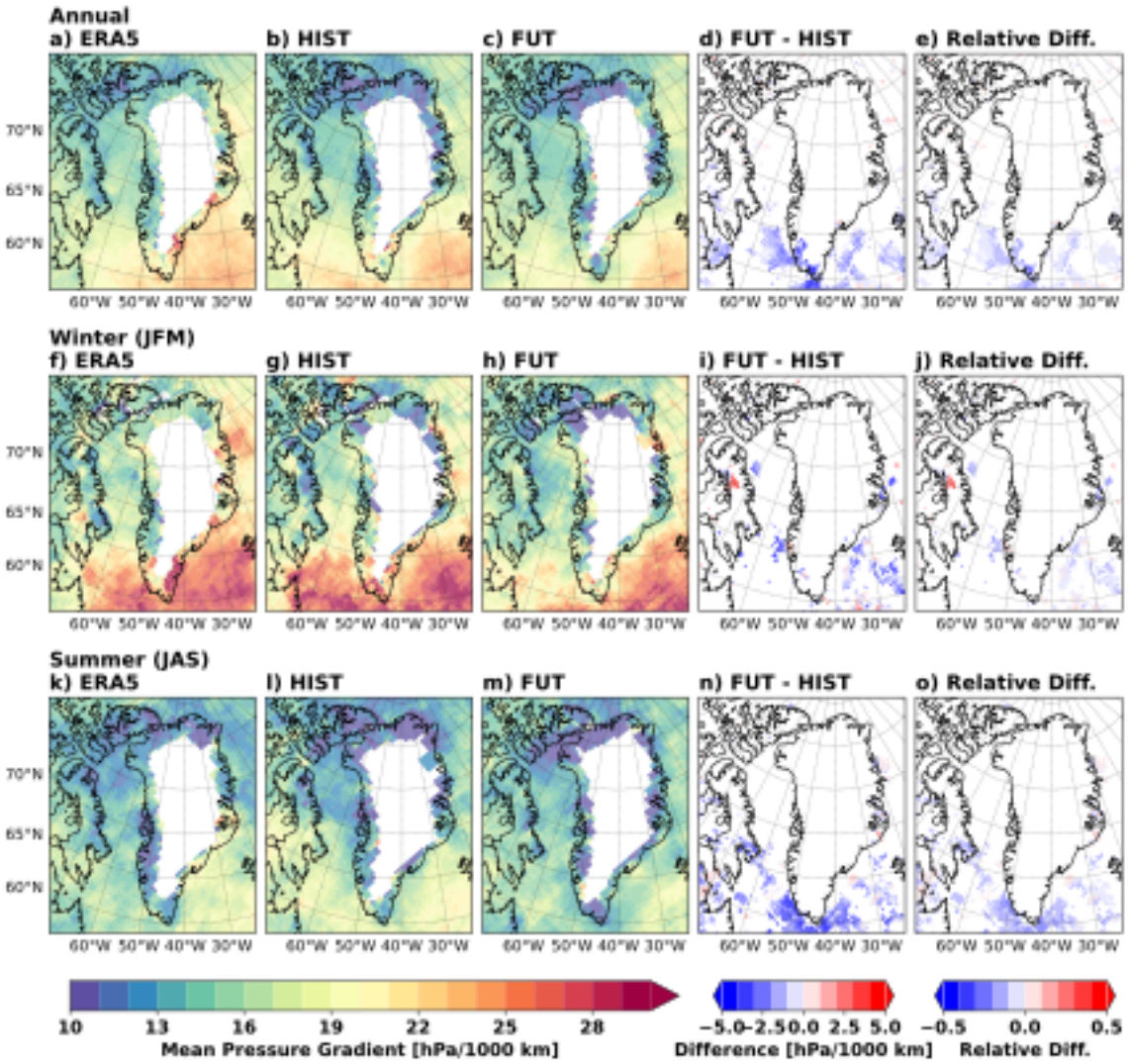

Figure B.11. Mean pressure gradient associated with cyclones from (a) ERA5 (1980-1999), (B) HIST (1980-1999), and (c) FUT (2080-2099). The differences between the future and historical conditions are shown in (c), with fractional differences (relative to HIST) shown in (e). Only differences that are statistically significant ($p < 0.05$) are shown.

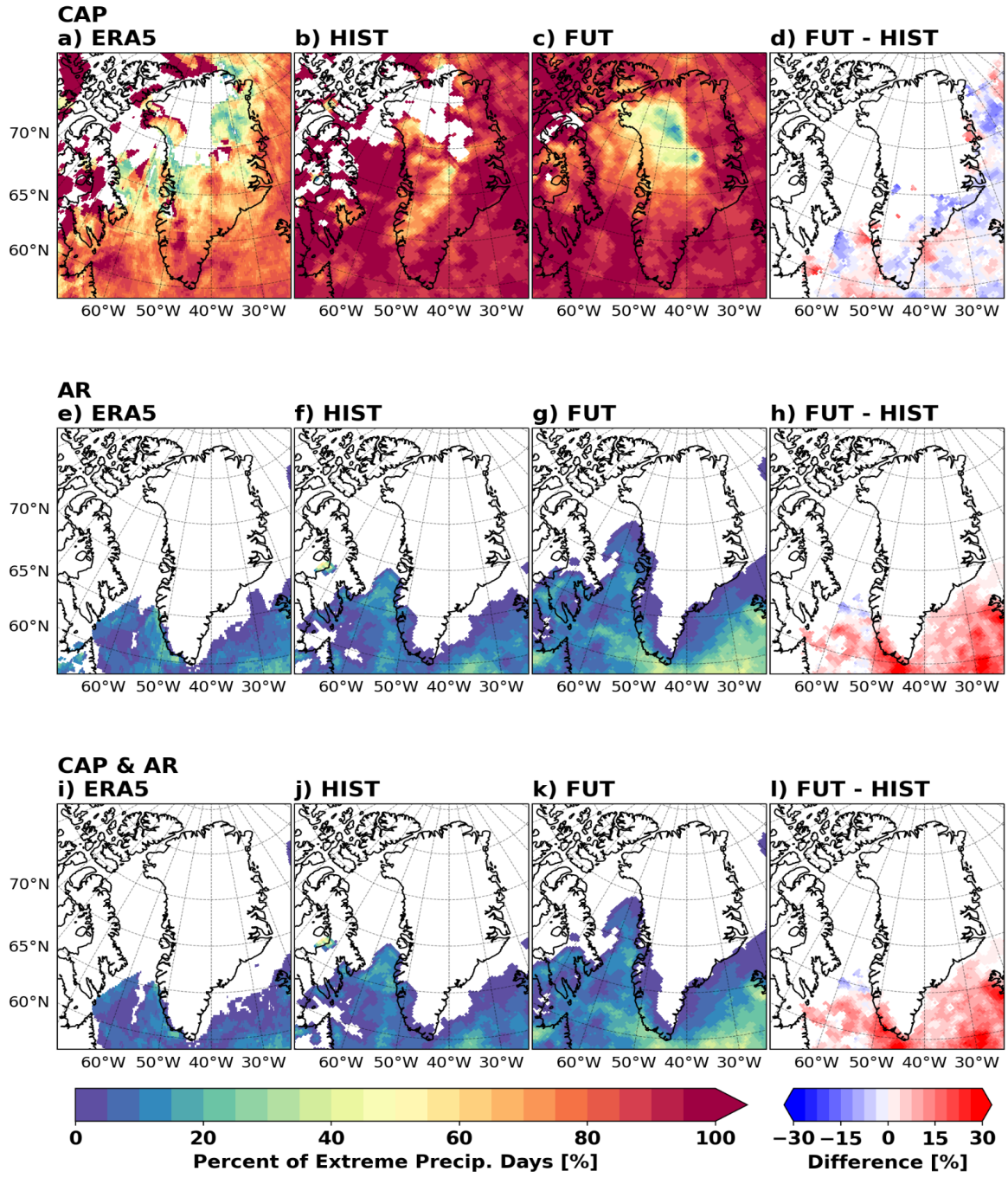

Figure B.12. As in Figure 4.9, but for winter (JFM).

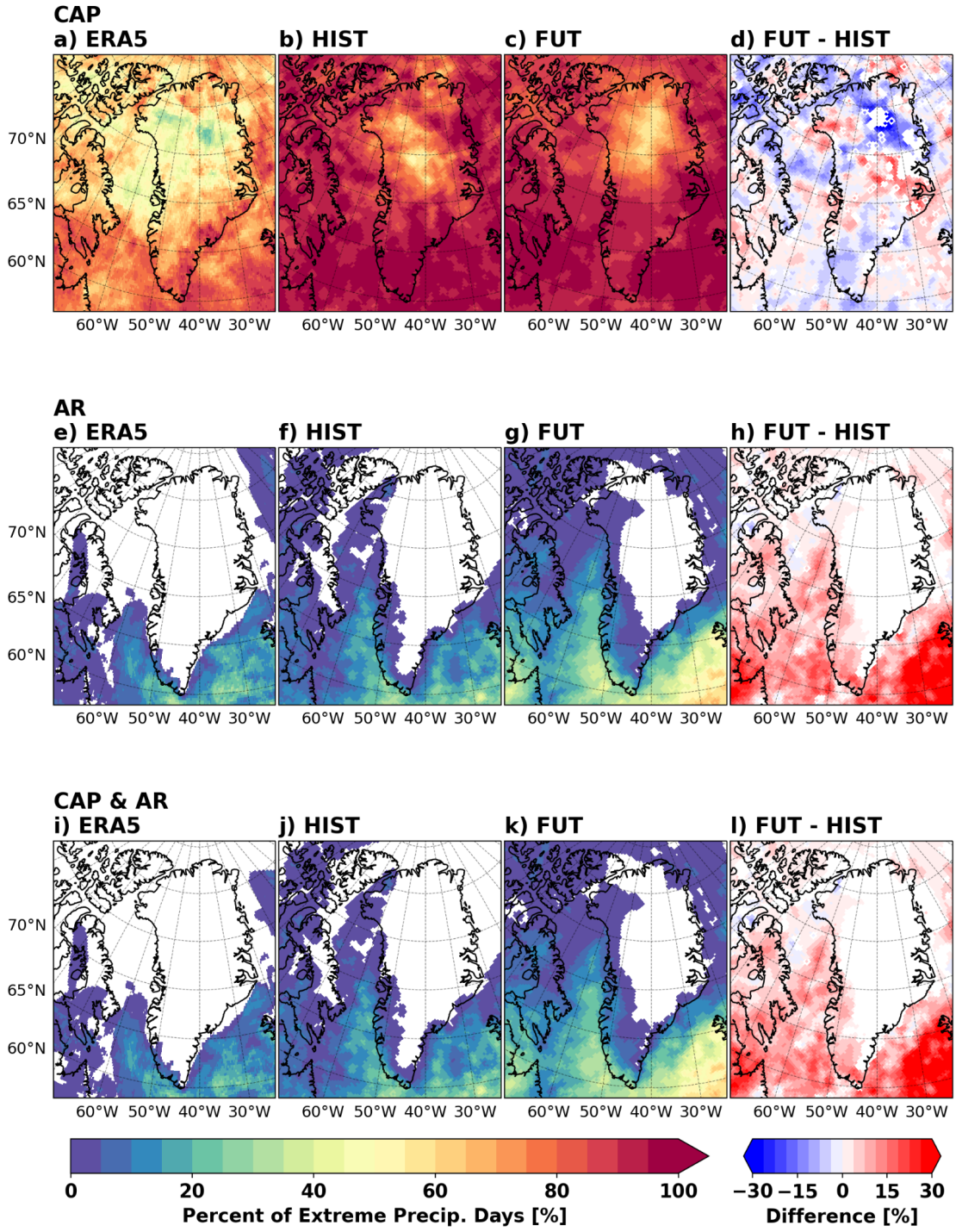

Figure B.13. As in Figure 4.9, but for summer (JAS).

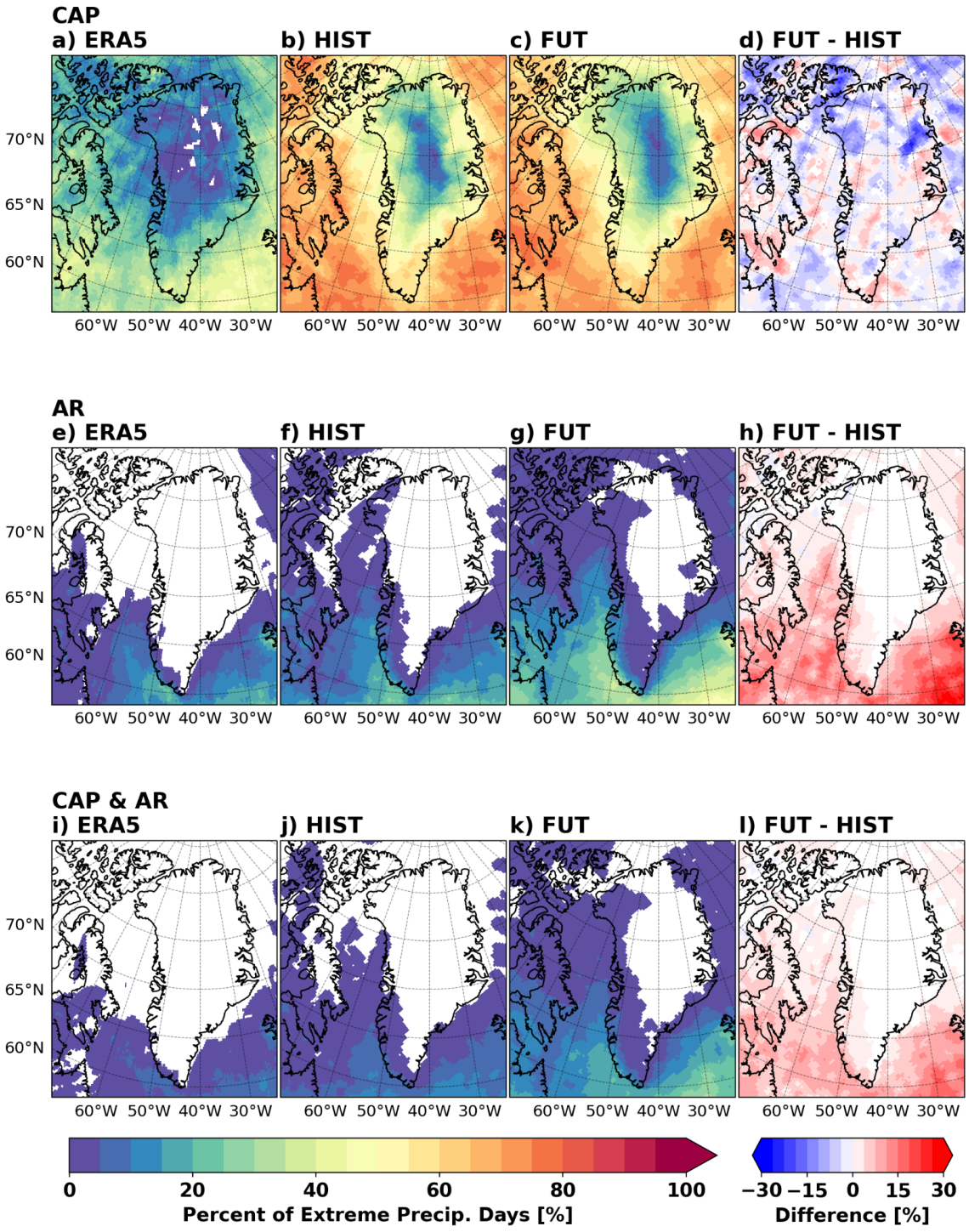

Figure B.14. As in Figure 4.9 (full year), but using a 600 km cyclone radius to determine cyclone-associated precipitation (CAP).

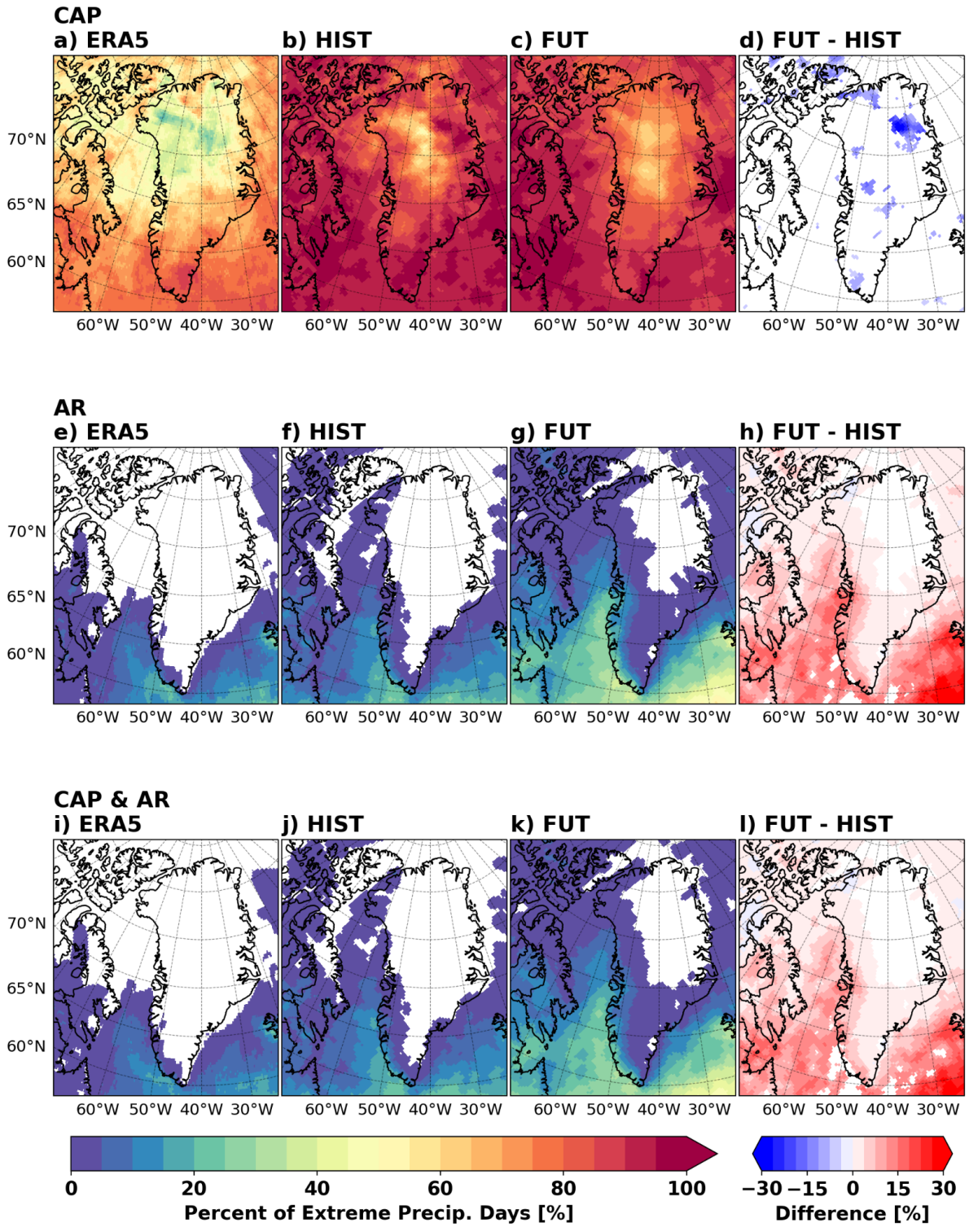

Figure B.15. As in Figure 4.9 (full year), but for the results of the second VR-CESM future run (FUT-102).

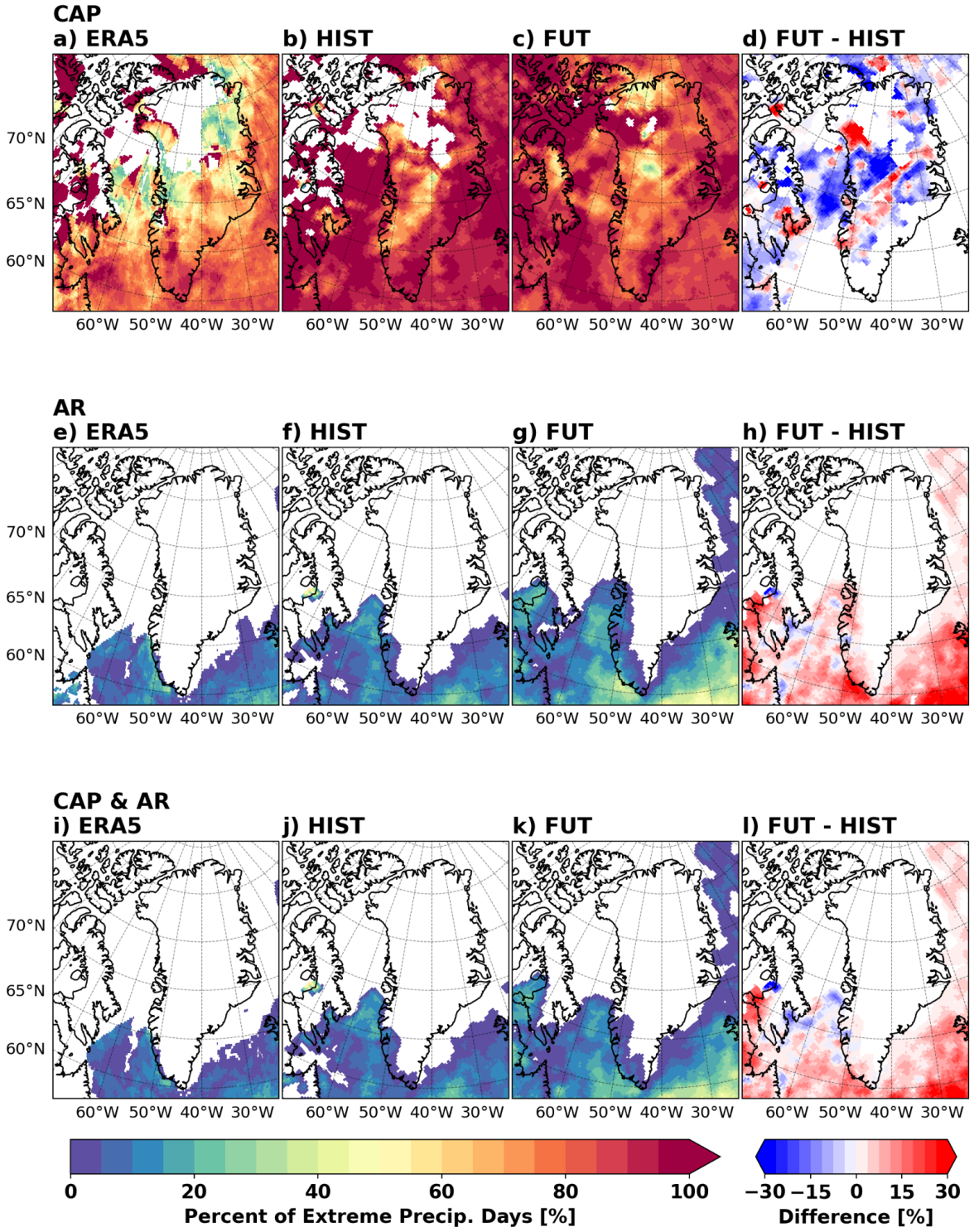

Figure B.16. As in Figure B.12 (JFM), but for the results of the second VR-CESM future run (FUT-102).

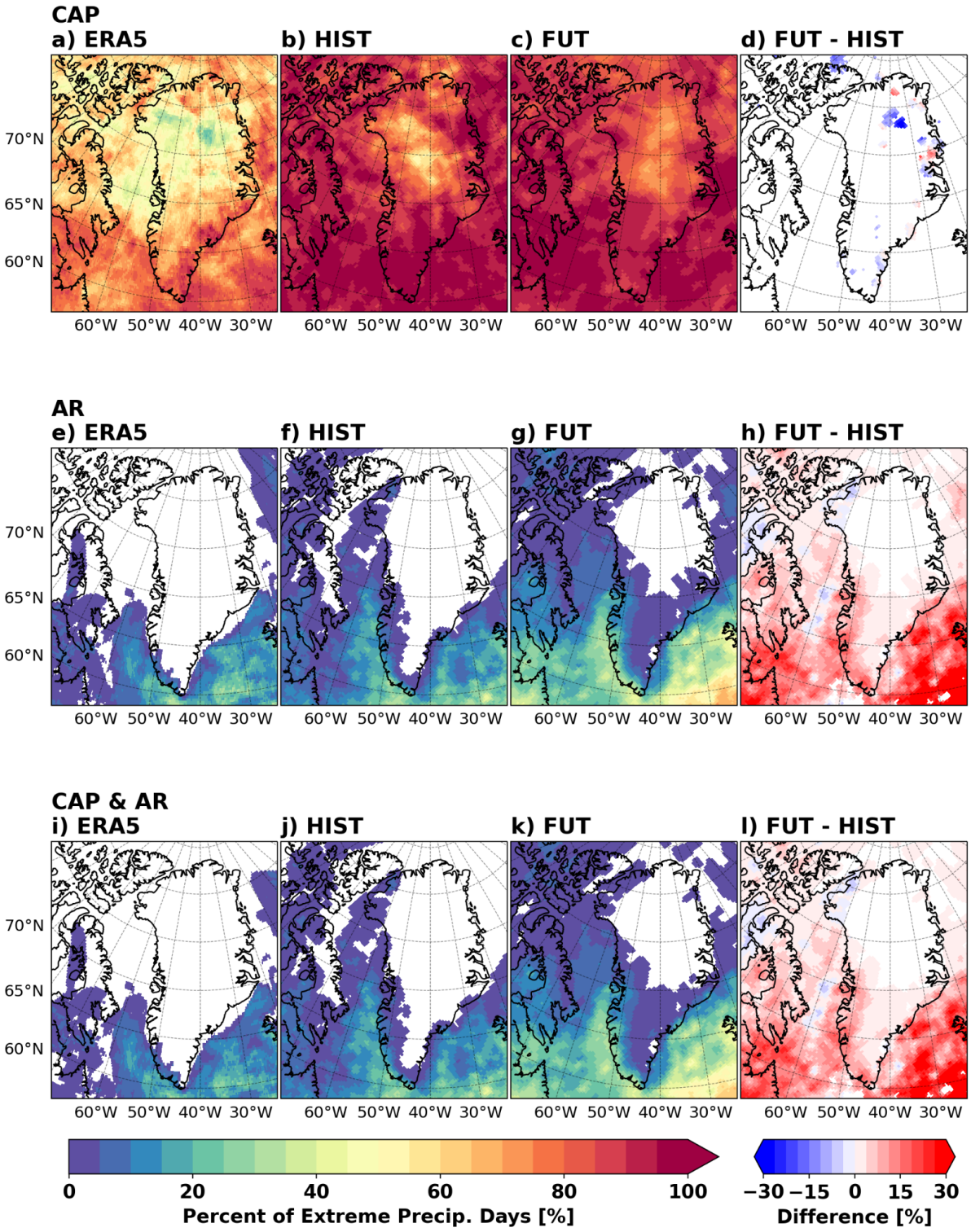

Figure B.17. As in Figure B.13 (JAS), but for the results of the second VR-CESM future run (FUT-102).

Appendix C. Supplementary Material for Chapter 5

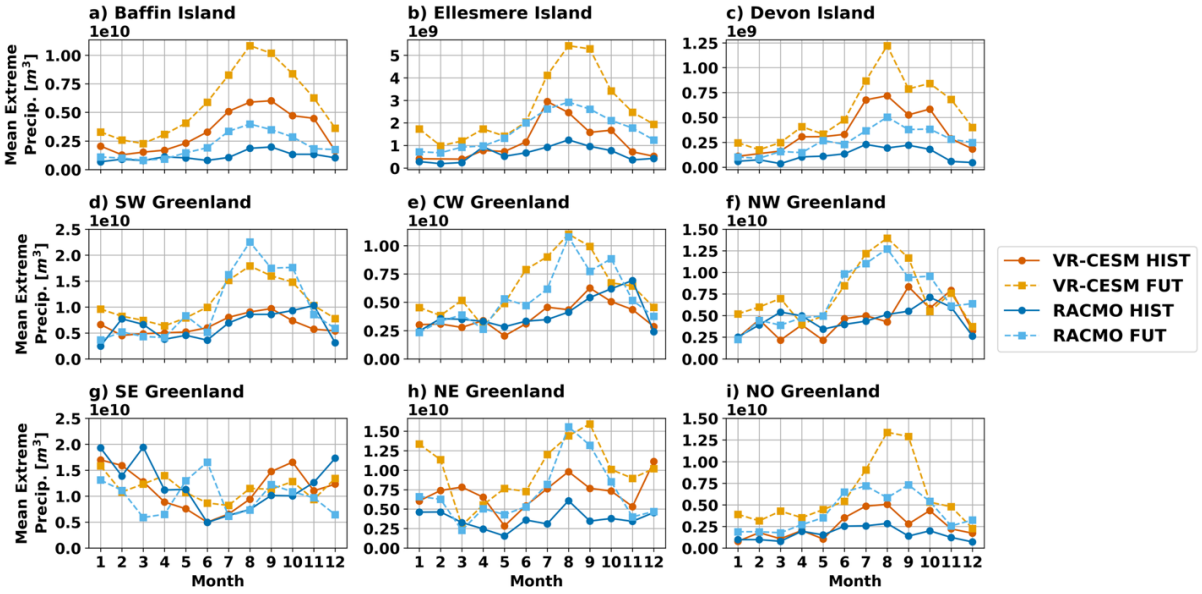

Figure C.1. As in Figure 5.2, but using the regional volume-based extreme precipitation definition, showing the mean monthly volume of extreme precipitation in each subregion.

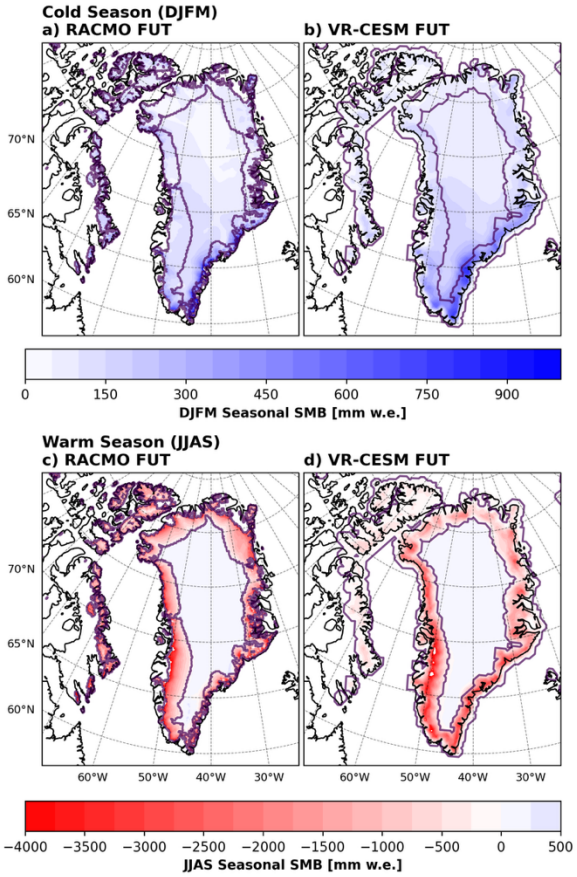

Figure C.2. Mean seasonal SMB in the region for the (a-b) cold season (DJFM) and (c-d) warm season (JJAS) for the future period (2080-2098; SSP5-8.5) from RACMO (a, c) and VR-CESM (b,d).

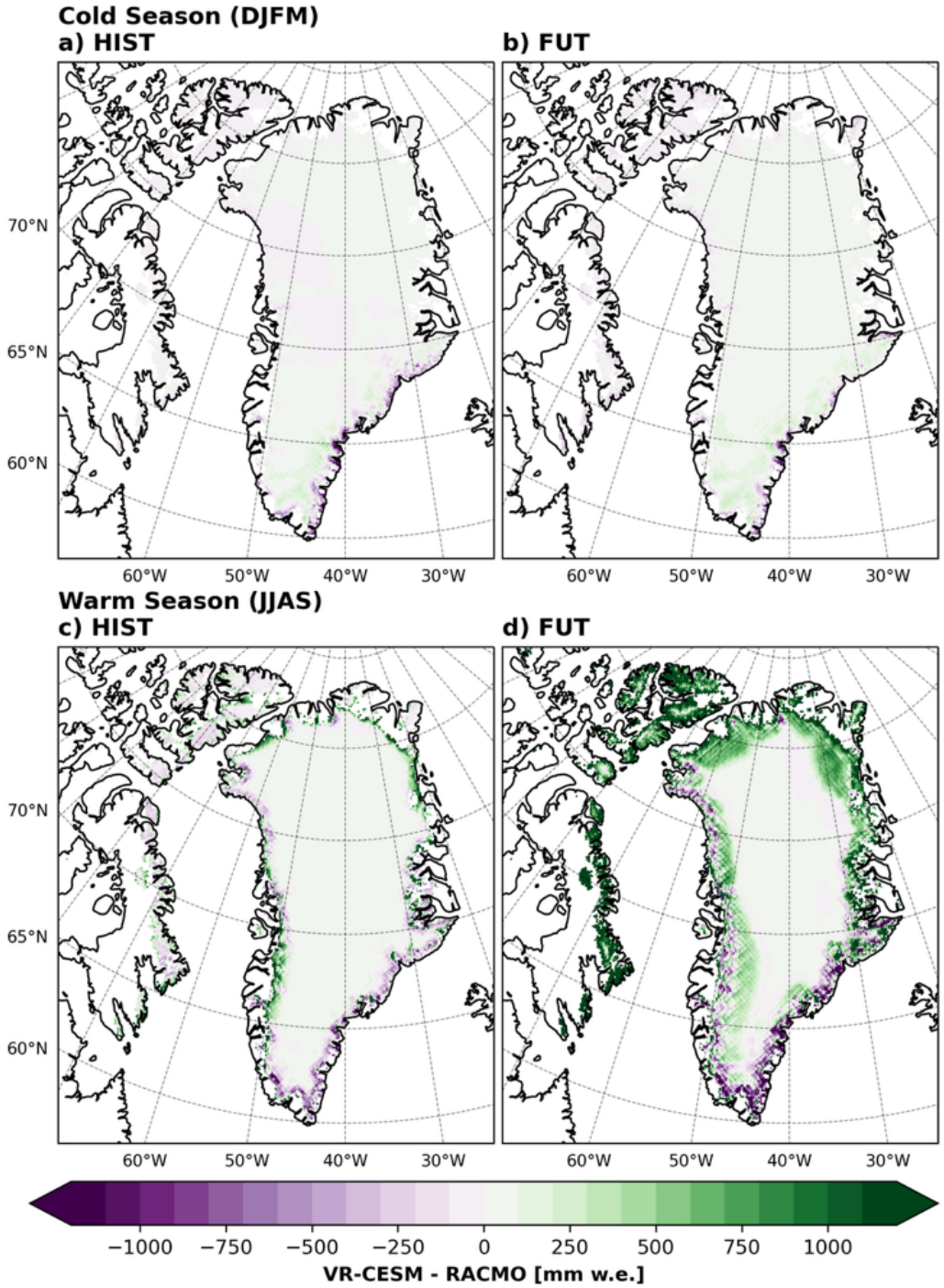

Figure C.3. Difference in mean seasonal SMB between VR-CESM and RACMO for the (a-b) cold season (DJFM) and (c-d) warm season (JJAS) in the (a,c) historical period (1980-1998) and (b, d) future period (2080-2098; SSP5-8.5). The green (purple) colours indicate that VR-CESM (RACMO) has a higher seasonal SMB.

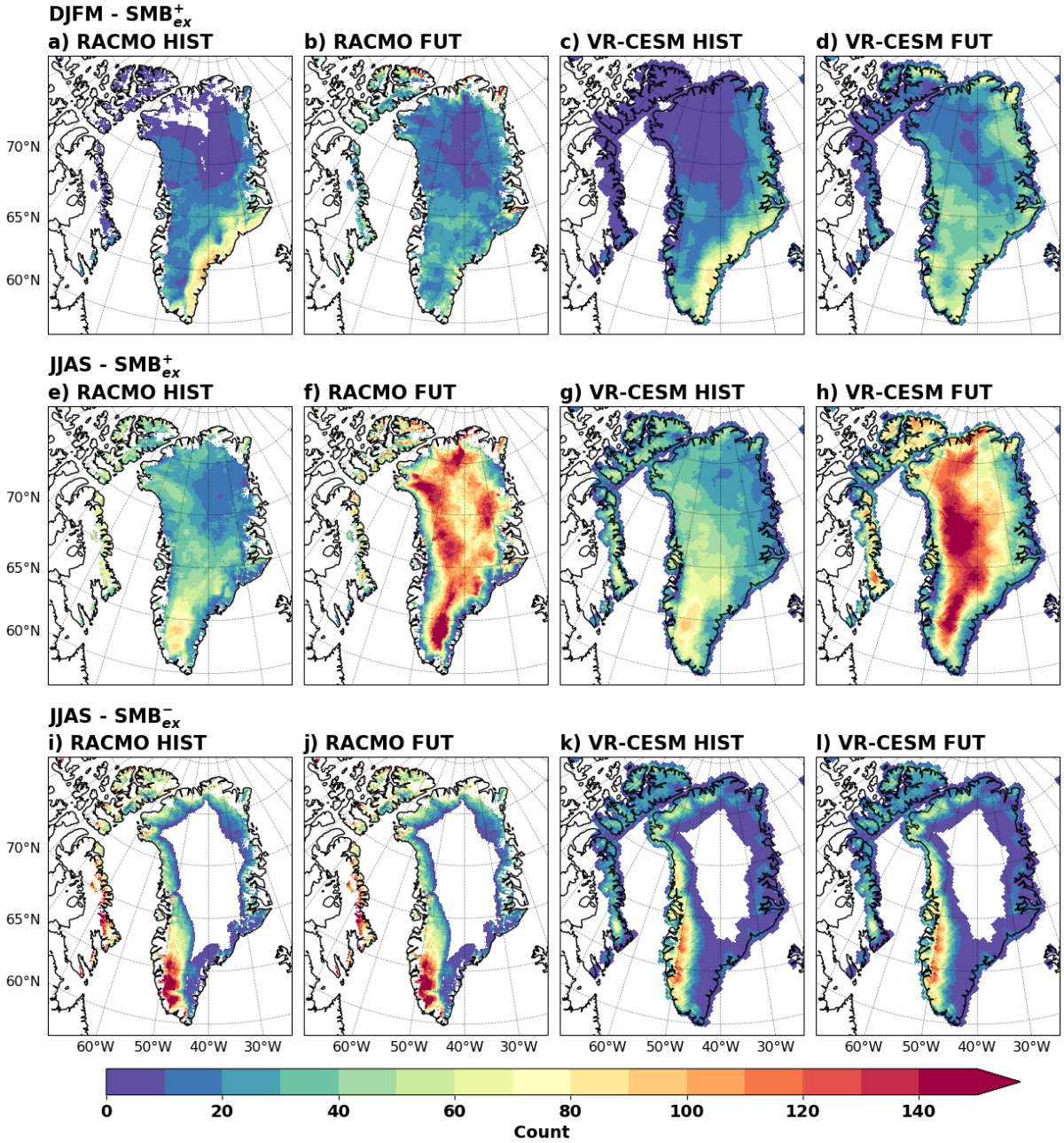

Figure C.4. Total number of extreme precipitation days occurring in each grid cell with positive SMB (a-h) or negative SMB (i-l) in the cold season (a-d) and warm season (e-l) in the historical (1980-1998; a,c,e,g,I,k) and future (2080-2098; b,d,f,h,j,l) periods. Counts from RACMO are shown in the first two columns (a-b, e-f, i-j) and VR-CESM is shown in the final two columns (c-d, g-h, k-l).

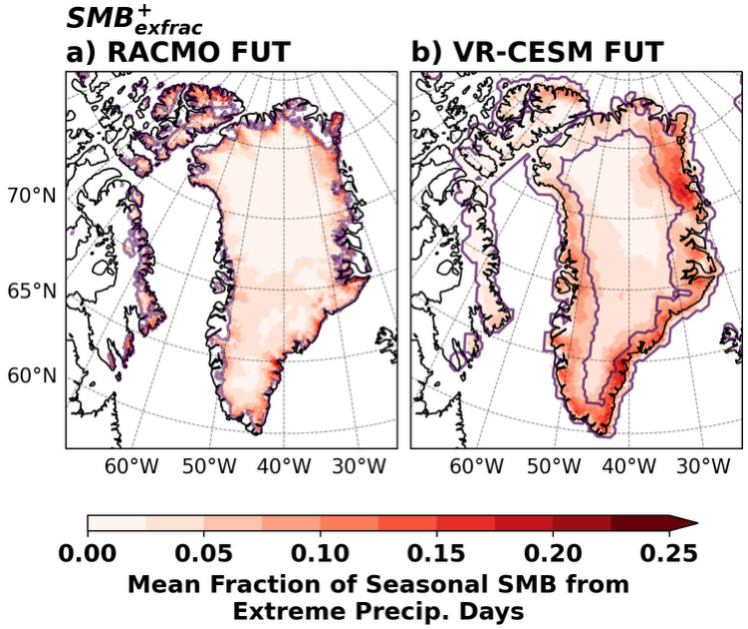

Figure C.5. Mean DJFM $SMB^{+}_{ex\ frac}$ for FUT (2080-2098; SSP5-8.5) from (a) RACMO and (b) VR-CESM. The solid purple line denotes the top of the ablation zone for the full simulation period.

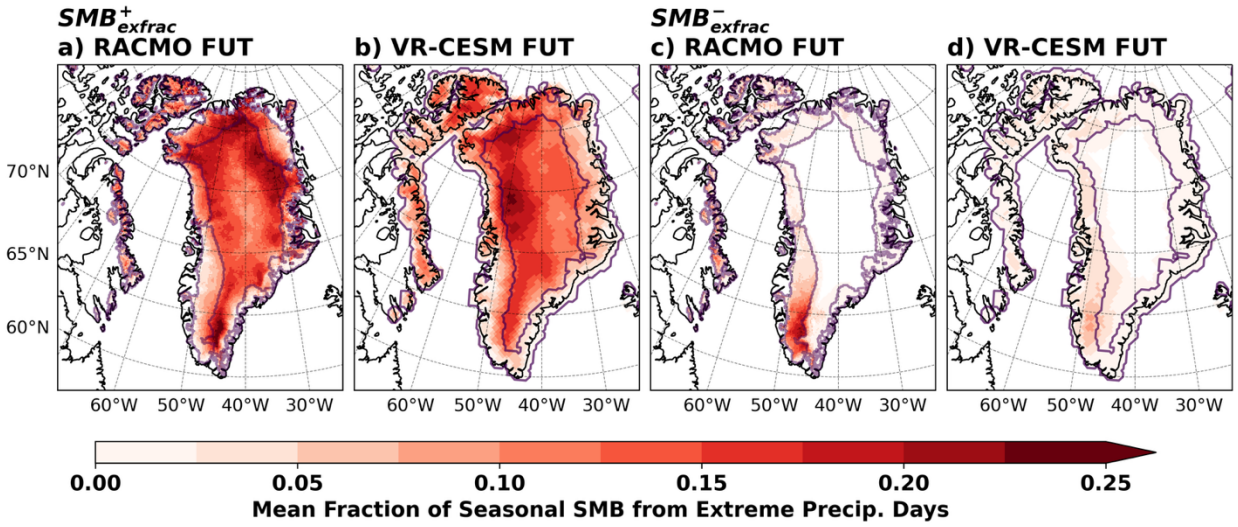

Figure C.6. Mean JJAS (a-b) $SMB^{+}_{ex\ frac}$ and (c-d) $SMB^{-}_{ex\ frac}$ for FUT (2080-2098; SSP5-8.5) from (a,c) RACMO and (b,d) VR-CESM. The solid purple line denotes the top of the ablation zone for the full simulation period.

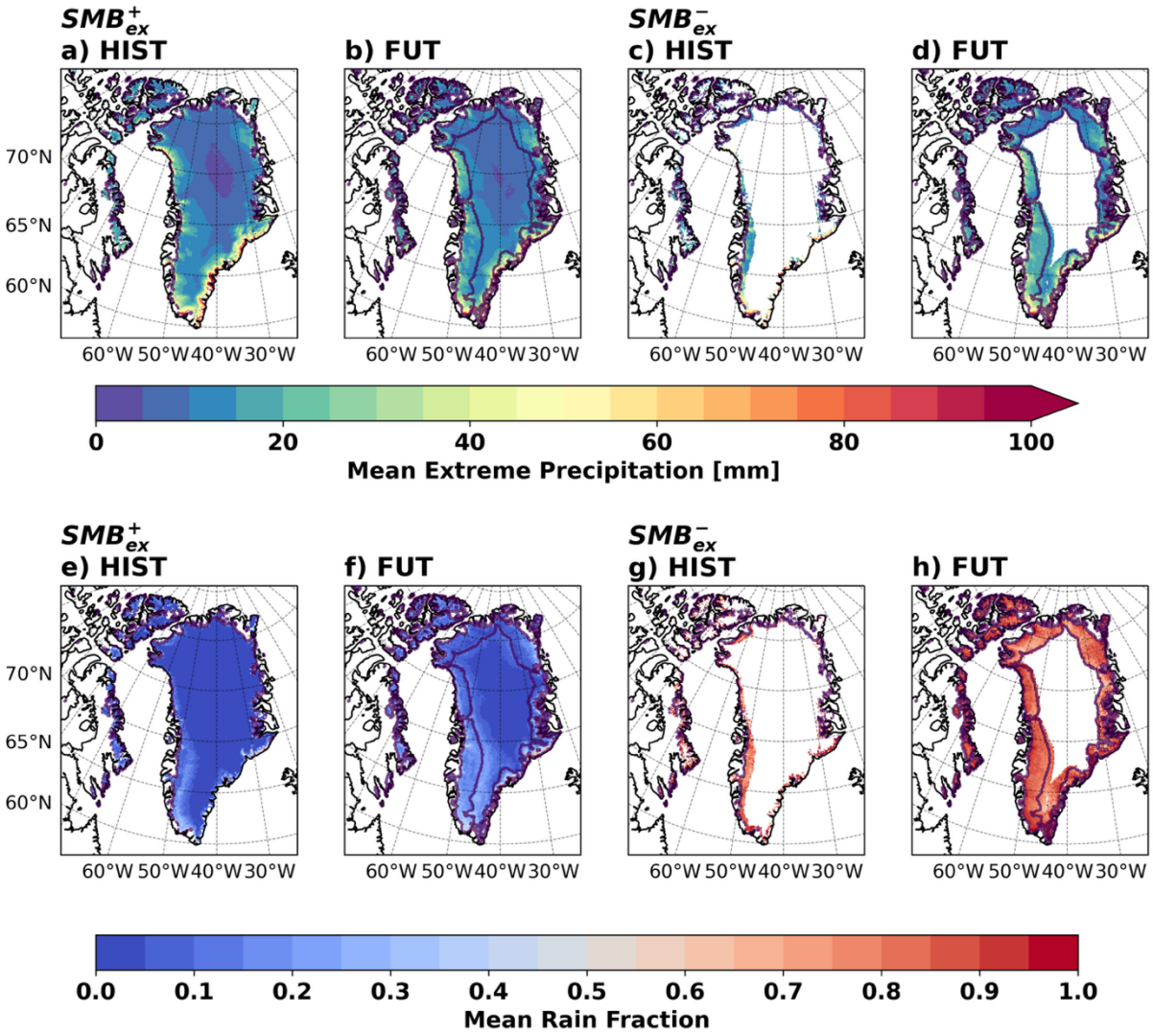

Figure C.7. Mean extreme precipitation (a-d) accumulations and (e-h) rain fraction in HIST (1980-1998; a,c,e,g) and FUT (2080-2098; b,d,f,h) for SMB_{ex}^{+} (a-b, e-f) and SMB_{ex}^{-} (c-d, g-h) from RACMO. The solid purple line denotes the top of the ablation zone for the full simulation period.

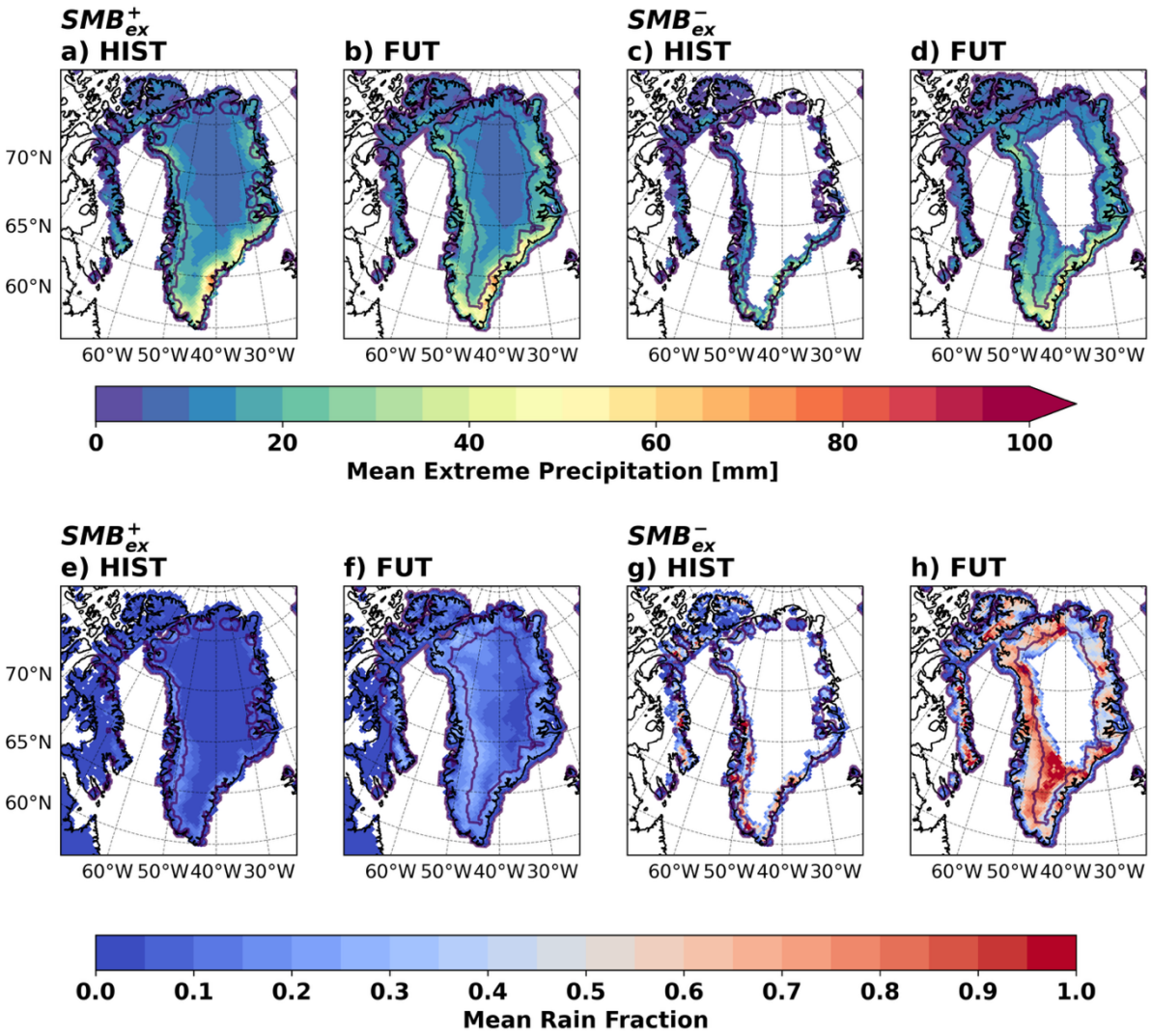

Figure C.8. As in Figure C.7, but from VR-CESM.

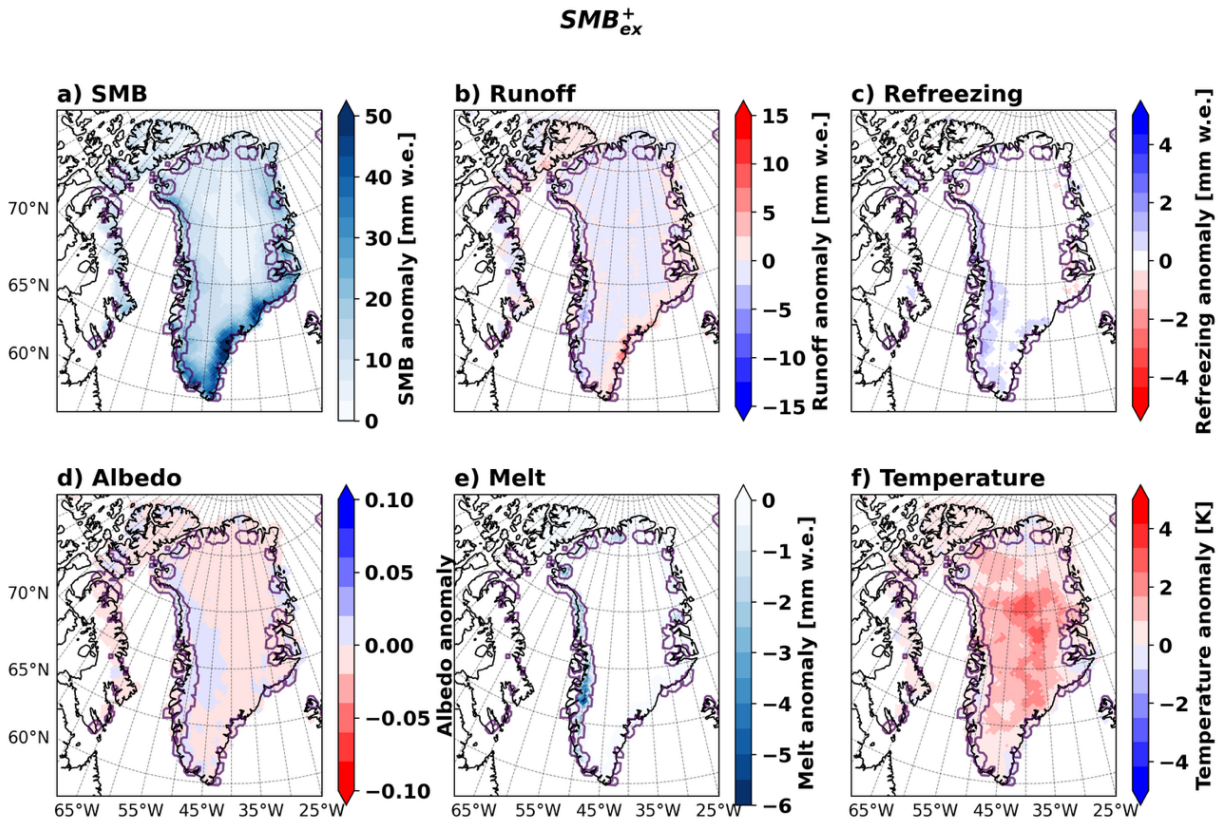

Figure C.9. Mean anomalies on positive SMB JJAS extreme precipitation days in the historical period (1980-1998) from VR-CESM. Anomalies are calculated for the extreme precipitation day relative to ±15 days. (Figure 5.9, but for VR-CESM)

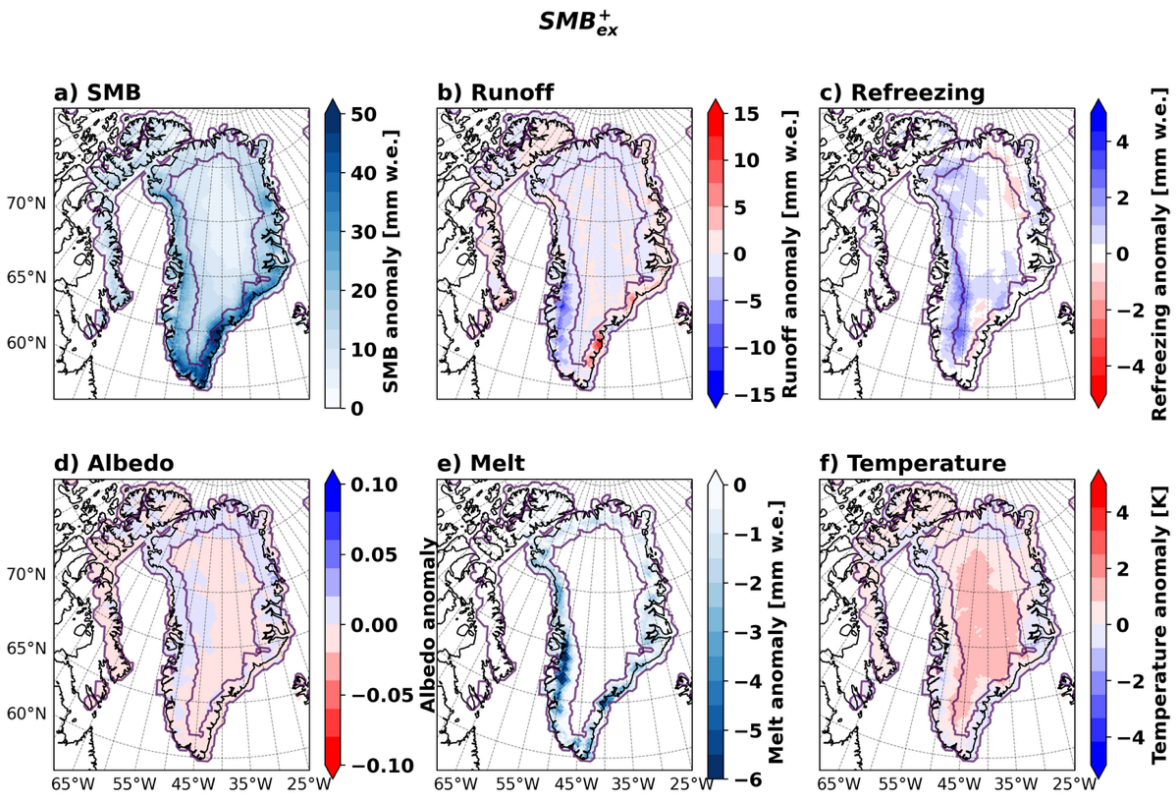

Figure C.10. As in Figure C.9, but for future positive SMB JJAS extreme precipitation days. (As in Figure 5.10, but for VR-CESM)

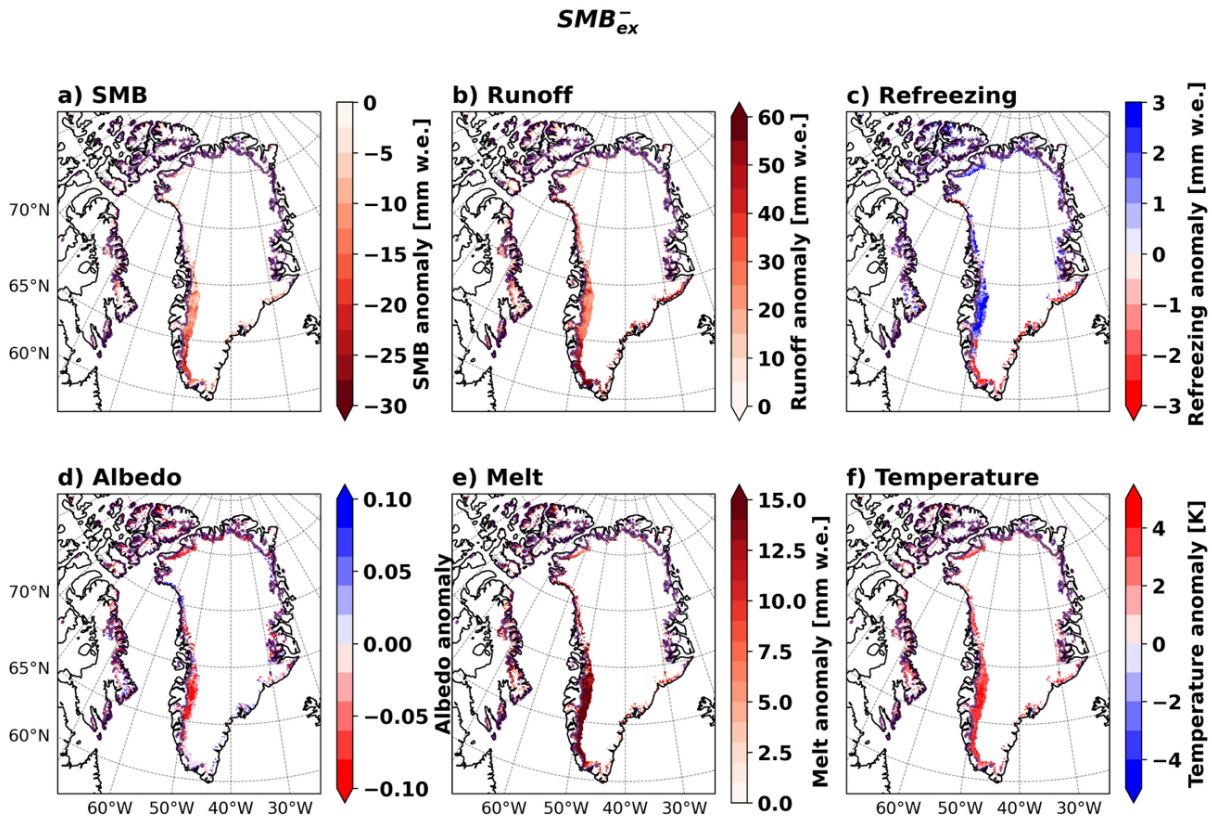

Figure C.11. As in Figure C.9, but for historical negative SMB JJAS extreme precipitation days from RACMO.

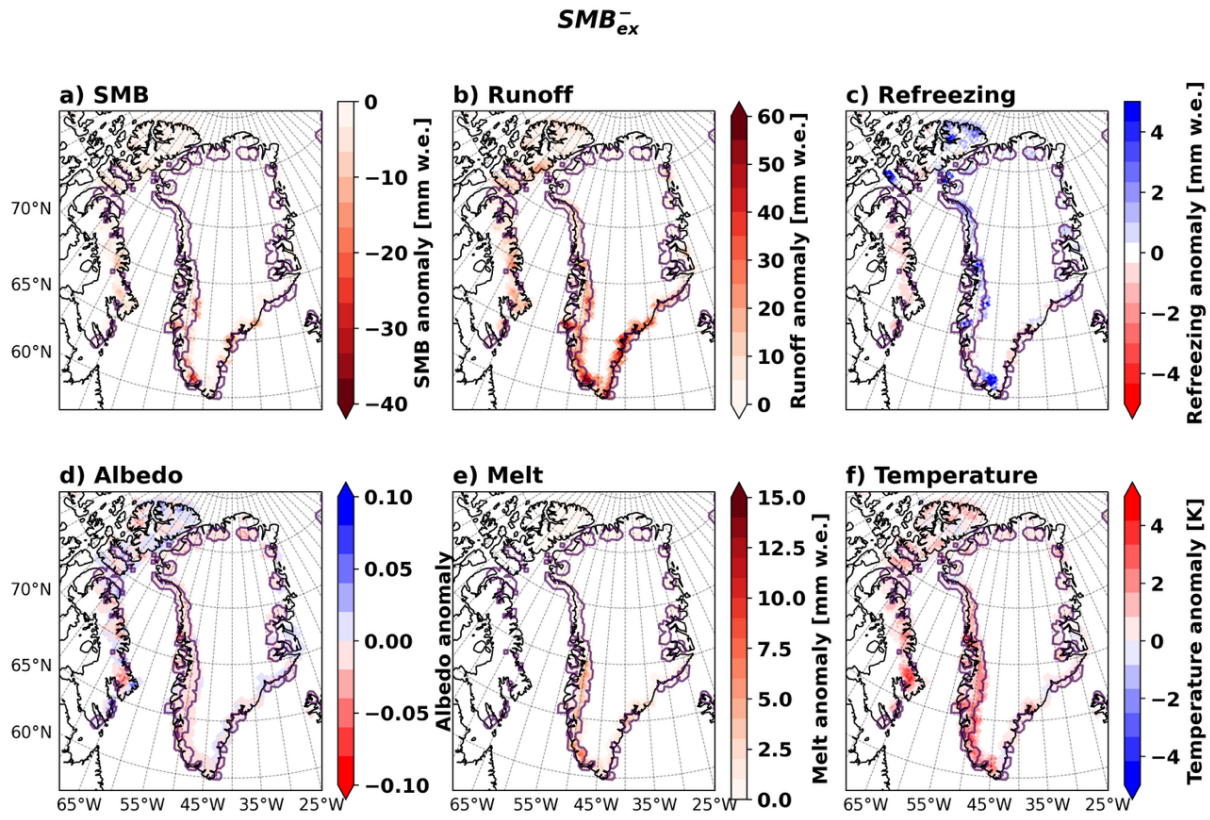

Figure C.12. As in Figure C.9, but for historical negative SMB JJAS extreme precipitation days from VR-CESM.

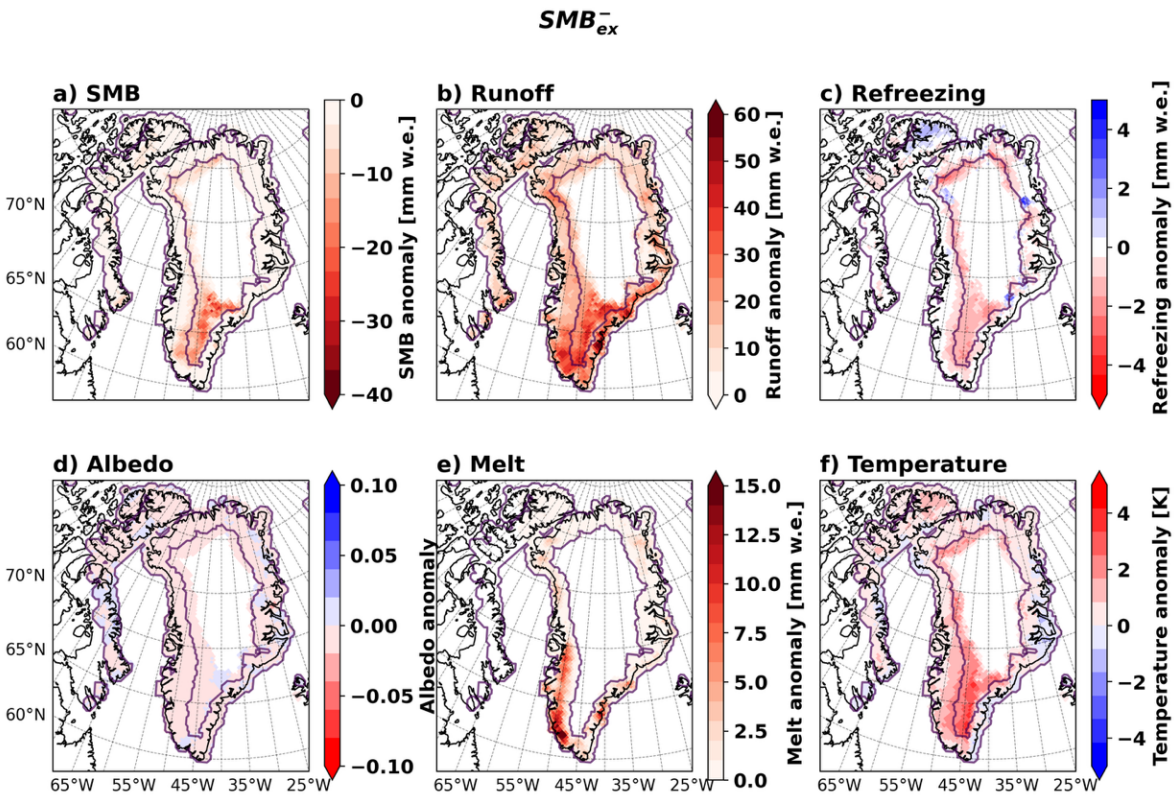

Figure C.13. As in Figure C.9, but for future positive SMB JJAS extreme precipitation days. (As in Figure 5.11, but for VR-CESM)